AUBURN

SAMUEL GINN
COLLEGE OF ENGINEERING

Research Report for ALDOT Project 930-889

FLAT SLAB BRIDGE MODEL FOR PERMIT LOAD ANALYSIS

Prepared by

Golpar Garmestani, Patryk J. Wolert, Marek K. Kolodziejczyk,

J. Michael Stallings and Andrzej S. Nowak

Department of Civil Engineering
Auburn University

Submitted to

Alabama Department of Transportation
Montgomery, Alabama

DECEMBER 2016

Highway Research Center
Harbert Engineering Center
Auburn, Alabama 36849

www.eng.auburn.edu/research/centers/hrc.html

DISCLAIMERS

The contents of this report reflect the views of the authors, who are responsible for the facts and the accuracy of the data presented herein. The contents do not necessarily reflect the official views or policies of Auburn University, the Alabama Department of Transportation, or the Highway Research Center. This report does not constitute a standard, specification, or regulation.

NOT INTENDED FOR CONSTRUCTION, BIDDING, OR PERMIT PURPOSES

Andrzej S. Nowak and J. Michael Stallings
Research Supervisors

ACKNOWLEDGEMENTS

The authors would like to acknowledge the financial support provided by the Alabama Department of Transportation that made this project possible. Also, the authors would like to acknowledge the efforts of many in the Alabama Department of Transportation who provided guidance and assistance that were essential to ensure that this project concluded in a useful and practical result.

ABSTRACT

ALDOT has an eleven-span flat slab concrete bridge over Barnes Slough and Jenkins Creek on the northbound side of US Highway 82/231 that was built in 1915 for which there are no construction drawings or other available data. This bridge is referred to as "Barnes Slough Bridge". The goals of this research are to define the capacity of Barnes Slough Bridge, rate the bridge, and provide a permit load model that can be included in the AASHTOWare software. ALDOT can then use this model to provide permits for non-standard trucks to travel over this bridge. The design methods from early 1900s were reviewed to identify the possible methods used in the original design of this bridge. Field measurements were taken using specialized equipment to assess the dimensions including span length, width, location and size of reinforcement, thickness of the slab, thickness of concrete cover and compressive strength of concrete. The collected data were analyzed and treated as input data to determine a preliminary load carrying capacity of the slab by AASHTOWare. An advanced finite element method program ABAQUS was used to develop a 3-D model of the slab. A sensitivity analysis served as a basis for identifying the most important parameters. The behavior of the bridge slab was then verified by load test, with the load applied using one and two 85-kip 3-axle trucks. The load test results were used to further improve the finite element model and in particular, to develop an improved value for the effective slab width. Proposed newly developed adjustments in the selection of input data in AASHTOWare result in a more rational evaluation and rating of the considered bridge.

TABLE OF CONTENTS

LIST OF TABLES

LIST OF FIGURES

1 Introduction

1.1 Motivation

ALDOT has an eleven-span flat slab concrete bridge over Barnes Slough and Jenkins Creek on the northbound side of US Highway 82/231 at milepost 162.56 (Figure 1-1) for which there are no construction drawings or other details that can be used to perform a load rating of the structure. This bridge is approximately one mile south of Taylor Road on the south side of Montgomery. ALDOT's "Bridge Card" for the structure indicates that the bridge was widened by approximately 4 ft in 1930, and the visual inspection of the bridge indicates that width has been added to the east side of the bridge twice and to the west side once. The sequence and time of these additions are unknown.

Figure 1-1: View of East Side of Barnes Slough Bridge

Figure 1-2: Bottom View of the Barnes Slough Bridge Looking East

Also the existence of some cracks on the sides of the slab near the supports were indicative of shrinkage or temperature cracking in the concrete, but there were no significant signs of flexural or shear cracking, nor evidence of anchorage or bond failure. Under two footings beneath the first and second support on the east side 6 in. scour has occurred. Currently the bridge carries unrestricted traffic. This is allowed by AASHTO's *The Manual for Bridge Evaluation* (2011) in cases where a reinforced concrete bridge of unknown details has carried unrestricted traffic without developing signs of distress. But, because the structural details of the bridge are unknown, ALDOT cannot perform an analysis to justify issuing a permit to any overweight, non-standard trucks. So, overweight, non-standard trucks are detoured around this bridge. ALDOT would like to have the ability to consider requests for permits on this heavily travelled route.

1.2 Historical Documentation

A search of historical documents was performed. The focus was to pinpoint an era when the bridge was built in order to achieve an understanding of the methods used to design the structure. By using the Auburn University library resources and the Alabama Department of Archives and History in Montgomery, the construction year was established as 1915 from a report of the state of Alabama Highway Commission (*State Highway Comission of Alabama* 1916).

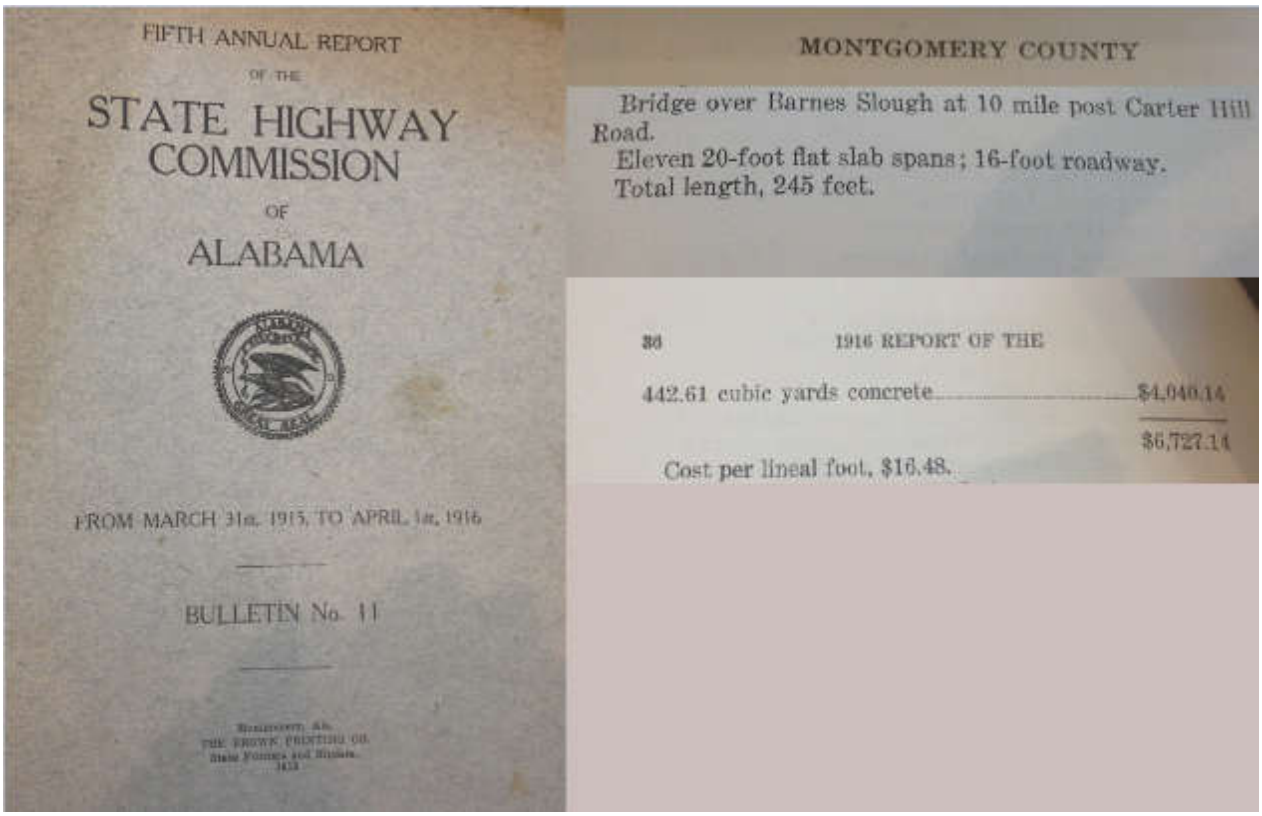
FIFTH ANNUAL REPORT
OF THE
STATE HIGHWAY COMMISSION
OF
ALABAMA

FROM MARCH 31st, 1915, TO APRIL 1st, 1916

BULLETIN No. 11

MONTGOMERY COUNTY

Bridge over Barnes Slough at 10 mile post Carter Hill Road.
Eleven 20-foot flat slab spans; 16-foot roadway.
Total length, 245 feet.

36 1916 REPORT OF THE

442.61 cubic yards concrete $4,046.14

$6,727.14

Cost per lineal foot, $16.48.

Figure 1-3: Records of Expenditure for Construction of Barnes Slough Bridge (State Highway Commission of Alabama 1916)

State Highway Commission of Alabama (1916) has the itemized list of infrastructure built between March 31, 1915 and April 1, 1916. A description of the Barnes Slough Bridge is shown on a photo of part of page 35 and 36 of that publication in Figure 1-3. These pages describe a bridge over Barnes Slough at the 10 mile post of Carter Hill Road. The description of the bridge as eleven 20-foot flat slab spans matches the original details of the existing bridge before it was widened. The location referred to as Barnes Slough is now referred to as Jenkins Creek, which is the location of the bridge that is the subject of this research. Through comparing the description of the location of the bridge on an old map of Montgomery County to a current map of Montgomery County it was confirmed that these are the same bridge.

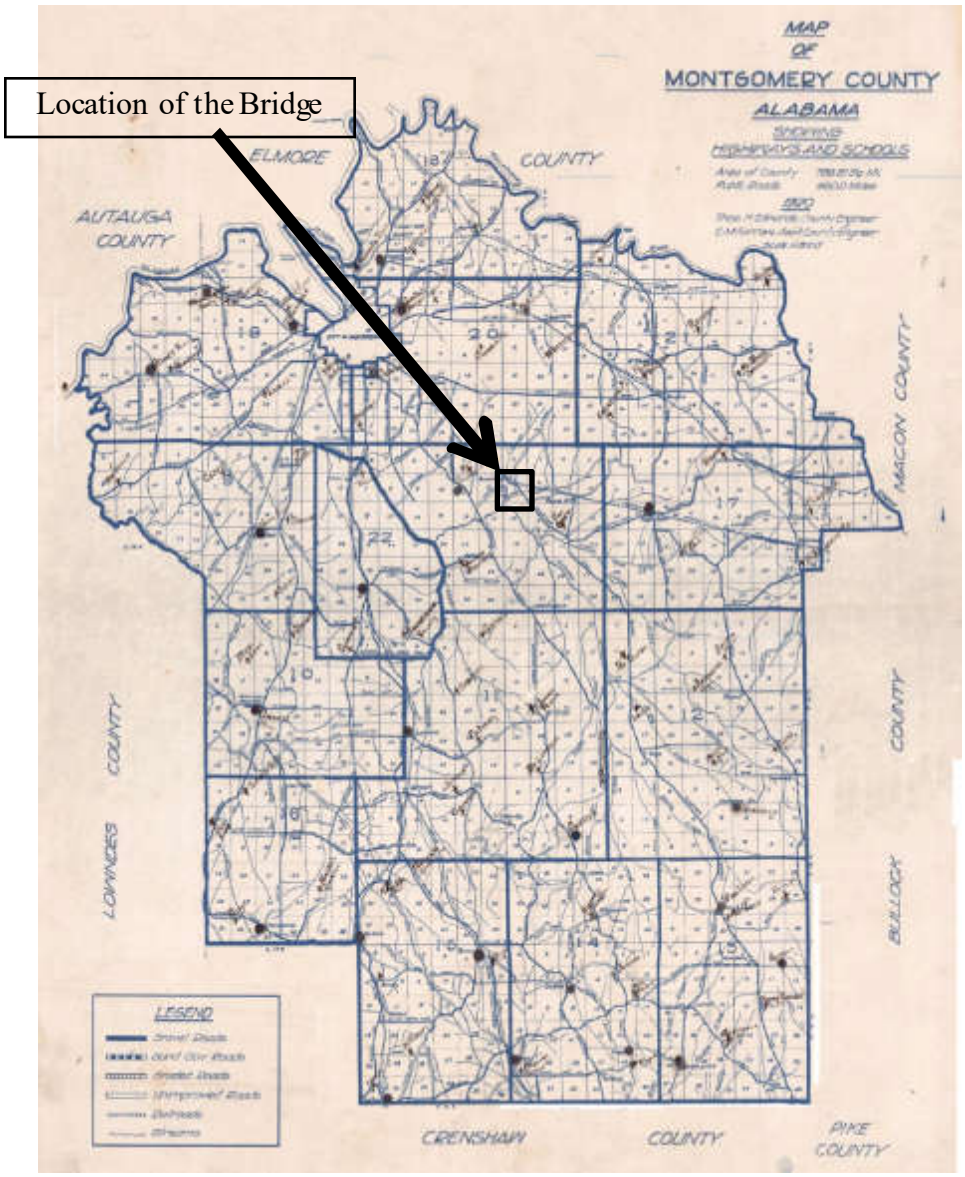

Figure 1-4: Map of Montgomery County, Alabama by Thomas H. Edwards, 1920 (http://alabamamaps.usa.edu)

Figure 1-5: Map of Montgomery County, Alabama by Thomas H. Edwards, 1920. Range 19 E, Township 15 N, Section 7
(http://alabamamaps.ua.edu)

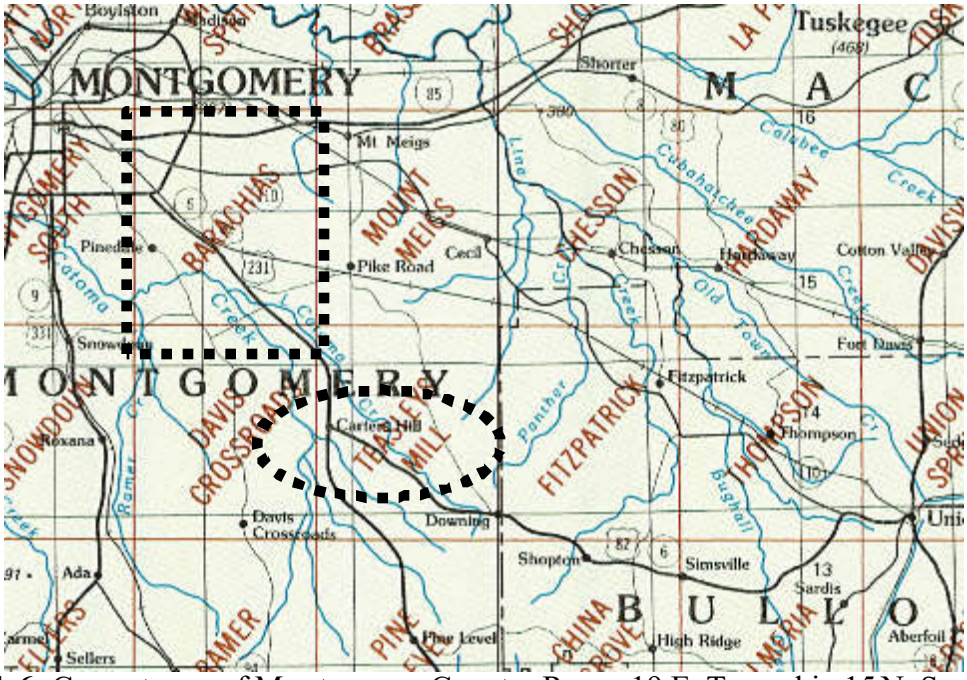

Figure 1-6: Current map of Montgomery County. Range 19 E, Township 15 N, Section 7 in 1993
(Alabama Index to topographic and other MAP COVERAGE. Scale: 1:24000. Denver Colorado. United States Geological survey, 1993)

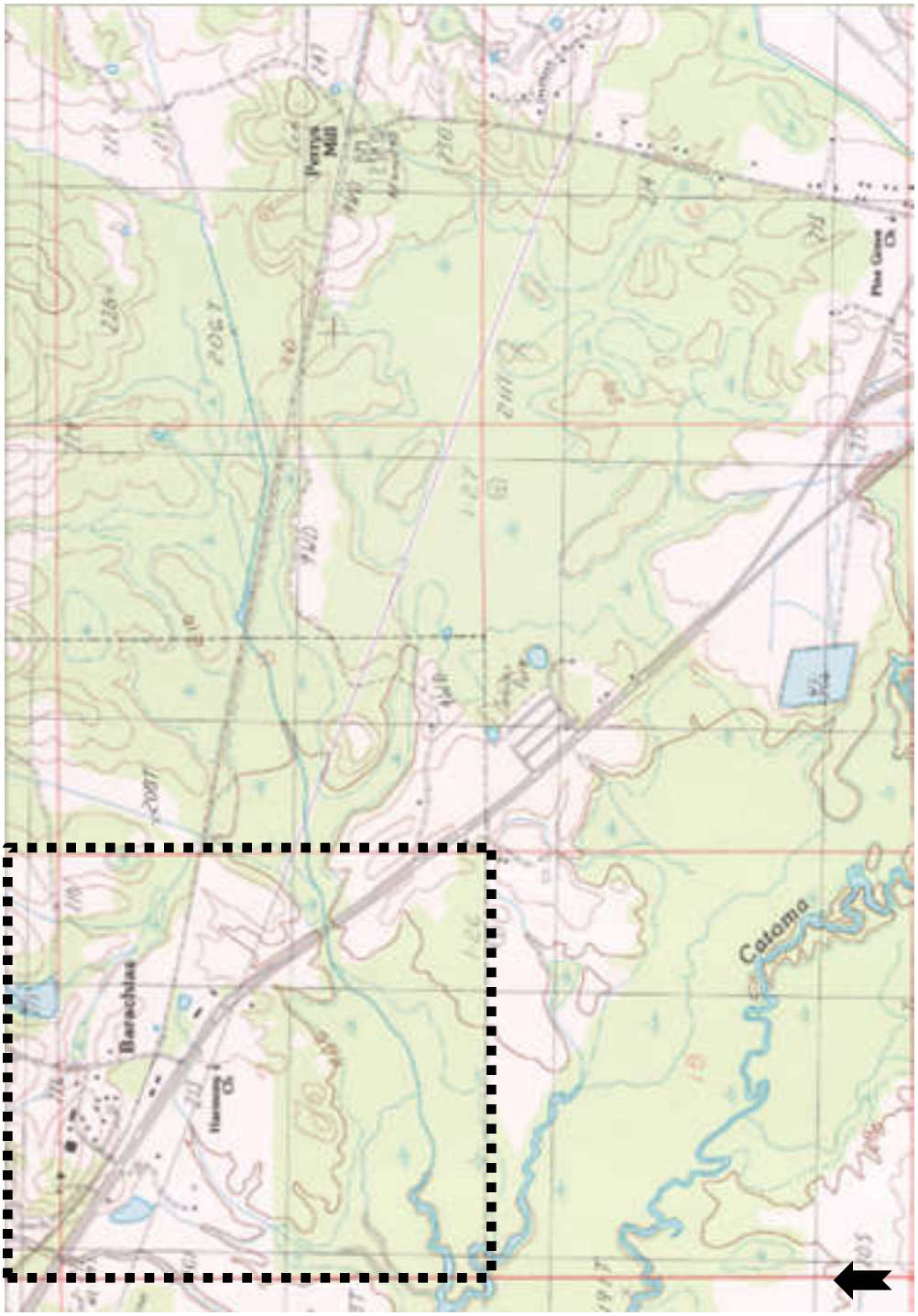

Figure 1-7: Current map of Montgomery County. Range 19 E, Township 15 N, Section 7 in 1999
(BARACHIAS Quadrangle ALABAMA-Montgomery CO. Scale: 1:24000. Denver Colorado. United States Geological survey, 1999)

A map of Montgomery County in Alabama from 1920 (Figure1-4) was found using the following link:

http://alabamamaps.ua.edu/historicalmaps/counties/montgomery/montgomery.html

Figure 1-4 shows the full map from 1920. Figure 1-5 is a portion of the map from Figure 1-4, and it shows Barnes Slough in section 7 of range 19 E, Township 15 N. A visual comparison can be made between the modern maps (Figure 1-6 and 1-7) and the old map (Figure 1-5) to confirm that the bridge on US Highway 82/231, which is the subject of this project, is the bridge over Barnes Slough reported by the State Highway Commission of Alabama (1916).

Although details of the bridge widening projects are not available, confirmation that the original construction of the bridge was in 1915 narrowed the research focus. Any bridge or found documents from that time frame became a useful reference for understanding the engineers' design process in 1915.

1.3 Project Objectives and Scope

The objective of this research is to provide ALDOT with a structural model of the eleven-span concrete flat slab bridge that can be used for analyses required for issuing permits to non-standard trucks. This objective is being accomplished by this Research Project completing the tasks listed in Table 1-1.

Table 1-1: Tasks of ALDOT Research Project 930-889

Task	Activity
1	Evaluation of Standard Reinforced Concrete Slabs
2	Baseline Structural Model
3	Field Test
4	Advanced Structural Analysis of Baseline Model
5	Final Structural Model
6	Study of ALDOT Permit Process
7	Development of the Final Report

Chapter 2 of this report includes a literature review of the concepts and methods used to design flat slabs in the early 1900s in addition to defining the expected values for parameters such as material properties and resistance. Chapter 3 addresses Task 1 and illustrates applications of these concepts for bridges from the 1920's to calculate the reinforcement required in the slab. Also the concept of bridge rating is introduced. ALDOT uses AASHTOWare software for the purpose of rating (Task 6), of which brief explanation is provided. In Chapter 4 these concepts are applied to estimate the amount of reinforcement needed in Barnes Slough Bridge. This fulfills Task 2 shown in Table 1-1. After the initial calculations and estimating the amount of steel and capacity of the bridge, field tests were carried out as Task 3. These tests included visual inspection, detection of the reinforcement using Proceq's Profometer, Ground Penetrating Radar and core tests. Results of the field measurements were processed and used to establish the material and cross sectional

properties. They also led to development of Advanced Structural Model (Task 4) and are reported in Chapter 4.

Advanced Structural Model was developed using two separate programs – AASHTOWare and ABAQUS, a Finite Element Software. In Chapter 5, a finalized AASHTOWare model of the bridge is presented. This model can be used for issuing permits for non-standard trucks. Results presented in Chapter 5 show ratings for various effective width of the model, ranging from the minimum width, specified in the code, up to a quarter of the total width. To understand the behavior of the structure, and as a second part of Task 3 fulfillment, the nondestructive live load testing was performed on the bridge. Results of these tests and discussion is shown in Chapter 6. Chapter 7 presents the development and calibration of the Finite Element Model. This model was used to determine the actual rating factors for the bridge that were compared with the ratings from AASHTOWare. The results led to the recommendation of the effective width to be used in the ASHTOWare. Chapter 8 provides conclusions and recommendations.

2 Literature Review

2.1 Introduction

The development of a structural model of the Barnes Slough Bridge requires the knowledge of material properties, dimensions, amount of reinforcement, cover thickness and so on. Because the technical documentation is not available, there is a need for understanding how engineers in the early 1900s designed a reinforced concrete slab for bridges. Therefore, the available historical documentation was searched. The obtained information is then verified by field measurements using specialized equipment.

Various sources were studied to confirm a series of methods and material properties that were used from the early 1900s until 1960s to calculate cross sectional capacity of the different segments of the slab. These studies include elastic cross section analysis, material properties, loadings of dead load and live loads and truck load, whether the concept of a multi-presence factor existed, impact, structural analysis methodology (how they loaded the structure to cause the maximum effect on the span), effective width of the slab, and the relationship between the cross-sectional components that resulted in a certain capacity. In Chapter 4, the amount of reinforcement from each time frame is listed to compare these results against the amount of reinforcement measured in field tests to gain an understanding of when these newer portions were added. Lastly, the shear and reinforcement development length requirements for slabs were reviewed to perform these checks for the slab. Below the concepts learned are divided by the year starting with the earliest years followed by the shear and development length requirements. The complete explanation of the process is documented in the early 1900s section, and the following years only explain the methods and concepts for that time frame that were different than the early 1900s.

2.2 Early Concepts

Engineers in early 1900s used an elastic analysis of a cracked section for reinforced concrete. The maximum concrete compression and tension in the reinforcement were limited to allowable values. In this section the relationship between different components of a reinforced concrete cross section and how to calculate the resisting moment according to these components are explained. The following discussion is similar to one presented by Kirkham (1932) and AASHO (1931).

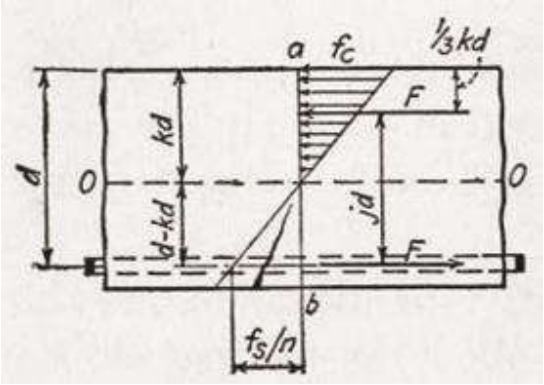

Figure 2-1: Stress Diagram for Reinforced Concrete Beam (Kirkham, 1932)

Figure 2-1 shows a generalized stress diagram of a reinforced concrete beam, in which the concrete below the neutral axis is cracked, and reinforcing bars take all the tension due to cross section bending. The stress diagram is defined in the same figure. The total force in the reinforcement and also for the total force in the concrete, Equation 1 defines the relationship below:

$$F = \frac{M}{jd} \qquad \text{(Eq-1)}$$

where:

F = Resultant compressive force in the concrete and also resultant tension in the reinforcement

M = Represents the bending moment on the beam

jd = Distance from the center of the reinforcement to the resultant compressive force in the concrete

For the total force in the concrete we also have:

$$F = \frac{1}{2}\frac{f_c}{kdb} \qquad \text{(Eq-2)}$$

where:

f_c = Compressive stress on the concrete at the top of the beam for positive moment

kd = Distance from the extreme compression fiber to the neutral axis

b = The width of flexure compression zone

From this last equation we obtain:

$$f_c = \frac{2F}{kdb} \qquad \text{(Eq-3)}$$

or

$$f_c = \frac{2M}{jkbd^2} \qquad \text{(Eq-4)}$$

for the maximum stress in the concrete. All the variables are defined previously.
From similar triangles (shown in Figure 2-1) we have:

$$\frac{f_c}{\frac{f_s}{n}} = \frac{kd}{d - kd} = \frac{k}{1 - k} \quad \text{(Eq-5)}$$

where:

f_s = Tensile stress in the reinforcement

d = Distance from the extreme fiber to the center of the reinforcement

From equilibrium of the resultant compression force and tension force:

$$\frac{1}{2} f_c b k d - n A_s \left(\frac{f_s}{n}\right) = 0 \quad \text{(Eq-6)}$$

Combining Eq-5 and Eq-6 results in:

$$k = \sqrt{2\rho n + (\rho n)^2} - \rho n \quad \text{(Eq-7)}$$

and,

$$\rho = \frac{A_s}{bd} \quad \text{(Eq-8)}$$

where:

n = Ratio of the modulus of elasticity of steel to that of concrete

ρ = Ratio of the area of flexural tension steel to the area of effective cross section

As seen in Figure 2-1, $jd = d - \frac{1}{3}kd$ and by dividing by d, we get:

$$j = 1 - \frac{1}{3}k \quad \text{(Eq-9)}$$

A_s is the area of steel required, calculated using the following equation:

$$A_s = \frac{F}{f_s} \quad \text{(Eq-10)}$$

or

$$A_s = \frac{M}{f_s jd} \quad \text{(Eq-11)}$$

The expectation was that the material strength in early 1900s was lower than the values used today, therefore, there was a need to find common material strengths used in that era. One of these findings was that the engineers of early the 1900s, like today, categorized the material strength depending on the type of the construction. Another finding was that they used allowable stress values for design. Although not one source categorized the material properties of steel and concrete used in design, the allowable stress values for steel and concrete were established through their use in various sources from the early 1900s period. Figure 2-2 and 2-3 show examples of notes found in two different sources. These values are listed in Table 2-1 below: (Hool and Whitney, 1921; S.E. Slocum, 1914)

Table 2-1: List of Material Properties found in various sources

Parameters	Values
Modulus of Elasticity of Steel, E_S (ksi)	30,000
Modulus of Elasticity of Concrete, E_C (ksi)	1200 - 2500
Allowable Steel Tensile Stress, f_s (ksi)	16000
Allowable Concrete Compressive Stress, f_c (ksi)	0.650

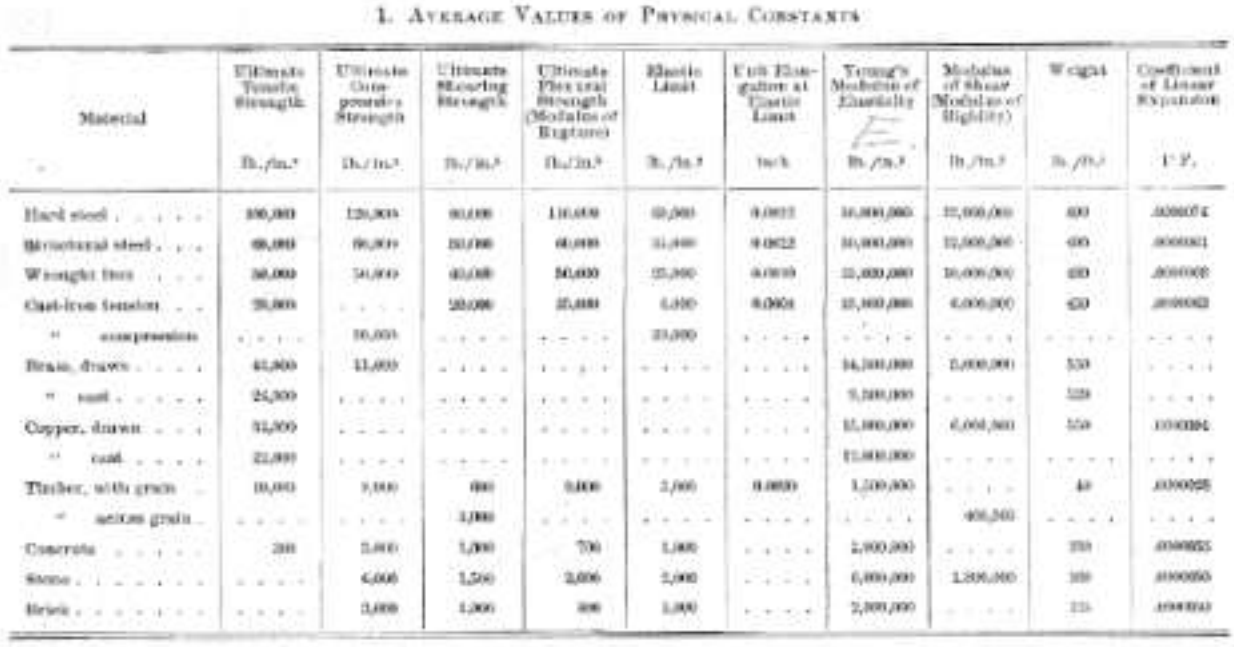

1. Average Values of Physical Constants

Material	Ultimate Tensile Strength lb./in.²	Ultimate Compressive Strength lb./in.²	Ultimate Shearing Strength lb./in.²	Ultimate Flexural Strength (Modulus of Rupture) lb./in.²	Elastic Limit lb./in.²	Unit Elongation at Elastic Limit inch	Young's Modulus of Elasticity lb./in.²	Modulus of Shear (Modulus of Rigidity) lb./in.²	Weight lb./in.³	Coefficient of Linear Expansion 1° F.
Hard steel	100,000	120,000	80,000	110,000	50,000	0.0017	30,000,000	12,000,000	490	.0000074
Structural steel	60,000	60,000	50,000	60,000	30,000	0.0012	30,000,000	12,000,000	490	.0000061
Wrought iron	50,000	50,000	40,000	50,000	25,000	0.0010	25,000,000	10,000,000	480	.0000060
Cast-iron tension	20,000		16,000	35,000	6,000	0.0001	15,000,000	6,000,000	450	.0000062
" compression		80,000			22,000					
Brass, drawn	40,000	15,000					14,500,000	5,000,000	530	
" cast	25,000						9,000,000		520	
Copper, drawn	32,000						15,000,000	6,000,000	550	.0000094
" cast	22,000						12,000,000			
Timber, with grain	10,000	5,000	600	9,000	2,000	0.0020	1,500,000		40	.0000025
" across grain			1,000					600,000		
Concrete	200	2,000	1,000	700	1,000		2,000,000		150	.0000055
Stone		4,000	1,500	2,000	2,000		6,000,000	2,500,000	160	.0000050
Brick		3,000	1,000	400	1,000		2,000,000		125	.0000050

Figure 2-2: The Modulus of Elasticity of Concrete (S.E. Slocum, 1914)

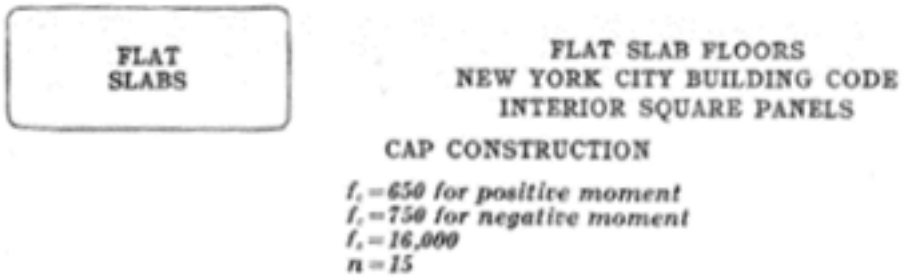

Figure 2-3: Concrete Designer's Manual (Hool and Whitney, 1921)

The modulus of elasticity of concrete was confirmed to be between 1200 ksi and 2500 ksi, and modulus of elasticity of steel was 30,000 ksi. Hence, two common values of 15 and 12 were used as modular ratio, n, which corresponded to higher and lower values of modulus of elasticity. Additionally the use of a modular ratio of 15 was confirmed in a few other sources (Turneaure and Maurer, 1911; Trusted Steel Company, 1910).

The engineers in early 1900s had a very similar understanding of dead load and live load as today. The dead load consists of the weight of the structure, including the floor, floor covering, sidewalks, railings, and any fixed loads due to car tracks, pipe lines, conduits, etc. In a case of concrete slab floors, an allowance was made in the design dead load to provide for the weight of the wearing surface. This allowance depended on the type of wearing surface, and it was considered less than 15 pounds per square foot of roadway. The weight of the pavement if not wood plank, was 150 pounds per cubic foot. The maximum live load depended upon the locality of the structure. The live load varied from interurban cars, streets cars, heavy trucks, and dense crowds of people in near cities and towns, to light trucks, slow-moving traction engines (Figure 2-4), and droves of livestock in outlying country districts.

As for highway live loads, the standard truck shown in Figure 2-4 can be considered as the unit of loading. These trucks are known as H20, H15, and H10. The numerals following the "H" in each case indicate the weight of the truck in tons. Figure 2-3 shows the spacing of axles and tires for a truck. In addition to truck loading, equivalent loading was used, which is also known as lane-loading. Equivalent loading consists of uniform load per linear foot of traffic lane combined with a single concentrated load so placed on the span as to produce maximum load effect. According to AASHO (1931) the equivalent loading was not used for spans less than 60 ft. Figure 2-5 shows the distribution of truck weight over four wheels, the axle spacing, and the lateral position of a truck on a roadway lane. Figure 2-7 shows the equivalent loading configurations.

Figure 2-4: Traction Engine from Early 1900s (http://www.cheffins.co.uk/assets/news/358_2-m.jpg)

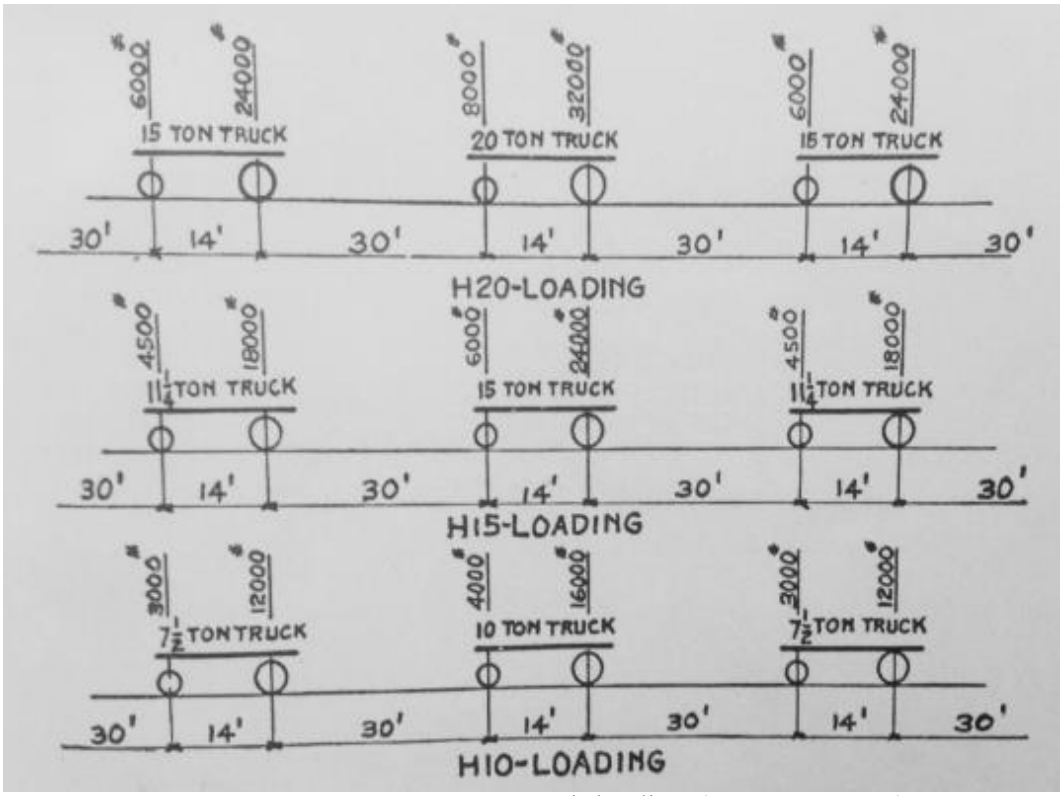

Figure 2-5: H20, H15, H10 Truck loading (AASHO, 1931)

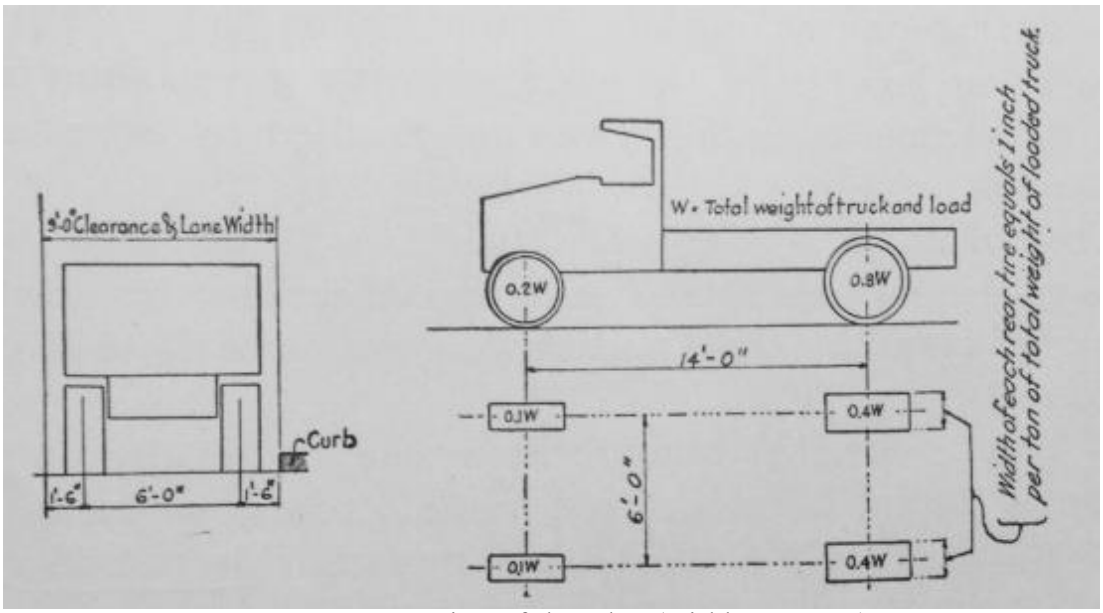

Figure 2-6: Spacing of the axles (Kirkham, 1932)

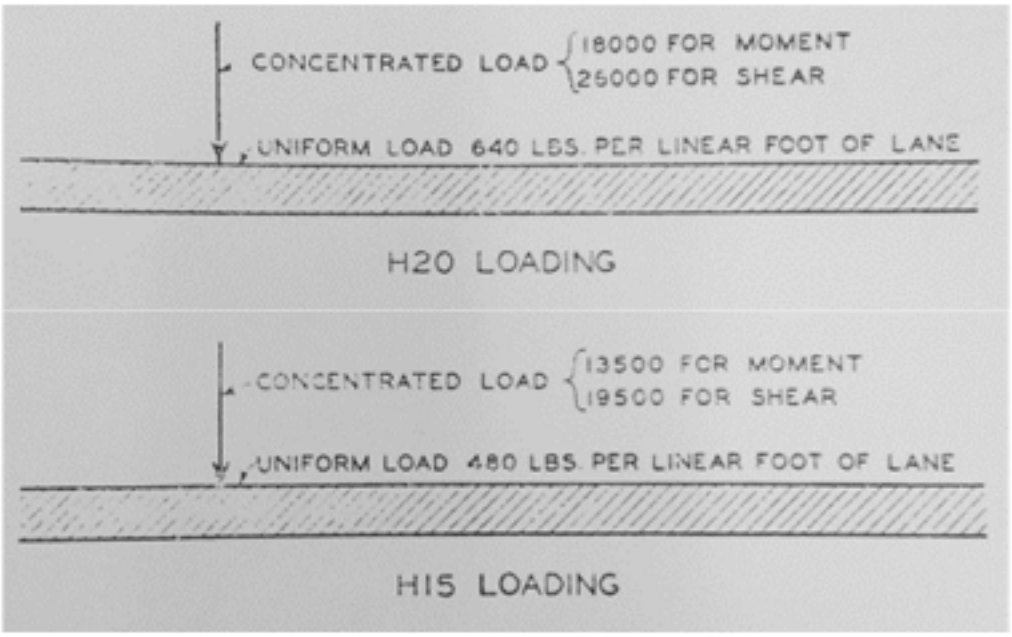

Figure 2-7: Equivalent Loading Configuration (Kirkham, 1932)

The relationship below gives the value for coefficient of impact, C_I, which would apply to live load from AASHO (1931).

$$C_I = \frac{50}{L + 125} \qquad \text{(Eq-12)}$$

where:

L = Length in ft of the portion of the span loaded to produce maximum live load effect in the member considered. (Kirkham, 1932)

According to AASHO (1931), if the loaded width of the roadway exceeded two lanes, width of 18 ft, the specified loads were reduced one percent for each foot of loaded roadway width in excess of 18 ft with a maximum reduction of 25 percent, corresponding to a loaded roadway width of 43 ft. When the loads were lane loads, the loaded width of the roadway was the aggregate width of the lanes considered; if the load lane were distributed over the entire width of the roadway, the loaded width of the roadway was the full width of roadway between curbs.

The number of traffic lanes was an important unknown since it impacted the effective width used in designing the slab. This number was decided based on the American Highway Engineers Handbook (Blanchard, 1919) to be two lanes. Equation 13 was used to define the number of traffic lanes.

$$Y = \frac{\mathrm{x}}{6} + 16 \geq 12 \text{ feet} \qquad \text{(Eq-13)}$$

where:

Y = roadway width in feet

X = number of vehicles traveling simultaneously

Also AASHO (1931) recommended a width of 10 ft for a lane of traffic and in case of a 16 ft roadway, the roadway would be designed for two traffic lanes. In cases where the roadway width was less than the desired 18 ft, and more than the minimum width of 16 ft, the effective width was calculated using the concept of overlap. The concept of overlap is explained in Section 2.2.7.

In 1931 the concept of effective slab width was used to calculate the required resistance for which the bridge should be designed. For roadways with two traffic lanes, the roadway had two zones. The inner zone, which carried a maximum moment due to the two trucks' wheels passing each other at the middle of the road, and outer zones that were designed to carry the lesser amount of live load moment due to one truck's wheel line. The method of calculating the effective widths were confirmed to be the same in two sources (Kirkham, 1932; AASHO, 1931).

In calculating bending moment due to wheel loads on concrete slabs, no distribution in the direction of the span of the slab was assumed. In the direction perpendicular to span of the slab, the wheel load was considered as distributed uniformly over an effective width of slab. This effective width was obtained from the following formula:

$$E_O = 0.7S + W \leq 7 \text{ feet} \qquad \text{(Eq-14)}$$

where:

$E_{I \text{ or } O}$ = Effective width in ft for one wheel in the inner zone or the outer zone as defined in the subscript.

S = Length in ft of the portion of the span loaded to produce maximum live load effect in the member considered

W = Width of the wheel or tire in ft

For cases when two wheels are located on a transverse element of the slab and when the roadway width is less than the recommended width of 18 ft, the concept of overlapped effective width was considered. The overlap meant that there was missing width in the middle of the roadway due to lane widths less than the recommended length; thus the effective width was overlapped. Equation 15 below shows how the effective width is calculated in a case of an overlap:

$$E_I = \frac{1}{2}\left(E_O + C_r\right) \qquad \text{(Eq-15)}$$

where:

C_r = The distance between centers of wheels of two adjacent trucks

1935 Design Methods

According to AASHO (1935) all of the concepts explained in section 2.1 applied to this era. Allowable stress design was the method of design; however, the loading used for design and the effective width formula was defined differently. Below these concepts are explained.

In 1935, different loadings applied to different classes of bridges. For any given class, the loading was applied to produce the maximum effect on the member considered. The loadings for class AA and class A were H20 and H15 respectively. The truck loading was used for spans less than 60 ft (Figure 2-4), and truck lane loadings were used for spans greater than 60 ft (Figure 2-6).

In 1935, the effective width formula was defined using the equation below:

$$E = 0.6\,S + 2W \qquad \text{(Eq-16)}$$

where:

E = effective width of slab in ft for one wheel Load.
S = length in ft of the portion of the span loaded to produce maximum live load effect in the member considered
W = width of the tire with a maximum value if 1.25 ft.

1936 Design Methods

All concepts defined in Section 2.2 applied to this era with the exceptions discussed below related to impact and loading in combination with effective widths as defined by GA DOT (1936).

The impact coefficient was defined in the *Standard Specification for Construction of Roads and Bridges for Georgia State Highway Department* (1936). The main formula was the same as the one in Equation 12; however, it had an exception for spans less than 45 ft. For such small spans, the impact coefficient was 0.3. (GA DOT, 1936)

An alternative method was described by GA DOT (1936). This method was for a case of a single load at the center of the span. Equation 17 was used to define the effective width for the outer zone:

$$E_O = 0.6S + 2W \qquad \text{(Eq-17)}$$

where:

$E_{I\text{ or }O}$ = Effective width in ft for one wheel in the inner zone or the outer zone as defined in the subscript.
S = Center to center span of slab in ft
W = Width of tire with a maximum value of 1.25 ft.

And in case of loadings on parallel elements of a slab, the maximum bending moment shall be calculated as shown in Section 2.2 and increased by the following percentage shown below:

$$\frac{B}{S} = 0 \;\; 100\,\% \qquad \text{(Eq-18-1)}$$

$$\frac{B}{S} = 0.1 \quad 60\ \% \qquad \text{(Eq-18-2)}$$

$$\frac{B}{S} = 0.4 \quad 30\ \% \qquad \text{(Eq-18-3)}$$

$$\frac{B}{S} = 1.0 \quad 10\ \% \qquad \text{(Eq-18-4)}$$

$$\frac{B}{S} = 1.4 \quad 0\ \% \qquad \text{(Eq-18-5)}$$

where:

B = Distance between the parallel loaded elements

In cases the ratio of B/S is in between the above values, intermediate values of B/S were obtained by interpolating the values above.

GA DOT (1936) defined the inner zone width as shown below:

$$E_I = \frac{1}{2}\left(E_O + C_r\right) \qquad \text{(Eq-19)}$$

where:

C_r = Distance between the center of exterior wheels of two adjacent trucks. This value was defined as 3 feet.

The design methodology used in 1937 was the allowable stress design. There was no different concept reported from this time. However, a document from this year by Hool (1937) showed that in the early 1900s the engineers believed that because the modulus of elasticity of a material is the ratio of stress to deformation, it followed that, for equal deformations, the stresses in the steel and concrete were as their moduli of elasticity, thus:

$$\frac{f_s}{f_c} = \frac{E_s}{E_C} = n \qquad \text{(Eq-20)}$$

And,

$$f_s = nf_c \qquad \text{(Eq-21)}$$

1941 Design Methods

The general method of design was still allowable stress design at this time. Some of the differences from the concepts introduced in the early 1900s were the steel allowable stress, the loadings, and the effective width. Below these concepts are explained.

The allowable steel stress changed from 16,000 psi to 18,000 psi in tension for flexural members. (AASHO, 1941)

In computing the maximum load effect due to either truck loading or lane loading, each 10 foot traffic lane or a single standard truck was considered as a unit. The loading configuration was so that it would produce the maximum load effect on a member. H-S lane-loading was used for spans

larger than 40 ft and H-S truck loading was considered for spans less than 40 ft. For H loading, either lane-loading or truck loading was used for design depending on which one caused the maximum effect. The lane-loading and truck loading configurations are shown in Figures 2-8, 2-9, 2-10, and 2-11.

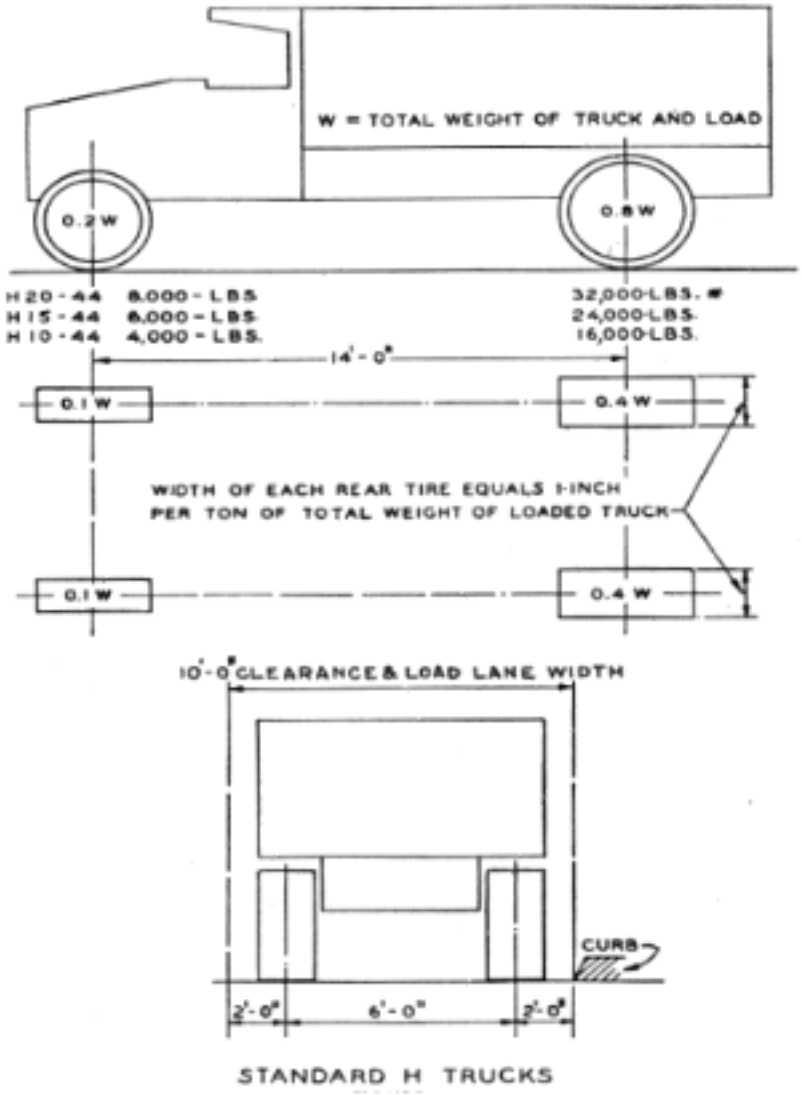

Figure 2-8: Standard H Truck Loading Configuration (Kirkham, 1932)

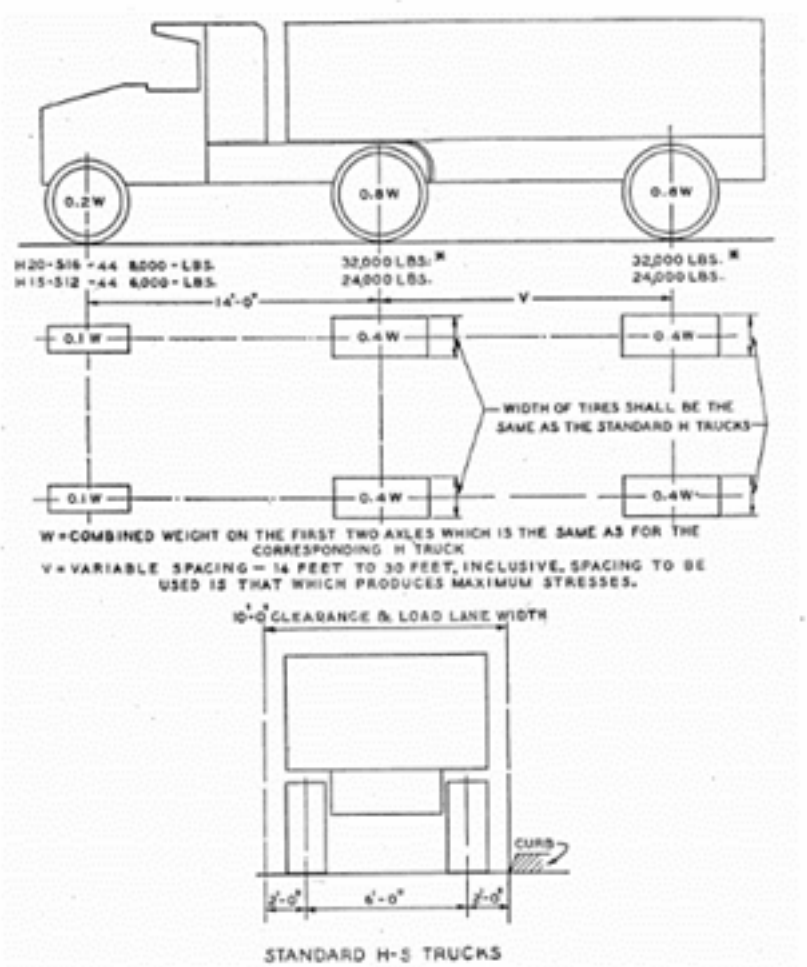

Figure 2-9: Standard H-S Truck Loading Configuration (Kirkham, 1932)

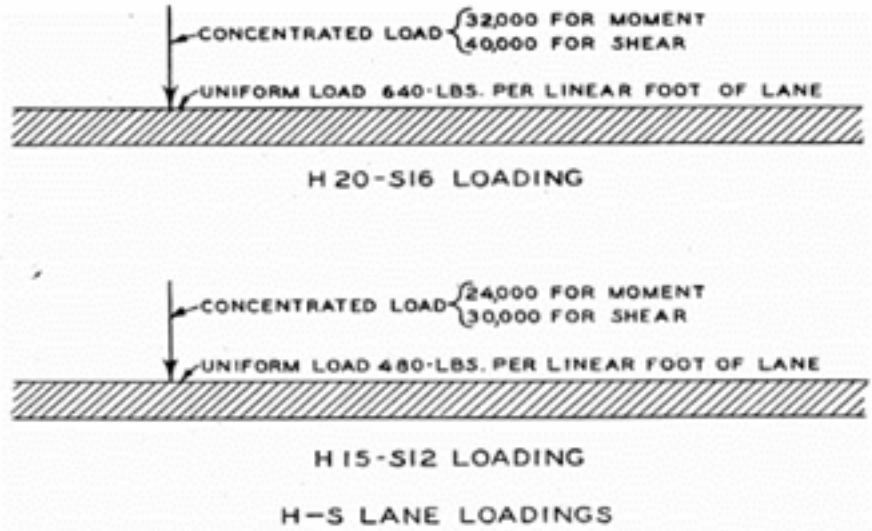

Figure 2-10: Standard H-S Lane-loading Configuration (Kirkham, 1932)

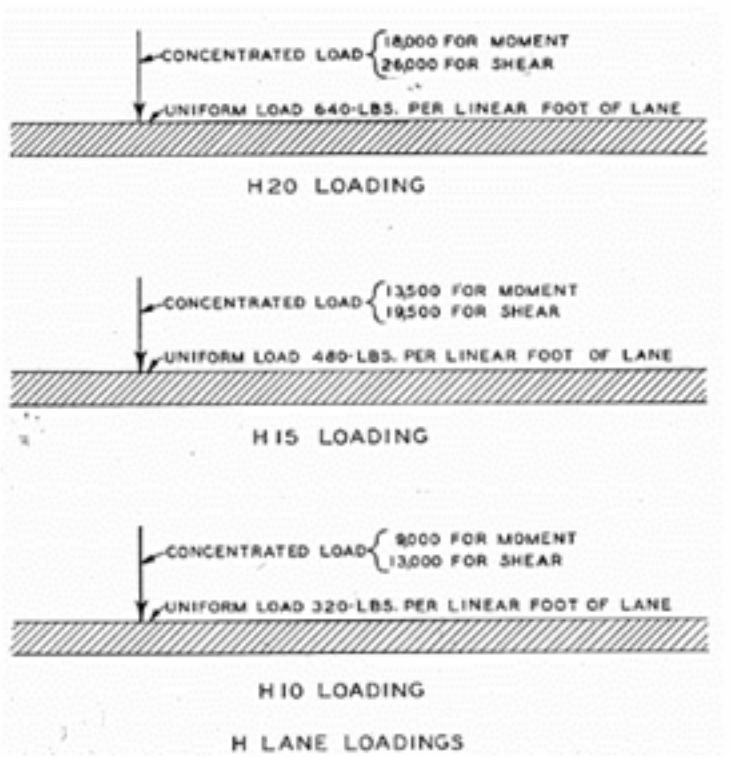

Figure 2-11: Standard H Lane-loading Configuration (Kirkham, 1932)

The maximum load effects were produced in any member by loading any number of traffic lanes simultaneously, the following percentages (Table 2-2) of the resultant live load was used in lieu of improbable coincident maximum loadings.

Table 2-2: Reduction in Load Intensity that Corresponds to the Number of Traffic Lanes

Number of Lanes	Percentage
One or two lanes	100
Three lanes	90
Four lanes or more	75

According to AASHO (1941) for H loading and spans over 12 ft the effective width for reinforcement parallel to traffic was calculated using two cases (a) and (b) below; whichever provided the more conservative results was applied in design. Below these formulas are explained:

(a) Wheel Load

$$E = \frac{10N + W_r}{4N} \qquad \text{(Eq-22)}$$

(b) Lane-loading

$$\text{Moment due to Uniform Load} = \frac{NQ}{0.5W + 5N} \text{ per square foot slab} \qquad \text{(Eq-23)}$$

$$\text{Moment due to Concentrated load} = \frac{NP'}{0.5W_r + 5N} \text{ per foot width of slab} \qquad \text{(Eq-24)}$$

where:

E = Width of slab over which a wheel load is distributed
N = Maximum number of lanes of traffic permissible on bridge
W_r = Width of roadway between curbs on bridge
Q = Uniform lane load per linear foot of lane
W = Width of graded roadway across culverts
S = For simple spans the span length shall be the distance center to center of supports but not to exceed clear span plus thickness of slab.
P = Load on one wheel
P' = Concentrated lane load per lane

In Case b, the values obtained from uniform load and concentrated load were added, and the final value would be the total live load moment in kips per foot of width. For main reinforcement parallel to traffic designed for H-S loading, for spans more than 12 ft and up to and including 40 ft truck loading was used. Lane-loading was used for lengths over 40 ft.

1949 Design Methods

In this era, the allowable stress design method was used to design a reinforced concrete slab. The differences in defining some of the concepts between early 1900s and 1949 were in the material properties, loadings, and effective width calculations. Below these concepts are reviewed.

In this era, the reinforcing steel had the same properties as that specified in 1941. The value of allowable steel tensile stress was 18,000 psi. (AASHO 1949) Also by this time the modular ratio was calculated independent of deformations using only the following relationship (Jensen, 1943):

$$n = \frac{E_S}{E_C} \qquad \text{(Eq-25)}$$

In 1960, Pauw (1960) also used this relationship in his article: S*tatic modulus of elasticity of concrete as affected by density.*

According to AASHO (1949) the type of loading used for design was the kind that causes the maximum load effect on the member considered, whether it was for continuous spans or simple spans. At this time there were no restrictions due to the length of the spans directly. Figure 2-12 shows the H and HS lane-loading configuration which were different than the previous years.

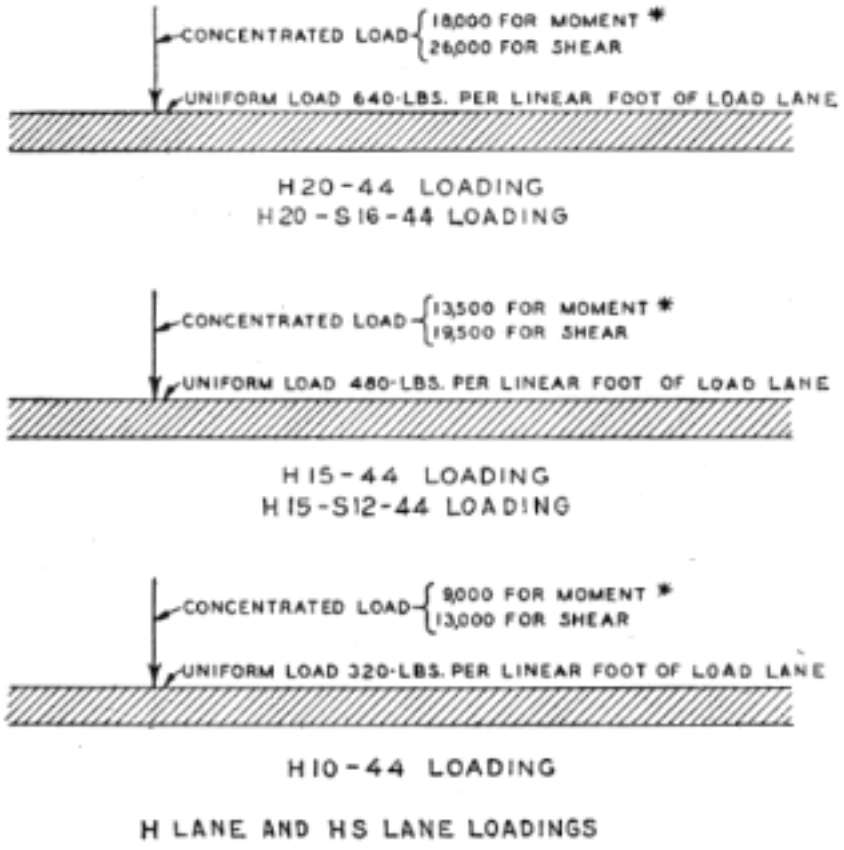

Figure 2-12: H and HS Lane-loading Configuration (AASHO, 1949)

In 1949, the load intensity reduction followed the same concepts developed in 1941.

The criterion in defining the number of traffic lanes was different. The lane-loading or standard truck was assumed to occupy a width of 10 ft. These loads were placed in design traffic lanes having a width of:

$$W_n = \frac{W_c}{N} \qquad \text{(Eq-26)}$$

where:

W_n = Width of design traffic lane
W_c = Roadway width between curbs exclusive of median strip
N = number of design traffic lanes as shown in the following table

Table 2-3 shows the number traffic lanes for increasing increments of roadway width.

Table 2-3: Number of Traffic Lanes for Different Roadway Widths

W_c (ft)	No. of Design Lanes
20 to 30 inc.	2
Over 30 to 42 inc.	3
Over 42 to 54 inc.	4
Over 54 to 66 inc.	5
Over 66 to 78 inc.	6
Over 78 to 90 inc.	7
Over 90 to 102 inc.	8
Over 102 to 114 inc.	9
Over 114 to 126 inc.	10

The effective width defined at this time was different than how engineers defined in early 1900s. According to AASHO (1949) the effective width was the same as that defined in 1941 in Section 2.4.3.

1957 Design Methods

In 1957 allowable stress design was used for design, and the all the concepts used in defining the cross section capacity were the same as in the early 1900s. However, the material properties, loadings, load intensity reduction, number of traffic lanes, and effective width were defined differently.

The allowable tensile stress value for steel at this time was considered to be 18,000 psi. (AASHO, 1957)

The loading configurations defined in AASHO (1957) were the same as those previously described in AASHO (1949). At this time there were also a series of tables used to define maximum moment and shear values for simple spans varying from 1 ft to 300 ft.

In 1957, the load intensity reduction followed the same concepts used in 1941. (AASHO, 1957)

The criterion for defining the number of traffic lanes was different than how it was defined in early 1900s. The concepts explained from 1949 are the basis for defining the number of traffic lane in 1957. (AASHO, 1957)

The effective width in 1957 was defined similarly to the effective width defined by AASHO in 1941.

1961 Design Methods

The design method considered at this time was also allowable stress design. Similarly to other time frames, some parameters were defined differently than the early 1900s. Of these different parameters are allowable steel stress, loadings, number of traffic lanes, and effective width. These concepts are explained below.

In this era, the reinforcing steel had the same properties as that specified in 1941. The value of allowable tensile stress was 18,000 psi. (AASHO, 1961)

The loadings at this time were the same as those used in 1949. (AASHO, 1961)

The number of traffic lanes on a roadway were defined the same as in 1949. (AASHO, 1961)

The effective was defined differently during this time. The formula used for effective width is the same as what is used in AASHTO (17th ed., 2002). The effective slab width is a width which carries one wheel-line of loading. The formula to define the effective width is presented below.

$$E = 4 + 0.06S \leq 7 \text{ feet} \qquad \text{(Eq-27)}$$

where:

E = Effective width with a maximum value of 7 ft. Lane loads are distributed over a width of 2E.

S = For simple spans the span length shall be the distance center to center of supports but not to exceed clear span plus thickness of slab.

For simple spans, the maximum live load moment per foot of width of slab, without impact, is closely approximated for two cases of H20 and H15 by the following formulas:

a) H20-S16 Loading:

For spans up to and including 50 ft:

$$\text{LLM} = 900\text{S (foot-pound)} \qquad \text{(Eq-28)}$$

For spans 50 ft to 100 ft:

$$\text{LLM} = 1000(1.30\ \text{S} - 20)\ \text{(foot-pound)} \qquad \text{(Eq-29)}$$

b) H15-S12 Loading:

Use ¾ of the values obtained from the Eq-28 and Eq-29 for H20-S16 loading.

$$LLM = 0.75(900\ S) \qquad \text{(Eq-30)}$$

Moment in continuous spans was obtained by suitable analysis using the truck or appropriate lane-loading.

2.3 Current Design and Analysis Methods

AASHTO 17th Ed. Method

Today the resistance of reinforced concrete slabs is calculated using ultimate strength design principles. The maximum moment due to live load for the load factor rating (LFR) method is calculated according to the AASHTO (17th ed., 2002). AASHTO (17th ed., 2002) follows the process used since 1961 to calculate moment and the effective width as described by Equations 27 through Equation 30.

AASHTO LRFD Method

One last check was to consider the LRFD method in AASHTO (LRFD, 2014) and compare the results with other methods in an aim for better understanding of how the engineers in early 1900s calculated the capacity of a slab. AASHTO (LRFD, 2014) is based on limit state design philosophy. Only the calculation of effective width in accordance to AASHTO (LRFD, 2014) was of an interest in this research since the other concepts such as loading criterion do not apply to the older methods reviewed so far. Below the concept of effective width is explained.

$$E_{I-1} = 84.0 + 1.44\sqrt{L_1 W_1} \leq E_{I-2}\ \frac{12.0\,W}{N} \qquad \text{(Eq-31)}$$

where:

W_1 = Modified edge to edge W equal or lesser than 60 ft for multiple lane, and 30 ft for one lane

W_p = Physical edge to edge W of bridge in feet

N = Number of design lanes as specified in Article 3.6.1.1.1. in AASHTO(LRFD, 2014)

L_{max} = 60 ft

All values in inches.

3 Bridge Design from 1920s and the Modern Rating Process

3.1 Introduction

In this chapter, the studies of bridges from the 1920s are presented as case studies. Design methods from 1910 until 1930 are referred to in report as the contemporary design, as these design concepts did not belong to one year or decade, and they are from the time period of the original design of the Barnes Slough Bridge. One case study is of standard simple span flat slab bridges from 1922. The geometry and reinforcement in the slabs is documented in a series of drawings provided by ALDOT. The other case study is a two-span continuous bridge from 1924 for which there are drawings. These case studies provided great examples of the outcome of the engineers' design in that era. After discussing these cases, the principles of modern rating of these structures are introduced using AASHTO LFR in addition to presenting the AASHTOWare software. This software is currently used by departments of transportation throughout the nation to rate bridges.

3.2 1922 Simple Span Bridges

A standard drawing provided by SHDA (1922) has tabulated values for the amount of reinforcement in simply supported spans with span lengths varying from 6 ft to 20 ft in 2 ft increments, and roadways widths of 16 ft, 18 ft, and 20 ft. The title block and the general notes from this drawing are shown in Figures 3-1 and 3-5 and Tables 3-1 through 3-2. With the information that was provided in the drawings the research focused on understanding how the amount of reinforcement required in the slab was calculated.


General Note:
Concrete is Class A 1-2-4 mix.
Reinforcing steel to be deformed and of structural grade
All exposed corners to be chamfered
one inch unless otherwise noted
Dimensions referring to reinforcement
are to centers of bars
Specifications: State Highway Department
Live Load: 15 Ton Typical Trucks, 30% Impact
Dead Load: 80 Lbs per sq ft of roadway.
Rub surface free from form marks to a smooth
and uniform finish. No plastering allowed

State Highway Department of Alabama
Office of Engineer, Montgomery, Ala.

STANDARD
REINFORCED CONCRETE
SLABS

Bridge Engineer

51

Figure 3-1: Title Block and General Notes for Standard Drawings of Simple Span Bridges (SHDA, 1922)

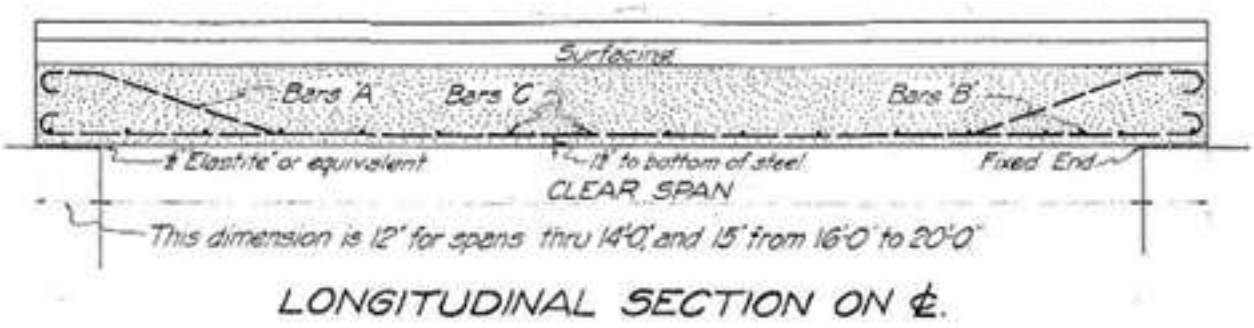

Figure 3-2: Details of Bars A, B, and C Configuration in a Section Cut for SHDA (1922)

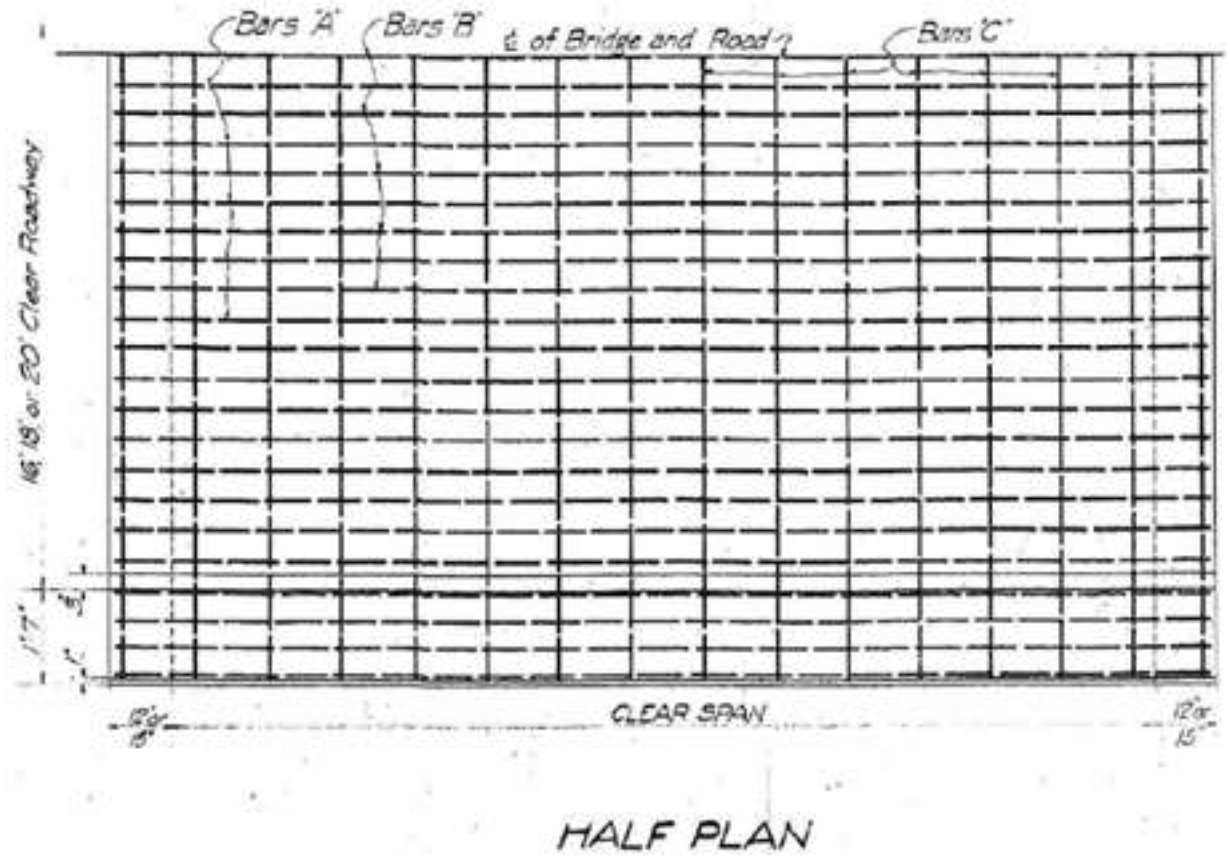

Figure 3-3: Bars A, B, and C Configuration in a Plan View for SHDA (1922)

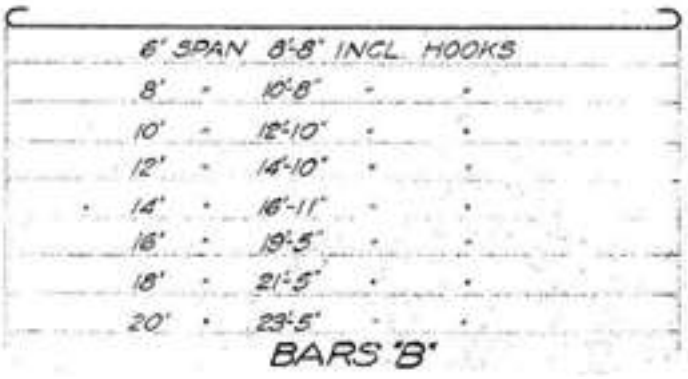

Figure 3-4: Bars "B" Dimension for Different Span Lengths for SHDA (1922)

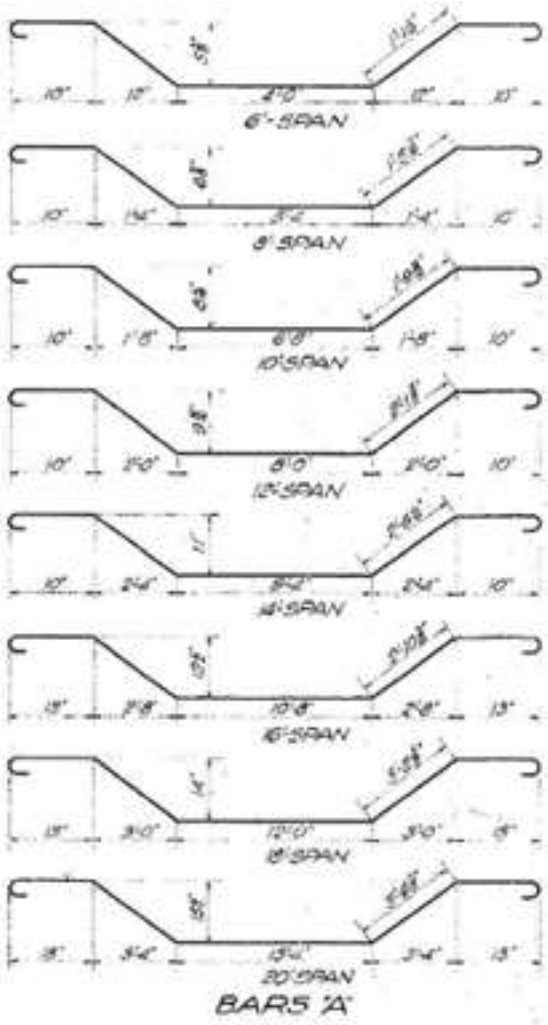

Figure 3-5: Bars "A" Dimensions for Different Span Length for SHDA (1922)

Table 3-1: 1922 Standards for Size and Spacing of the Bars for Different Lengths of Spans (SHDA, 1922)

DESIGN DATA						
CLEAR SPAN	DIMENSIONS		BARS "A" & "B"		BARS "C"	
	"H" DEPTH OF SLAB	TO C.G. OF STEEL	SIZE	C. TO C.	SIZE	C. TO C.
6	8⅝"	7⅜"	¾"ϕ	7"	½"□	18"
8	10⅝"	9⅜"	¾"ϕ	6"	½"□	18"
10	11⅞"	10⅝"	⅞"ϕ	7"	½"□	18"
12	12⅝"	12"	⅞"ϕ	6"	½"□	18"
14	14⅜"	13⅛"	1"ϕ	7½"	½"□	18"
16	16"	15"	1"ϕ	6½"	½"□	18"
18	17⅝"	16⅝"	1"ϕ	6"	½"□	18"
20	19"	18"	1"ϕ	5½"	½"□	18"

Table 3-2: Number of Bars, Length, and Types of Bars for Different Lengths and Roadway Widths for SHDA (1922)

STEEL ESTIMATE, I-SLAB									
CLEAR SPAN	16'-ROADWAY			18'-ROADWAY			20'-ROADWAY		
	BARS	LENGTH	NO. REQUIRED	BARS	LENGTH	NO. REQUIRED	BARS	LENGTH	NO. REQUIRED
6	A	8'-10"	16	A	8'-10"	18	A	8'-10"	20
	B	8'-8"	17	B	8'-8"	19	B	8'-8"	21
	C	18'-9"	6	C	20'-9"	6	C	22'-9"	6
8	A	10'-10"	19	A	10'-10"	21	A	10'-10"	23
	B	10'-8"	20	B	10'-8"	22	B	10'-8"	24
	C	18'-9"	8	C	20'-9"	8	C	22'-9"	9
10	A	13'-3"	16	A	13'-3"	18	A	13'-3"	20
	B	12'-10"	17	B	12'-10"	19	B	12'-10"	21
	C	18'-9"	9	C	20'-9"	9	C	22'-9"	9
12	A	15'-3"	19	A	15'-3"	21	A	15'-3"	23
	B	14'-10"	20	B	14'-10"	22	B	14'-10"	24
	C	18'-9"	10	C	20'-9"	10	C	22'-9"	10
14	A	18'-5"	15	A	18'-5"	17	A	18'-5"	19
	B	16'-11"	16	B	16'-11"	18	B	16'-11"	20
	C	18'-9"	12	C	20'-9"	12	C	22'-9"	12
16	A	20'-5"	17	A	20'-5"	19	A	20'-5"	21
	B	19'-5"	18	B	19'-5"	20	B	19'-5"	22
	C	18'-9"	13	C	20'-9"	13	C	22'-9"	13
18	A	22'-2"	19	A	22'-2"	21	A	22'-2"	23
	B	21'-5"	20	B	21'-5"	22	B	21'-5"	24
	C	18'-9"	15	C	20'-9"	15	C	22'-9"	15
20	A	24'-3"	20	A	24'-3"	22	A	24'-3"	24
	B	23'-5"	21	B	23'-5"	23	B	23'-5"	25
	C	18'-9"	16	C	20'-9"	16	C	22'-9"	16

3.2.1 Area of Tension Reinforcement Required

By applying the concepts that were introduced in Chapter 2 the required amount of reinforcement was calculated. The parameters used here to calculate the amount of reinforcement required are listed in Table 3-3. Figure 3-6 shows the design truck configuration on the span. The methods used to calculate the amount of reinforcement in the slab were based on the earliest methods learned from the contemporary time. These methods were defined by AASHO (1931) and Kirkham (1932). According to Kirkham (1932), although the calculations were done both for the inner zone and the outer zones, in practice the one that controlled the design was applied across the whole cross section. The uniform distribution of the reinforcement in the slab (Figure 3-3) confirmed that this concept was applied. The concept of inner zone explained by Kikham (1932) is the same as effective width used by other sources. In all cases the amount of reinforcement calculated for the inner zone controlled the design. For example calculations, refer to Garmestani, (2016).

Table 3-3: Summary of Parameters Used for the Analysis of 1922 Standard Simple Spans

Parameters	Value
Allowable Concrete Compressive Stress, fc	650 psi
Allowable Steel Tensile Stress, fs	16,000 psi
Modular Ratio	15
Reinforced Concrete Unit Weight	150 pcf
Live Load	H 15 Truck
Impact Allowance (Contemporary)	30%
Impact Allowance (OFOR Loading)	30%
Superimposed Dead Load (Contemporary)	80 psf
Superimposed Dead Load (OFOR Loading)	80 psf
Slab Thickness, H	19 in.
Depth to Tension Reinforcement, d	18 in.
Effective Width of Slab (Contemporary)	5 ft
Effective Width of Slab (OFOR Loading)	4 ft
Span Length – Clear Span Length	20 ft

In addition to studying the contemporary methods to calculate the amount of reinforcement in the slab, another method of loading was considered. This different loading was used to evaluate the effect of roadway width on the design. In this method the roadway was loaded by two trucks, 4 wheel-lines, and this load effect plus impact was divided by the roadway width to calculate the moment per foot of width. In this configuration the effective width is one-fourth of the roadway. This configuration is referred to as OFOR (One-fourth of the Roadway). Below the results for both methods are presented in Table 3-4.

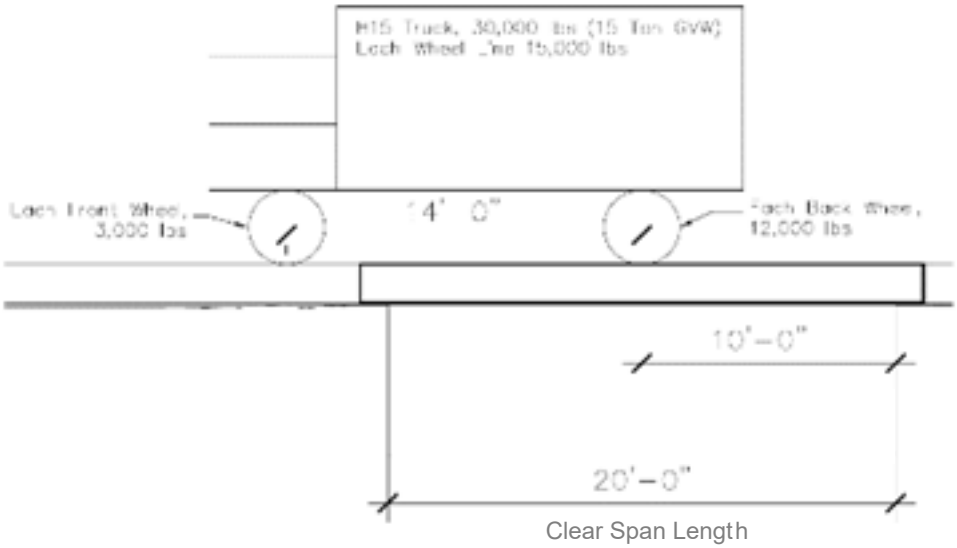

Figure 3-6: Diagram of 20-ft Simply Supported Span with One Wheel-Line of an H15 Truck Positioned To Cause Maximum Moment

Table 3-4: Required Area of Steel for 1922 Simple Spans (in^2/ft of Width)

Clear Span	Method	Roadway Width		
		16 ft	18 ft	20 ft
6 ft	Table 3-2	0.757	0.769	0.779
	Contemporary	0.707	0.707	0.707
	OFOR	0.742	0.669	0.612
8 ft	Table 3-2	0.895	0.894	0.893
	Contemporary	0.741	0.741	0.741
	OFOR	0.877	0.798	0.732
10 ft	Table 3-2	1.03	1.05	1.06
	Contemporary	0.865	0.865	0.87
	OFOR	1.025	0.936	0.87
12 ft	Table 3-2	1.22	1.22	1.22
	Contemporary	0.981	0.981	0.98
	OFOR	1.15	1.06	0.98
14 ft	Table 3-2	1.28	1.31	1.33
	Contemporary	1.10	1.10	1.10
	OFOR	1.27	1.18	1.10
16 ft	Table 3-2	1.44	1.46	1.47
	Contemporary	1.23	1.23	1.23
	OFOR	1.41	1.31	1.23
18 ft	Table 3-2	1.61	1.61	1.60
	Contemporary	1.36	1.36	1.36
	OFOR	1.54	1.44	1.36
20 ft	Table 3-2	1.69	1.68	1.67
	Contemporary	1.5	1.5	1.50
	OFOR	1.69	1.58	1.50

A comparison made between the results from these two methods and the tabulated values from SHDA (1922) showed that the studies generated results that were similar to the amount of reinforcement listed in the drawings, but the results from these three methods did not follow the same pattern. These patterns increased and decreased differently for different span lengths and roadway widths. Only the results for a case of 20-ft span and 16-ft roadway width matched SHDA (1922). These replicas suggested that our understanding of dead load and live load were sufficient; however, the process which was used to identify the effective width remained unknown.

To isolate the value that was used as the effective width by the contemporary design, firstly, a series of fixed values were considered as effective width such as 3 ft, 4 ft, and 5 ft to calculate the amount of reinforcement in the slab. Secondly, another method by Georgia State Highway Department (Georgia State Highway Department - *Standard Specification for Construction of Roads and Bridges*, 1936) was used to define effective width in combination with additional loading due to parallel loadings on the same element. Equations 17, 18-2, and 18-3 were used by GA DOT to identify the effective width and loading while the rest of the process is the same as contemporary method. However, these results did not follow the same pattern for all span lengths and roadway widths, and the three methods of Contemporary, OFOR loading, and GA DOT did not uncover how the engineers calculated the effective width.

3.2.2 Identification of Effective Width

The effective slab width is defined in AASHTO (17th ed., 2002) as the width of slab that resists one wheel-line of loading. Applying this definition, it is possible to use the amounts of reinforcement listed in Table 3-1 to back-calculate the effective width used by the original designers of the 1922 simple spans.

Using the definition above, the applied live load moment with impact per foot of width is equal to

$$\frac{M_{l+I}}{E} \qquad \text{(Eq-32)}$$

where:

M_{L+I} = Live load moment due to one wheel-line of truck loading plus impact
E = Effective width in ft

Assuming moment resistance per foot of width, M, is equal to the applied live load with impact plus the dead load per foot of width results in:

$$M = \frac{M_{L+I}}{E} + M_D \qquad \text{(Eq-33)}$$

where:

M_D = Dead load moment

By rearranging:

$$E = \frac{M_{L+I}}{M - M_D} \qquad \text{(Eq-34)}$$

Values of effective width were calculated for each combination of span length and roadway width listed in Table 3-2. The moment resistance was calculated using an elastic analysis of a cracked section with the parameters listed in Table 3-3. The live loading included truck loading plus impact, and the dead load included the weight of the slab plus superimposed dead load as described in Table 3-3.

The results of the effective width calculations are listed in Tables 3-5 through 3-7 and plotted in Figure 3-7. The values back-calculated using Equation 34 are shown under the heading "1922". Results are also shown for three other methods: AASHTO (17th ed., 2002), LRFD method, and GA DOT (1936).

Table 3-5: Effective Width Values for a 16-ft Roadway

Span Length (ft)	Effective Width for 16 ft Roadway (ft)			
	1922	GA DOT	AASHTO LRFD	AASHTO 17th ed.
6	4.17	4.82	4.09	4.36
8	4.13	5.28	4.18	4.48
10	4.30	5.00	4.26	4.60
12	4.20	4.83	4.33	4.72
14	4.14	4.71	4.40	4.84
16	4.10	4.63	4.46	4.96
18	4.09	4.57	4.52	5.08
20	4.11	4.52	4.57	5.20

Table 3-6: Effective Width Values for a 18-ft Roadway

Span Length (ft)	Effective Width for 18 ft Roadway (ft)			
	1922	GA DOT	AASHTO LRFD	AASHTO 17th ed.
6	4.17	4.82	4.09	4.36
8	4.13	5.28	4.18	4.48
10	4.30	5.00	4.26	4.60
12	4.20	4.83	4.33	4.72
14	4.14	4.71	4.40	4.84
16	4.10	4.63	4.46	4.96
18	4.09	4.57	4.52	5.08
20	4.11	4.52	4.57	5.20

Table 3-7: Effective Width Values for a 20-ft Roadway

Span Length (ft)	Effective Width for 20 ft Roadway (ft)			
	1922	GA DOT	AASHTO LRFD	AASHTO 17th ed.
6	4.17	4.82	4.09	4.36
8	4.13	5.28	4.18	4.48
10	4.30	5.00	4.26	4.60
12	4.20	4.83	4.33	4.72
14	4.14	4.71	4.40	4.84
16	4.10	4.63	4.46	4.96
18	4.09	4.57	4.52	5.08
20	4.11	4.52	4.57	5.20

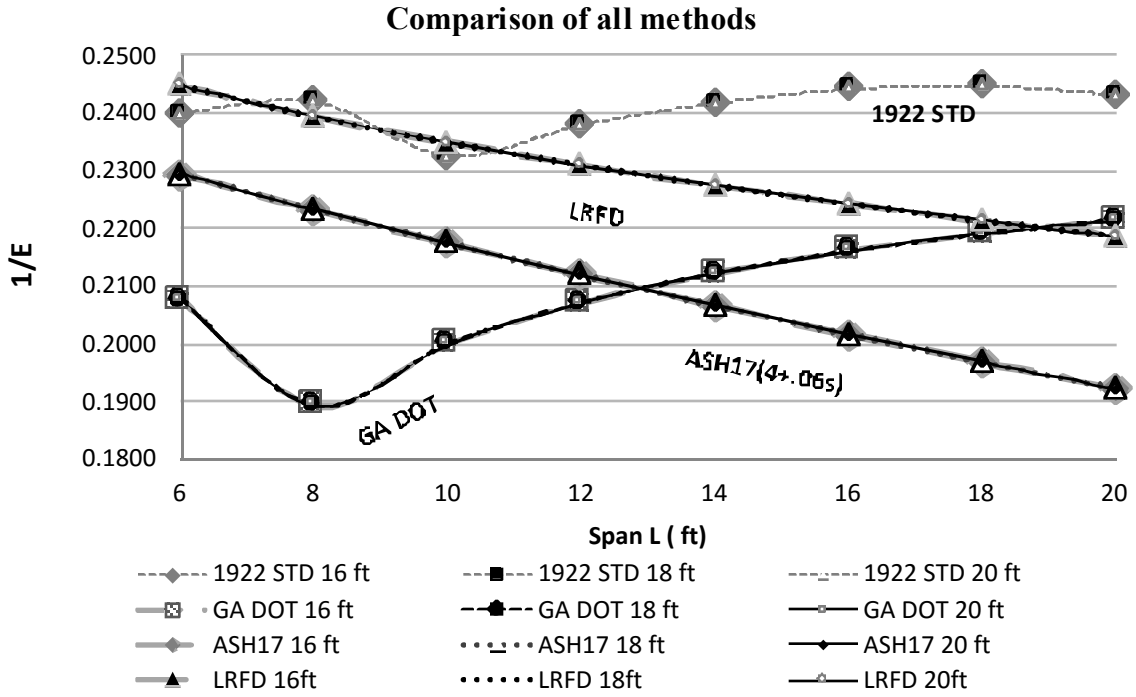

Figure 3-7: Graph of 1/E versus Span Length for Different Methods

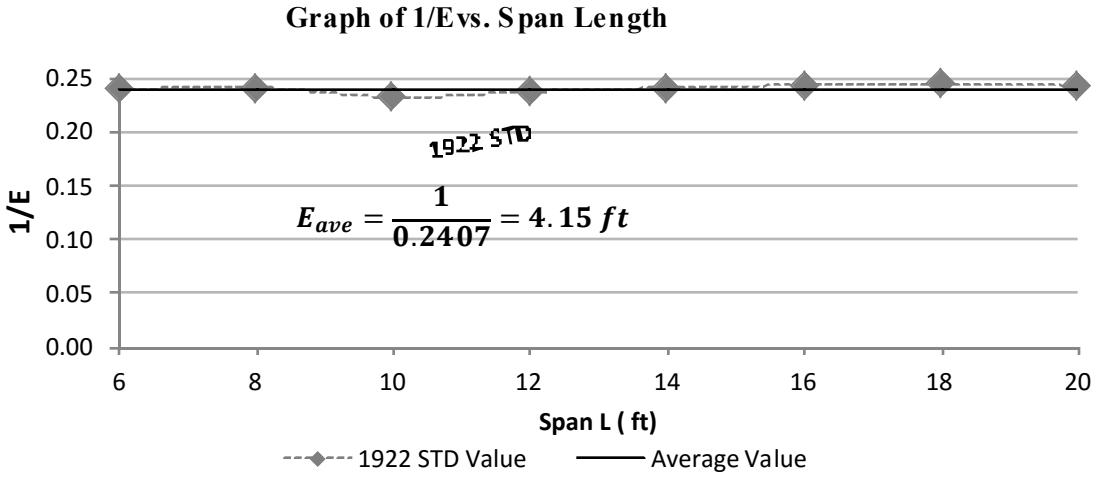

Figure 3-8: The Ratio of 1/E for Different Span Lengths and Roadway Widths

From the back-calculations it was concluded that the average effective width in these calculations was the value of 4.15 ft. When this effective width was applied to calculate the amount of steel in the slab, the results matched the values listed in Table 3-2. This study suggested that the effective width could possibly have been calculated by considering the geometry of the roadway. For a 16-ft roadway the maximum effective width, one-fourth of roadway for a two-lane roadway, would be 4 ft. Alternatively, the distance between two adjacent trucks was considered to be 3 ft, and the spacing between two wheel-lines was considered to be 6 ft. If an effective width was calculated as half the distance between two trucks plus half the distance between two wheel-lines, the effective width would be 4.5 ft. The original designers probably used an effective width such as 4 ft or 4.5 ft. The value of 4.15 ft determined from the back-calculations agrees well with either value.

3.3 1924 Two-Span Continuous Bridge in Fayette County

The same process learned from the contemporary method was used to calculate the reinforcement in the slab for a two-span continuous bridge of Fayette Co. documented in SHDA (1924). From Figures 3-9, through Figure 3-11 it was determined that the area of steel per foot of width is 1.44 in^2/ft in the positive moment region and negative moment region.

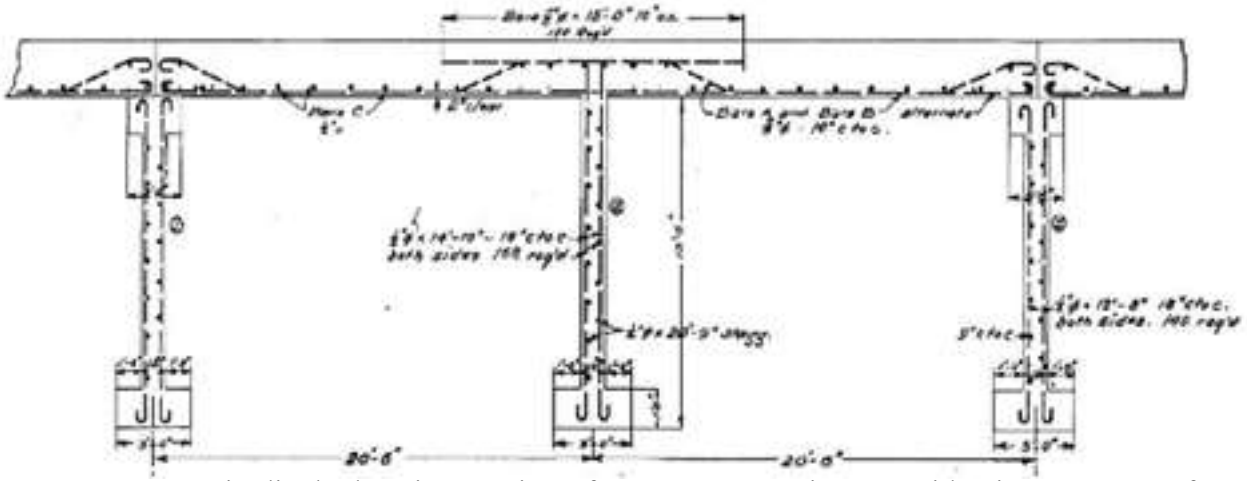

Figure 3-9: Longitudinal Elevation Section of Two-Span Continuous Bridge in Fayette Co. from SHDA (1924)

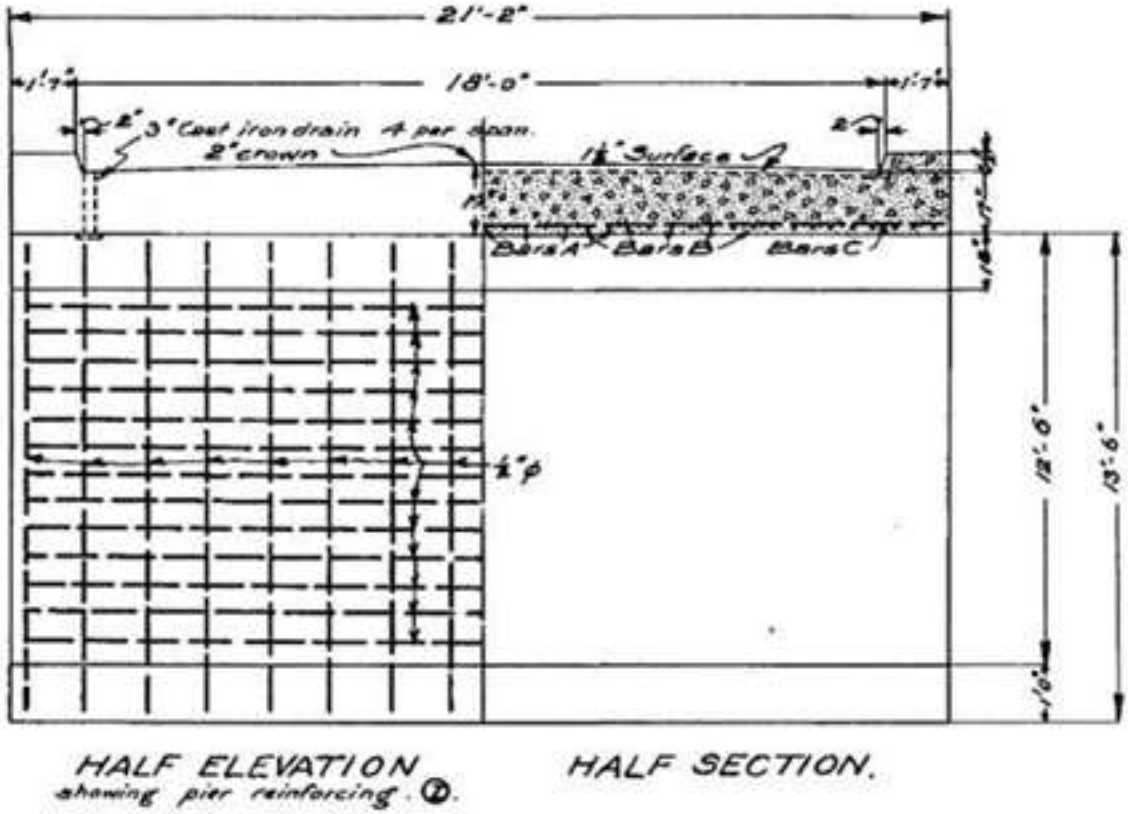

Figure 3-10: 1924 Drawings of Roadway Section of Two-Span Continuous Bridge in Fayette Co. from SHDA (1924)

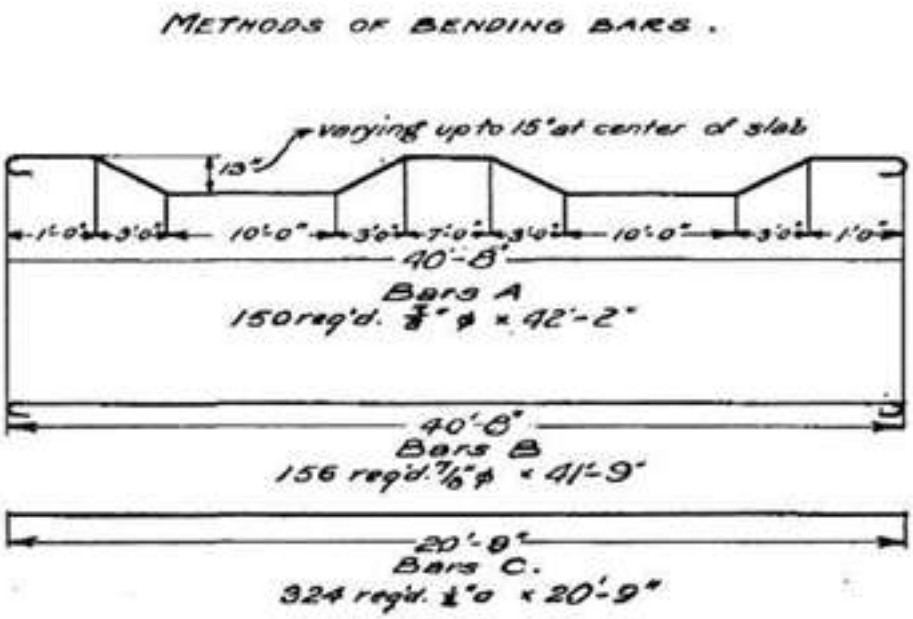

Figure 3-11: Bar Geometry of Two-Span Continuous Bridge in Fayette Co. from SHDA (1924)

Table 3-8: Summary of the Cross Sectional Properties and Material Properties Needed to Calculate the Reinforcement Required in the Slab of Fayette Co. Bridge

Parameters	Value
Allowable Concrete Compressive Stress, fc	650 psi
Allowable Steel Tensile Stress, fs	16,000 psi
Modular Ratio	15
Reinforced Concrete Unit Weight	150 pcf
Live Load	H 15 Truck
Impact Allowance (Contemporary)	30%
Super Imposed Dead Load (Contemporary)	80 psf
Slab Thickness, H	17 in.
Depth to Tension Reinforcement, d	15 in.
Effective Width of Slab (Contemporary)	4.15 ft
Span Length (center to center of supports)	20 ft

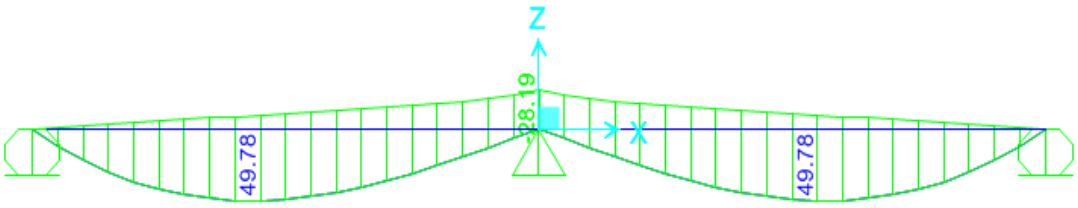

Figure 3-12: The Moment Envelope for a Moving H15 Truck on 20-ft Two-Span Continuous in Fayette Co. (Values are in kip-ft)

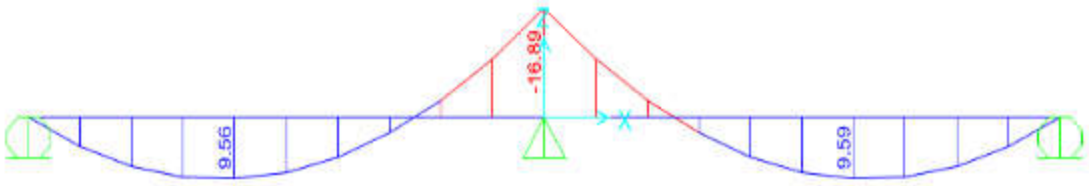

Figure 3-13: The Dead Load Moment Diagram for a 20-ft Two-Span Continuous in Fayette Co. (Values are in kip-ft)

Using the provided characteristics in Table 3-8, a structural analysis was done using SAP2000 (*SAP2000. Computer software. Https://www.csiamerica.com/products/sap2000. Vers. 17.1. N.p., 2015. Web.*) to define the maximum live load moment from the moment envelopes. The moment of inertia was kept constant throughout both spans. Figure 3-12 shows the moment envelop for a H15 Truck on this two-span continuous configuration, and Figure 3-13 shows the dead load moment diagram of this bridge. The results for the amount steel needed per foot of width and the spacing of the bars were calculated and the results match the drawings. These calculations were done both for the positive moment region and negative moment region, and the results were the same for both regions. The results from the calculations confirmed the reinforcement of 1.4 in^2 per foot of width, and if Number 7 bars were used as per the SHDA (1924), the spacing would be 5 in. on center. The amount of steel per foot of width was calculated based on the OFOR method and the results were the same for this analysis. The GA DOT (1936) method for effective width however, did not prove to be reliable for this case as the spacing for Number 7 bars was 4 in. on center.

3.4 Conclusions from Case Studies

The method of back-calculating the effective width for the 1922 simple spans (SHDA, 1922) resulted in values that were approximately constant. None of the design methods of calculating effective width matched this finding. Additionally, it was concluded that the effective width was calculated independently of the roadway width and span length for the simple spans. The outcome of this study showed that the average effective width was determined to be 4.15 ft for all roadway widths and spans. Besides the effective width concept, these case studies confirmed that the researchers understanding of the parameters used in the contemporary method was accurate, and although there is no evidence on how the single value of effective width was chosen, there was enough data to show that the 4.15 ft value was reliably used in contemporary design.

It was concluded that the SHDA (1922) used the clear span for simple spans of the bridge to design the reinforcement in the slab. This observation was made when the effective width was back-calculated using center to center of the support as the span length. When the center-to-center of the supports was considered the effective width values ranged from 4.75 ft to 6.25 ft with an average effective width of 5.56 ft. However, calculating the reinforcement for all span length by using an effective width of 5.56 ft did not generate the same reinforcement listed in SHDA (1922). For the two-span continuous bridge, the center-to-center of the support was considered for the design span length and not the clear span.

With this knowledge, the research could focus on predicting the cross sectional capacity and material properties in the Barnes Slough Bridge.

3.5 Modern Rating of Bridges

The aim of this section is to describe the load factor rating process for bridges according to AASHTO (MBE, 2011) and the AASHTO (17^{th} ed., 2002). Additionally the process of rating bridges using AASHTOWare is presented in this chapter. Today, AASHTOWare is used by the DOTs nationwide for the purpose of rating the structures in accordance with AASHTO specifications.

3.5.1 Modern Methodology

A rating analysis of a bridge is a structural evaluation of the overall condition of the bridge superstructure with regard to its load-carrying capacity. Live load is the primary concern for rating, and the structure is assumed to be sufficient for its dead load; however, the dead load effect is considered in the calculations. The result of a rating is a fraction where a value of one means that the structure is exactly sufficient for a given truck live load, and zero means that it is capable of carrying no live load. Any value greater than zero shows the proportion of the truck's nominal weight as the bridge's load carrying capacity; therefore, the trucks' weight should be limited to that proportion for the safety of the structure. AASHTO (MBE, 2011) has a series of standard trucks that are commonly used for rating bridges. These trucks are a good representation of many trucks although their configuration may not be exactly the same as any truck. ALDOT uses slightly different trucks shown in Figures 3-14 through 3-17 for calculating bridge ratings.

Below the concept of rating is explained in accordance with AASHTO (MBE 2011). The general equation for rating is

$$RF = \frac{C - A_1 D}{A_2 L(1+I)} \qquad \text{(Eq-35)}$$

where:

RF = Rating factor for the live load capacity.
C = Capacity of the member
D = Dead load effect on the member.
L = Live load effect on the member.
I = Impact fraction to be used with the live load
A_1 = Factor for dead load
A_2 = Factor for live load

This value multiplied by the nominal truck weight gives the load capacity for that truck configuration, usually reported in tons:

$$RT = (RF)\ W \qquad \text{(Eq-36)}$$

where:

RT = Bridge member rating (ton)
W = Weight of the nominal truck in determining live load effect, L.

There are two kinds of ratings for bridges: operating and inventory. The operating rating is used by ALDOT for evaluation of an existing structure and the factors A_1 and A_2 are equal to 1.3. For an inventory rating the factor A_1 is 1.3 and A_2 is 2.17, which corresponds to design of new structures according to AASHTO (17^{th} ed., 2002). The equations above are used for both operating and inventory cases with different nominal values used for A_1 and A_2 factors. In the above equation the "load effect" refers to vertical shear force, axial force, bending moment, axial stress, shear stress, and bending stress, etc. In our case, a flat slab bridge, the primary concern is the bending moment in the slab. The rating of a bridge is controlled by the member yielding the least rating factor. For a flat slab bridge, one effective width resists the load from one wheel-line for a given truck; therefore, the wheel-load distribution factor for this effective width is one, and the evaluation of the bridge cross-sectional capacity is done for one effective width.

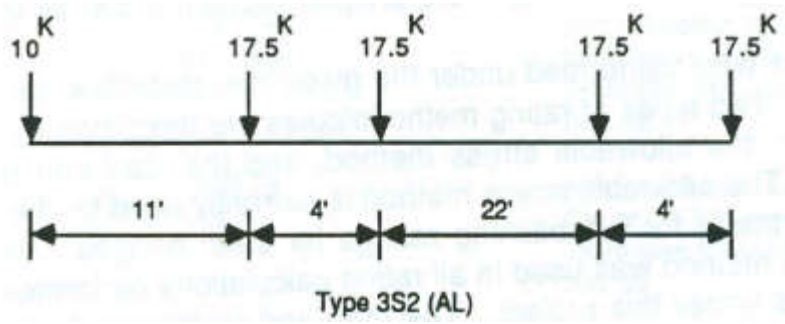

Figure 3-14: ALDOT Standard Trucks Type 3S2

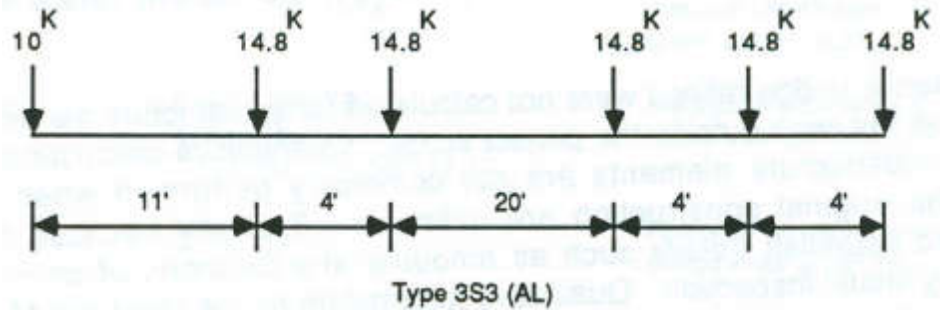

Figure 3-15: ALDOT Standard Trucks Type 3S3

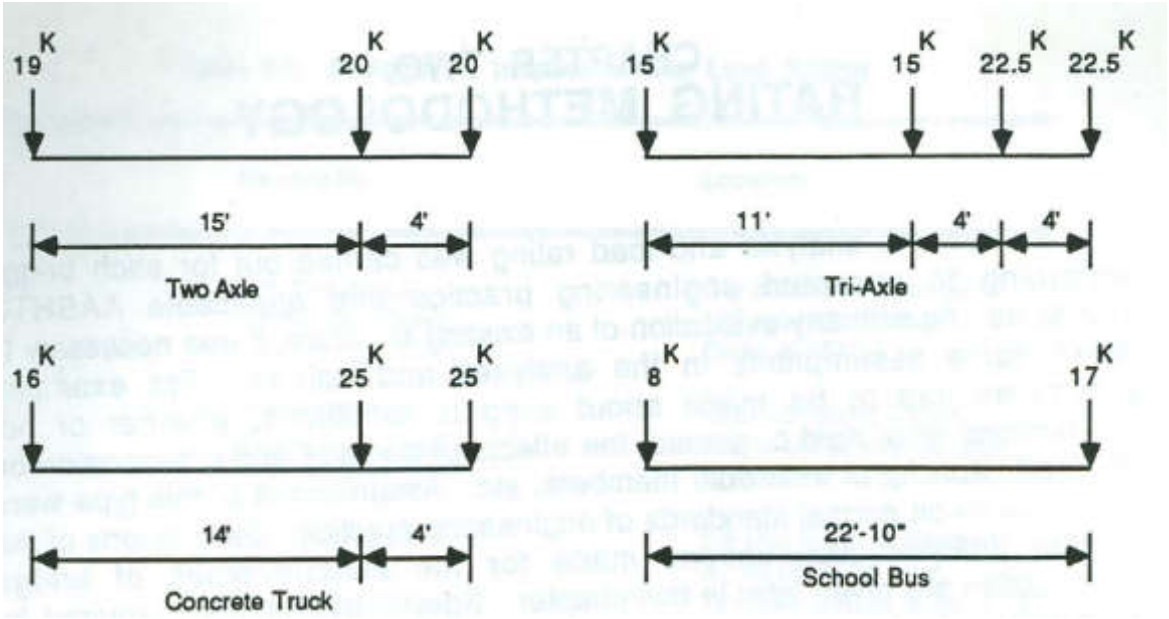

Figure 3-16: ALDOT Standard Trucks for Two Axle, Tri-Axle, Concrete Truck, and School Bus

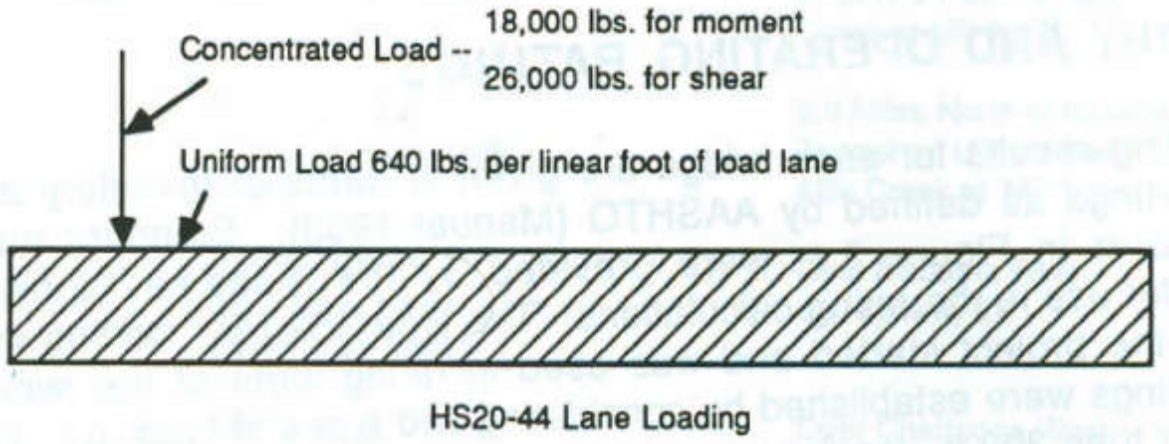

Figure 3-17: AASHTO Standard Trucks for HS20-40 Used by ALDOT

3.5.2 H15 Ratings of 1922 Simple Span Bridges

A series of ratings were done for bridges from the 1920s: one for the simple spans, and another for the two-span continuous bridge of Fayette Co. In this section these calculations are presented for 20-ft simple spans from SHDA (1922) with the characteristics listed in Table 3-9. For detailed calculations refer to Garmestani (2016).

Table 3-9: Summary of the Characteristics Used for Modern Rating of 20-ft Simple Span from 1922

Parameters	Value
Concrete Compressive Strength, f_c	2500 psi
Steel Yield Tensile Strength, f_y	33,000 psi
Reinforced Concrete Unit Weight	150 pcf
Live Load	H15 Truck
Impact Allowance (LFD)	30%
Span Length	20 ft
Slab Thickness, H	19
Depth to Tension Reinforcement, d	18
As (Area of Steel per Foot)	1.68 in^2/ft
Effective Width of Slab (LFD)	5.2 ft

AASHTO (17th ed., 2002) has specified the material properties for structures that were built prior to 1954 for which the material properties are unknown. These specifications are listed in Table 3-9, and these values are the concrete compressive strength and steel tensile yield strength.

The number of traffic lanes was assumed to be two lanes. This assumption allowed having a full effective width in the 16 ft roadway for rating purposes. As for the type of loading, since the documents showed that these spans were designed for H15, the same truck was used to perform the rating; however, this process applies for all other types of trucks. According to AASHTO the impact fraction of 0.3 should be added; therefore, the total effect would be 1.3 times the live load effect. For the purpose of rating the bridge the effective width was calculated in accordance with AASHTO (17th ed., 2002). Since the main reinforcement was parallel to traffic, Equation 27 governed for effective width of simple spans. For the H15 truck, ¾ of this value will apply as effective width. For the H15 truck, the maximum live load moment is 60 kip-ft for one wheel-line. (Figure 3-6 shows the truck configuration on the bridge) The dead load moment was 15.9 kip-ft, and the impact fraction was 0.3. The cross section capacity was calculated using the equation below:

$$C = \emptyset M_n = \emptyset A_s f_y (d - \frac{a}{2}) \qquad \text{(Eq-37)}$$

where:

$\phi = 0.9$

and

$$a = \frac{A_s f_y}{0.85 f`_c d b_w} \qquad \text{(Eq-38)}$$

From the above equation, the capacity of the cross section is 68.2 kip-ft, and by applying Equation 36, the operating rating factor is 2.5, which means the slab can carry 2.5 times the nominal weight of the H15 truck.

3.5.3 H15 Ratings of 1924 Two-Span Continuous Bridge

For the two-span continuous bridge, the same process was used with the addition of identifying the maximum moment through the use of SAP2000 and generating moment envelopes from the software for moving truck loadings, and influence lines for lane loadings. Figures 3-12 and 3-13 show the moment diagram for the dead load and the moment envelope and for the live load of the H15 truck on the two-span continuous beam. The rating for Fayette County Bridge used the parameters listed in Table 3-10. Applying the same equations (Eq-36 and Eq-37) the operating rating factor for the positive moment region is 2.33, and operating rating factor for the negative moment regions is 3.00.

Table 3-10: Summary of the Characteristics Used for Modern Rating of Two-Span Continuous Bridge from 1924

Parameters	Value
Concrete Compressive Strength, f_c	2500 psi
Steel Yield Tensile Strength, f_y	33,000 psi
Reinforced Concrete Unit Weight	150 pcf
Live Load	H15
Impact Allowance (LFD)	30%
Span Length	20 ft
Slab Thickness, H	17 in.
Depth to Tension Reinforcement, d	15 in.
As (Area of Steel per Foot)	1.44 $In.^2$/ft
Effective Width of Slab (LFD)	5.2 ft

This process also indicated that this structure was more than sufficient for the H15 truck load. The next step was to investigate the rating for other span lengths and truck types. The results from these ratings are listed in section 3.6.1.

3.6 AASHTOWare

AASHTOWare is a software used by the bridge engineers for evaluation and design. This software is organized so that the user can describe the structure through a series of inputs, such as material properties, cross-sectional properties, effective width, bar pattern, bar size, bar spacing, etc. A series of screenshots are shown in Figures 3-18 through 3-21 to demonstrate the process. Once a new file is created and labeled, other inputs are inserted. Figure 3-20 shows a series of the branches that are used to describe the structure. First branch is the material properties of the concrete and reinforcement. Then the method desired to rate the structure is defined, in this case LFR. The next folder is the "Superstructure Definition". Here the structure is defined as a "Girder Line Superstructure", and then the impact, dead load, and the wheel-load distribution factor are defined. Under the "Bar Mark Definition" folder different bar sizes and their geometry are defined, and under the "Member" folder, other cross sectional properties are defined such as the bar spacing, clear distances, modular ratio, asphalt thickness, web geometry, etc. Next, a bridge alternative is defined, and lastly the trucks for which the bridge is being rated are chosen (Figure 3-21). Finally, this analysis is run to determine the ratings for the structure.

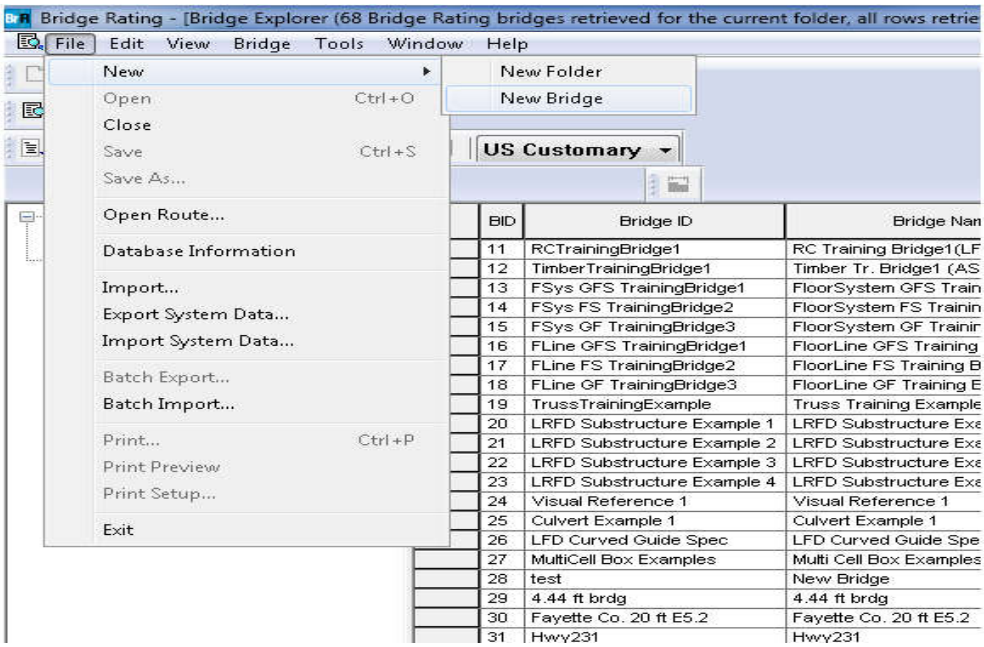

Figure 3-18: Creating a New File in AASHTOWare (2014)

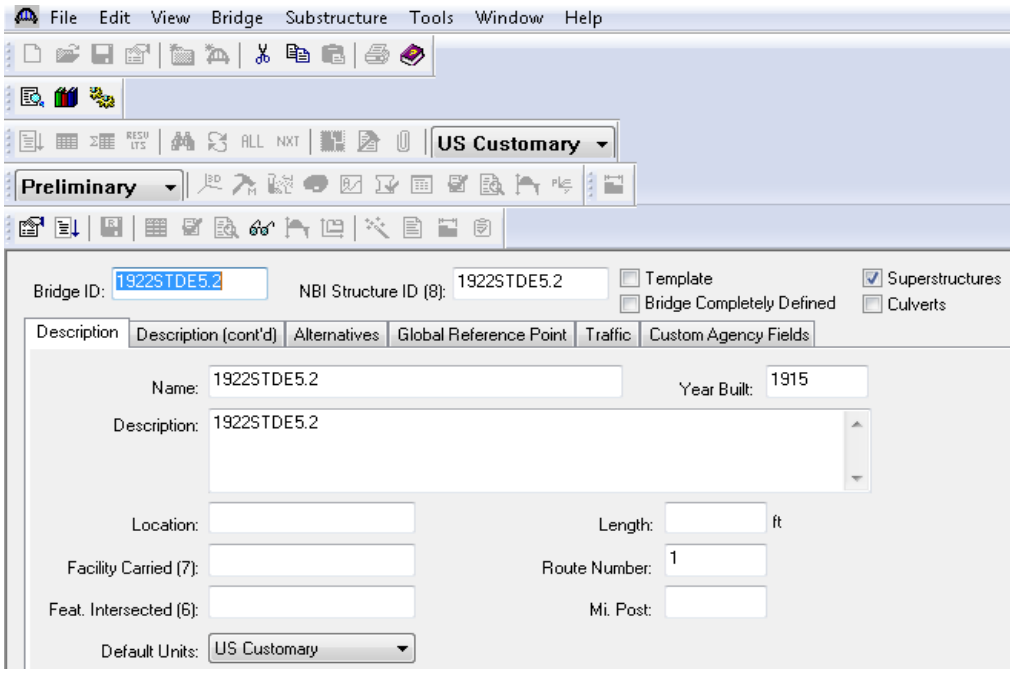

Figure 3-19: Labeling the File in AASHTOWare (2014)

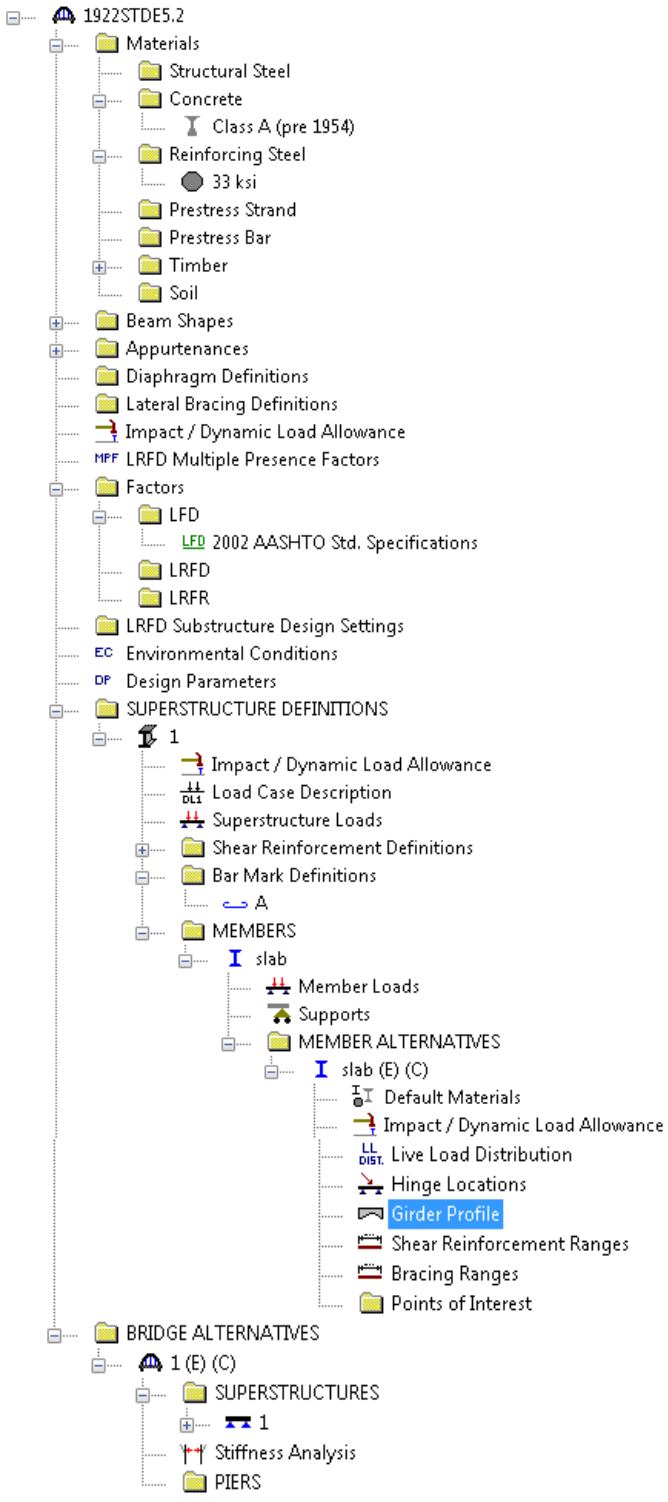

Figure 3-20: Tree of Folders to Insert Inputs in AASHTOWare (2014)

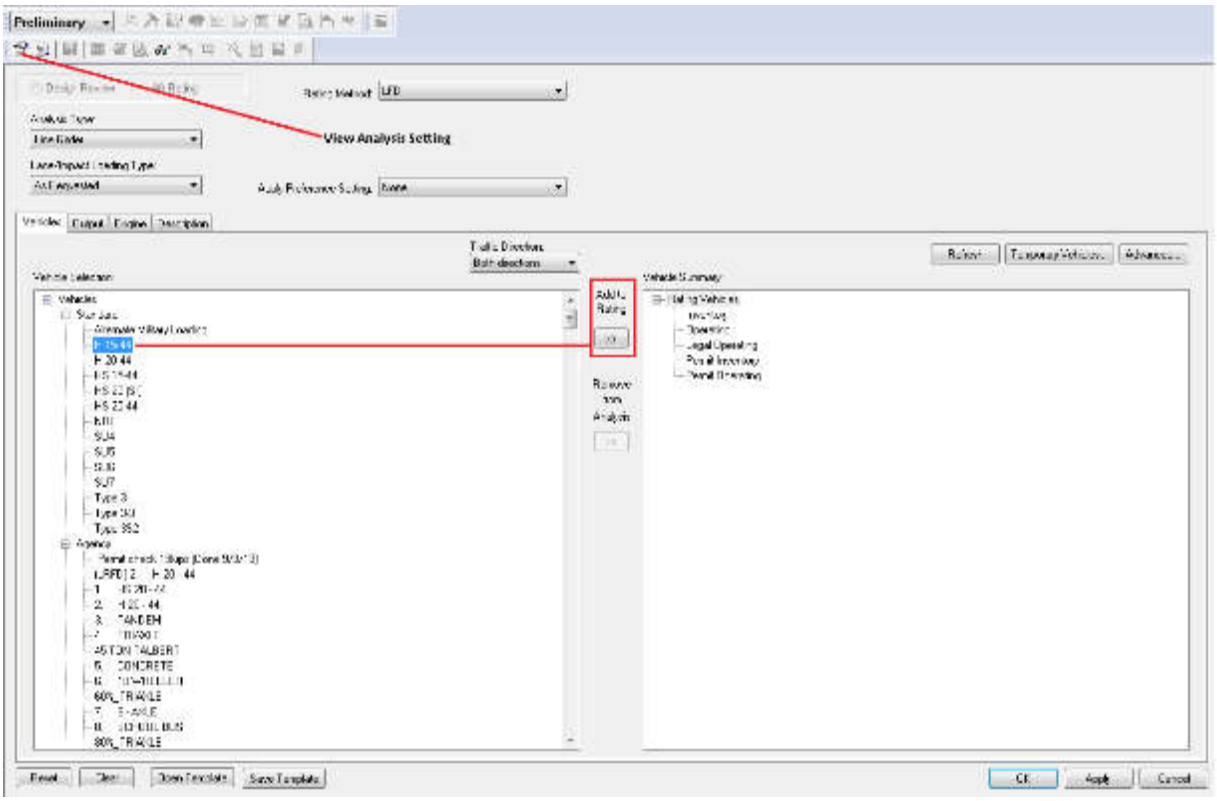

Figure 3-21: Under View Analysis Settings Chose the Truck Types (AASHTOWare, 2014)

3.6.1 AASHTOWare Ratings for ALDOTs' Standard Trucks

A series of ratings were generated using AASHTOWare for ALDOT standard trucks both for the 20-ft simple span and the two-span continuous bridge defined in the SHDA (1922, 1924). The results are listed in Tables 3-11 and 3-13. The results for the simple span matched the hand calculations. The operating rating results from hand calculations for the two-span continuous case are reported in Table 3-12. AASHTOWare considers the development length of the bar as well as the size and spacing. The bars in the negative moment region were terminated at 7.5 ft from the center of the support. This cut off length resulted in lower values than the hand calculations for the negative moment region only since the rating formula does not consider the termination of bars. The ratings for all ALDOT trucks for two-span continuous are listed in Table 3-13.

Table 3-11: Ratings of 20-ft Simply Supported Span by AASHTOWare for All ALDOT Standard Trucks

Vehicle	Inventory Rating Factor	Operating Rating Factor
School Bus	2.19	3.6
H 15-44	1.55	2.5
Type 3S2 (AL)	1.33	2.2
HS 20-44	1.16	1.9
Two Axle	1.16	1.9
Type 3S3 (AL)	1.14	1.9
Concrete	0.93	1.5
Triaxle	0.82	1.3

Table 3-12: Ratings of 20-ft Two-Span Continuous with Full Length Bars

Vehicle	Inventory Rating Factor	Operating Rating Factor
H 15-44	1.28	2.3

Table 3-13: Ratings of 20-ft Two-Span Continuous with Top Bars Terminated 7.5 ft on Either Side of the Support

Vehicle	Inventory Rating Factor	Operating Rating Factor
School Bus	1.14	1.91
H 15-44	0.81	1.36
Type 3S2 (AL)	0.58	0.97
HS 20-44	0.61	1.02
Two Axle	0.51	0.85
Type 3S3 (AL)	0.50	0.84
Concrete	0.41	0.68
Triaxle	0.36	0.60

Table 3-14: Summary of the Characteristics Used for Modern Rating of all Simple Span Bridges from 1922

Parameters	Value
Concrete Compressive Strength, f_c	2500 psi
Steel Yield Tensile Strength, f_y	33,000 psi
Reinforced Concrete Unit Weight	150 pcf
Live Load	All ALDOT Trucks
Impact Allowance (LFD)	30%
Span Length	Table 3-1
Slab Thickness, H	Table 3-1
Depth to Tension Reinforcement, d	Table 3-1
As (Area of Steel per Foot)	Table 3-2
Effective Width of Slab (LFD)	Defined by Eq-27

Lastly, the operating and inventory ratings for all simple span flat slab bridges form SHDA (1922) are listed in Table 3-15 and 3-16. The parameters used for these modern ratings are summarized in Table 3-14.

Table 3-15: Operating Rating Factor for ALDOT Trucks and for 1922 Simple Spans

Vehicle	Operating Rating Factor							
	Span Length (ft)							
	6	*8*	*10*	*12*	*14*	*16*	*18*	*20*
HS 20-44	1.29	1.30	1.38	1.62	1.58	1.89	2.03	1.76
Triaxle	1.64	1.53	1.33	1.36	1.22	1.38	1.47	1.36
Concrete	1.48	1.37	1.21	1.32	1.23	1.43	1.624	1.47
School Bus	2.44	2.45	2.60	3.04	2.98	3.57	3.74	3.79
Two Axle	1.85	1.72	1.51	1.65	1.54	1.79	2.03	1.83
Type 3S3 (AL)	2.50	2.32	2.01	2.00	1.76	1.97	2.00	1.92
Type 3S2 (AL)	2.12	1.96	1.73	1.89	1.76	2.05	2.30	2.04

Table 3-16: Inventory Rating Factor for ALDOT Trucks and for 1922 Simple Spans

Vehicle	Inventory Rating Factor							
	Span Length (ft)							
	6	*8*	*10*	*12*	*14*	*16*	*18*	*20*
HS 20-44	0.77	0.78	0.82	0.97	0.94	1.13	1.21	1.05
Triaxle	0.98	0.92	0.79	0.81	0.73	0.83	1.22	0.81
Concrete	0.88	0.82	0.72	0.79	0.74	0.86	1.38	0.88
School Bus	1.46	1.47	1.55	1.82	1.78	2.14	0.89	2.27
Two Axle	1.11	1.03	0.90	0.99	0.92	1.07	1.19	1.10
Type 3S3 (AL)	1.50	1.39	1.20	1.20	1.05	1.18	0.88	1.15
Type 3S2 (AL)	1.27	1.16	1.03	1.13	1.05	1.23	0.97	1.22

3.7 Conclusions

Form these case studies, it is concluded that the method which the effective width was calculated remains unknown; however, there was enough data to consider this value to be 4.15 ft for all designs. Additionally, all the ratings for simple span bridges shown in section 3.6.1 and, Table 3-15, for a case of an operating rating factor prove that the contemporary methods used to design the flat slab bridges for simple spans were so that the cross-sectional capacity was adequate for all ALDOT trucks. Thus there is no need for posting on these bridges. However, for two-span continuous bridges, the reinforcement in the negative moment region was not developed properly. By modern standards as a result the operating rating factor for five of the eight standard trucks were less than one. So, posting of weight restrictions for these trucks would be necessary.

With the information gained in Chapters 2 and 3, the research focused on identifying the capacity of Barnes Slough Bridge in Chapter 4.

4 Barnes Slough Bridge

4.1 Introduction

This chapter is focused on using the contemporary method to estimate the amount of reinforcement required in the Barnes Slough Bridge, presenting the field measurements of the slab properties, and rating the bridge. The capacity of the slab depends upon the cross-sectional characteristics, material properties, the loading conditions, and the effective width.

Initially, the capacity of the slab was calculated for the Original segment. The cross sectional characteristics were defined based on the methods used in contemporary design. The material properties were the allowable stress values chosen from the literature review. The loading was H15 Truck loading. The effective width value was concluded from Chapter 3. Using the above information, the amount of reinforcement in the slab was estimated.

After the initial calculations, a series of field measurements were done. These field measurements indicated in a different amount of reinforcement in the slab, changed the clear cover. Core tests identified the concrete strength. Also from these field measurements, it was concluded that the structure was behaving as a simple span. A comparison made between the field measurements and the estimated capacity of the slab concluded that methods learned from Chapter 2 and 3 were not able to establish a method which was used to design the reinforcement during the contemporary time. Next, a series of decade studies were done with an aim to estimate a time when the additions were built by comparing these results with the field measurements.

Lastly, the capacity and the characteristics of the slab were used to build a baseline structural model of Barnes Slough Bridge, and ratings were generated for all four segments. For the purpose of modern evaluation of the bridge and rating, the cross-sectional characteristics measured in the field were used. Other characteristics such as the loading, impact, effective width, and the number of traffic lanes were considered in accordance with AASHTO (17^{th} ed., 2002), and did not depend on the contemporary design methods.

Figure 4-1: View of East Side of Barnes Slough Bridge

Figure 4-2: View of West Side of Barnes Slough Bridge

4.2 Estimating the Reinforcement using the Contemporary Design Methods

Firstly, the task was to calculate the amount of reinforcement required in Barnes Slough Bridge based on the design methods in the 1920s. These calculations were done to estimate the amount of steel in the original 18 ft wide segment in the middle.

The geometry of the existing bridge was measured through initial visual inspection of the bridge. Figures 4-3 through 4-5 show these measurements that were taken on the site. The field measurements showed an average span length of 21 ft-10 in. center-to-center of the supports with a clear span length of 19 ft-10 in. The thickness of the piers was 2 ft. A layer of asphalt 1.75 in. thick existed over the full roadway, and the thickness of the slab was measured to be 19 in. and an 18 in. of effective depth was assumed as it was specified in the SHDA (1922) for similar span lengths of 20 ft.

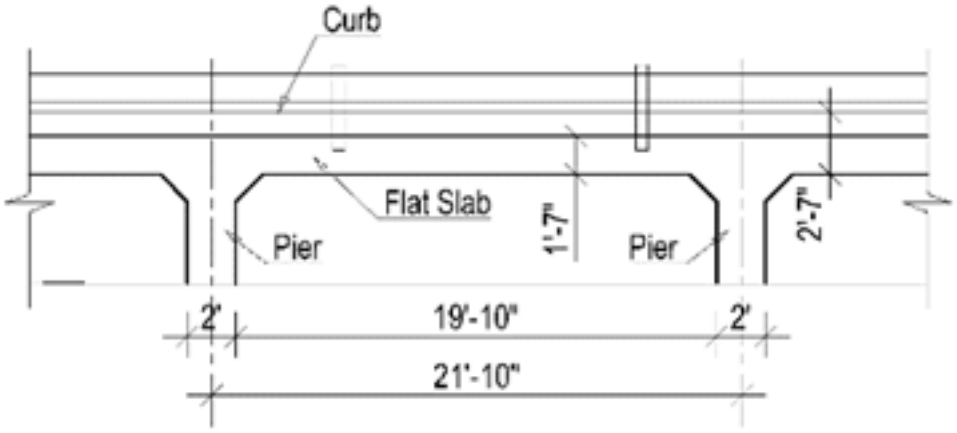

Figure 4-3: Elevation of Typical Span of Barnes Slough Bridge

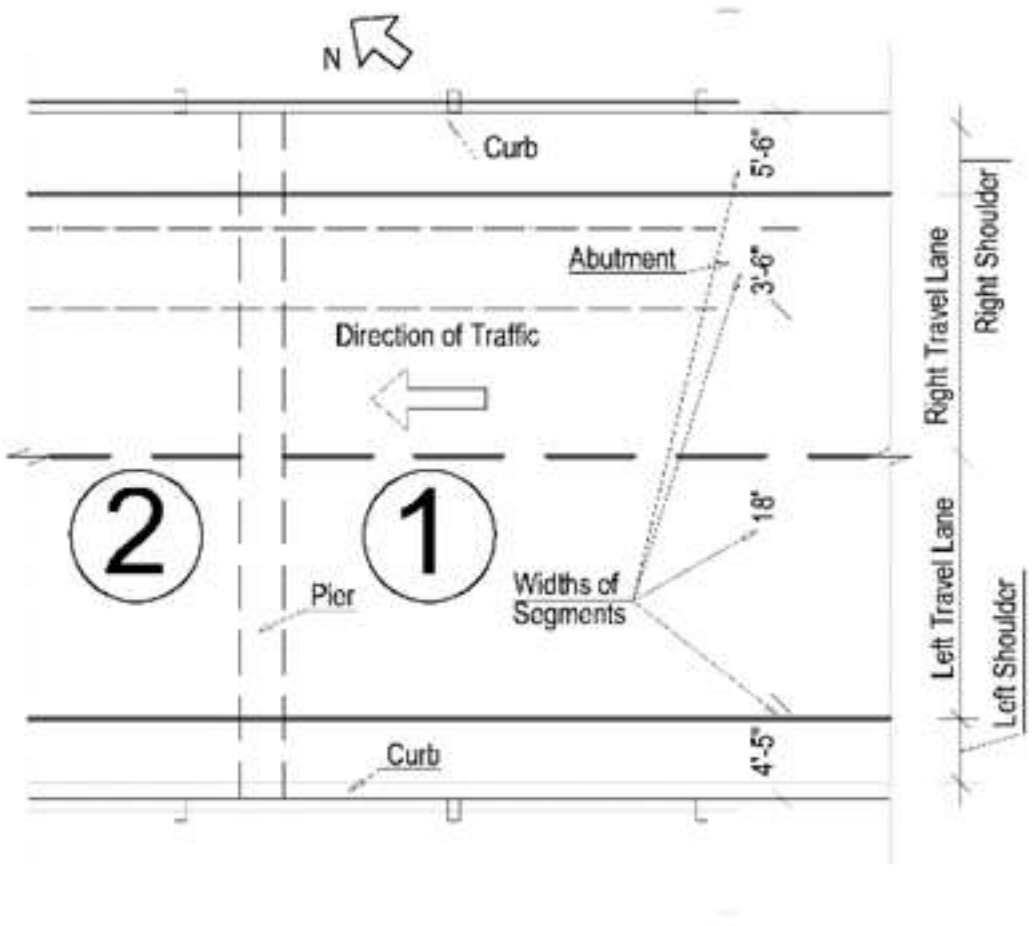

Figure 4-4: Partial Plan of Barnes Slough Bridge

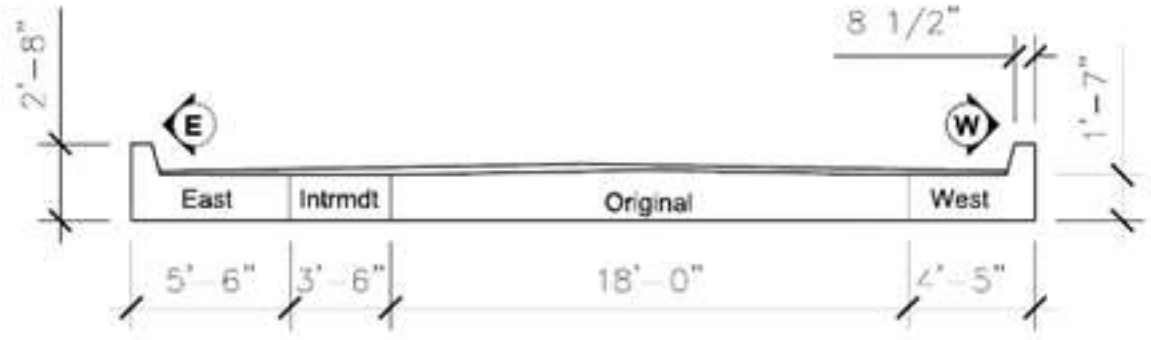

Figure 4-5: Cross Section of Barnes Slough Bridge

In the initial calculations the structure was modeled both as simple spans and as a series of continuous spans. The estimation of reinforcement in the slab was done for simple span moment diagrams and continuous spans' moment envelopes generated for an H15 Truck since this truck was used by contemporary designers. Required bar spacings were calculated for three different bar

sizes, Number 7 bar, Number 8 bar, and Number 9 bar. The effective width for the purpose of defining steel in the slab was considered to be 4.15 ft as it was established in Chapter 3 for the contemporary design method. Table 4-1 lists the parameters used to calculate the amount of steel in the slab. Additionally the amount of steel was calculated for this slab based on OFOR method. The two methods provided a range of amount of steel that could be expected to be detected in the slab of Barnes Slough Bridge.

Table 4-1: Assumed Parameters Used to Calculate the Amount of Reinforcement in the Slab Using Contemporary Design Method

Parameters	Value
Allowable Concrete Compressive Stress, fc	650 psi
Allowable Steel Tensile Stress, fs	16,000 psi
Modular Ratio	15
Reinforced Concrete Unit Weight	150 pcf
Live Load	H 15 Truck
Impact Allowance (Contemporary)	30%
Impact Allowance (OFOR)	30%
Super Imposed Dead Load (Contemporary)	80 psf
Super Imposed Dead Load (OFOR)	80 psf
Slab Thickness, H	19 in.
Depth to Tension Reinforcement, d	18 in.
Effective Width of Slab (Contemporary)	4.15 ft
Effective Width of Slab (OFOR)	7.78 ft

Tables 4-2 and 4-3 have listed the results for all the conditions listed above. For calculations refer to Garmestani (2016). This initial calculation was done to see if the results matched the case studies from the 1920s. The amount of steel for both cases of simple spans and continuous spans were within 5% of the results from SHDA (1922; 1924). For continuous spans, Number 7 bars resulted in a spacing of 5in. in the positive moment region and 5.5 in. in the negative moment region, which are very close to the Fayette Co. Bridge (SHDA, 1924) with Number 7 bars at 5 in. on center. For simple spans, Number 8 bars provided the same 5.5 in. spacing as in Table 3-1. Next the reinforcement was designed based on OFOR method and the difference in the expected amount of steel was less than 10%. From these studies it was expected to detect similar amount of reinforcement through field measurements.

Table 4-2: Bar Spacing for Different Conditions in the Original Segment According to Contemporary Methods for H15 Truck

Bar size	Simple Span		11-Spans Continuous			
	+M		+M		-M	
	Contemporary	OFOR	Contemporary	OFOR	Contemporary	OFOR
	Spacing (in.)	Spacing (in.)	Spacing (in.)	Spacing (in.)	Spacing (in.)	Spacing (in.)
#7	4.75	4.25	5.25	5.0	5.75	5.75
#8	6.25	5.5	7.0	6.5	7.5	7.5
#9	8.0	7.0	8.5	8.5	9.75	9.5

Table 4-3: Amount of Steel per foot of Width for Different Conditions in the Original Segment According to Contemporary Methods for H15 Truck

Simple Span		11-Spans Continuous			
+M		+M		-M	
Contemporary	OFOR	Contemporary	OFOR	Contemporary	OFOR
As ($in.^2$)/ft	As ($in.^2$)/ft	As ($in.^2$)/ft	As ($in.^2$)/ft	As ($in.^2$)/ft	As ($in.^2$)/ft
1.50	1.69	1.36	1.39	1.23	1.24

4.3 Field Measurements

Field measurements were made to determine as many as practical of the parameters that are needed to calculate the cross-sectional capacity. These tests included the use of Profometer (http://www.proceq.com, 2015) device to read the rebar spacing, bar size, and cover for the bottom layer of reinforcement. Ground penetration radar (GPR) was used to check the spacing of the bars at the top layer of reinforcement, and concrete was removed to expose rebar to confirm the bar diameter.

Figure 4-6: Reinforcement Detection and Measurements with Proceq Profometer

Figure 4-7: Ground Penetrating Radar Tests

Concrete was removed from the bottom of the slab in the original segment and from the intermediate segment. Some bars were exposed in the East and West segments due to concrete spalling, which helped to confirm the size of the bars in those segments. Information gained from exposing the rebar confirmed Profometer measurements. Table 4-4 lists the bar size and clear cover for all four segments. These tests also resulted in slightly different characteristics than the ones tabulated in SHDA (1922; 1924). The clear cover was confirmed to be 1.25 in., and it was confirmed that all segments have Number 8 bars except the Intermediate segment which has Number 7 bars. The spacings of these bars are listed in Table 4-4. The amount of steel measured in the slab was considered to be distributed equally for calculation purposes, and the measured values were used in the models without any modifications.

Table 4-4: Tension Reinforcement at Bottom of Slab from Field Measurements

	Cross Sectional Properties				
Segment	**Segment Width**	**Cover (in.)**	**Bar Size**	**# of Rebars**	**Spacing (in.)**
East	5.5 ft	1.25	#8	10	6.8
Intermediate	3.5 ft	1.25	#7	9	4.5
Original	18 ft	1.25	#8	53	4.0
West	4.4 ft	1.25	#8	7	7.5
TOTAL	31.4ft				

The concrete core tests were done at three locations: the first location was over the first support from the south end in the original segment of the slab, second location was over the first support from south end in the East segment, and the third location was at the middle of the first span from the south end in the East segment. The results from the core tests are listed in Table 4-5. The result from the core test showed strength of 3340 psi in the first location. However, it was decided to use the suggested value of 2500 psi in accordance with AASHTO (MBE, 2011) since the tested value

was much higher than the core strengths at the other locations. The concrete compressive strength of 1850 psi was applied to East, Intermediate, and West segments. This value was the average value of the two core test results from the east segment. Also the core tests from the top of the slab exposed the reinforcement in the top layer of reinforcement, and they were confirmed to be Number 4 bars at 10.5 in. on center.

Figure 4-8: Drilled Concrete Core

Table 4-5: Concrete Core Test Results and the Adjusted Values

Location of Sample	Measured Strength	Adjusted Strength
East@ Mid-Span	1760 psi	1850 psi
East @ Support	1940 psi	1850 psi
Original @ Support	3340 psi	2500 psi

The field measurements showed that the expected amount of reinforcement in the slab calculated using contemporary methods (Table 4-2) for continuous spans in the positive moment region was less than the amount detected in field measurements (Table 4-4). Additionally the amount of reinforcement in the negative moment region was only 18% of that expected in a continuous span (compare Table 4-2 with 0.229 in^2/ft measured at the field). The GPR detected some cracks beneath the asphalt over the supports. These results from the field measurements suggested that the designers of Barnes Slough Bridge reinforced this bridge as if it was a series of simple spans and not as an 11-span continuous bridge.

From the field measurements it was concluded that the four segments of the bridge had different characteristics and had to be evaluated separately. With this conclusion a series of studies was done for different decades from 1930s through 1960s in an aim to estimate a time when the additional segments were built.

4.4 Decade Studies

An attempt was made to estimate when the East and West additions were performed. Once it was concluded that the structure was designed as a series of simple spans, the reinforcement for the slab was calculated based in AASHO codes from 1930s through 1960s. The characteristics used in designing the slab for different times are listed in Table 4-6. Tables 4-7 and 4-8 show the results for the amount of reinforcement needed in the slab for different eras throughout the 20th century. The design truck loading that controlled the design of 21 ft-10in. span for the time that the additions were built was H20; however, it is suggested that the truck loading for which the Barnes Slough Bridge was designed for was H 15 Truck.

Table 4-6: Design Characteristics of Simple Span Slab for Different Times

Parameters	Value					
	1931	**1935**	**1941**	**1949**	**1957**	**1961**
Allowable Concrete Compressive Stress, f_c (psi)	650	1,000	1,000	1,000	1,000	1,000
Allowable Steel Tensile Stress, fs (psi)	16,000	16,000	18,000	18,000	18,000	18,000
Reinforced Concrete Unit Weight (pcf)	150	150	150	150	150	150
Live Load (Truck Loading)	H15 & H20	H15 & H20	H15 & H20	H15 & H20	H15 & H20	H15 & H20
Impact Allowance	30%	30%	30%	30%	30%	30%
Super Imposed Dead Load (Asphalt, in.)	1.5	1.5	1.5	1.5	1.5	1.5
Slab Thickness, H (in.)	19	19	19	19	19	19
Depth to Tension Reinforcement, d (in.)	17.25	17.25	17.25	17.25	17.25	17.25
Effective Width of Slab (ft)	7	15.6	4.94	4.94	4.94	5.31
Effective Width of Slab (OL)	6.5 ft	NA*	NA*	NA*	NA*	NA*

NA*: The concept of overlap does not apply to these years.

Table 4-7: Calculated Spacing of Reinforcement for 1931

Truck Loading	Spacing (in.)			
	#7 bars STD. Eff. Width 7 ft	**#7 bars Overlapped Width 6.5 ft**	**#8 bars STD. Eff. Width 7 ft**	**#8 bars Overlapped Width 6.5ft**
H15 Truck	5	4.50	6.5	6
H20 Truck	3.75	3.50	5	4.50

Table 4-8: Calculated Spacing of Reinforcement for 1935-1961

Year	Effective Width (ft)	Truck Loading	Spacing (in.)	
			# 7 Bars	#8 Bars
1935	15.6	H15 Truck	6.75	9
		H20 Truck	6.25	8.25
1936	5	H15 Truck		7.75
		H20 Truck		7
1941	4.94	H15 Truck		7.25
		H20 Truck		6.25
1949	4.94	H15 Truck		7.25
		H20 Truck		6.5
1957	4.94	H15 Truck		7.25
		H20 Truck		6.5
1961	5.31	H15 Truck		6.75
		H20 Truck		6

In 1931 the concept of overlap was considered to define the effective width. This concept was explained previously in Chapter 2 Section 2.2.7. The amount of reinforcement in the slab for the overlapped case and Number 7 bars matches the reinforcement in the Intermediate segment measured in the field. There was a note on the "Bridge Card" from 1930 stating that an addition, Intermediate segment, was added. The match between the result shown above and the reinforcement measured in the slab and the note from the "Bridge Card" suggest that the case of overlapped effective width was used to calculate the reinforcement in the Intermediate segment.

Table 4-4 lists a uniform bar spacing determined by dividing the width of the segment by the number of bars in that segment. This decision represents the spacing measured in the original segment, the intermediate segment, and the East segment properly; however, the actual spacing listed for the West segment was different than the 7.5 in. listed in Table 4-4. (Figure 4-9) On the east side of the West segment there was a larger gap between the last bar of the West segment and the first bar of the Original segment. This gap is about 1 ft. This difference influenced the average spacing of bars in the West segment. If this gap was considered, the spacing for West segment would be 7.25 in. A comparison made between the results from Table 4-4 to Tables 4-6 and 4-7 and considering this gap influence, can attempt to estimate when these additions were built. This spacing would suggest that the segments on the East and West of the roadway were built sometime between 1941 and 1959, and that the slab was designed for a H15 Truck loading.

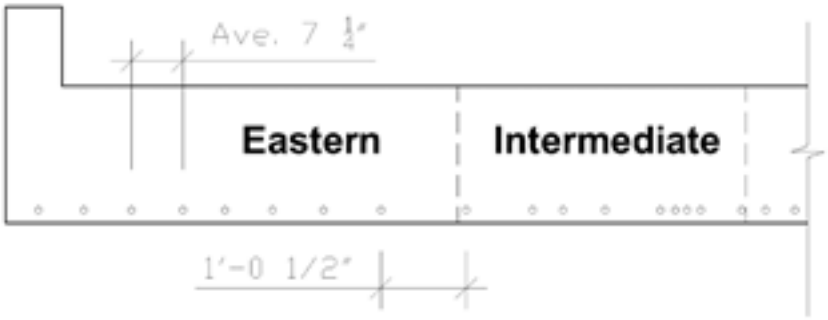

Figure 4-9: The Spacing of Reinforcement in the East Segment

4.5 Modern Rating and the Baseline Structural Model of the Barnes Slough Bridge

Based on the field measurements described above, each segment of the cross section was modeled in AASHTOWare to provide the section capacity and the rating of the segment. A model for each segment was necessary for the final evaluation of the whole structure. In AASHTOWare the effective width of slab was modeled as a single girder with a distribution factor of one both for moment and shear. The Intermediate and West segments were not as wide as the effective width from AASHTO (17th ed., 2002). The Intermediate segment width is 3.5 ft. AASHTO (17th ed., 2002) specifies an effective width of 5.31 ft for a 21 ft–10 in. span (Equation 27). The intermediate segment was modeled by assuming the effective width was symmetrically centered over the 3.5 ft as shown in Figure 4-10. This arrangement led to 10.75 in. into the adjacent segments on either side. The amount of steel over the 5.31 ft effective width was assumed to be the equal distribution of the total reinforcement in the intermediate segment and the reinforcement in the two 10.75 in. adjacent segments. The West segment width is 4 ft - 5 in., which is also less than the effective width of 5.31 ft. The segment is an edge segment, so the effective width started from the West side and continued 10.75 in. into the original segment as shown in Figure 4-11.

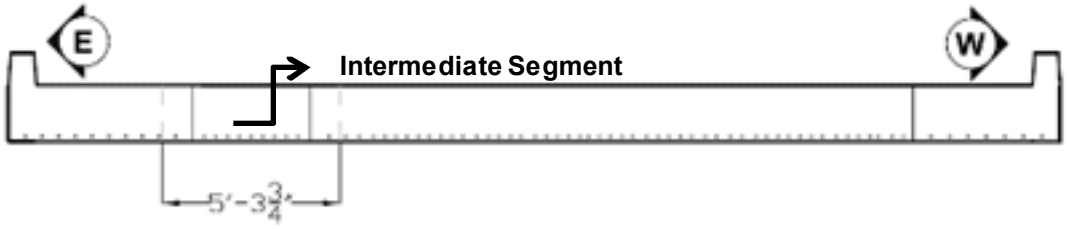

Figure 4-10: Effective Width Used for the Intermediate Segment

Figure 4-11: Effective Width Used for the West Segment

The amount of steel over this width was an equal distribution of the reinforcement over West segment and the reinforcement in the additional 10.75 in. of the adjacent segment for the purpose of rating.

The rating results from AASHTOWare for each segment are listed in Tables 4-7 through 4-10. These segments include the original, the intermediate, the West, and East segments. These ratings were generated for all ALDOT standard trucks based on LFR method. Figures 3-14 through 3-17 and 4-12 show the configuration of all trucks. Additionally ratings were generated for LC-5 load test truck, which was the truck used for the non-destructive live load testing of this bridge. This truck's configuration is shown in Figure 4-12.

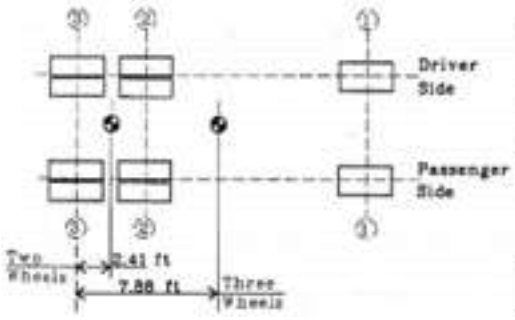

Wheel Loads				
Total Wt (lbs)	85,700	Wheel 3 (lbs)	Wheel 2 (lbs)	Wheel 1 (lbs)
Driver		15,800	16,000	11,100
Passenger		15,600	15,800	11,400
Average		15,700	15,900	11,250

Figure 4-12: LC-5 Load Testing Truck Configuration

The four cross section segments were rated both as simple spans and 11-spans continuous to check the capacity for both cases. Table 4-9 shows the results of AASHTOWare rating for the case of 11-span continuous. These ratings for the continuous spans were zero due to insufficient negative moment capacity. The ratings are not zero by hand calculations. The rating factors should be a negative value of about 7%; however, AASHTOware indicated the lack of cross section capacity in the negative moment region as zero. The negative moment cross section capacity over the supports is enough to support to the unfactored dead load; however, the dead load is multiplied by a factor of 1.3 (Equation 36) and deducted from the capacity in the rating calculations. The factored dead load is greater than the capacity, thus the rating factors for this structure are negative, for which the software generates zero in such cases.

The amount of steel in the negative moment region was confirmed through field tests to be 0.229 in^2 per ft. This area of steel was provided by spacing of Number 4 bars at 10.5 in. on center. These

bars were continuous along the whole length of the span. The bar size at the existing spacing must be Number 6 bars to provide enough cross sectional capacity to generate ratings that are bigger than zero. Through these negative moment ratings it was confirmed once more that the structure is behaving as a simple span. Tables 4-10 through 4-11 show the operating and inventory rating factors for the Barnes Slough Bridge as a series of simple spans. From these tables it was concluded that the East segment has the least capacity.

Table 4-9: AASHTOWare Ratings of Barnes Slough Bridge as 11- Span Continuous

Vehicle	Inventory Rating Factor	Operating Rating Factor
School Bus	0	0
Type 3S2 (AL)	0	0
HS 20-44	0	0
Two Axle	0	0
Type 3S3 (AL)	0	0
Concrete	0	0
LC 5 Test Truck	0	0
Triaxle	0	0

Table 4-10: Ratings of Original Segment of Barnes Slough Bridge as Simple Spans

Vehicle	Inventory Rating Factor	Operating Rating Factor
School Bus	2.44	4.08
Type 3S2 (AL)	1.45	2.43
HS 20-44	1.30	2.17
Two Axle	1.27	2.12
Type 3S3 (AL)	1.24	2.07
Concrete	1.01	1.70
LC 5 Test Truck	0.93	1.56
Triaxle	0.90	1.50

Table 4-11: Ratings of Intermediate Segment of Barnes Slough Bridge as Simple Spans

Vehicle	Inventory Rating Factor	Operating Rating Factor
School Bus	1.49	2.49
Type 3S2 (AL)	0.88	1.48
HS 20-44	0.79	1.32
Two Axle	0.77	1.29
Type 3S3 (AL)	0.75	1.26
Concrete	0.62	1.04
LC 5 Test Truck	0.57	0.95
Triaxle	0.55	0.91

Table 4-12: Ratings of West Segment of Barnes Slough Bridge as Simple Spans

Vehicle	Inventory Rating Factor	Operating Rating Factor
School Bus	1.14	1.90
Type 3S2 (AL)	0.68	1.35
HS 20-44	0.60	1.01
Two Axle	0.59	0.99
Type 3S3 (AL)	0.57	0.96
Concrete	0.47	0.79
LC 5 Test Truck	0.43	0.73
Triaxle	0.42	0.70

Table 4-13: Ratings of East Segment of Barnes Slough Bridge as Simple Spans

Vehicle	Inventory Rating Factor	Operating Rating Factor
School Bus	1.03	1.72
Type 3S2 (AL)	0.61	1.02
HS 20-44	0.55	0.91
Two Axle	0.53	0.89
Type 3S3 (AL)	0.52	0.87
Concrete	0.43	0.71
LC 5 Test Truck	0.39	0.66
Triaxle	0.38	0.63

5 Models for Permit Loads

5.1 Introduction

Barnes Slough Bridge cross section has four segments, and the capacity of each segment is different. In Chapter 4, a description and an operating rating factor for each segment is reported. To provide ALDOT with a structural model of the Barnes Slough Bridge, a single model has to be developed that represents all segments appropriately. The goal of this chapter is to accomplish this task through a series of effective width studies. Adjusting the effective width in AASHTOware is the most appropriate way to modify the calculated capacity of this structure.

According to finite element studies (Chapter 7), it is concluded that the location of lowest rating in the bridge is the new segment on the east side of the roadway. However, the performance of the structure through its life and during the live load tests suggests that the structure has significant capacity and perhaps more than the expected capacity shown by the AASHTOWare ratings. When the measured strains and deflections from the field tests were compared to those of the finite element model, it was shown that there is more capacity in this structure, and modeling the weakest portion of the structure in AASHTOWare is not an accurate way of representing the overall structure.

In addition to the field tests and the rating analysis presented in Chapter 4, the structure was checked for shear and development of the bars in the slab to confirm that flexure is the controlling limit state for this structure. The factored shear capacity of the cross section is 15.5 kip per foot of width for the concrete strength of 2500 psi, and 13.4 kip per foot of width for the concrete strength of 1850 psi. Both of these values are larger than shear demands caused by the dead load and live load on the slab. The shear due to dead load is 3.67 kip per foot of width, and the shear due to the LC-5 load testing truck is 5.9 kip per foot of width which result in 9.57 kip total shear demand. The same shear force for dead load added to the triaxle truck load of 4.9 kip per foot of width result in a total of 8.58 kip of shear demand. These calculations confirmed that the slab is sufficient for ALDOT's heaviest trucks. For calculations refer to Garmestani (2016).

The embedment details of the positive moment reinforcement over the supports is unknown. The drawings from SHDA (1922; 1924) suggested that half of the bottom bars were bent at the support. Based on the field measurements, it was concluded that two-thirds of the reinforcement continued to the supports and only one-third was either terminated or bent. The ground penetration radar did not detect any Number 8 bar or Number 7 bars at the top of the slab; therefore, it was confirmed that the missing one-third of the bars did not bend into the top layer of the reinforcement, so they are assumed to be terminated. Also the core tests at the support from the top of the slab only showed Number 4 bars reinforcement at the top of the slab, and there was no evidence of bottom bars that were bent up. With this evidence the development length of the bars at the bottom of the slab was checked for a case where only two-thirds of the bars continued to the support and one-third was terminated at 3.5 ft from the support. This check confirmed the safety of the structure under this worst case configuration of bars. The development length was more than sufficient for this configuration for all four segments of the roadway.

By concluding that there were only Number 4 bars at 10.5 in. on center over the supports and in the negative moment region, the cross section capacity was estimated based on this small amount of reinforcement. This capacity was too small to carry any truck load in addition to the slab self-weight. Therefore, it was decided that the most appropriate model of the Barnes Slough Bridge is a simple span model. Some cracking at the top of the slab at the supports was identified by the ground penetration radar which also suggested there is not enough negative moment capacity in the cross section. All of the above checks confirmed that the limit state that controlled the rating was the ultimate cross section capacity in flexure.

5.2 Model for Permit Load

The final model of this bridge is a model of one effective width with a distribution factor of one both for shear and moment in AASHTOWare. The span length is 21 ft-10 in. from center-to-center of supports. This span is simply supported with pinned connection on one end and a roller on the other end. The slab height is 19 in. with 1.25 in. of clear cover, the effective depth of 17.25 in. and Number 8 bars with area of 0.79 in^2 that are spaced at 4 in. on center. One-third of the bars are cut off at 3.5 ft from the center of the support and two-thirds of bars are full length. The ratings presented here are not affected by the bar cutoff details. But these details are appropriate for permitting non-standard loads. The asphalt is considered to be 1.75 in. as defined in AASHTOWare under girder profile menu. The concrete strength is 2500 psi and reinforcement yield strength is 33,000 psi. These parameters are shown in Figures 5-1 and 5-2 below.

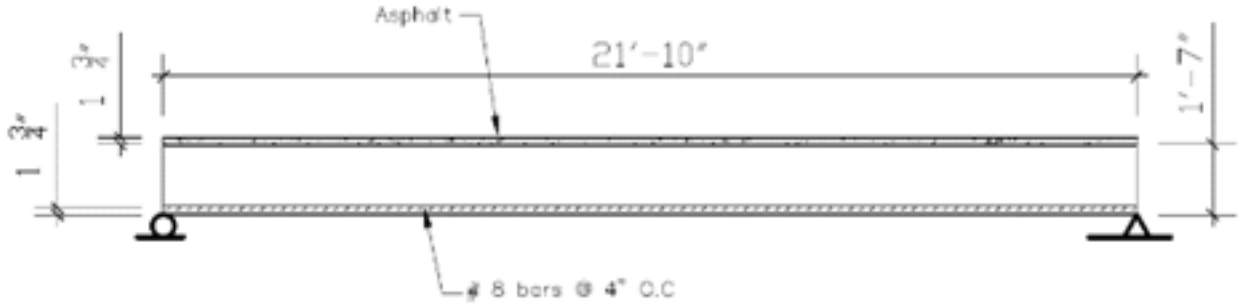

Figure 5-1: The Elevation View of the Final Model

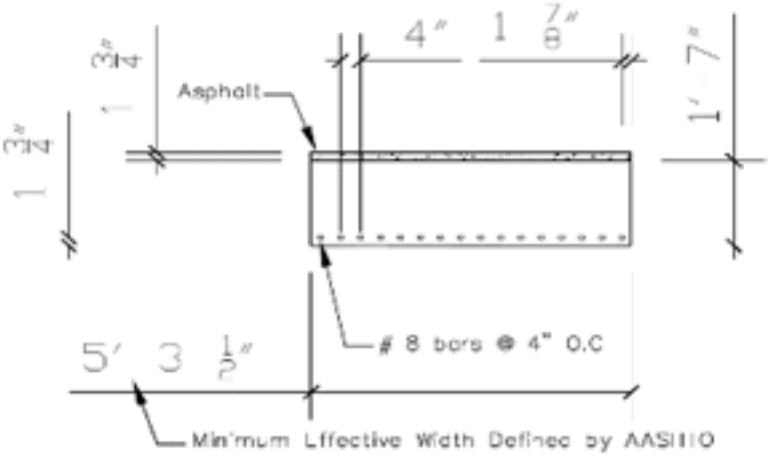

Figure 5-2: The Final Configuration of the Model as One Effective Width

One method of defining the capacity is rating of this structure such as the LFR rating. A rating is a function of dead load, live load, and the cross sectional capacity. Dead load is a function of the weight of the structure and for this exiting structure with known geometry dead load cannot be modified. Live load is a function of the truck load and boundary conditions. The best evaluation of live load is considered upon the maximum effect that the truck has on the structure through structural analysis. The cross sectional capacity is a function of effective depth, the amount of steel, material strength, and the effective width. Although the impact of the dead load and live load are not adjustable, increasing the cross sectional capacity can increase the rating of the structure. The amount of reinforcement, geometry, and the strength of the concrete were defined through field tests; hence, choosing an effective width larger than the value defined by AASHTO was the most appropriate parameter that could incorporate additional capacity into an AASHTOWare model while keeping the measured parameters the same as those measured in the field.

In this chapter, load ratings of AASHTOware models are investigated for effective widths ranging from the value specified by AASHTO (MBE, 2011), which is the lower bound, to an upper bound of one-fourth of the roadway width. The lower bound is defined using Equation 27 in Chapter 2 and for a 21 ft-10 in. span. This formula results in an effective width of 5.31 ft, that is 63.72 in. The effective widths were incrementally increased by 4 in. until the width reached an upper bound of one-fourth of the roadway width which is 91.72 in. The reason for this upper bound comes from the geometry of the roadway and the number of traffic lanes. The current AASHTO (17th ed., 2002) requires a minimum value of 12 ft as the lane width. The full road way is 31.4 ft. This width provides sufficient width for two traffic lanes allowing for two trucks simultaneously on the roadway. This configuration results in a maximum number of four wheel-lines, two wheel-lines per truck, on the road which means one-fourth of the roadway width is the maximum effective width which carries one wheel-line without overlap of the effective widths. These effective widths were rated for the LFR operating rating for all ALDOT standard trucks. First, these models are based on the original segment of the roadway. This segment is the widest segment and it has the highest capacity in the structure. The parameters used to model these effective widths are listed above and Figure 5-1 shows the cross section.

Table 5-1: Summary of Reinforcement for Each Effective Width of Slab in the Original Segment

Effective Width (E)(in.)	Bar Size	# of Full Length Bars	# of Bars Cut off at 3.5 ft from supports	Edge Distance (in.)	Spacing (in.)	Effective Depth (in.)
63.7	# 8	11	5	1.86	4	17.25
67.7	# 8	12	5	1.86	4	17.25
71.7	# 8	12	6	1.86	4	17.25
75.7	# 8	13	6	1.86	4	17.25
79.7	# 8	14	6	1.86	4	17.25
83.7	# 8	14	7	1.86	4	17.25
87.7	# 8	15	7	1.86	4	17.25
91.7	# 8	16	8	1.86	4	17.25

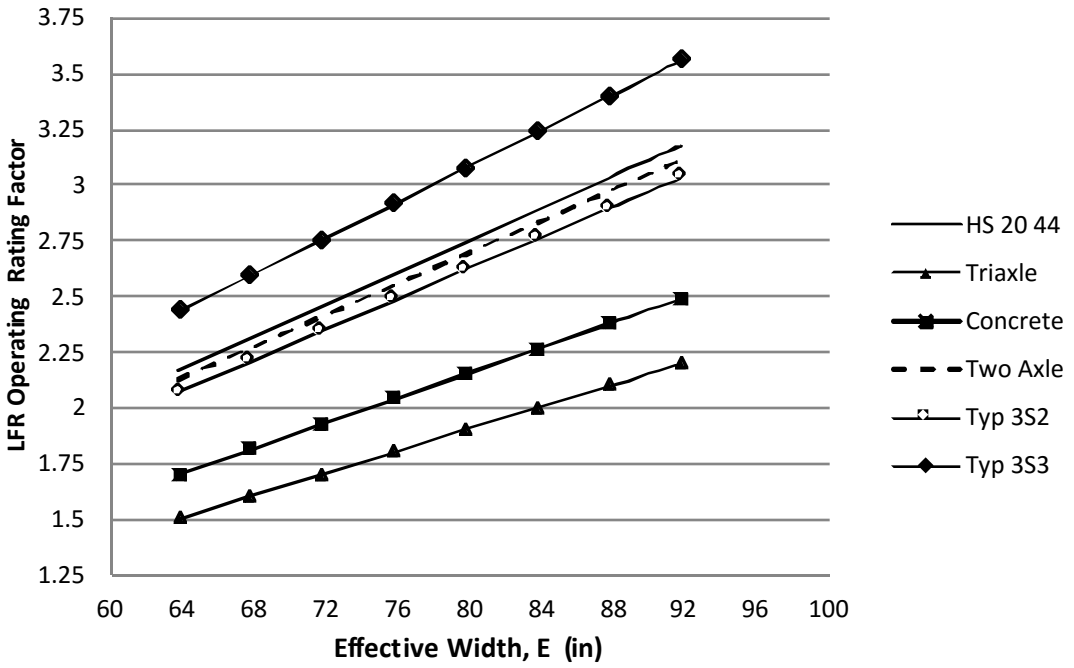

Figure 5-3: LFR Operating Rating Factor of the Original Segment of the Barnes Slough Bridge for Six of the ALDOT Standard Trucks

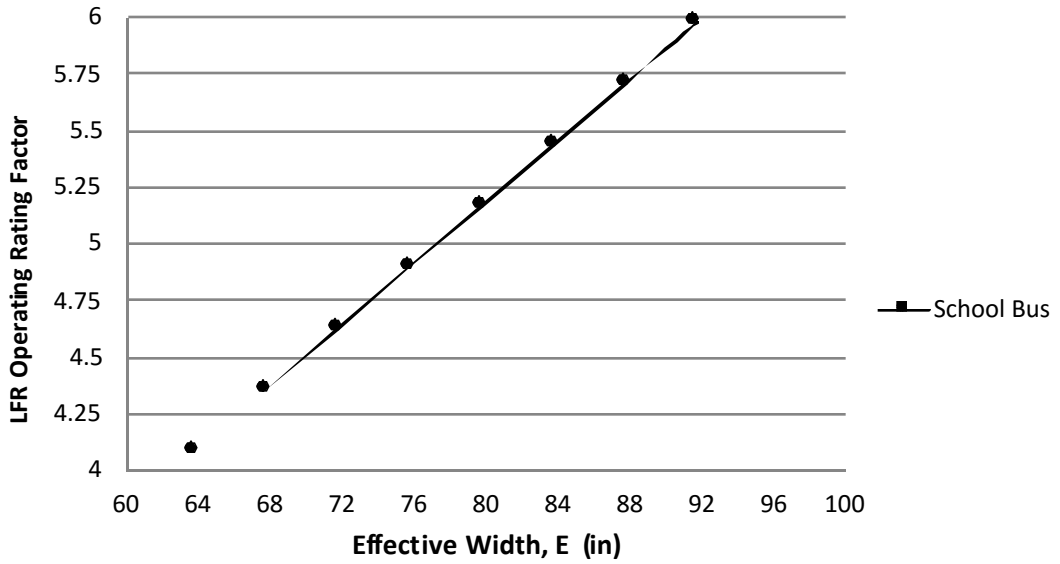

Figure 5-4: LFR Operating Rating Factor of the Original Segment of the Barnes Slough Bridge for the School Bus

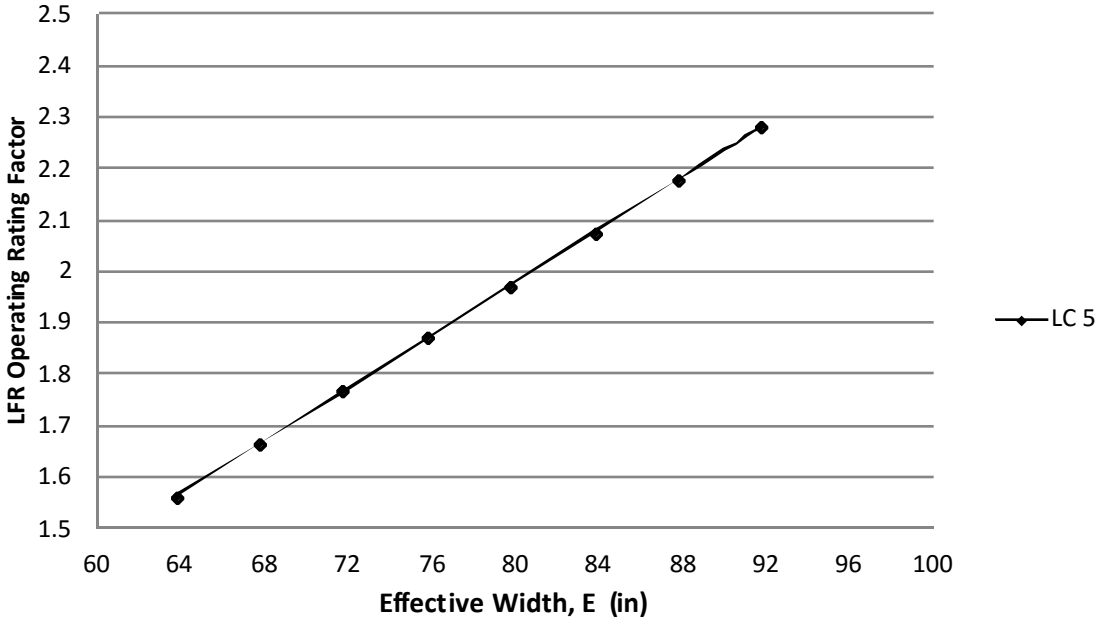

Figure 5-5: LFR Operating Rating Factor of the Original Segment of the Barnes Slough Bridge for the LC 5 Test Truck

AASHTOWare uses the number of bars in the effective width, and not the bar spacing, to calculate the capacity. For this reason, the effective width was increased in increments of the bar spacing at 4 in. Table 5-1 shows the number of bars for the model of each effective width. Figures 5-3 through

5-5 show the graphs of effective widths versus the operating rating factors for Barnes Slough Bridge.

In addition to modeling the strongest segment of the bridge and providing ratings, the weakest segment, the East segment, was also modeled to investigate the smallest ratings for this bridge. This comparison allows for a better judgment of the structures' capacity and choosing an appropriate effective width as the width of the final model. Table 5-2 shows the summary of bar configuration for each effective width of slab in the East segment. Figures 5-6 through 5-8 show the operating rating factors for all ALDOT standard trucks of these effective widths.

Table 5-2: Summary of Reinforcement for Each Effective Width of Slab in the East Segment

Effective Width (E)(in.)	Bar Size	# of Full Length Bars	# of Bars Cut off at 3.5 ft from supports	Edge Distance (in.)	Spacing (in.)	Effective Depth (in.)
63.7	#8	6	3	1.9	7.5	17.25
67.7	# 8	7	3	1.9	7.5	17.25
71.7	# 8	7	4	1.9	7.5	17.25
75.7	# 8	9	3	1.9	7.5	17.25
79.7	# 8	9	4	1.9	7.5	17.25
83.7	# 8	9	5	1.9	7.5	17.25
87.7	# 8	10	5	1.9	7.5	17.25
91.7	# 8	11	5	1.9	7.5	17.25

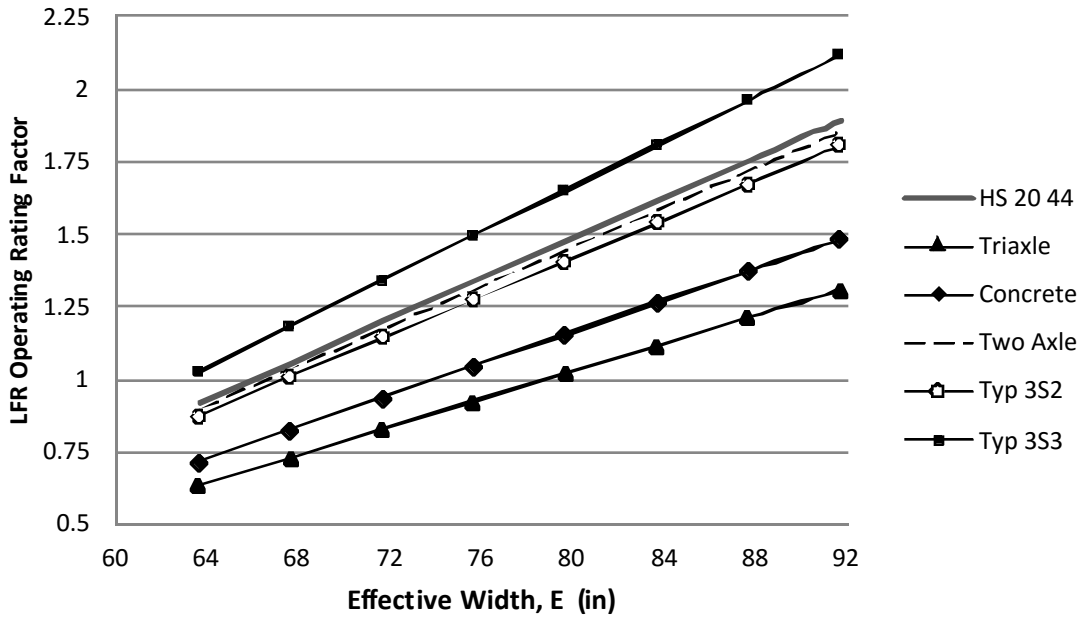

Figure 5-6: LFR Operating Rating Factor of the East Segment of the Barnes Slough Bridge for Six of the ALDOT Standard Trucks

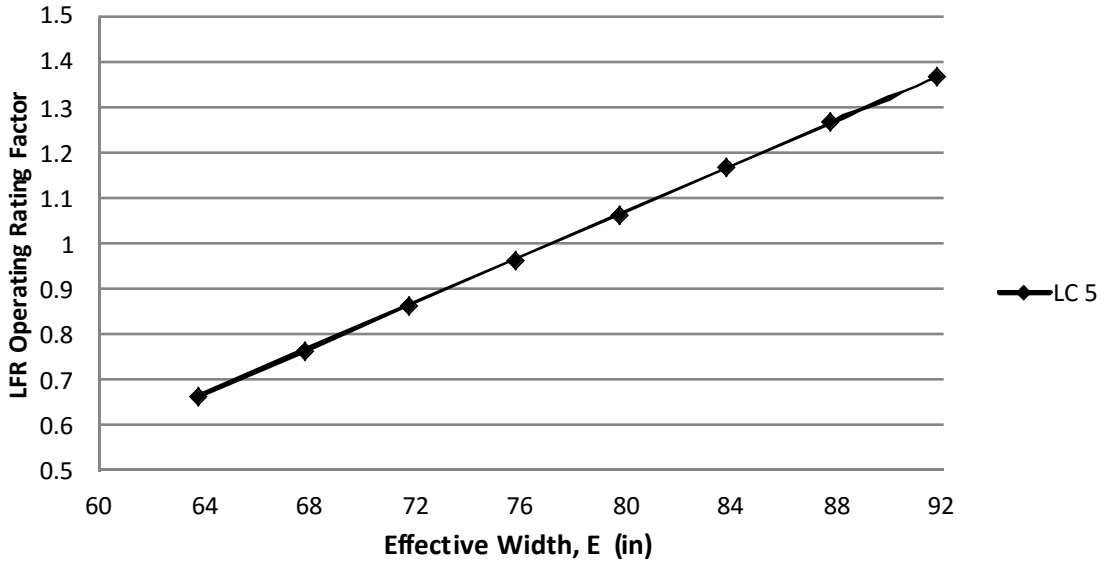

Figure 5-7: LFR Operating Rating Factor of the East Segment of the Barnes Slough Bridge for the LC 5 Test Truck

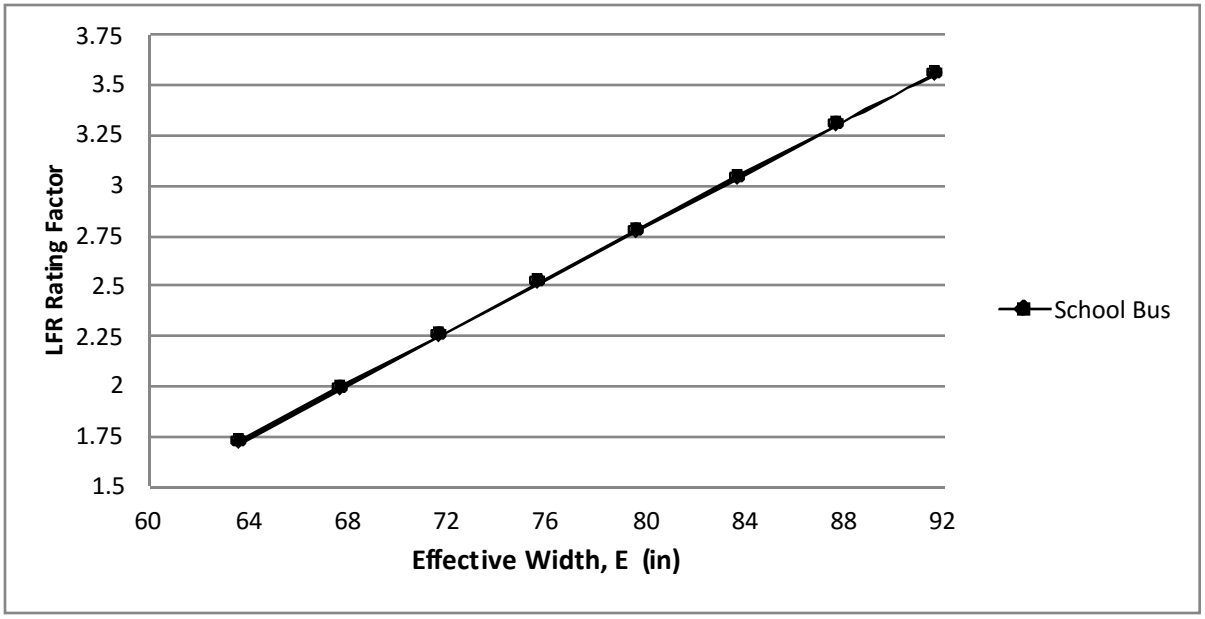

Figure 5-8: LFR Operating Rating Factor of the East Segment of the Barnes Slough Bridge for the School Bus

5.3 Application of Results

The previous section presented relationships between effective slab width and the rating factor of the model for permit loads determined by ASHTOWare. These relationships provide a means of linking the live load tests and finite element analyses (reported in Chapter 7) to an AASHTOWare model. If the rating factor determined by the finite element analyses is 2 for the triaxle truck, Figure 5-3 shows that an effective width of 84 in. should be used in AASHTOWare to have the same rating factor for the permit model of Figure 5-1.

6 Live-Load Tests

6.1 Introduction

Three kinds of tests were conducted. The first test was conducted for determining the static response under multiple load patterns. This test was performed with one or two trucks stopped at specific locations. Load patterns with one truck placed in the middle of travel lane were repeated three times for left lane and four times for right lane. Load patterns with one truck placed 1 ft from curb were repeated three times for both lanes. Load patterns with two trucks side-by-side placed 1 ft from curb were repeated two times for both lanes. Then, load patterns with one truck in the middle of travel lane were repeated with the trucks moving at a crawling speed (three times for right lane, four times for left lane). Finally, the trucks moved over the bridge at a speed of 61 mph, to check the dynamic response of the bridge. This load pattern was conducted only for right travel lane and repeated two times. All load patterns are presented in detail in the Appendix A-1.

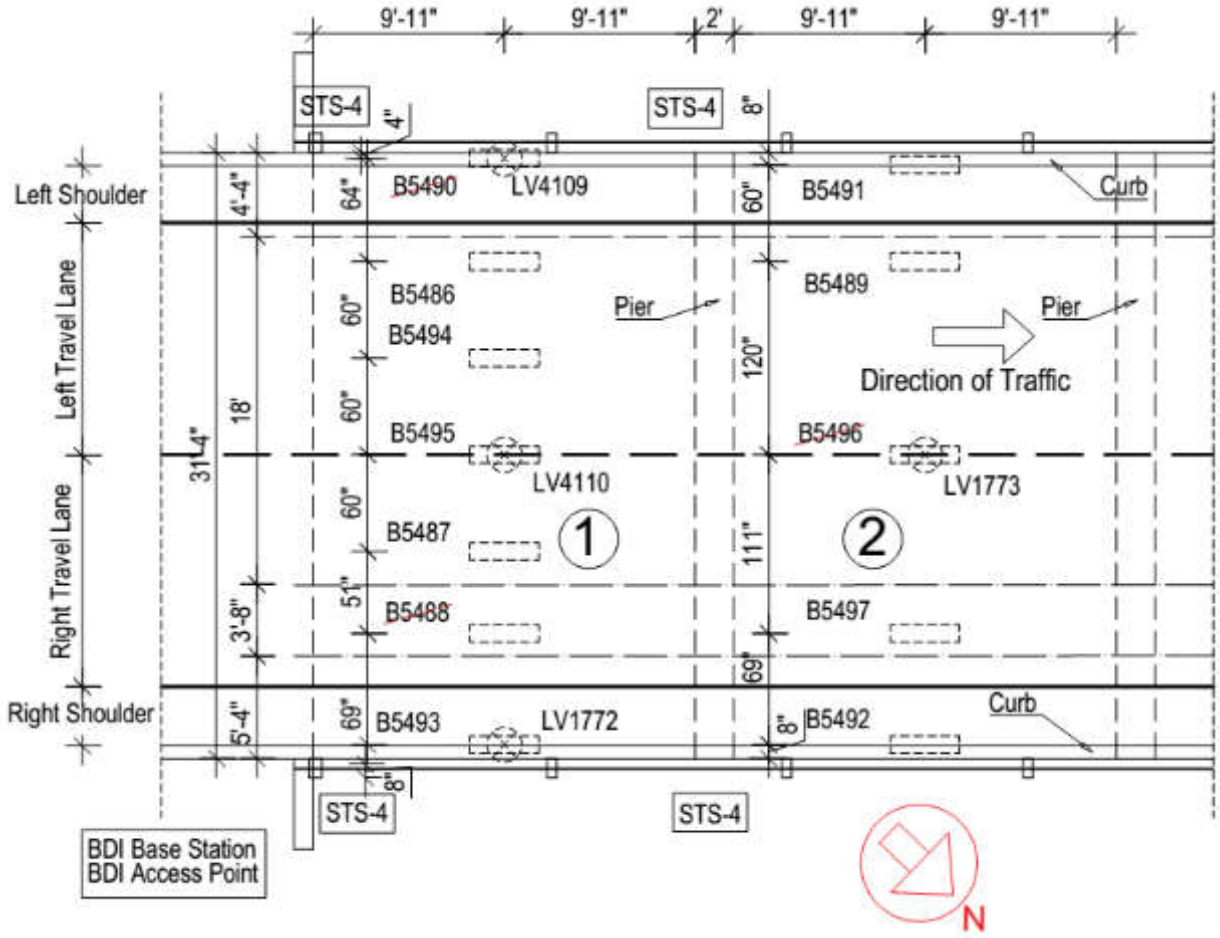

Figure 6-1: Location of Strain Transducers (BXXXX) and LVDT's (LVXXXX) at the Bottom of the Bridge Slab

Various equipment was utilized during the live load tests. For measurements of the strain, strain transducers with special extensions were mounted at the bottom of the slab (Figure 6-1) and covered with aluminum foil to reduce "drift" effect which comes from the change of the temperature of the sensor (Figure 6-2, Figure 6-3). The deflections were measured using LVDT's and optical devices.

Figure 6-2: Strain Transducer Covered with Aluminum Foil and One LVDT (Photo by ALDOT)

Figure 6-3: Sensors Mounted Under the Bridge (Photo by ALDOT)

6.2 Measuring Devices

Twelve strain transducers (Figure 6-4 left) with extensions and four LVDT's (Figure 6-4 right) from Bridge Diagnostics, Inc. Company were used.

Figure 6-4: Strain Transducer (left) and LVDT (right)

The BDI system consisted of Base Station, Access Point, Data Acquisition Nodes and Sensors (Figure 6-5). Sensors were connected to Data Acquisition Nodes with cables. Data Acquisition Nodes were connected to Base Station and Access Point through Wi-Fi. Computer was also connected with Access Point through Wi-Fi. To record data, BDI STS-Live software was used and it generated files which were later processed in MS Excel to summarize and plot the results. Furthermore, the whole system was tested and checked in the university lab before the field tests.

Figure 6-5: BDI Testing System

6.3 Applied Test Load

Two 85-kip trucks (Figure 6-6) were used as the load and they were placed on the bridge in 9 different configurations. Trucks were placed in both lanes of the bridge to check if there was an agreement and symmetry in the transverse response in the slab (Figure 6-7).

After analysis of the results, data recorded by three of the strain transducers (B5488, B5490 and B5496) were concluded to be unusable and they were excluded (see crossed-out sensors in the Figure 6-1).

Due to usage of 18-inch aluminum extensions (original gage length is 3 inch), recorded values of strains were multiplied by 6 and divided by the factor of 1.1 according to BDI documentation. Additionally, the speed of the trucks during dynamic load tests was confirmed. The most valuable and interesting plots and tables are presented in detail in the Appendix A-2.

Figure 6-6: ALDOT's LC-5 Truck (Photo from ALDOT)

Figure 6-7: Example of Load Pattern (Photo by ALDOT)

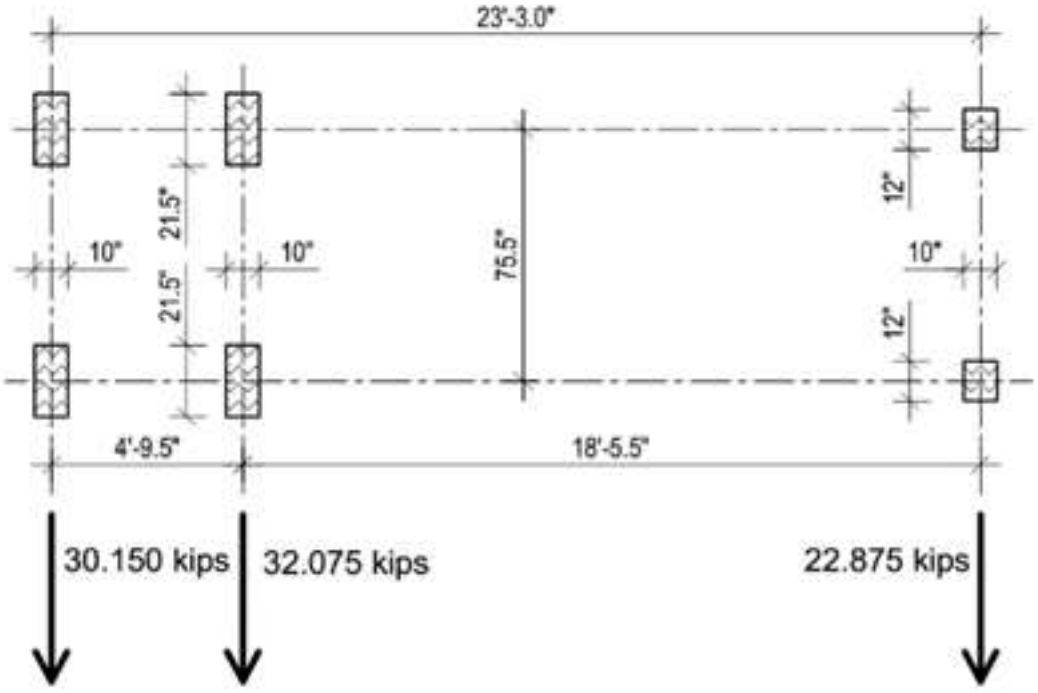

Figure 6-8: Axle Weights and Axle Spacing of ALDOT's LC-5 Truck

Figure 6-9: Preparations to the Load Tests (Photo by ALDOT)

Figure 6-10: Longitudinal Position of the Test Truck During the Load Tests (Photo by ALDOT)

Figure 6-11: Adjustment of the Location of the Test Truck During Load Test (Photo by ALDOT)

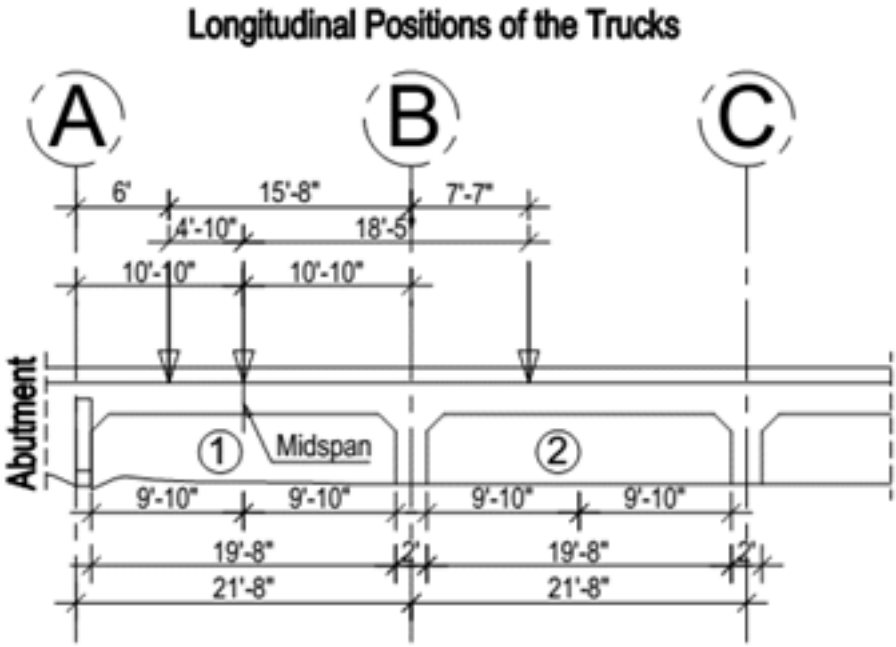

Figure 6-12a: Longitudinal Positions of the Test Trucks for Span 1

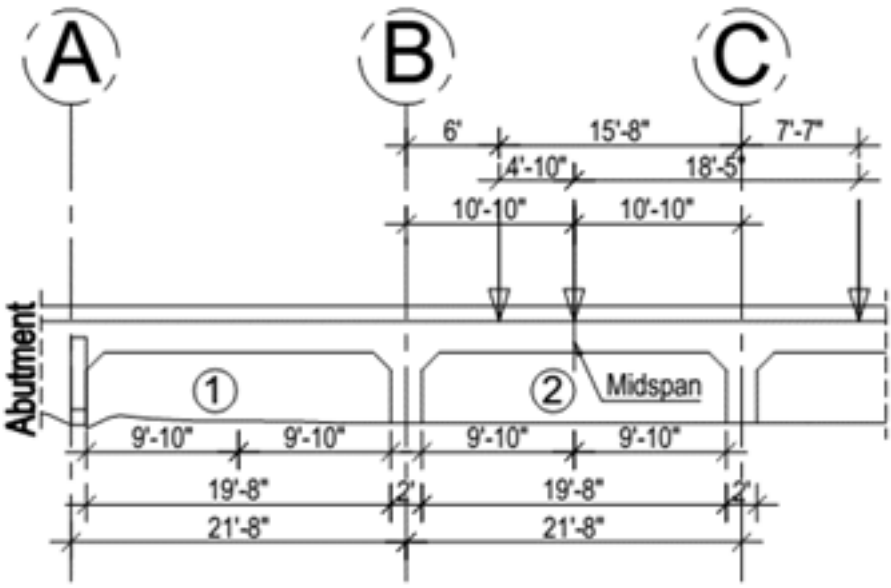

Figure 6-12b: Longitudinal Positions of the Test Trucks for and Span 2

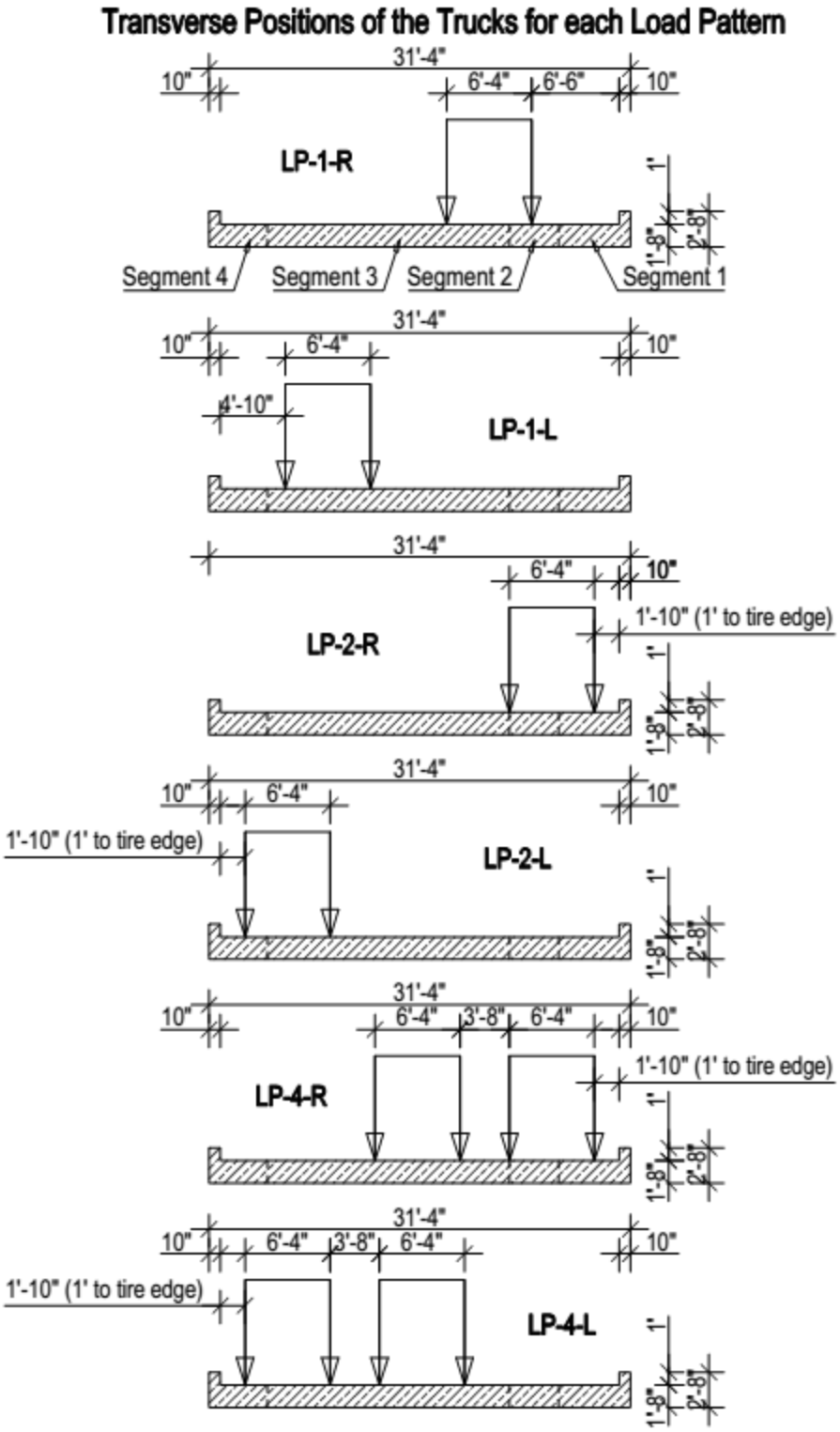

Figure 6-13: Transverse Positions of the Test Trucks for Each of the Load Patterns

6.4 Strain Measurements

For all of the static load patterns, measured values of the strains for span 1 and span 2 (averaged values for each load pattern) were compared. For span 1, the pattern of strains measured for the oldest (middle) part of the slab are symmetrical for corresponding load patterns as shown in Figure 6-14. Figure 6-15 shows the strains measured in span 2, and for corresponding load patterns these values are reasonably symmetric for both edges of the slab (newer parts of the bridge).

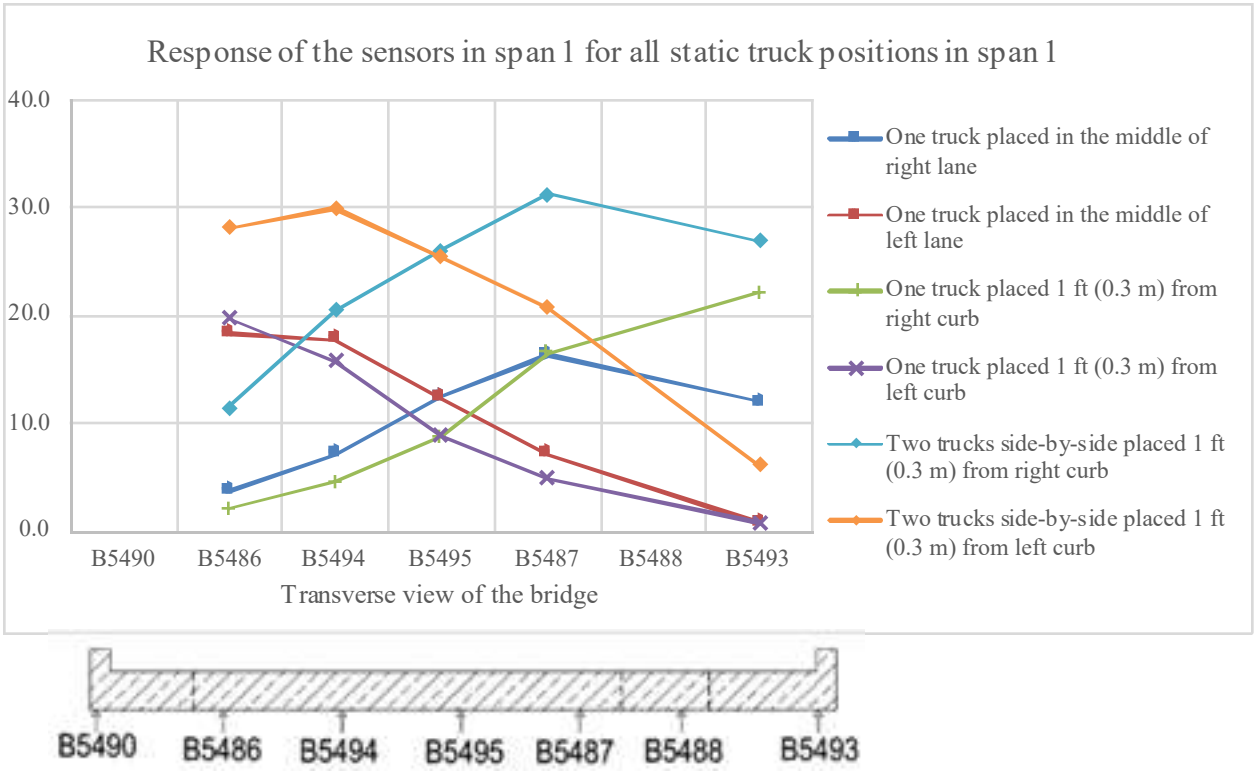

Figure 6-14: Transverse Response of Span 1 for All of the Static Load Patterns – Strains (με)

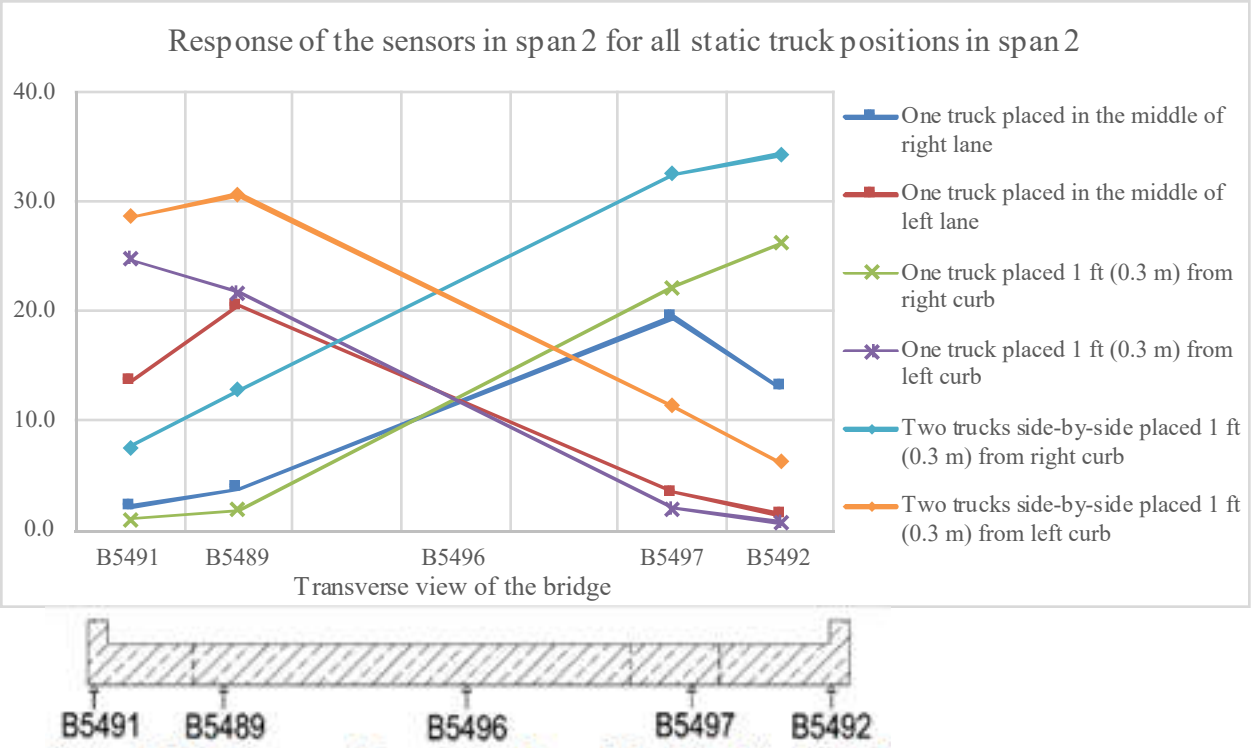

Figure 6-15: Transverse Response of Span 2 for All of the Static Load Patterns – Strains (με)

Table 6-1a and Table 6-1b present a summary of strains recorded during the load tests (averaged values for each load pattern). The largest measured strain was 34με under span 2. The critical load pattern was LP-4-R with two trucks side-by-side close to the curb on the right side of the bridge.

Table 6-1a: Summary of Strains for Each Static Load Pattern (με) – Span 1

Load Pattern	Description	B5486	B5494	B5495	B5487	B5493
LP-1-R	One truck placed in the middle of right lane	4	7	12	16	12
LP-1-L	One truck placed in the middle of left lane	18	18	12	7	1
LP-2-R	One truck placed 1 ft from right curb	2	4	9	16	22
LP-2-L	One truck placed 1 ft from left curb	20	16	9	5	1
LP-4-R	Two trucks side-by-side placed 1 ft from right curb	11	20	26	**31**	27
LP-4-L	Two trucks side-by-side placed 1 ft from left curb	28	30	25	21	6

Table 6-1b: Summary of Strains for Each Static Load Pattern (με) – Span 2

Load Pattern	Description	B5491	B5489	B5497	B5492
LP-1-R	One truck placed in the middle of right lane	2	4	19	13
LP-1-L	One truck placed in the middle of left lane	14	20	4	1
LP-2-R	One truck placed 1 ft from right curb	1	2	22	26
LP-2-L	One truck placed 1 ft from left curb	25	22	2	1
LP-4-R	Two trucks side-by-side placed 1 ft from right curb	8	13	32	**34**
LP-4-L	Two trucks side-by-side placed 1 ft from left curb	29	31	11	6

6.5 Deflection Measurements

Measured deflections for span 1 and span 2 were compared. The pattern of deflections shown in Figure 6-16 and Figure 6-17 is consistent with expectations and the deflections in span 1 are reasonably symmetric.

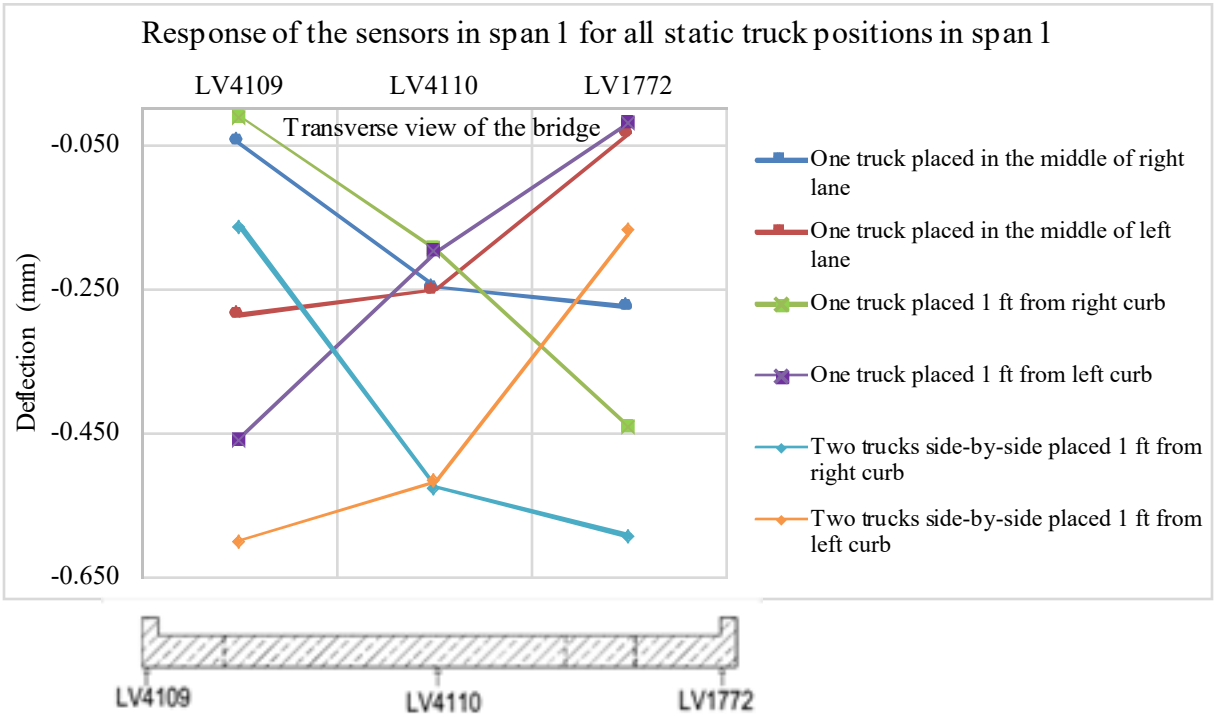

Figure 6-16: Deflections for Each of the Static Load Patterns – Span 1

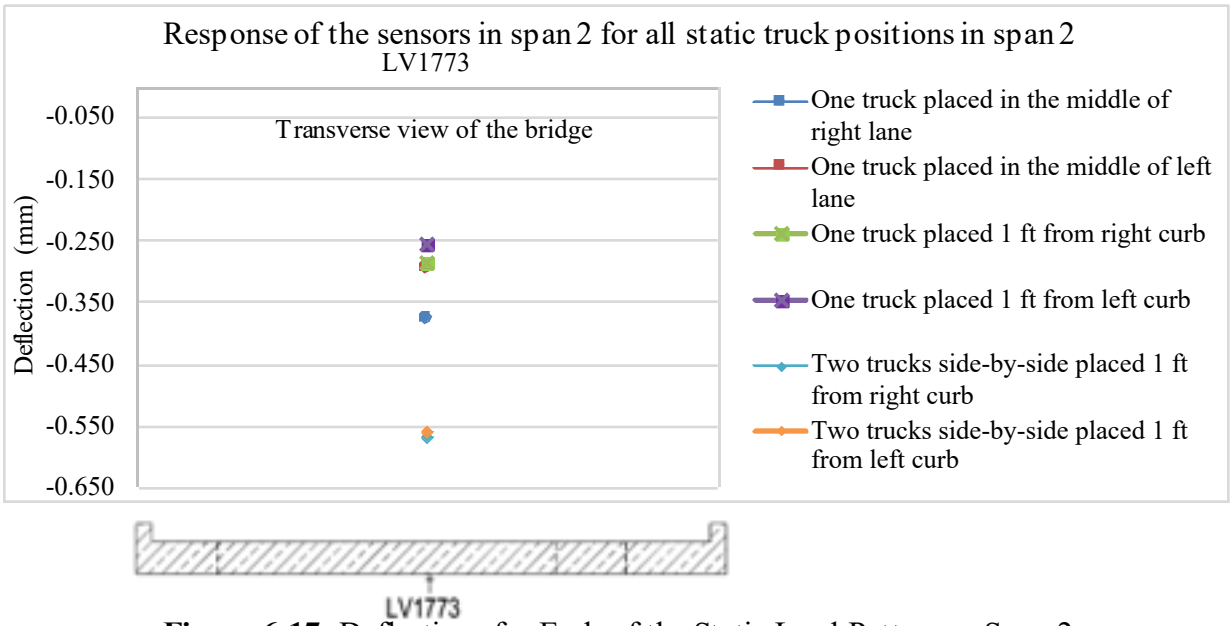

Figure 6-17: Deflections for Each of the Static Load Patterns – Span 2

Measured values of deflections at midspan, at the middle of the bridge's width were also compared for all of the load patterns. Behavior of the slab for both spans is very similar. Deflections recorded for span 2 are slightly higher than those measured in span 1 (Figure 6-18).

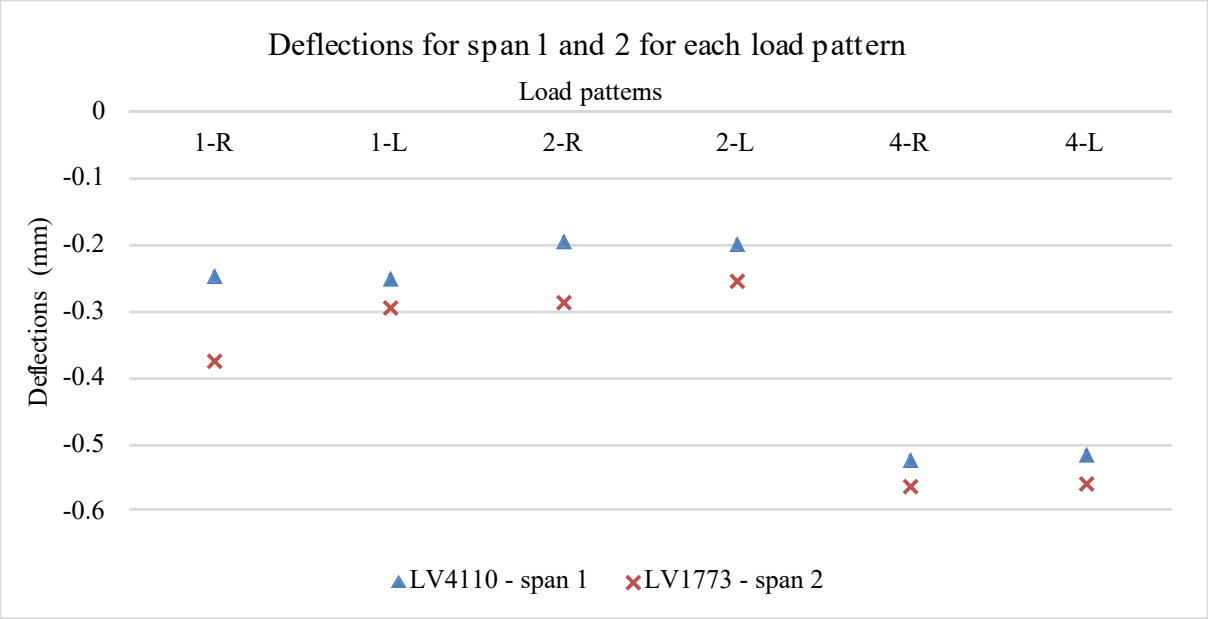

Figure 6-18: Comparison of Deflections Measured in Span 1 and Span 2 at the Middle of the Bridge Width

Table 6-2 presents a summary of the deflections recorded during load test. The largest deflection of 0.598 mm was recorded at the west side of span 1. That deflection occurred under load pattern LP-4-L with two trucks placed side-by-side close to the curb on the west side of the bridge.

Table 6-2: Summary of Deflections for Each Static Load Pattern (mm)

Load Pattern	Description	SPAN 1			SPAN 2	
		LV4109	LV4110	LV1772	Load Pattern	LV1773
LP-1-R	One truck placed in the middle of right lane	-0.046	-0.248	-0.273	**LP-1-R**	-0.376
LP-1-L	One truck placed in the middle of left lane	-0.286	-0.250	-0.033	**LP-1-L**	-0.295
LP-2-R	One truck placed 1 ft from right curb	-0.011	-0.193	-0.442	**LP-2-R**	-0.287
LP-2-L	One truck placed 1 ft from left curb	-0.458	-0.198	-0.018	**LP-2-L**	-0.253
LP-4-R	Two trucks side-by-side placed 1 ft from right curb	-0.162	-0.524	-0.592	**LP-4-R**	**-0.566**
LP-4-L	Two trucks side-by-side placed 1 ft from left curb	**-0.598**	-0.515	-0.167	**LP-4-L**	-0.558

6.6 Comparison of Strains and Deflections

Strains and deflections for load patterns with one truck in the middle of right travel lane during the state, crawling speed, and normal speed tests are compared in Figure 6-19 and Figure 6-20. They were measured by sensors B5487 and LV1772 respectively. For each of the load patterns, the truck was in the middle of the east traffic lane. The first load pattern (LP-1-R) was static, for the span 2 (LP-3-R-CS) the truck passed over the bridge at a crawling speed, and for the third (LP-5-R-Dyn) the truck was at a normal traffic speed (61mph). There is no significant difference in strains caused by the speed of the truck. For deflections in Span 2, value for the static load pattern is approximately 20% higher than for the other load patterns.

Table 6-3: Comparison of Strains for Different Load Pattern (με) – Span 1 and Span 2

Load Pattern	Description	SPAN 1	SPAN 2
LP-1-R	One truck placed in the middle of right lane	16	19
LP-3-R-CS	One truck, middle of right lane, Crawling Speed	18	19
LP-5-R-Dyn	One truck, middle of right lane, Normal Speed	15	20

Table 6-4: Comparison of Deflections for Different Load Pattern (mm) – Span 1 and Span 2

Load Pattern	Description	SPAN 1	SPAN 2
LP-1-R	One truck placed in the middle of right lane	-0.273	-0.376
LP-3-R-CS	One truck, middle of right lane, Crawling Speed	-0.300	-0.290
LP-5-R-Dyn	One truck, middle of right lane, Normal Speed	-0.266	-0.322

6.7 Comparison of Measured and Calculated Values

Maximum theoretical values of strains and deflections were calculated according to the AASHTO simplified analysis procedure using one wheel-line of loading on an effective width of slab. The uncracked transformed properties of the slab cross section were used for the calculations. Two situations were considered: simply supported and fixed-fixed boundary conditions. Effective width, effective depth, reinforcement properties and concrete strength were assumed according to Chapter 5 of this report. These calculated values were compared with the maximum measured values of strains (34 με) and deflections (0.598 mm) from the live load tests. Calculated values of strains for simple support and fixed-fixed boundary conditions are 117 με and 36 με, respectively. Calculated deflections for simple support and fixed-fixed boundary conditions are 2.160 mm and 0.490 mm, respectively.

6.8 Summary and Conclusions

In this Chapter live load test procedure and results were described. Values for deflections and for strains recorded during the load tests were very small, as expected. Even for the most critical load pattern with two test trucks together in one span, the bridge did not crack. This confirms the overall good condition of the structure and its reserve flexural capacity. Measured values of strains and deflections show reasonable symmetry in bridge's behavior, especially for the oldest part of the slab. Comparison between calculated theoretical values of strains and deflections and measured during live load tests shows that calculated strains both for simply support and fixed-fixed boundary conditions are larger that measured during load tests. For deflections, for simply support boundary conditions calculated values are significantly larger, for fixed-fixed boundary conditions, they are slightly smaller than measured on the field.

7 Finite Element Method Analysis

7.1 Introduction

A three dimensional Finite Element (FE) Model of a single span, the first span at the south end of the bridge, was developed in Simulia Abaqus FE Software (Abaqus 2014). Findings from field measurements (Chapter 4 Section 4.3), as well as relative similarity of the measured deflections and strains for both spans tested (Chapter 6) led to the conclusion that the model of one span will best reflect the behavior of the bridge. The model was developed using solid and beam elements, which allowed for a detailed investigation of local stress and strain distributions as well as overall bridge behavior.

The model contains upper pieces of the piers, slab, bottom reinforcing bars, and curbs. Dimensions of the piers, segments of slab and reinforcement are as specified in Section 4.2 of this report. The curbs have cross-sectional dimensions of 8x10in. Four different width segments, fully bonded with each other, create the slab cross section of the bridge.

Preliminary analyses assured researches that the bridge was capable of carrying two LC-5 Trucks with GVW=85kip each during live load tests. After the load tests were performed the FE model was calibrated to have the same response as the real structure.

This chapter contains description and discussion of the finite element types used in the model, the development and application of numerical, nonlinear material models and presents boundary conditions, constraints and loads applied. Results of Finite Element Analyses (FEA) are shown in section 7-5, while section 7-6 presents determination of bridge ratings from FEA.

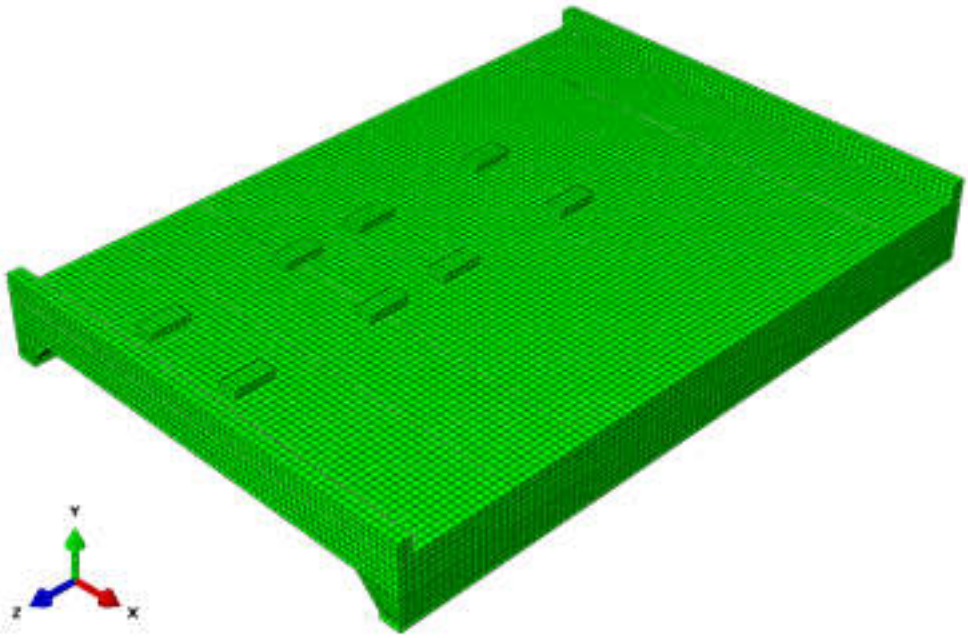

Figure 7-1: Isometric View of the FE Model of the Bridge

7.2 Element Types

Among various element types available in Finite Element Method only elements that were used in the model of the bridge are presented. The concrete elements - curbs, slab segments and piers were modelled with 8-noded linear brick elements with reduced integration (C3D8R) - Figure 7-2a. Reduced integration element was chosen due to its computational cost, which is smaller than for a full-integration element. The element type used for reinforcing bars is a 2-node linear beam element (B31) - Figure 7-2b. The advantage of the beam, over widely used link elements in FE modelling of reinforcement, is its ability to act in compression as well as in tension. Both element types selected, C3D8R and B31, have six degrees of freedom at each node – translations and rotations in the nodal x, y, and z directions. For stress/displacement simulations the degrees of freedom are the translations for brick elements, and for the beam elements rotations and translations at each node. The application of solid elements for concrete elements allowed for a more detailed investigation of local stress and strain distributions.

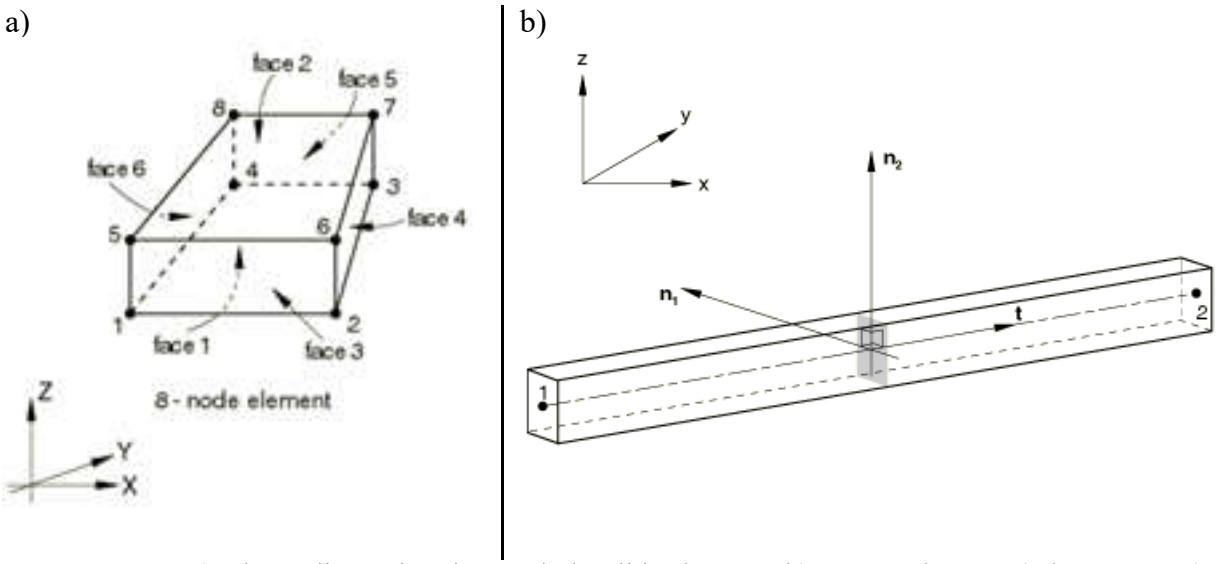

Figure 7-2: a) Three-dimensional 8-noded Solid Element, b) Beam Element (Abaqus 2014)

The reinforcing bars were modelled as in the real structure (Table 4-4), the reinforcement is embedded into slab. From the numerical method point of view an embedded rebar acts as fully bonded with concrete slab. Although, the rebars occur in all of the concrete elements they were modelled in the slabs only. Modelling of the reinforcement in other elements was not critical.

The mesh study showed that the most effective mesh size, in terms of accuracy and computing time, is 4x4x3.8 in. for the brick elements and 4 in. of length for the beam elements.

7.3 Numerical Material Models

To develop numerical material models all collected data with available literature was reviewed. The FE method requires specification of material parameters such as modulus of elasticity,

Poisson's ration and stresses with corresponding strains in non-linear stress ranges. Two non-linear material models, Concrete Damage Plasticity (CDP) for concrete and elasto-plastic for steel, were implemented into the FE model. Material non-linearity is justified by need for accurate stress investigation under loads causing concrete cracking and non-linear material behavior. Details on material models development is described in following sections.

7.3.1 Concrete Material Model

The CDP model available in Abaqus software requires parameters are associated with simplified Drucker-Prager concrete strength hypothesis. The dilation angle, eccentricity, f_{b0}/f_{c0} ratio (point in which the concrete undergoes failure under biaxial compression), K_c parameter (ratio of the distances between compression and tension meridians in the deviatoric cross section) as well as Viscosity parameter describe behavior of concrete in biaxial stress state. Description and selection of these parameters are available in Abaqus Manual (Dassault Systèmes 2014) and in (Kamiński 2011). In addition to those, CDP model requires stress-strain data within inelastic region for compressive and tensile behavior. These can be determined from strain-stress curve. Due to the lack of accurate stress-strain data for the concrete samples taken, the relationship curves had to be approximated as described below.

ACI 318-14 provides the formula (Eq-39), where modulus of elasticity E_c is a function of f'c.

$$E_c = 57000\sqrt{f_c'} \qquad \text{(Eq-39)}$$

where:

E_c = Initial Modulus of Elasticity (psi)
f'_c =Compressive Strength of concrete (psi)

During the calibration process it was found out that Eurocode formula (EN 1992-1-1 2004) for the modulus of elasticity (Eq-40, Eq-41) adopted to the FE model produce values of strains and deflections which match the measured values better. The Eurocode formula for modulus of elasticity was used and is presented below.

$$E_c = 22000\,(f_c')^{\frac{1}{3}} \qquad \text{(Eq-40)}$$

$$E_c = 3191\left(\frac{f_c'}{1.45}\right)^{\frac{1}{3}} \qquad \text{(Eq-41)}$$

Where in Eq-40 E_c and f'_c are in MPa, while in Eq-41 E_c and f'_c are in ksi. The equation Eq-41 is a transformation of Eq-40 to US units.

The compressive stress-strain relationship curves were modelled with the Desayi and Kirshnan (Desayi, 1964) equation (Eq-42).

$$\sigma_c = \frac{E\varepsilon_c}{1 + \left(\frac{\varepsilon_c}{\varepsilon_0}\right)^2} \qquad \text{(Eq-42)}$$

where:

σ_c = Compressive stress
ε_c = Compressive strain
ε_0 = Strain at maximum stress
E = Initial tangent modulus, assumed to be twice the secant modulus at maximum stress σ_{max}

It is assumed that numerical concrete material models perform linearly up the stress of $0.4f'_c$. The difference in stress-strain curve shape for different values of modulus of elasticity are shown in Figure 7-3.

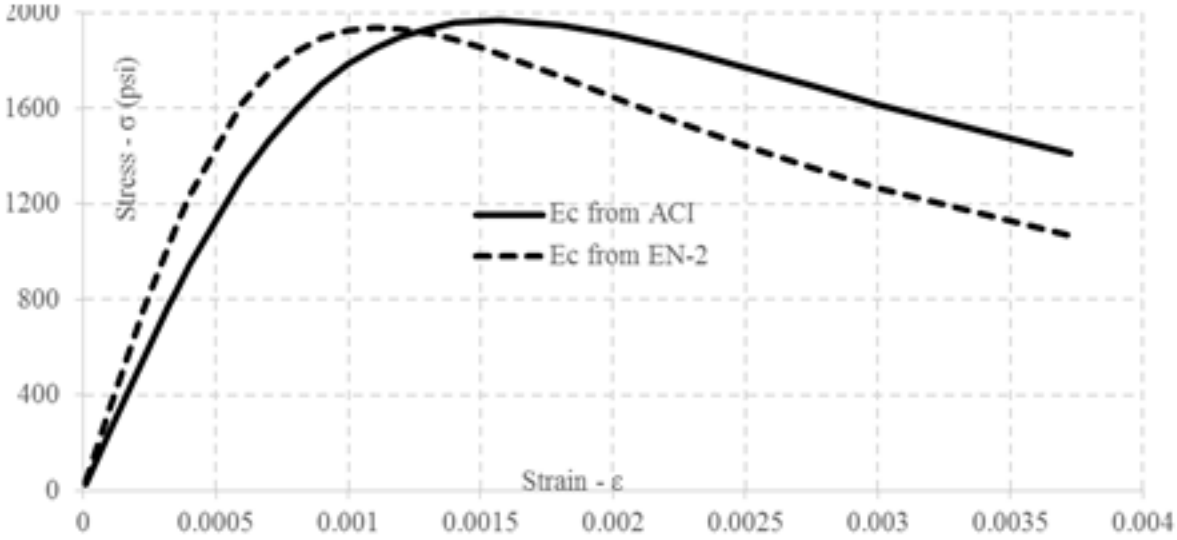

Figure 7-3: Stress-strain Curves for Concrete with Compressive Strength 1960psi

The tensile stress-strain relationship was developed using the Wang and Hsu formula (Hsu, Wang 2001) which most accurately describes concrete tension stiffening.

$$\sigma_t = E_c \varepsilon_t \; if \; \varepsilon_t \leq \varepsilon_{cr}$$
and
$$\sigma_t = f'_c \left(\frac{\varepsilon_{cr}}{\varepsilon_t}\right)^{0.4} \; if \; \varepsilon_t > \varepsilon_{cr} \qquad \text{(Eq-43)}$$

where:

σ_t = Tensile stress
ε_t = Tensile strain
ε_{cr} = Cracking strain

To establish cracking strain the modulus of rupture must be known. AASHTOs' formula, equation Eq-44, was used to establish the tensile strength of the concrete.

$$f_r = 7.5\sqrt{f'_c} \qquad \text{(Eq-44)}$$

Based on concrete core test results (Table 4-5), four different compressive strengths of concrete were taken for each of the four segments of the bridge. For each of the slab's segments, the approximated stress-strain relationships were developed for the compressive and the tensile behavior. The compressive strengths used as well as the values of corresponding moduli of elasticity are shown in the Table 7-1.

Table 7-1: Parameters of Concrete for each Slab Segment

Segment	4 (West Bound)	3	2	1 (East Bound)
Compressive Strength, *f'c* (psi)	1850	3340	1760	1940
Modulus of Elasticity, *E* (ksi)	3433	4098	3382	3482

The developed stress-strain relationships for each of the slab segments are shown in Figure 7-4.

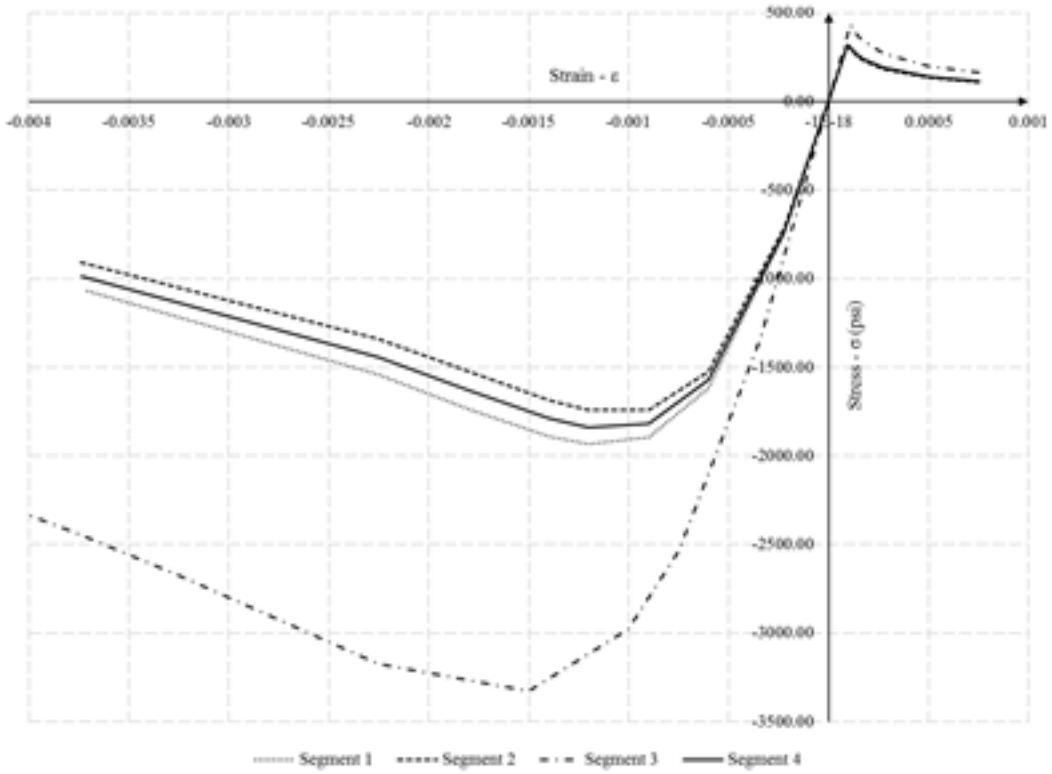

Figure 7-4: FEM Input Stress-Strain Curves for Segments 1-4

7.3.2 Steel Material Model

Provisions from AASHTO Manual for Bridge Evaluation (AASHTO, 2011) allowed to develop the material model for reinforcing steel bars. The Manual recommends the yield strength of steel of 33ksi for unknown reinforcing steels in bridges built prior to 1954. For assumed modulus of elasticity of 29000ksi the reinforcing bars reach yielding at strain value of 0.1% The ultimate tensile strength of steel was taken as 55ksi (CRSI, 2001) and assumed to occur at strain of 1.0%. Within the inelastic region the stress-strain relationship is assumed linear for computational stability.

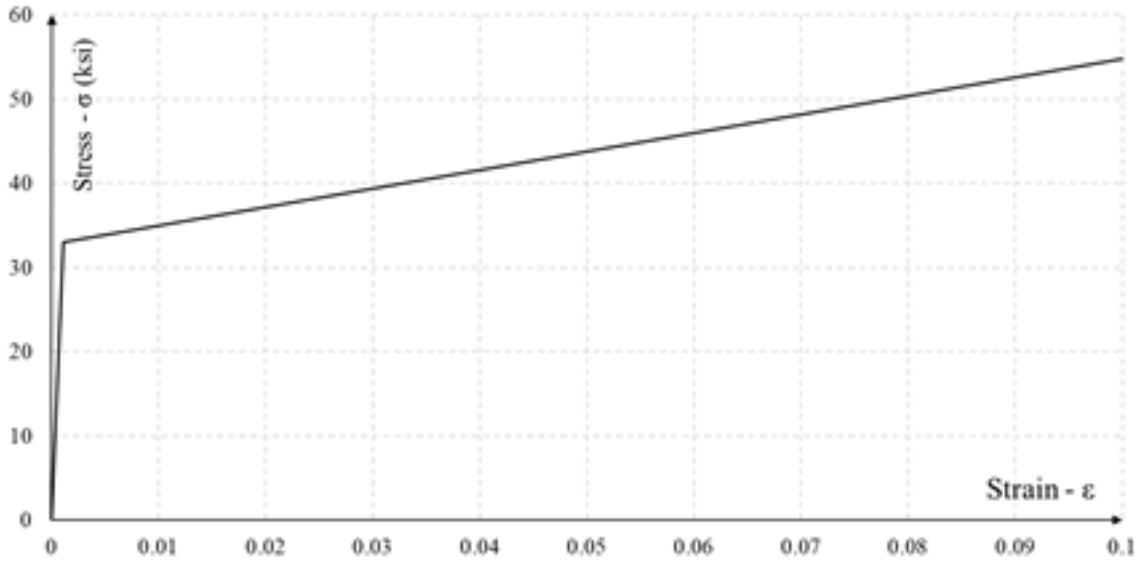

Figure 7-5: Stress-Strain Relationship for Reinforcing Steel

7.4 Boundary Conditions and Loads

First supporting pier has restrained displacements in Y and Z directions for nodes on vertical and horizontal, contact surfaces. Unrestrained displacement in X direction allows it to move in longitudinal direction – parallel to direction of traffic. Second pier has all the displacements restrained. The rotations for both piers are allowed in all the directions. Allowed displacement in X and Y directions at the front and back surfaces of the slab imitates it's discontinuity due to the transverse cracks detected over the supports.

Figure 7-6: Boundary Conditions for the Bridge Model

Contact conditions specified in the model are as follows: full bond of reinforcing bars with concrete in all segments, full connection to the side surfaces of the adjacent segments, pressure transfer interaction between tire footprint elements and concrete segments.

Load applied to the model during the calibration process was the actual truck used during load tests – ALDOT's LC-5 Test Truck. Wheel and axle spacing as well as tire contact dimensions were provided by ALDOT. The LC-5 axle spacing, footprint area and axial loads are presented in Figure 6-8. Load application was done through tire footprint imitating rigid plate elements (Figure 7-1, 7-6). Each of these elements transfer uniformly distributed total force of half of an axle weight.

Dead load effects were determined based on the following assumptions: concrete density 150pcf, asphalt density 140pcf, additional layer of 1.5in. of concrete, due to gable concrete shape at the mid-with of the bridge and 1.75in. thickness of the asphalt layer. The FE model uses actual weight of each of concrete finite elements to calculate the dead load effects, while additional loads of concrete and asphalt layers are applied as uniformly distributed pressure on the top surface of the slab.

Analyses on calibrated FE Model were conducted for the Tri-Axle and ALDOT's LC-5 Test Truck. These two vehicles were selected because they generated the lowest values of bridge ratings (Section 5.2). For the TriAxle vehicle (Figure 3-15) the AASTHO recommended footprint area of 10x20in. was used.

7.5 FEA Results

Results presented in this chapter were obtained from the calibrated FE model. Section 7.5.1 shows comparison of FEA obtained and field measured values of strains and deflections. The load patterns used in the field live load tests are described in Chapter 6 and Appendix A. Section 7.5.2 presents stress analysis results and discusses behavior of the structure.

7.5.1 FEA and Field Test Results Comparison

The calibrated FE model, with parameters described in sections above, replicates strains and deflections within acceptable tolerance for the integration points at the same locations as sensors. Maximum offset in the strains is 12με, while for deflections it is 0.09mm. Summary of differences between measured and FEA values is shown in Tables 7-2 through 7-5. This allowed plotting the values obtained through FE analyses and field test measurements for all the static load patterns (Figures 7-7 and 7-8). Just two comparison plots for critical load patterns are presented in this sections; plots for remaining static load cases are shown in Appendix B-1.

Table 7-2: Measured Values to FEA Utilized Comparison of Strains

	Span 1					Span 2			
	Distance along the width (in)					Distance along the width (in)			
Load Pattern	*68*	*128*	*188*	*248*	*368*	*8*	*68*	*300*	*368*
LP-1-L	0.90	0.95	0.82	0.77	0.16	0.80	1.00	0.55	0.32
LP-1-R	0.62	0.78	0.81	0.84	0.70	0.48	0.65	0.84	0.76
LP-2-L	0.87	0.85	0.85	0.78	0.25	0.82	0.96	0.47	0.22
LP-2-R	0.50	0.71	0.83	0.85	0.72	0.35	0.46	0.94	0.85
LP-4-L	0.87	0.89	0.89	0.83	0.50	0.76	0.94	0.68	0.51
LP-4-R	0.75	0.84	0.91	0.90	0.70	0.63	0.84	0.95	0.89

Table 7-3: Differences between Measured Strains and FEA Values (με)

	Span 1					Span 2			
	Distance along the width (in)					Distance along the width (in)			
Load Pattern	*68*	*128*	*188*	*248*	*368*	*8*	*68*	*300*	*368*
LP-1-L	-2	-1	-3	-2	-4	-3	0	-3	-3
LP-1-R	-2	-2	-3	-3	-5	-2	-2	-4	-4
LP-2-L	-3	-3	-2	-1	-2	-5	-1	-2	-2
LP-2-R	-2	-2	-2	-3	-9	-2	-2	-1	-5
LP-4-L	-4	-4	-3	-4	-6	-9	-2	-5	-6
LP-4-R	-4	-4	-2	-3	-12	-4	-2	-2	-4

Table 7-4: Measured Values to FEA Utilized Comparison of Deflections

	Span 1			Span 2
	Distance along the width (in)			Distance along the width (in)
Load Pattern	*4*	*188*	*368*	*188*
LP-1-L	1.06	0.92	0.52	1.08
LP-1-R	0.73	0.89	1.00	1.36
LP-2-L	0.95	1.02	0.40	1.30
LP-2-R	0.24	0.98	0.90	1.46
LP-4-L	1.01	0.98	0.92	1.06
LP-4-R	0.92	1.00	0.98	1.08

Table 7-5: Differences between Measured Deflections and FEA Values (mm)

	Span 1			Span 2
	Distance along the width (in)			Distance along the width (in)
Load Pattern	*4*	*188*	*368*	*188*
LP-1-L	-0.02	0.02	0.03	-0.02
LP-1-R	0.02	0.03	0	-0.10
LP-2-L	0.02	0	0.03	-0.06
LP-2-R	0.03	0	0.05	-0.09
LP-4-L	-0.01	0.01	0.01	-0.03
LP-4-R	0.01	0	0.01	-0.04

The values of deflections and longitudinal strains at sensor mounting locations along the width of the bridge are shown as points in the plots of Figure 7-7 and 7-8. FEA values present the actual distribution of longitudinal strains and deflections in the cross-section. Vertical dashed lines indicate the boundaries between the different cross section of segments. West side of the bridge corresponds to the distance along the width of 0 inches, while East side corresponds to the value of 376 inches.

It is concluded that the model shows overall good correlation with measured values and the bridge, although is a hybrid structure with different widths of slab's segments, behaves symmetrically.

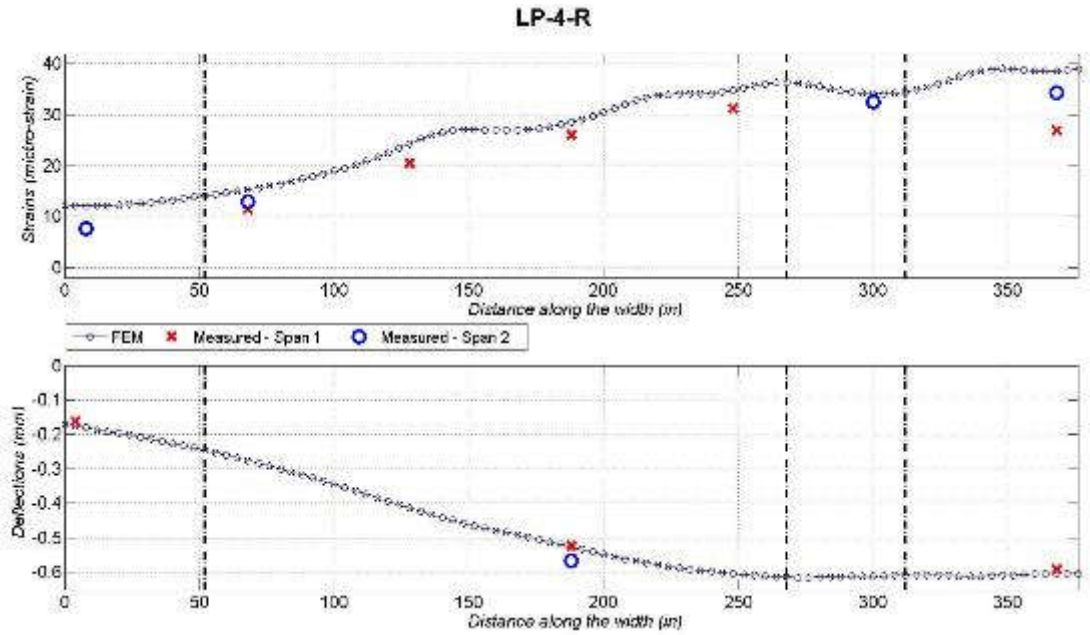

Figure 7-7: Comparison Plot of Strains and Deflections for LP-4-R
(1 mm = 0.02 in)

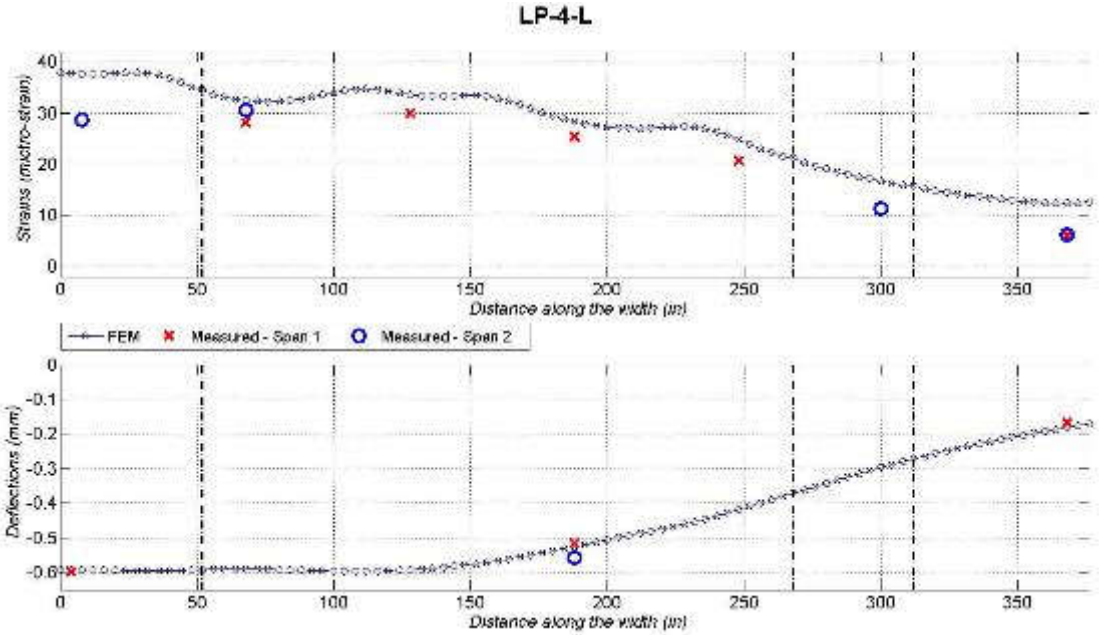

Figure 7-8: Comparison Plot of Strains and Deflections for LP-4-L
(1 mm = 0.02 in)

7.5.2 Stress Analysis

In this chapter maximum principal stresses for rebars and concrete segments due to LC-5 truck(s) loading are presented and discussed. Values presented in tables in this chapter come from FE Model of the bridge. Maximum resulting stresses in concrete are shown in figures 7-9 through 7-11, others can be found in output figures attached in Appendix B-2 of this report.

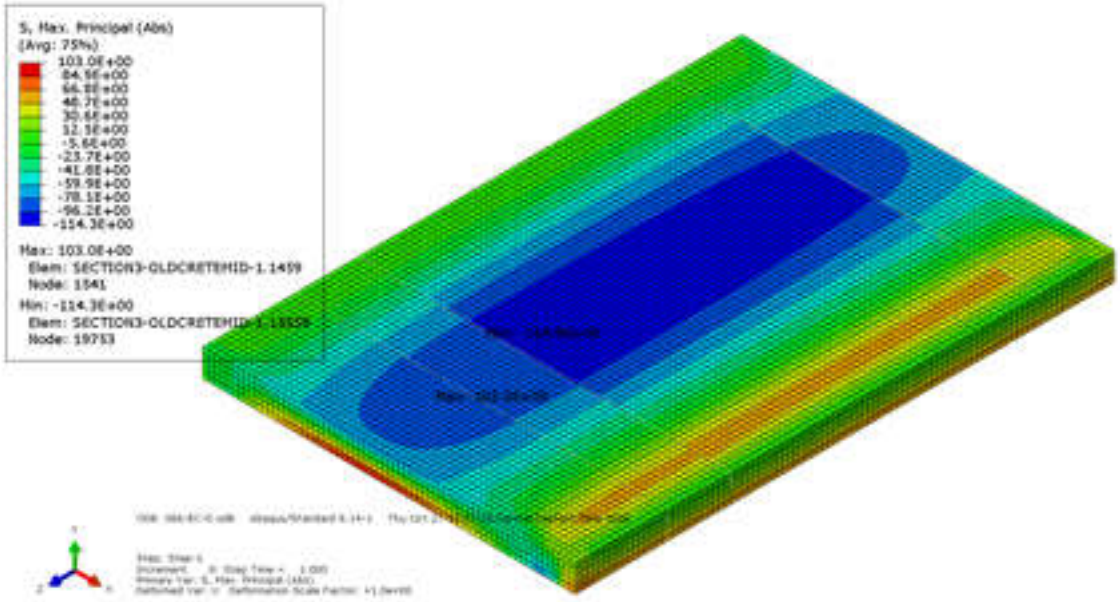

Figure 7-9: Stresses in Concrete Slab for Dead Load (psi)

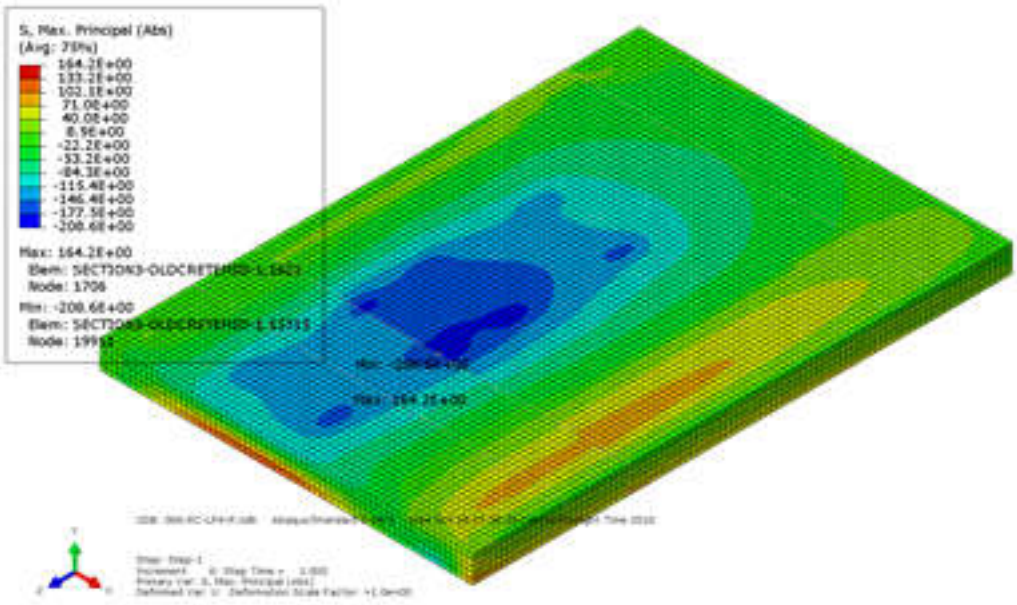

Figure 7-10: Stresses in Concrete Slab for LP-4-R (psi)

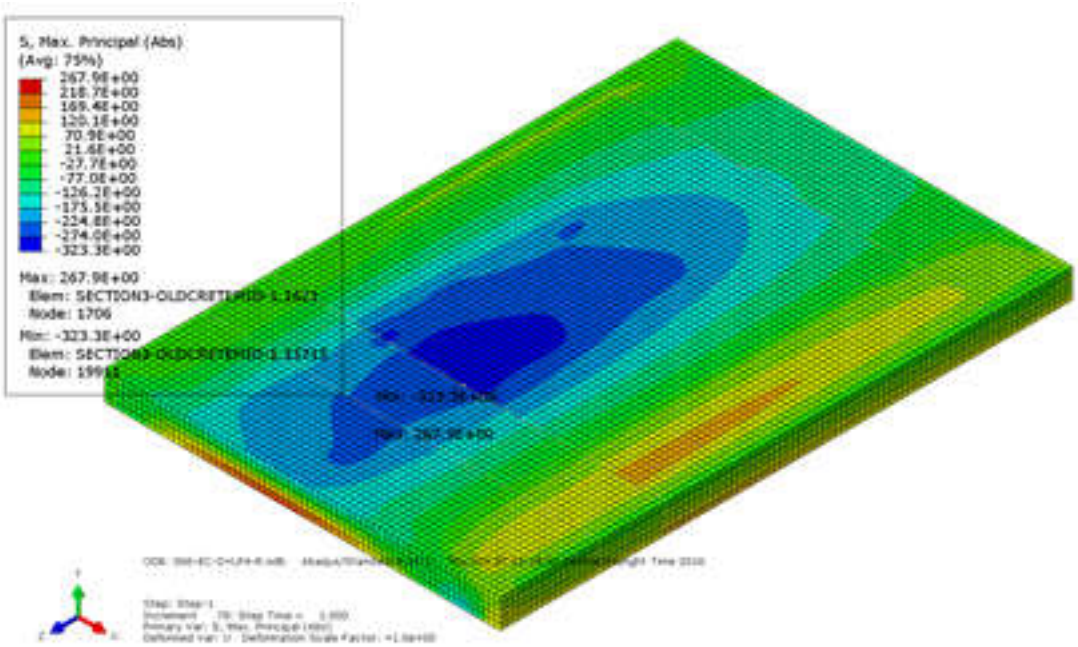

Figure 7-11: Stresses in Concrete Slab for D+LP-4-R (psi)

Table 7-6: Resulting Stresses for Static Live Load Cases

1	Load Configuration*	LP-1-L	LP-1-R	LP-2-L	LP-2-R	LP-4-L	LP-4-R	Dead Load
2	**Truck(s)**	**LC-5**	**LC-5**	**LC-5**	**LC-5**	**2xLC-5**	**2xLC-5**	**-**
3	$\sigma_{c,min}$** (psi)	-137	-135	-140	-144	-201	-209	-114
4	$\sigma_{c,max}$*** (psi)	+102	+96	+112	+117	+157	+164	+103
5	$\sigma_{s,min}$** (psi)	-430	-465	-804	-842	-773	-815	-502
6	$\sigma_{s,max}$*** (psi)	+693	+746	+991	+1021	+1237	+1273	+882

* *LP=Load Pattern, R=Right Traffic Lane/Side, L=Left Traffic Lane/Side,*
** *σ_{min}=compressive stress with negative sign,*
*** *σ_{max}=tensile stress with positive sign.*

Table 7-7: Resulting Stresses for Static Live Load Cases with Dead Load

1	Load Configuration*	D+LP-1-L	D+LP-1-R	D+LP-2-L	D+LP-2-R	D+LP-4-L	D+LP-4-R
2	**Truck(s)**	**LC-5**	**LC-5**	**LC-5**	**LC-5**	**2xLC-5**	**2xLC-5**
3	$\sigma_{c,min}$** (psi)	-243	-245	-247	-255	-310	-323
4	$\sigma_{c,max}$*** (psi)	+200	+197	+212	+212	+256	+268
5	$\sigma_{s,min}$** (psi)	-801	-856	-1279	-1345	-1243	-1270
6	$\sigma_{s,max}$*** (psi)	+1431	+1502	+1848	+1903	+2095	+2158

* *D=Dead Load, LP=Load Pattern, R=Right Traffic Lane/Side, L=Left Traffic Lane/Side,*
** σ_{min}*=compressive stress with negative sign,*
*** σ_{max}*=tensile stress with positive sign.*

Table 7-6 shows maximum principal stresses in concrete and rebars for static live load cases. Table 7-7 presents the stresses due to dead load and live load. The smallest modulus of rupture for this bridge, for compressive strength from Table 7-2, calculated with Equation 43 is 315 psi. Comparing it with tensile stresses in concrete (Table 7-6 and 7-7, row 4) for all the static live load cases show a level of stress less than required to cause cracking. Tensile stresses due to two side-by-side trucks slightly exceeded 52% of the expected cracking stress. Adding the dead load to the model, gives most probable stresses achieved during the live load tests. Maximum expected tensile stress due to two side-by-side trucks and dead load is 267psi, which is 85% of the smallest predicted cracking stress. Analysis confirmed that the bridge would not crack under the live load used during load tests.

The linear compressive stress-strain relationship for concrete was assumed up to 40% of its compressive strength. Therefore, for the weakest concrete in the segment 2, the non-linear behavior starts to occurs at stress higher than 704 psi. Maximum compressive stresses due to dead load and two side-by-side trucks (Table 7-7, row 3) did not exceed 46% of maximum linear stress and 19% of the smallest compressive strength of the concrete in the slab (Table 7-2).

7.6 Finite Element Model Aided Bridge Ratings

The FEM results were used to determine rating factors for the LC5 test truck and the standard TriAxle truck. The ratings were determined by limiting the stress in the concrete and reinforcing steel to allowable values. So, the load factors A1 and A2 for the rating equation (Equation 35) are one. The allowable unit stresses are given in Table 7-8. The ratings were determined by applying the full dead load to the FEM model and then incrementally increasing the truck weigh until the stress in either the concrete or steel reached its allowable value. The truck weight at that point is represented by *RF(1+I)L* as shown in Figure 7-12.

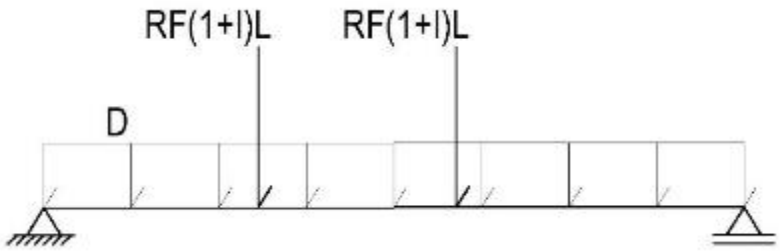

Figure 7-12: Scheme of Load Application in FEM

Tables 6B.5.2.3-1 and 6B.5.2.4.1-1 in Manual (AASHTO 2011) specify respectively allowable stresses for reinforcing steel and compression due to bending in concrete. These stresses were used to perform rating calculations (Table 7-8). The dynamic allowance was taken as 0.3 to achieve the conservative values of the ratings. 0.3 is much larger than the dynamic effect observed in a limited number of tests described in Chapter 6.

Table 7-8: Allowable Unit Stresses

	Stresses (psi)	
	Inventory Level	**Operating Level**
Reinforcing bars	18,000	25,000
Concrete in compression	800	1200

The model was used to investigate the stresses in the concrete and the reinforcing bars for various load configurations. To determine the rating factor of the bridge the FE model was loaded with dead load and a fraction of the live load which was incrementally increased as described above. These analyses were performed for two live load configurations, two ALDOT's LC-5 trucks side-by-side (Figure 6-8) and two side-by-side Triaxle vehicles (Figure 3-15). Vehicles were placed at the most critical longitudinal and transverse locations, resulting in the highest stresses and compared with allowable bending unit stresses in concrete and steel. It turned out that stresses in concrete control, therefore only ratings due to concrete in bending are considered. The live load multiplier, *RF(1+I)*, was read at concrete stresses corresponding to inventory and operating level of rating and divided by dynamic allowance, *(1+I)*. Such approach gives the most realistic rating factors determined from 3D FEM. Table 7-10 shows calculations performed for the two truck configurations.

Table 7-9: Allowable Stress Ratings

Vehicle	**Allowable compressive stress (psi)**		**Live Load Multiplier, *RF(1+I)***		**Dynamic Allowance, *I***	***RF*- Inventory**	***RF*- Operating**
	Inventory Level	**Operating Level**	**Inventory Level**	**Operating Level**			
2xLC5	800	1200	3.74	5.08	0.3	2.88	3.91
2xTriAxle	800	1200	4.15	5.43	0.3	3.19	4.18

Resulting values of rating factors are higher than those calculated in Chapter 5. Comparison of rating factors obtained through AASHTO procedures, presented in section 5-2, and FEM are shown in Table 7-10. Values for the east and original segments are as presented in Figures 5-3, 5-5, 5-6, 5-7.

Table 7-10: Comparison of Obtained Rating Factors

Vehicle	RF-Operating				
	East Segment E=63.7in	East Segment E=91.7in	Original Segment E=63.7in	Original Segment E=91.7in	FEM
2xLC5	0.66	1.37	1.56	2.28	3.91
2xTriaxle	0.64	1.31	1.50	2.20	4.18

Operating rating factors in Table 7-10 determined from FEM are nearly six times larger than those calculated by AASHTOWare for the east segment using the AASHTO (17th Ed. 2002) effective width of 63.7in. Rating factors determined from FEM are more than 70% above those determined those determined by AASHTOWare for the original segment with an effective width of 91.7in. These comparisons support a recommendation for a model for permit loads for use in AASHTOWare having the characteristics of the original segment with an effective width equal to one-quarter of the bridge width, 91.7in.

8 Summary of Findings, Conclusions and Recommendations

The purpose of this research is to develop an AASHTOWare model of a flat slab reinforced concrete bridge that could be used for issuing permits to overweight trucks. This bridge has 11 spans with a total length of 245 ft and crosses Jenkins Creek and Barnes Slough on the northbound side of US Highway 82/231 at milepost 162.56. ALDOT's "Bridge Card" for the structure indicates that the bridge was widened by approximately 4 ft in 1930, and the visual inspection of the bridge indicated that the width was increased twice on the east side of the bridge and once to the west side.

The information about bridge design a 100 years ago was reviewed using the Auburn University Library resources and the Alabama Department of Archives and History in Montgomery. The construction year of the considered bridge was established as 1915 from a report of the state of Alabama Highway Commission (*State Highway Comission of Alabama* 1916). These findings were confirmed by a comparison made between maps from 1920 and 1992. The sequence and time which the additional segments were built remain unknown, although additional segments were most likely added between 1941 and 1959 based on the amount of reinforcement present in the slab. A literature review is provided with the aim of describing the methods used for designing flat slab bridges throughout the 20th century.

The older methods to calculate the required reinforcement in the slab were reviewed. A historical development of the concept of rating is presented and compared with the AASHTOWare software used by DOTs. Two case studies from the 1920s were used to apply these methods to establish a single method used to design the original segment from the contemporary time. From these case studies it was concluded that although the methods used to design the reinforcement in the slab were established, the concept that defined the effective width remained unknown. The value of effective width was calculated by inversing the ratio of capacity deducted by dead load effect divided by live load effect plus impact. Through this study, not only it was concluded that the effective width was calculated independent of span length or roadway widths, but that in the 1920s the designers used the clear span for simple spans bridges to design the reinforcement in the slab. For the two-span continuous case study, center to center of the supports was used for design. From these studies there was enough data generated to consider the effective width value to be 4.15 ft for all designs. Additionally, all the operating ratings for the simple span bridges showed that the contemporary methods used to design the flat slab bridges provided adequate cross section capacity for all ALDOT trucks. Thus there would be no need for postings on these bridges if any still exists. For the two-span continuous bridge, the reinforcement in the negative moment region was not developed properly, which resulted in lower rating values than 100% of the truck load, and there would be a need for postings for ALDOT trucks.

The old methods were applied to estimate the amount of reinforcement needed in all four segments of Barnes Slough Bridge. After the initial calculations and estimating the amount of steel and capacity of the bridge, field tests and measurements were performed. Based on field measurements, the bar size in all segments was one size smaller than those predicted. Additionally, the clear cover was different than that used in the standard simple span bridges (SHDA, 1922). From the concrete core tests, the strength of the concrete was identified. The concrete strength was

less than assumed earlier, and this resulted in a different cross section capacity of the slab. The amount of reinforcement detected in the positive moment region was more than the estimated amount, and the reinforcement in the negative moment region was far less than the expected amount. Some cracks were detected in the top of the slab (under the asphalt) over the supports by the GPR device. From these findings it was concluded that the bridge was reinforced as if it is a series of simple spans. This observation resulted in narrowing down the focus of research to one type of structure.

The live load tests resulted in strains and deflections that were very small and smaller than expected. This confirms the overall good condition of the structure and its reserve flexural capacity. Measured values of strains and deflections show reasonable symmetry in bridge's behavior, especially for the oldest part of the slab. Comparison between calculated theoretical values of strains and deflections and measured during live load tests shows that calculated strains both for simply support and fixed-fixed boundary conditions are larger than measured during load tests. For deflections, for simple support boundary conditions calculated values are significantly larger, for fixed-fixed boundary conditions, they are slightly smaller than measured in the field.

Finite Element Model of the bridge shows overall good correlation with measured values of strains and deflections during live load tests. The model showed that bridge would not crack under two LC-5 trucks load which was confirmed during the load tests. The rating factors corresponding to the load carrying capacity calculated using FEM are nearly twice higher than the rating factors calculated using the AASHTOWare.

Based on the performed analysis and field testing, it is recommended to modify the value of effective width of the slab in the AASHTOWare for use with the structural model defined for the original portion of the bridge as defined in Section 5.2. For the considered bridge, the effective width can be taken as the total width of the slab divided by the number of wheel lines which is 4 in this case. Therefore, in calculation of the rating factor for permit vehicles, the effective width is a quarter of the total width, equal to 91.7 in which is 43% more than what is used in the AASHTOWare.

9 References

AASHTO. (2014). AASHTO LRFD *Bridge design specifications*. 7th Ed., Farmington Hills, MI.

AASHTO. (2011). *Manual for bridge evaluation*, 2nd Ed., Farmington Hills, MI.

AASHTO. (2002). *Standard specifications for highway bridges*. 17th ed., Farmington Hills, MI.

AASHTOWare. Computer software. Http://www.aashtoware.org/Pages/default.aspx. Vers. 2014.

AASHO. (1931). *Standard specifications for highway bridges and incidental structures.* Association Central Office. Washington DC.

AASHO. (1935). *Standard specifications for highway bridges*. 2nd Ed., Association Central Office. Washington DC.

AASHO. (1941). *Standard specifications for highway bridges*. 3rd Ed., Association Central Office. Washington DC.

AASHO. (1949). *Standard specifications for highway bridges.* 5th Ed., Association Central Office. Washington DC.

AASHO. (1957). *Standard specifications for highway bridges*. 7th Ed., Association Central Office. Washington DC.

AASHO. (1961). *Standard specifications for highway bridges.* 8th Ed., Association Central Office. Washington DC.

ACI Committee 318. 2014b. *ACI 318-14 Building Code Requirements for Structural Concrete and Commentary*. American Concrete Institute.

Blanchard, Arthur H. (1919). *"American Highway Engineering Handbook."* New York, NY, USA: John Wiley and Sons.

Dassault Systèmes. (2014). *ABAQUS: Abaqus Analysis User's Manual, Version 6.14*.

Desayi P., Kirshnan S. (1964). *"Equations for the stress-strain curve of concrete"*, J. Amer. Concr. Inst., 61, pp. 345-350, 1964.

EDR 48 *"Evaluation of Reinforcing Bars in Old Reinforced Concrete Structures"*, CRSI 2001.

European Committee for Standarization. 2004. *EN 1992-1-1: Design of Concrete Structures -Part 1-1: General Rules and Rules for Buildings.*

Garmestani, G. (2016) *Model for Permit Loads for Barnes Slough Bridge* (Master thesis). Retrieved from Auburn University Library.

Georgia State Highway Department. (1936). *"Standard Specification for Construction of Roads and Bridges."*, GA: State of Georgia, GA.

Hool, George A. (1937). *"Principle of Reinforced Concrete Construction."* New York, NY, USA: McGraw-Hill Book Company, Inc.

Hool, George A., and Charles S. Whitney (1921). *"Concrete Designer's Manual."* New York, NY, USA: McGraw-Hill Book Company, Inc.

Hsu T.T.C., Wang T. 2001. "Nonlinear Finite Element Analysis of Concrete Structures Using New Constitutive Models." *Computers and Structures,* 79 (32): 2781–91.

Jensen, V. P. (1943). *"The plasticity ratio of concrete and its effect on the ultimate strength of beams."* Proceedings of The American Concrete Institute Vol. 39. 565-582.

Kirkham, John E. (1932). *"Highway Bridges."* New York, NY, USA: McGraw-Hill Book Company, Inc.

Kamiński M., Kmiecik P. 2011. "*Modelling of Reinforced Concrete Structures and Composite Structures with Concrete Strength Degradation Taken into Consideration.*" Archives of Civil and Mechanical Engineering, Vol. XI, No. 3, pp. 623-636.

Pauw, A. (1960) "S*tatic modulus of elasticity of concrete as affected by density."* The Proceedings of American Concrete Institute Vol. 57, 679-688.

Shanley, F.R. (1957). *"Strength of Materials."* New York, NY, USA: McGraw-Hill Book Company, Inc.

SHDA. (1922). *Standard Reinforced Concrete Slabs, Drawing No. 51.* State Highway Department of Alabama, Montgomery, Alabama.

SHDA. (1924). *Plan and Profile of Proposed State Highway Project No. 16A, Fayette County, Windfield to Fayette.* State Highway Department of Alabama, Montgomery, Alabama.

Slocum, S.E. (1914). *"Resistance of Materials."* Boston, New York, Chicago, London: Ginn and Company, 1914.

State Highway Commission of Alabama. Montgomery, Alabama, USA. (1916). The Brown Printing Co.

Singer, L. Ferdinand. (1951). *"Strength of Materials."* New York, NY: Harper & Brothers Publishers.

Troxel, George E., Harmer E. Davis, and Joe W. Kelly. (1968). *"Composition and Properties of Concrete."* New York, NY, USA: McGraw-Hill Book Company, Inc.

Trusted Steel Company. (1910). "A *hand book of practical calculation and application of reinforced concrete."* Detroit, MI, USA: Trusted Steel Company.

Turneaure, F.E., and E.R. Maurer. (1911)."*Principles of reinforced concrete construction."* New York, NY, USA: John Wiley and Sons.

Http://www.proceq.com/. N.P./2016. Web. 27 July 2015.

10 List of Abbreviations

A_s	Area of Steel
ALDOT	Alabama Department of Transportation
AASHTO	American Association of State Highway and Transportation Officials
B	Distance between the parallel loaded elements
β_b	Ratio of the area of reinforcement cut off to the total area of tension reinforcement at the section
b_d	Bar diameter
b_w	The width which the shear is considered
C_c	Clear cover
C_I	Notation for "Coefficient of Impact"
C_r	Distance between centers of wheels
D	Distance in ft from the center of the nearer support to the venter of wheel
d	Distance from the top of the beam down to the center of the reinforcement
E	Design effective width
E_I	Effective width of road in inner zone
E_O	Effective width of road in outer zone
E'	Ratio of live load of a wheel line to the maximum moment due to live load
Es	Modulus of elasticity of steel
E_c	Modulus of elasticity of concrete
F	Resultant compressive force in the concrete and also resultant tension in the reinforcement
f_s	Strength of steel
f_c	Strength of concrete
fy	Ultimate strength of steel
H_{number}	Truck with the number of ton as its weight
h	Slab depth
j	A multiplier of d that measures the distance between the center of steel and the center of compression in the cross section
jd	Distance from the center of the reinforcement to the resulted compressive force in the concrete
k	Effective length factor for compression members
kd	Distance from the extreme compression fiber to the neutral axis
L	Length of span
L_d	Required development length of reinforcement
L_a	Embedment length of reinforcement
LFR	Load factored rating
LLM	Live load moment
M	Bending moment
N	Number of traffic lane on the road
n	Modular Ratio
ρ	Ratio of steel to the area of effective cross section
P	It is most often the force. Refer to the definition of notation on the page Load on one wheel

P’	Concentrated lane load per lane
P_s	Strength of steel
P_c	Strength of concrete
Q	Uniform lane load per linear foot of lane
S	Span of Slab
s	Spacing of shear reinforcement
V_c	Concrete shear strength
W	Width of the wheel or tire in ft
W	Width of graded roadway across culverts
Wr	Width of roadway between curbs on bridge
W_r	Modified edge to edge width
W_P	Physical edge to edge width of bridge
W_n	Width of design traffic lane
W_C	Roadway width between curbs exclusive of median strip
X	Number of vehicles traveling
Y	Roadway width in ft
DOT	Department of Transportation
DL	Dead load
ft	feet
in.	Inches
in^2	Inches squared
lb	Pound
lbs	Pounds
LL	Live load
Ksi	Kips per square in.
psi	Pound per square in.
STD	Standard

Appendix A: Load Test Patterns and Results

The aim of this section is to show all considered load patterns. Additionally, results and comparisons for different load configurations are presented here.

A-1 Load Patterns

In Appendix A-1 all considered load patterns are presented.

Static Load Patterns:

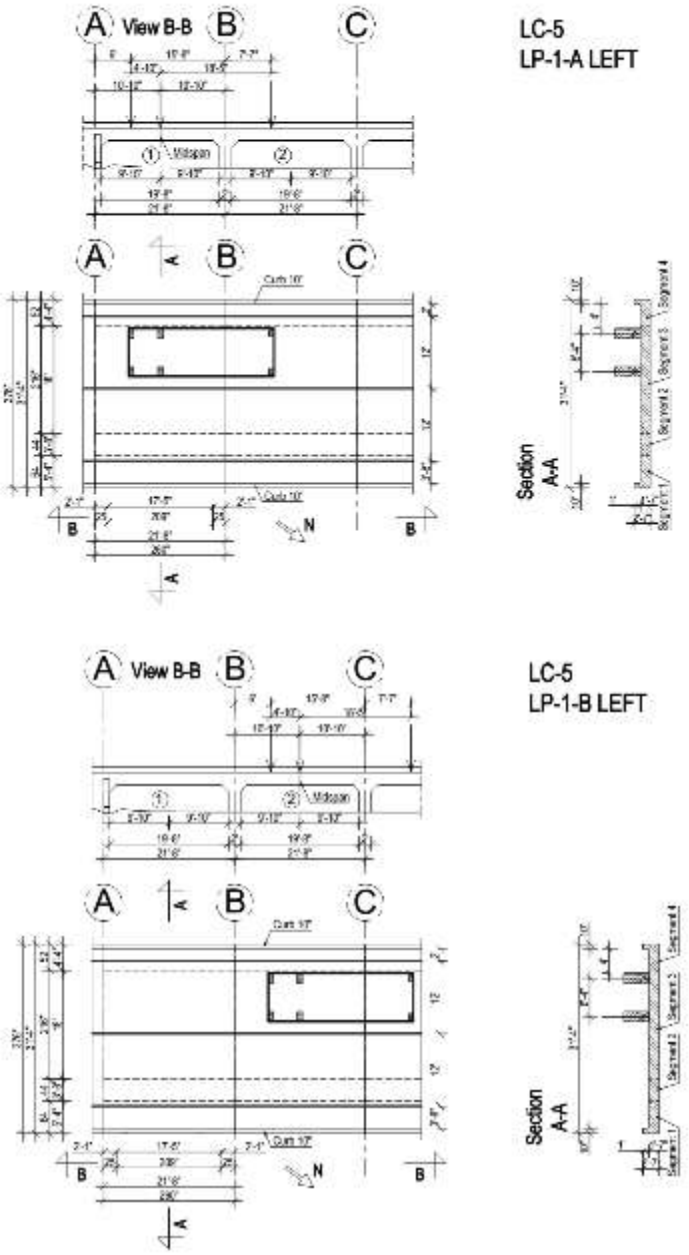

Figure A-1-1: Load Pattern LP-1-L

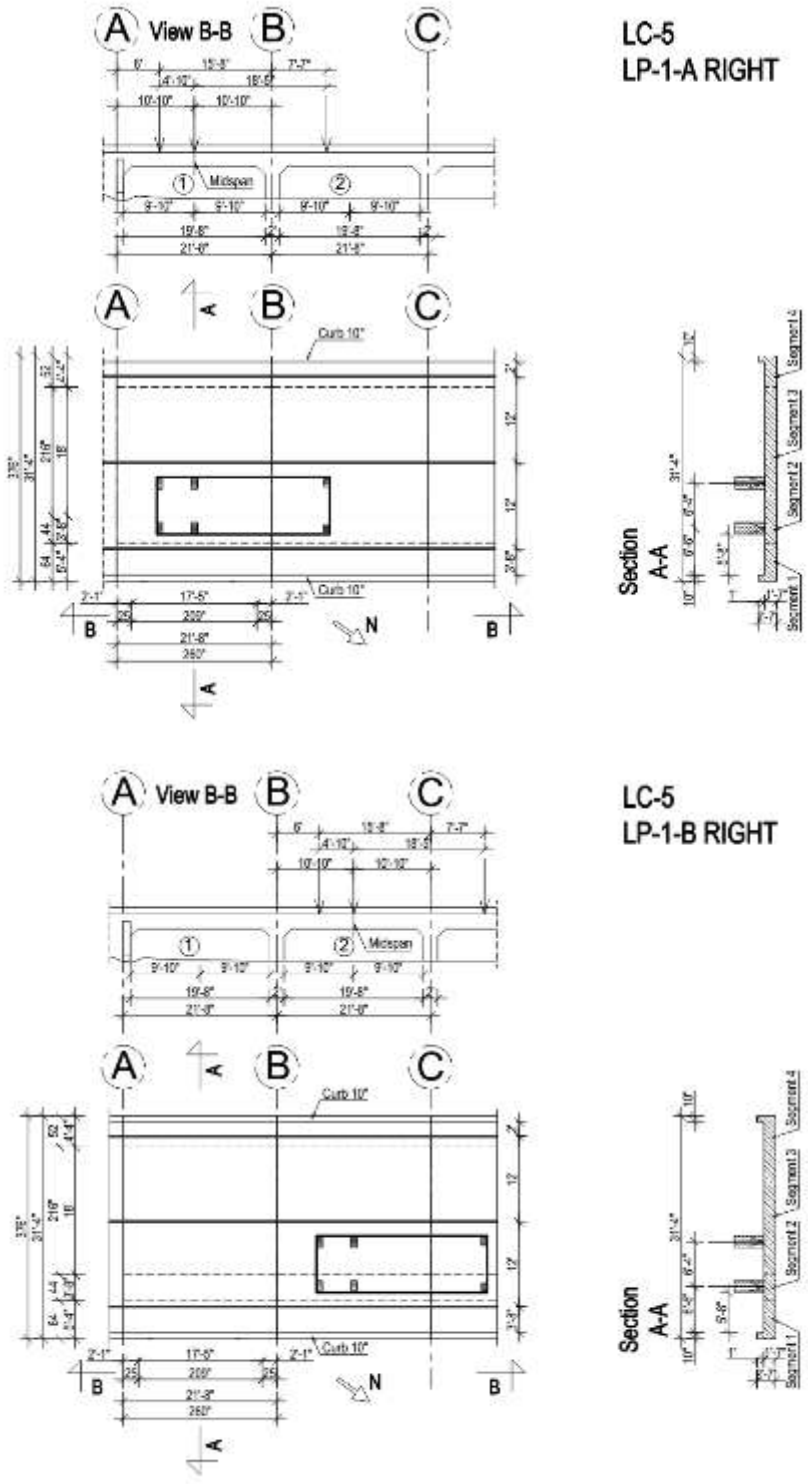

Figure A-1-2: Load Pattern LP-1-R

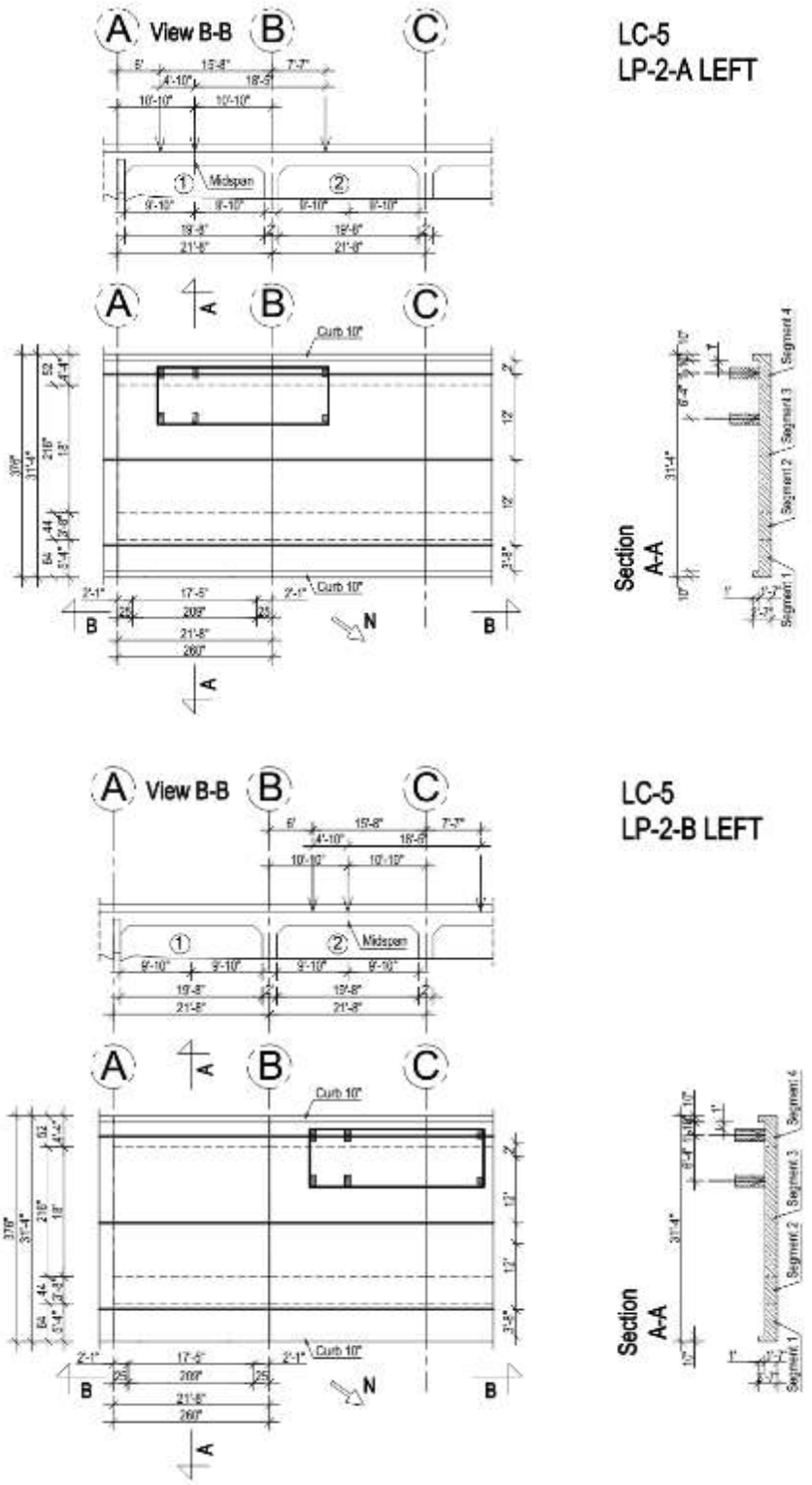

Figure A-1-3: Load Pattern LP-2-L

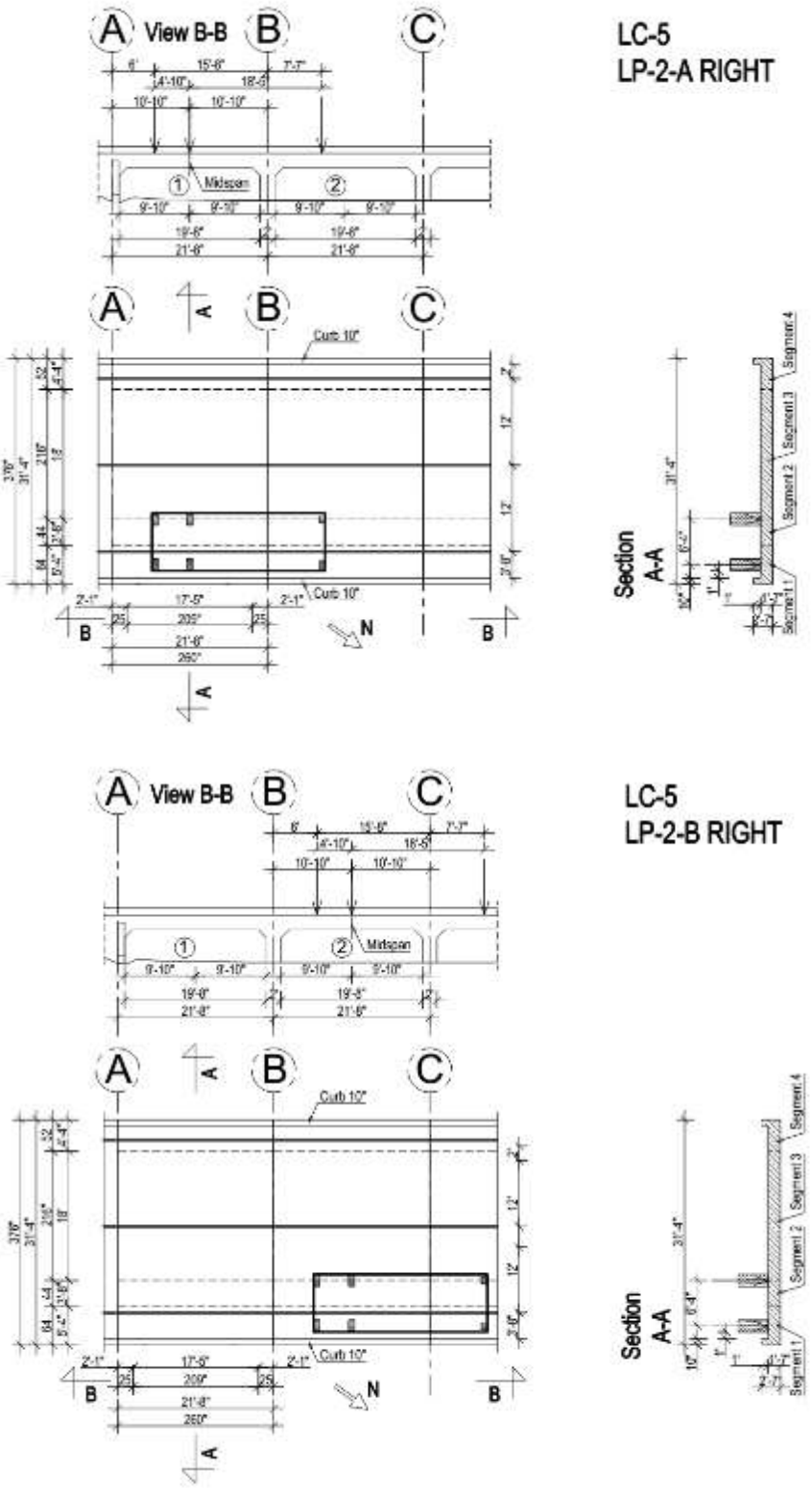

Figure A-1-4: Load Pattern LP-2-R

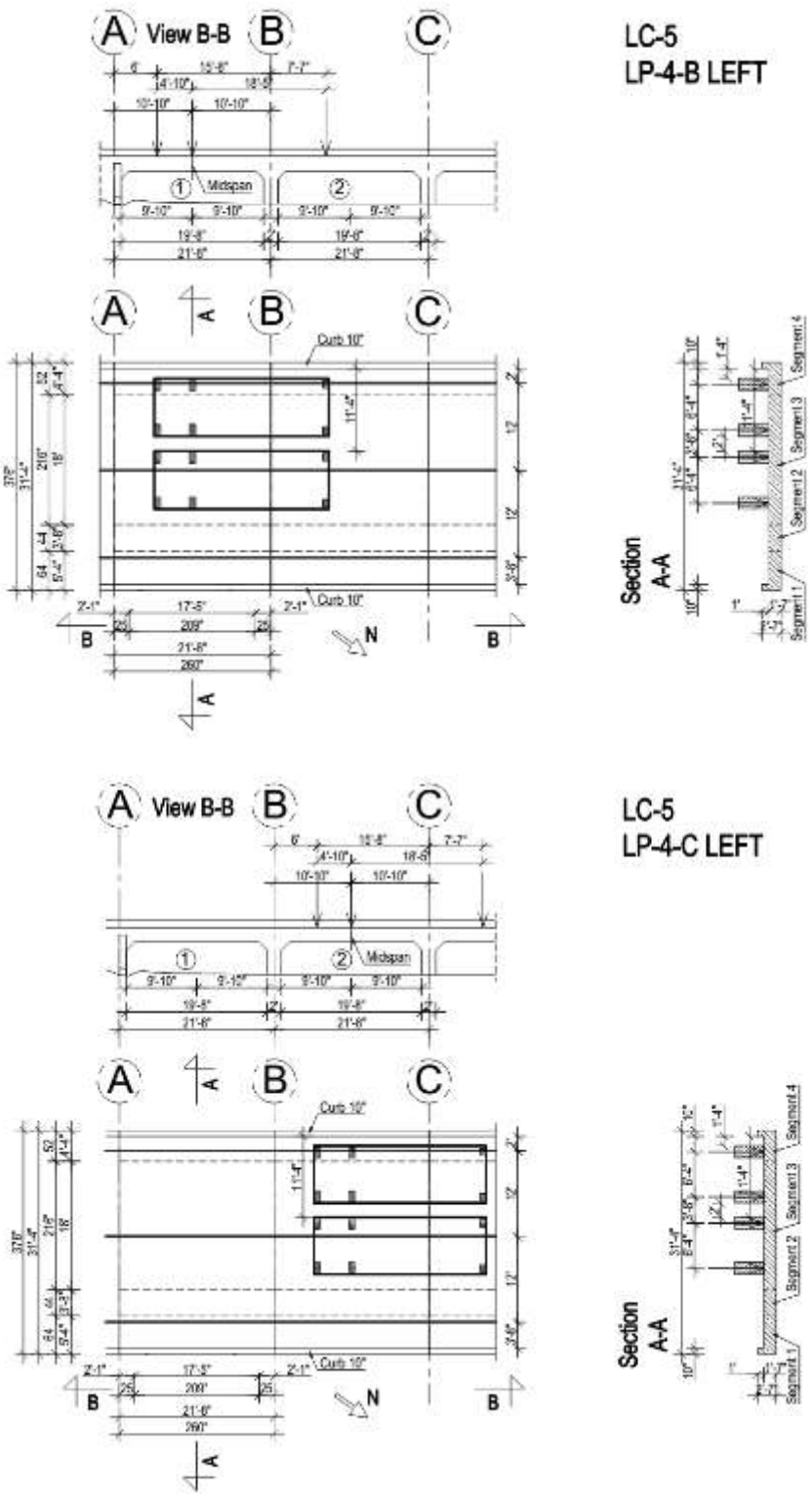

Figure A-1-5: Load Pattern LP-4-L

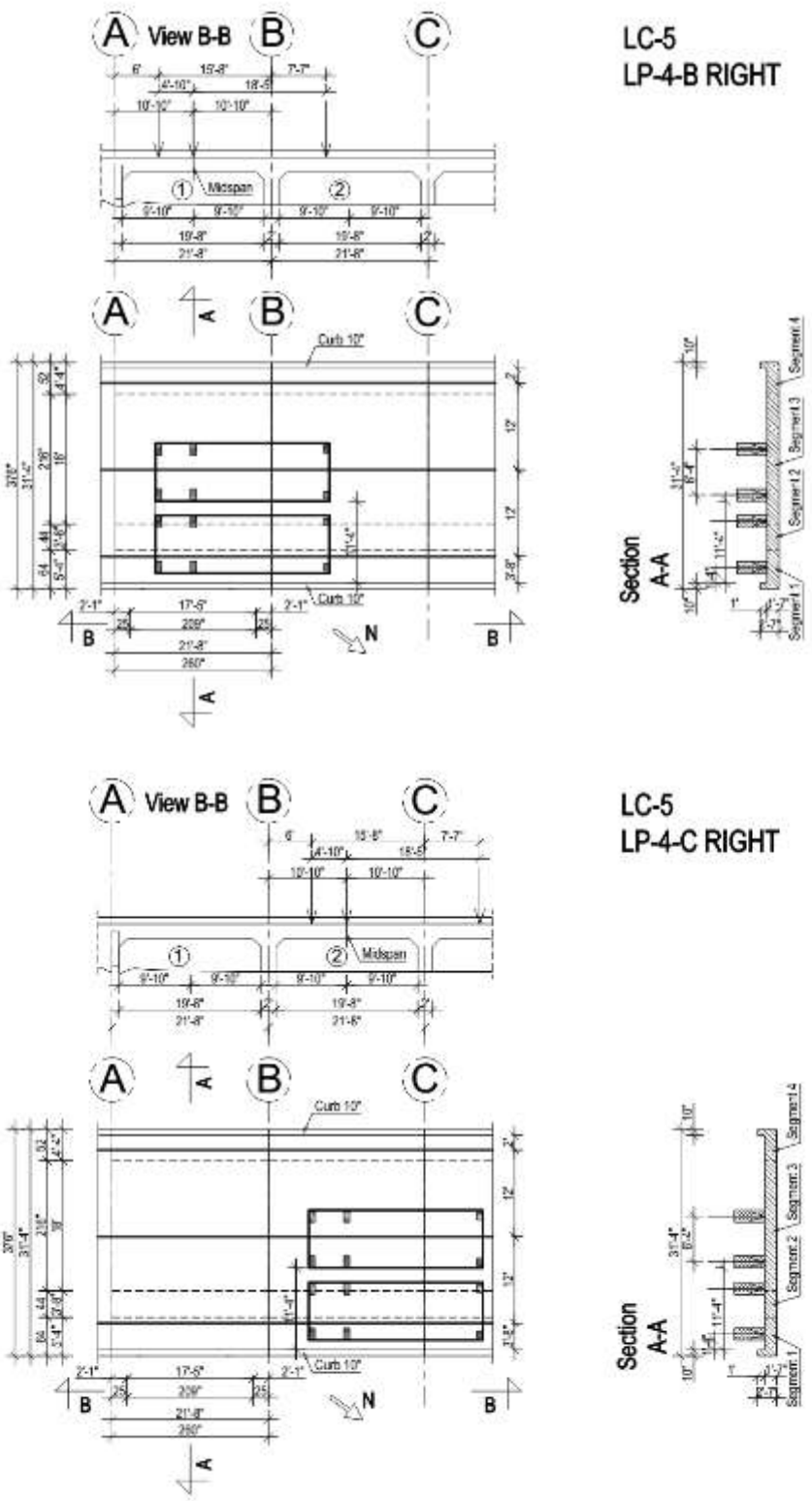

Figure A-1-6: Load Pattern LP-4-R

Load Patterns with Crawling Speed:

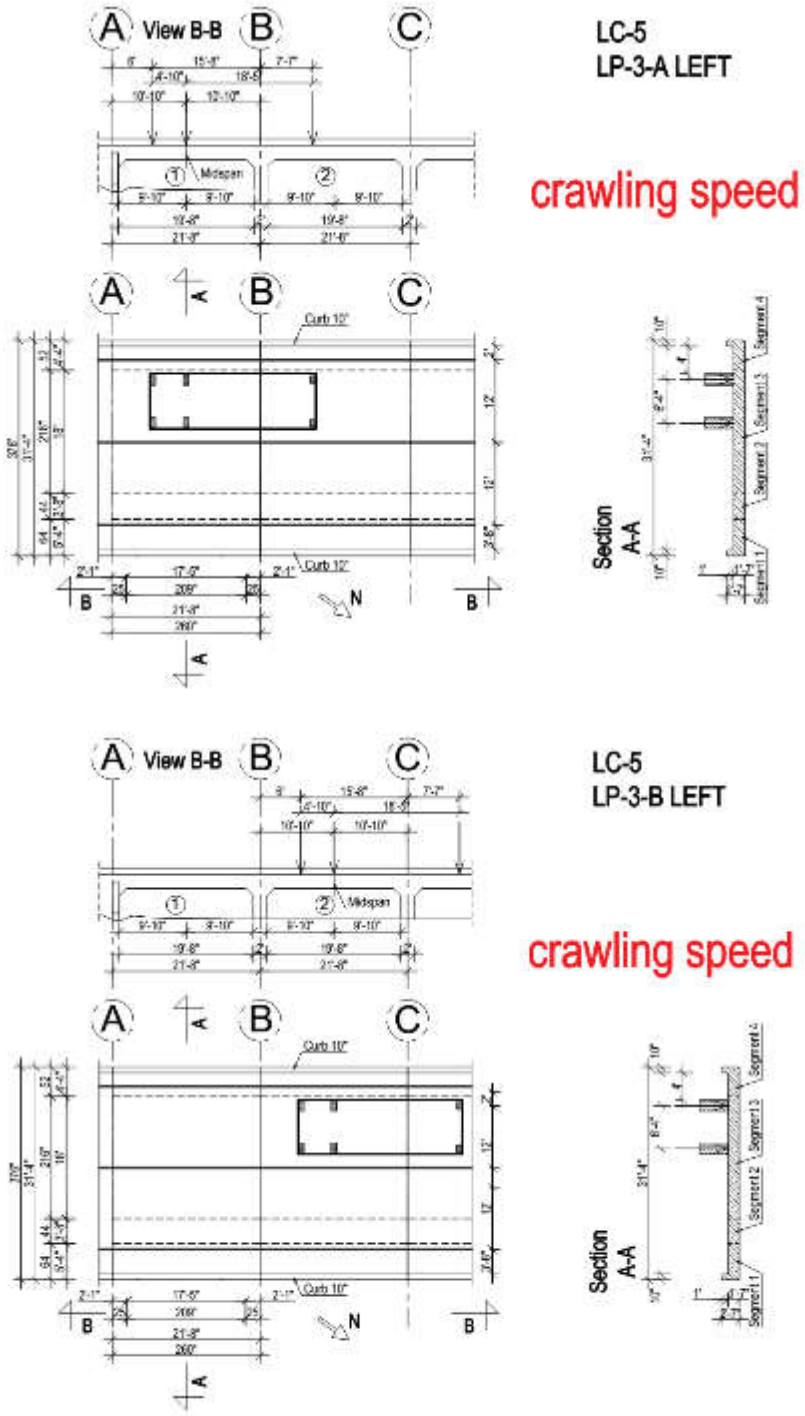

Figure A-1-7: Load Pattern LP-3-L-CS

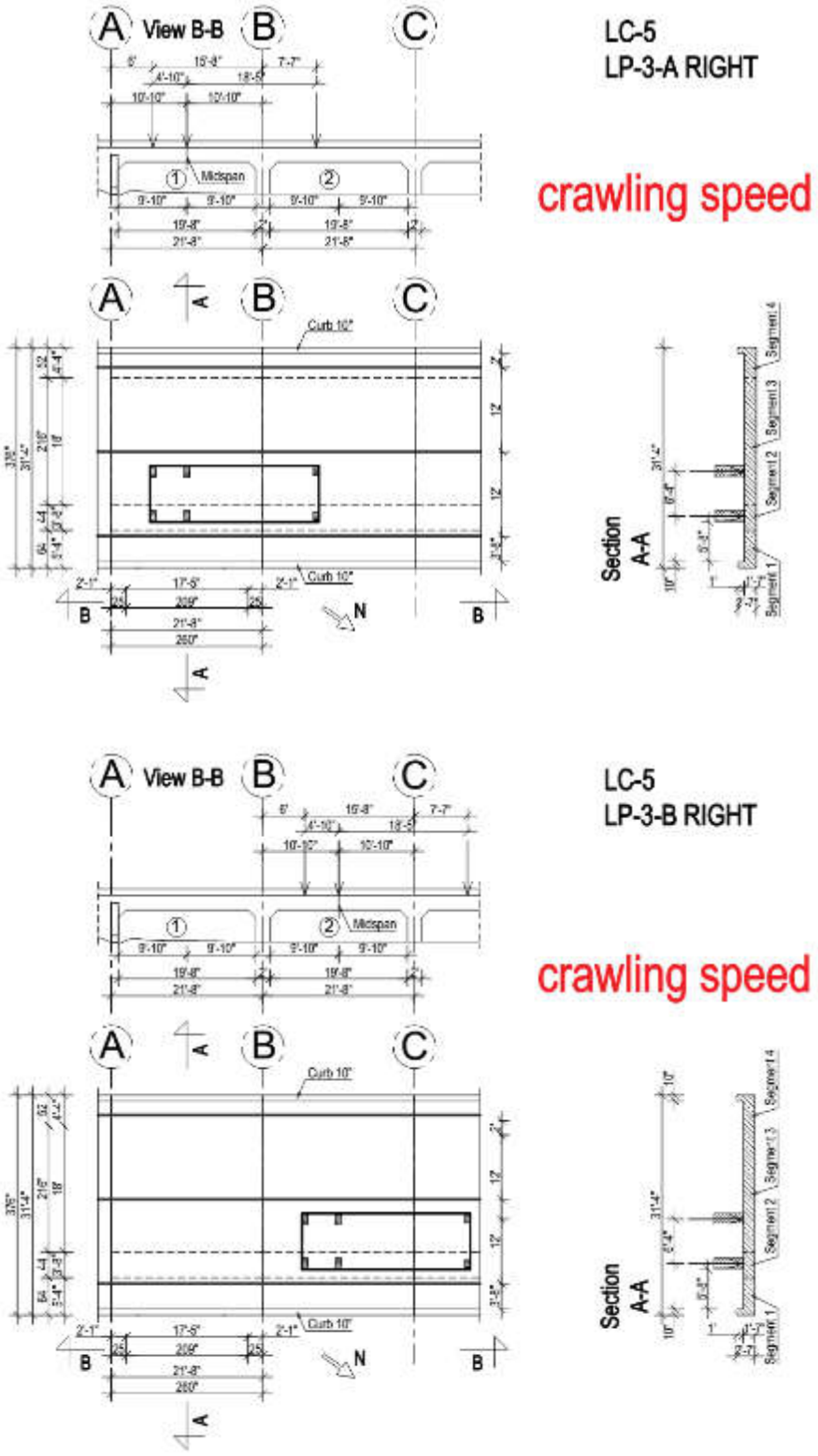

Figure A-1-8: Load Pattern LP-3-R-CS

Load Pattern with Normal Speed (61mph):

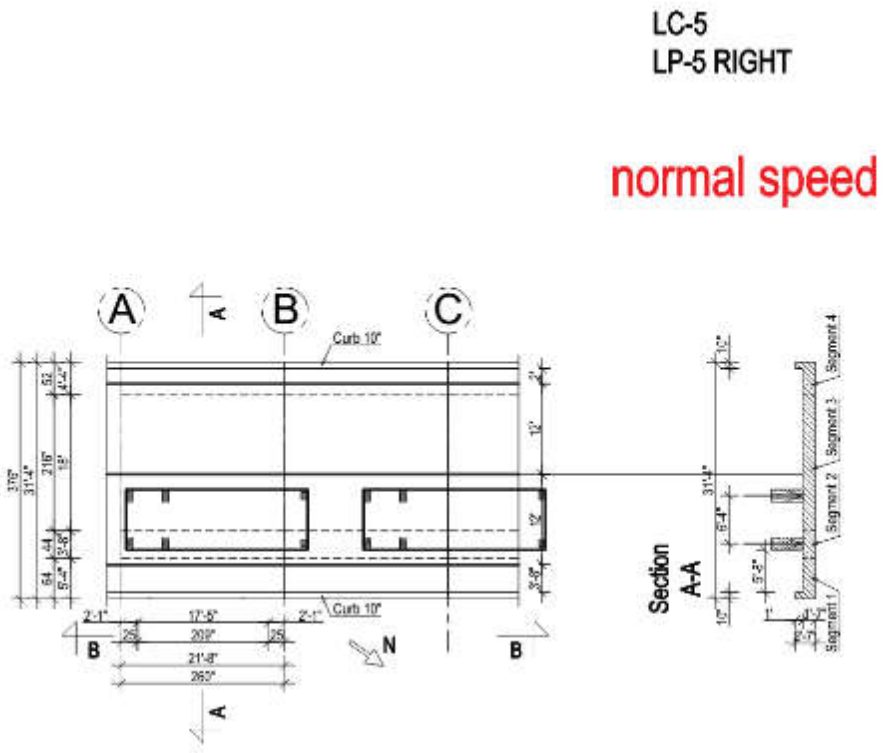

Figure A-1-9: Load Pattern LP-5-R-Dyn

A-2: Results and Comparisons

In Appendix A-2 the most significant results and comparisons are presented.

Load Pattern LP-1-L:

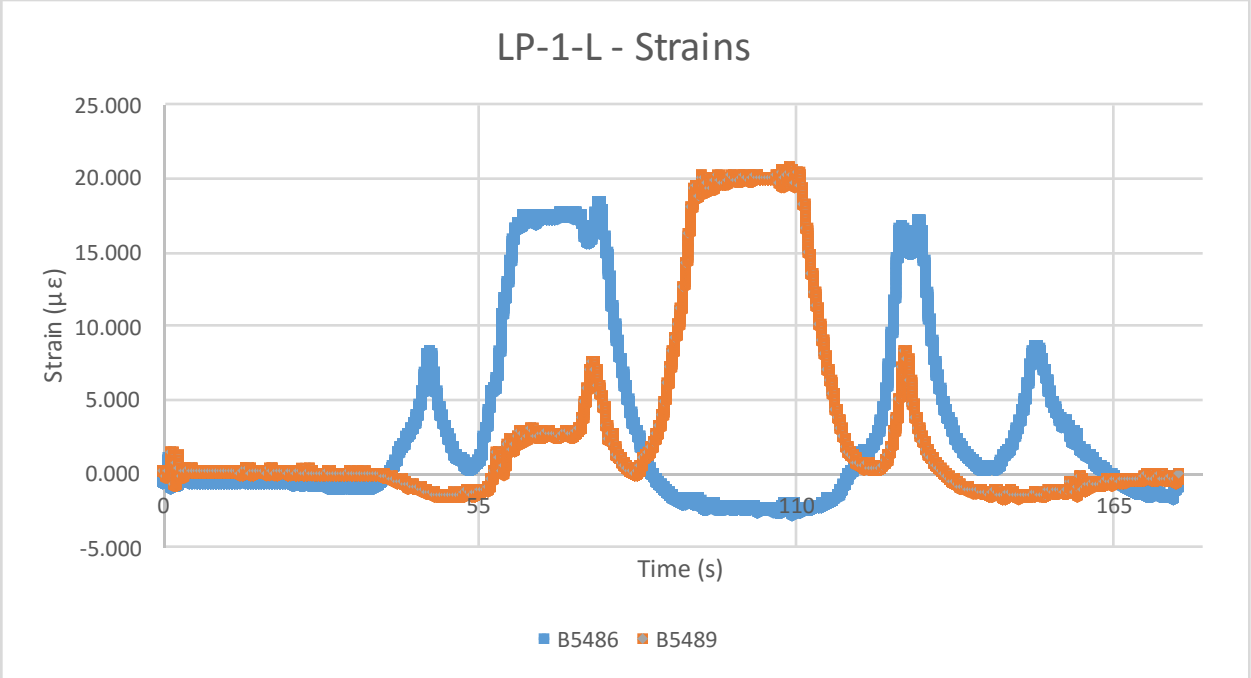

Figure A-2-1: Strains in Time for Second Run

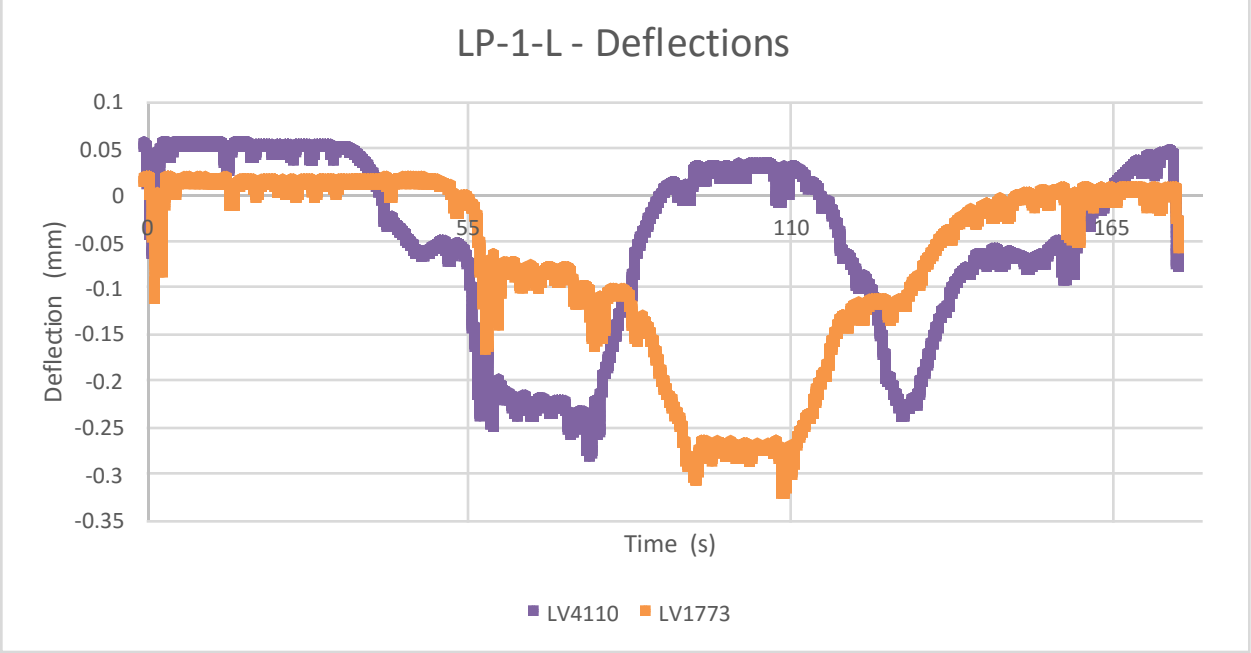

Figure A-2-2: Deflections in Time for Second Run

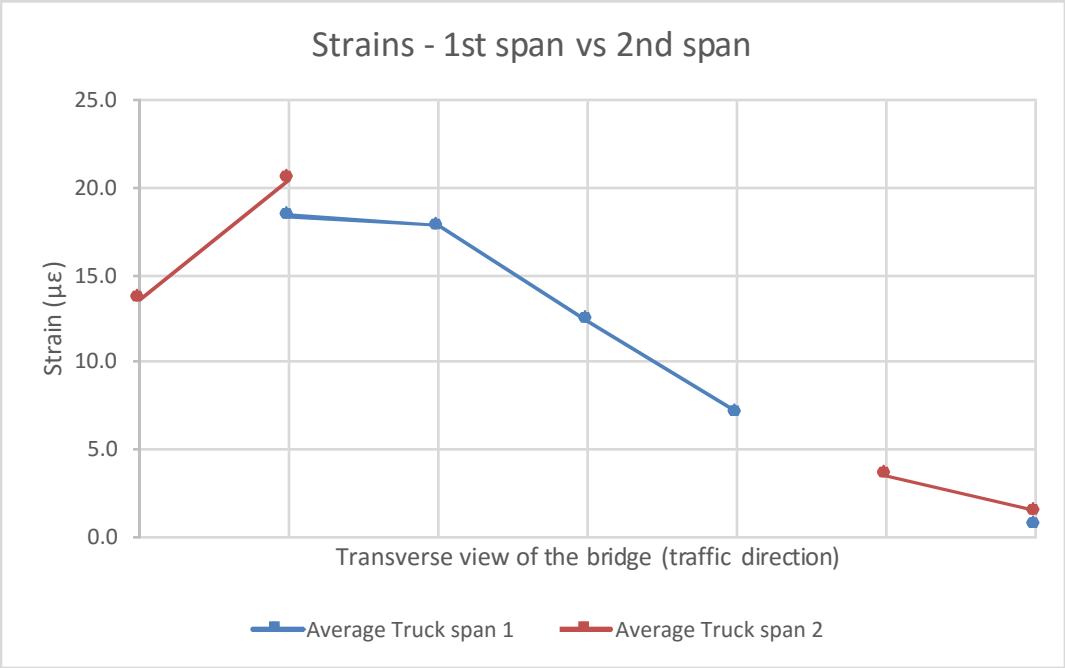

Figure A-2-3: Comparison of Averaged Strains for 1st and 2nd Span

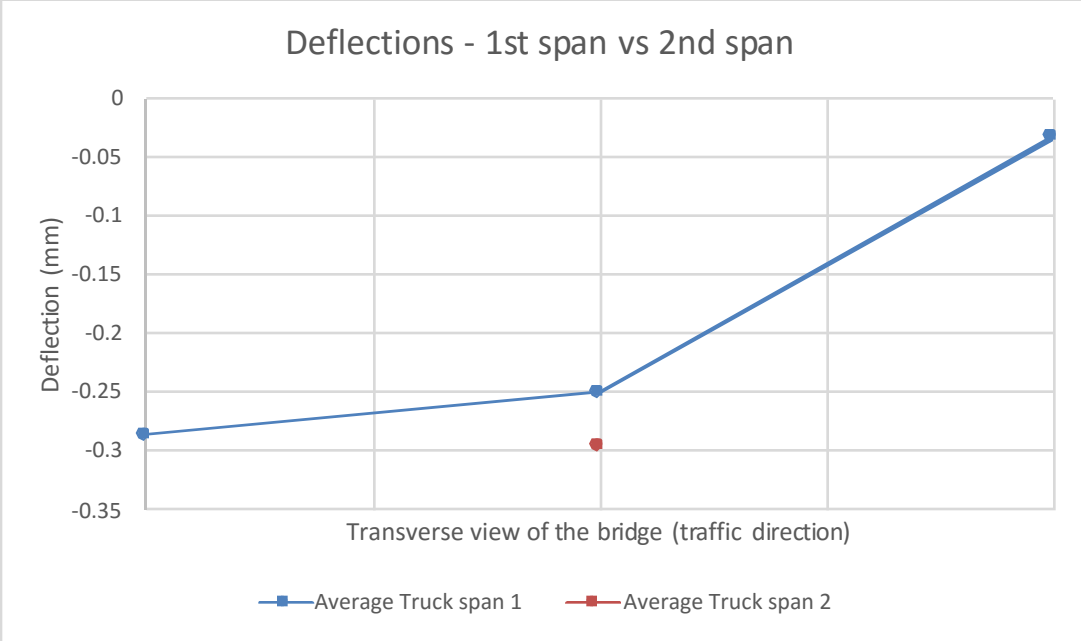

Figure A-2-4: Comparison of Averaged Deflections For 1st and 2nd Span

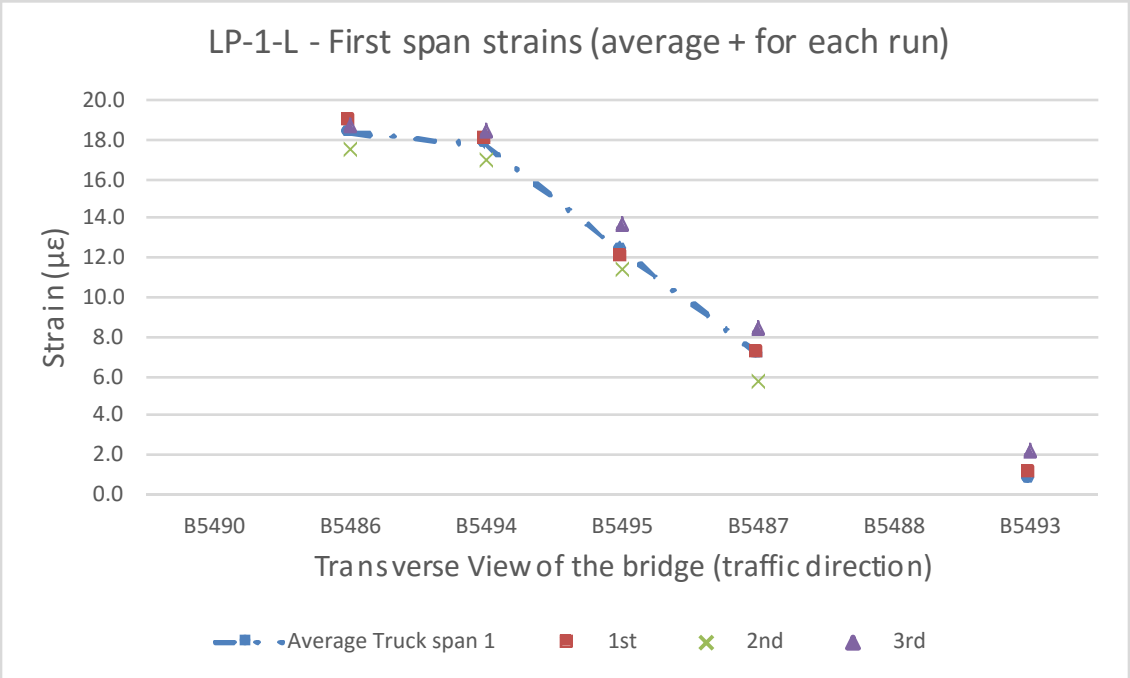

Figure A-2-5: Comparison of Averaged Strains and Strains for Each Run – 1st Span

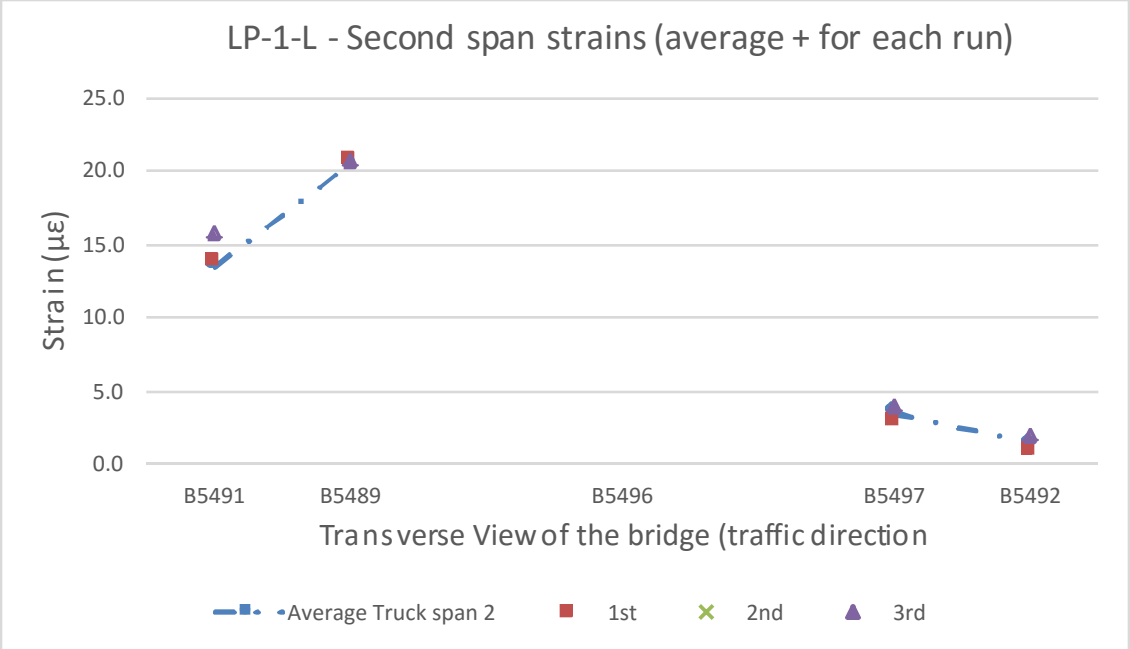

Figure A-2-6: Comparison of Averaged Strains and Strains for Each Run – 2nd Span

Load Pattern LP-1-R:

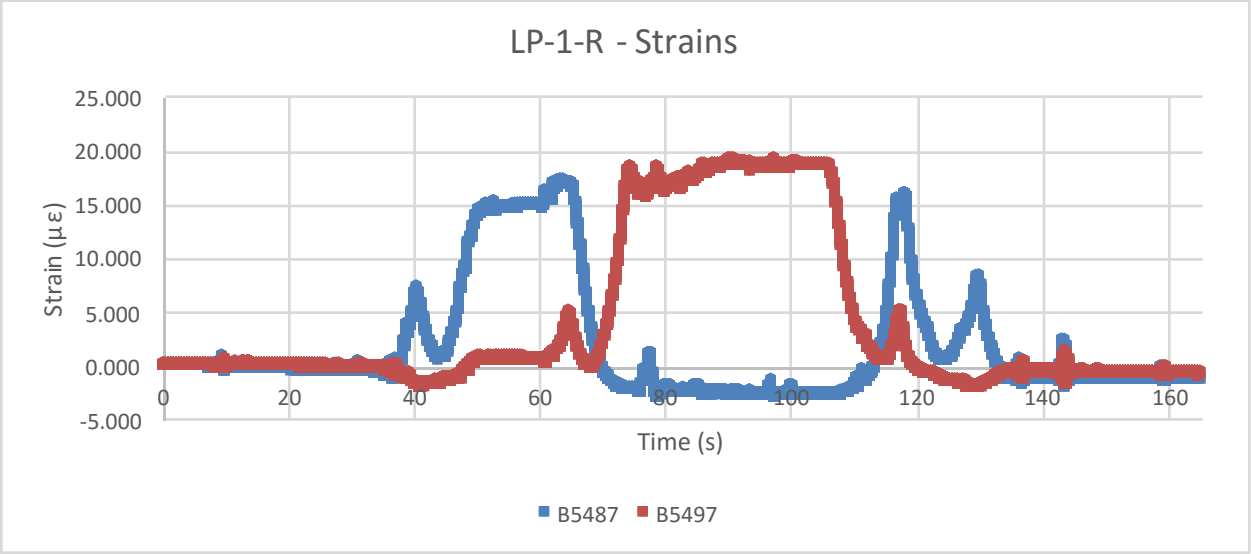

Figure A-2-7: Strains in Time for Second Run

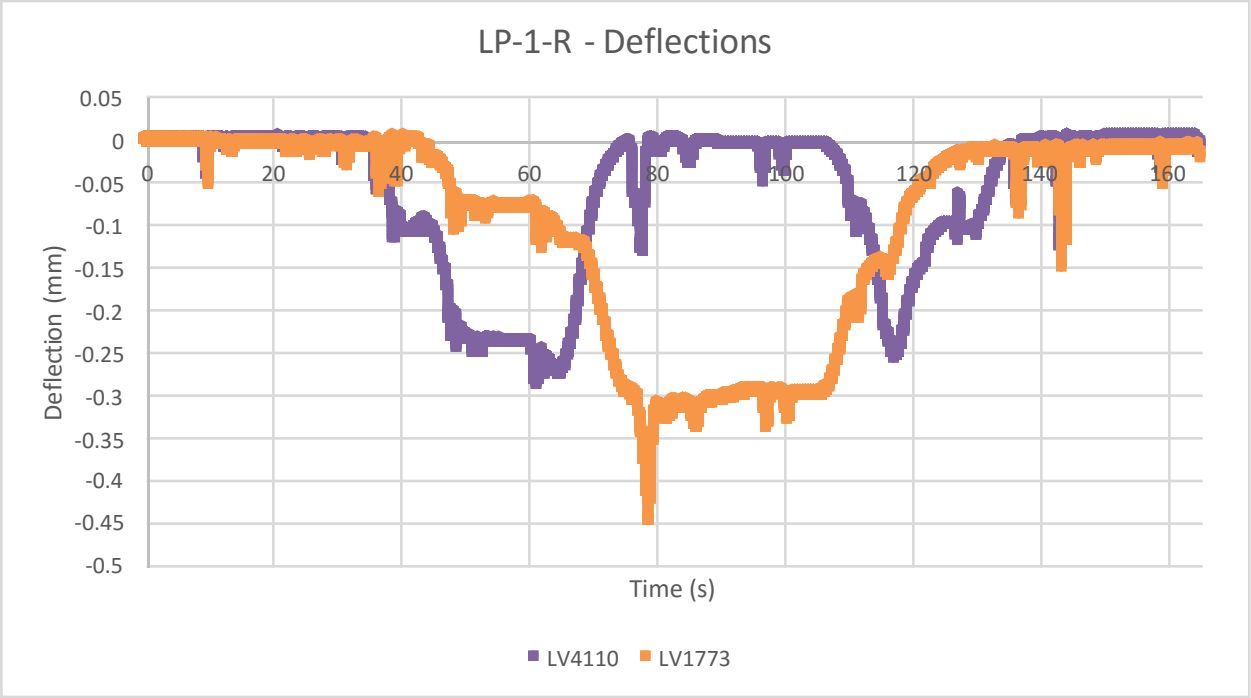

Figure A-2-8: Deflections in Time for Second Run

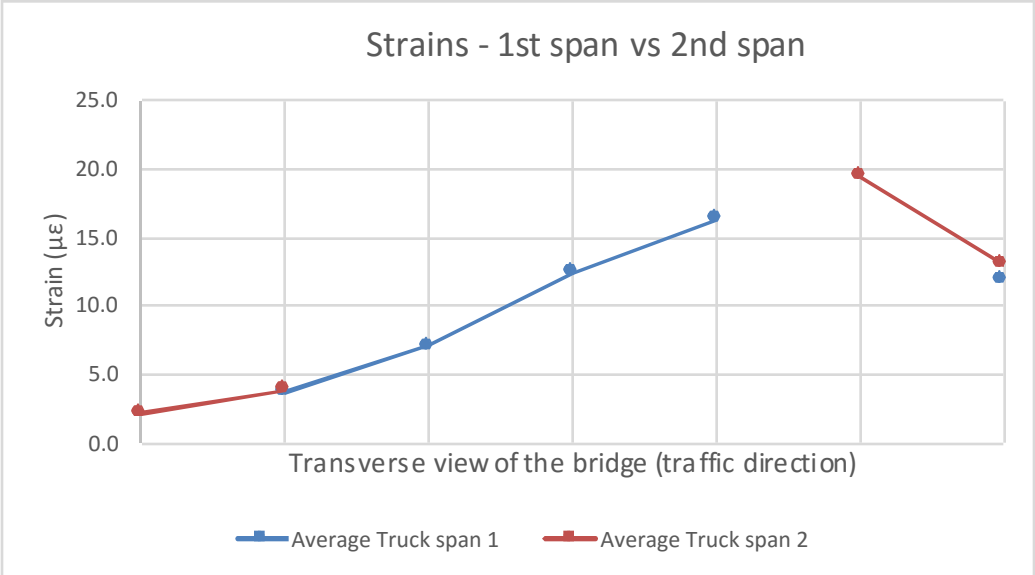

Figure A-2-9: Comparison of Averaged Strains for 1st and 2nd Span

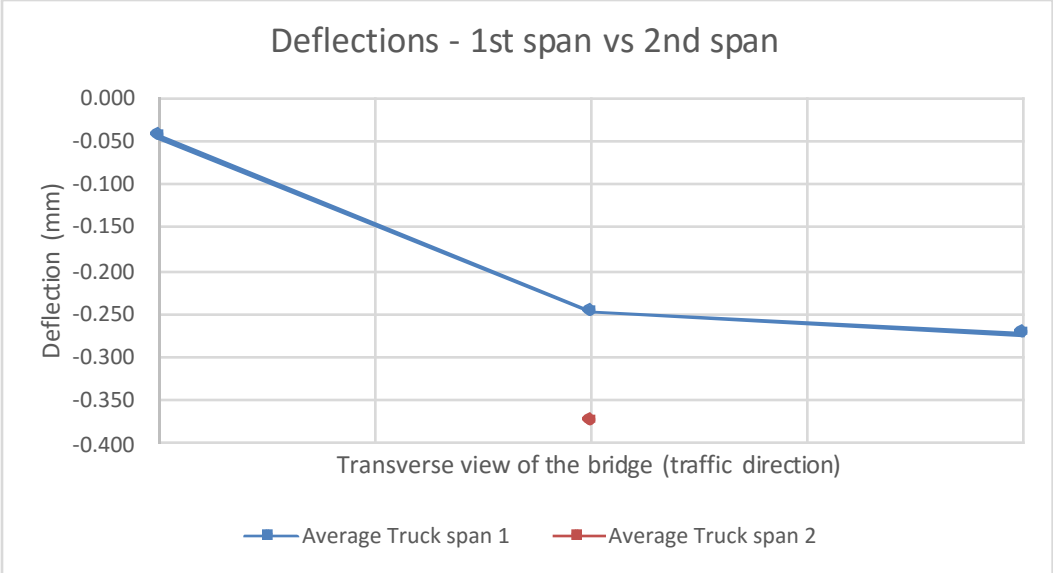

Figure A-2-10: Comparison of Averaged Deflections for 1st and 2nd Span

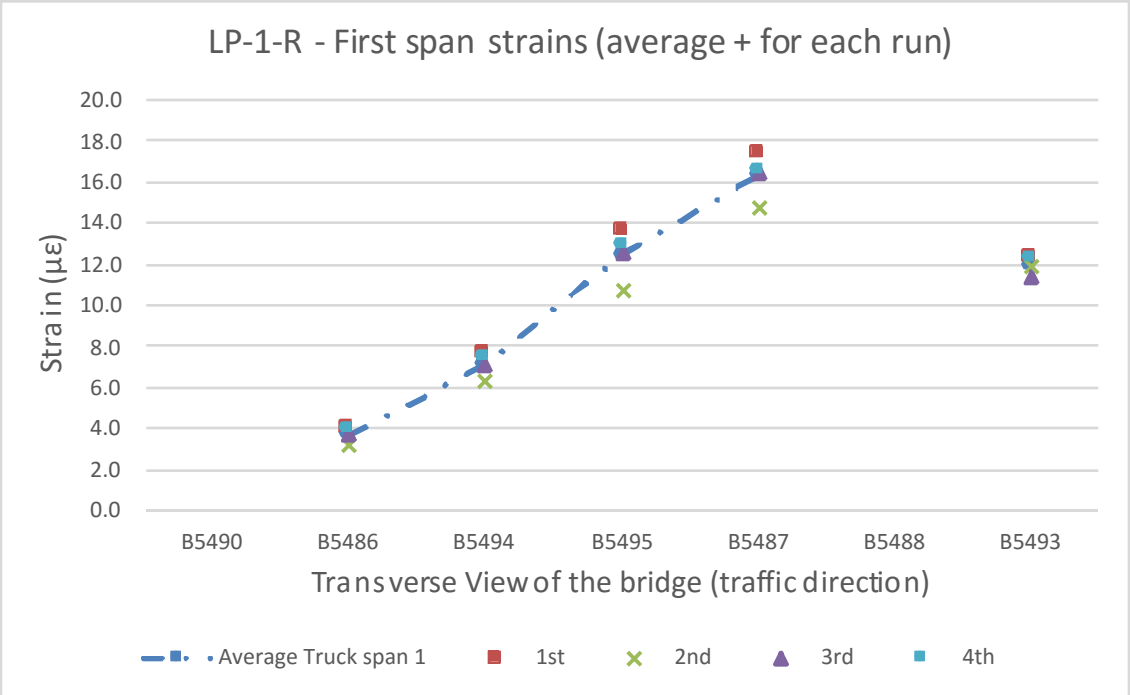

Figure A-2-11: Comparison of Averaged Strains and Strains for Each Run – 1st Span

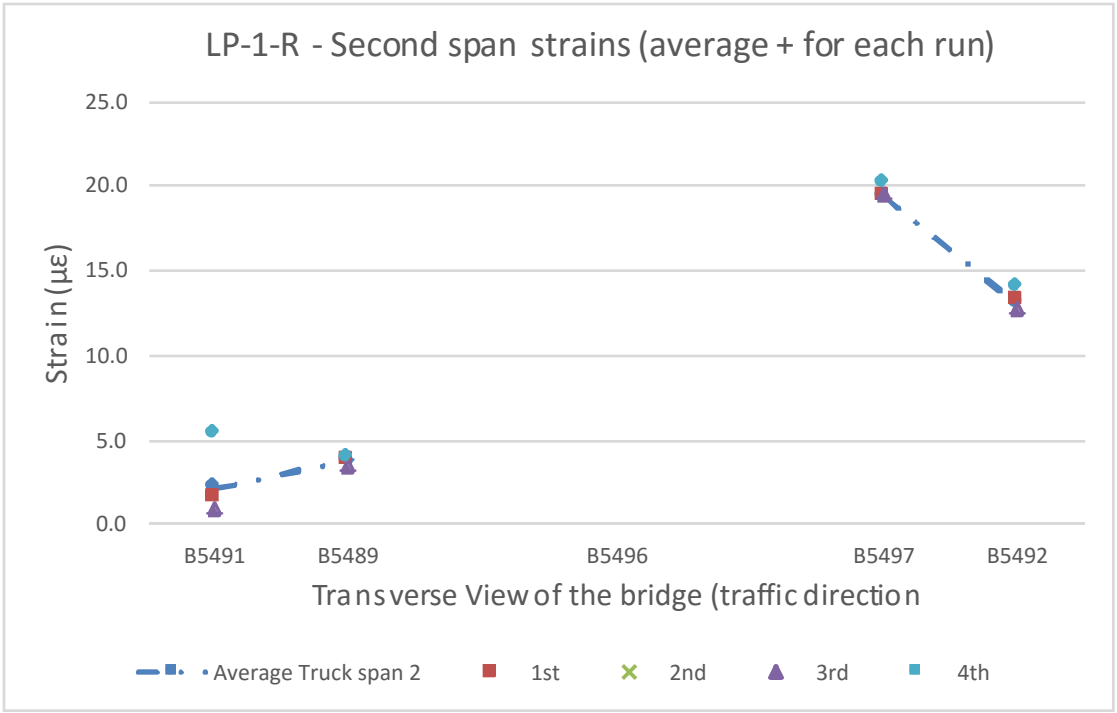

Figure A-2-12: Comparison of Averaged Strains and Strains for Each Run – 2nd Span

Load Pattern LP-2-L:

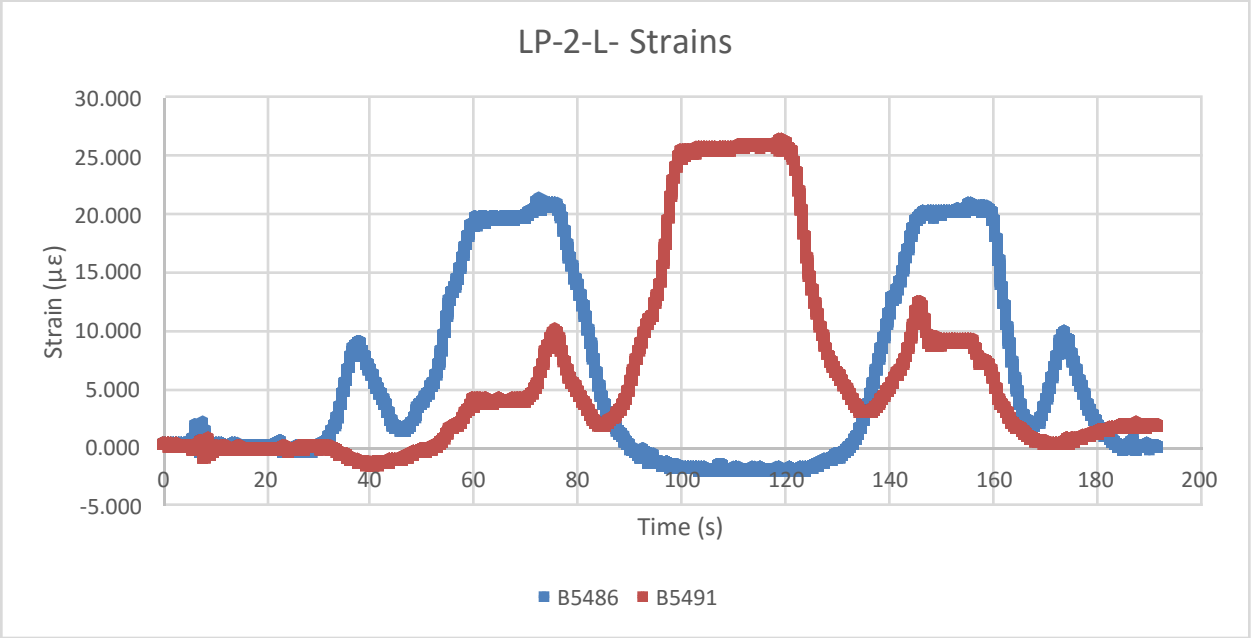

Figure A-2-13: Strains in Time for Second Run

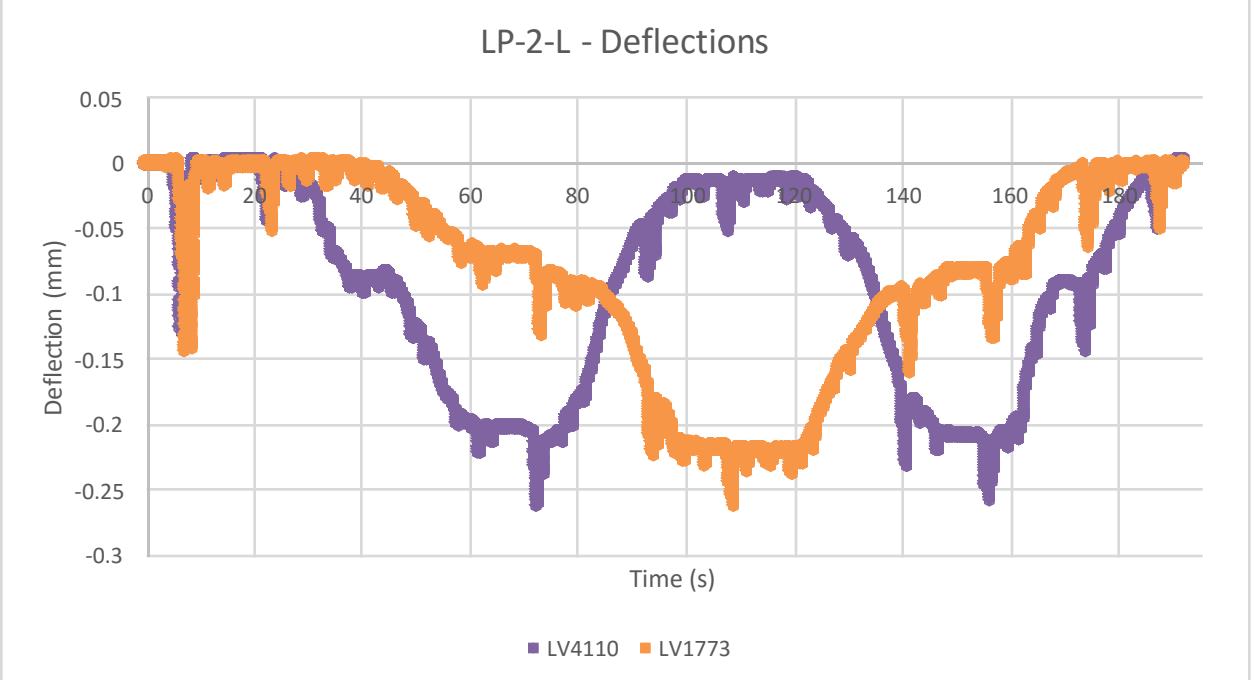

Figure A-2-14: Deflections in Time for Second Run

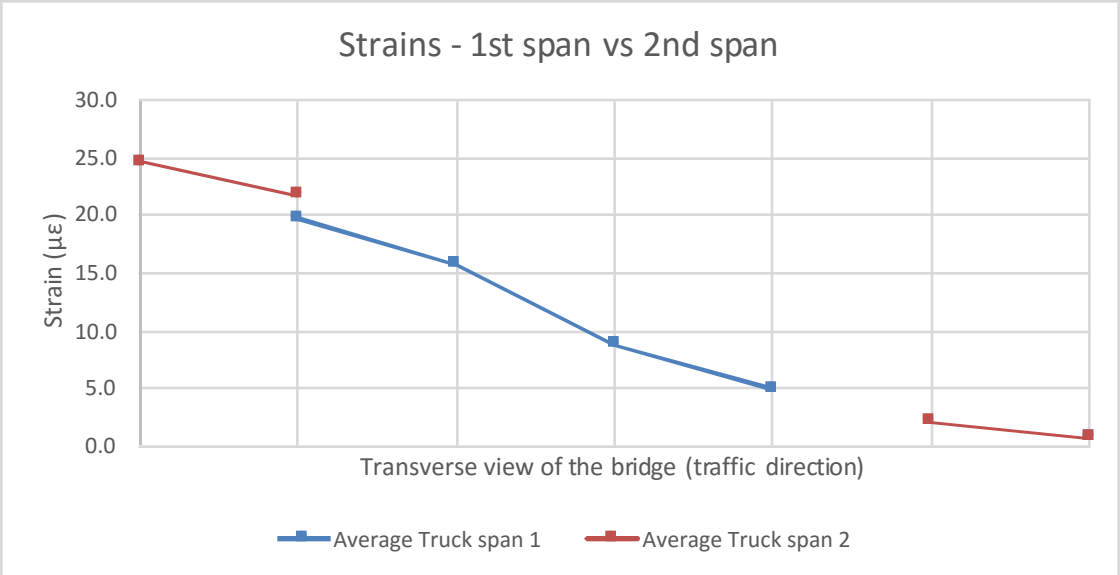

Figure A-2-15: Comparison of Averaged Strains for 1st and 2nd Span

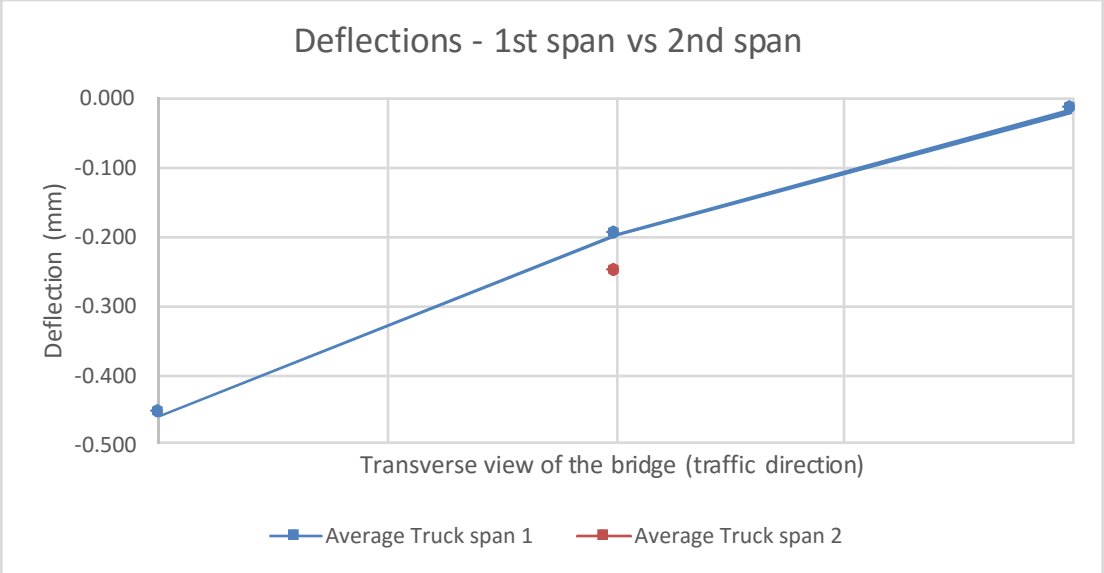

Figure A-2-16: Comparison of Averaged Deflections for 1st and 2nd Span

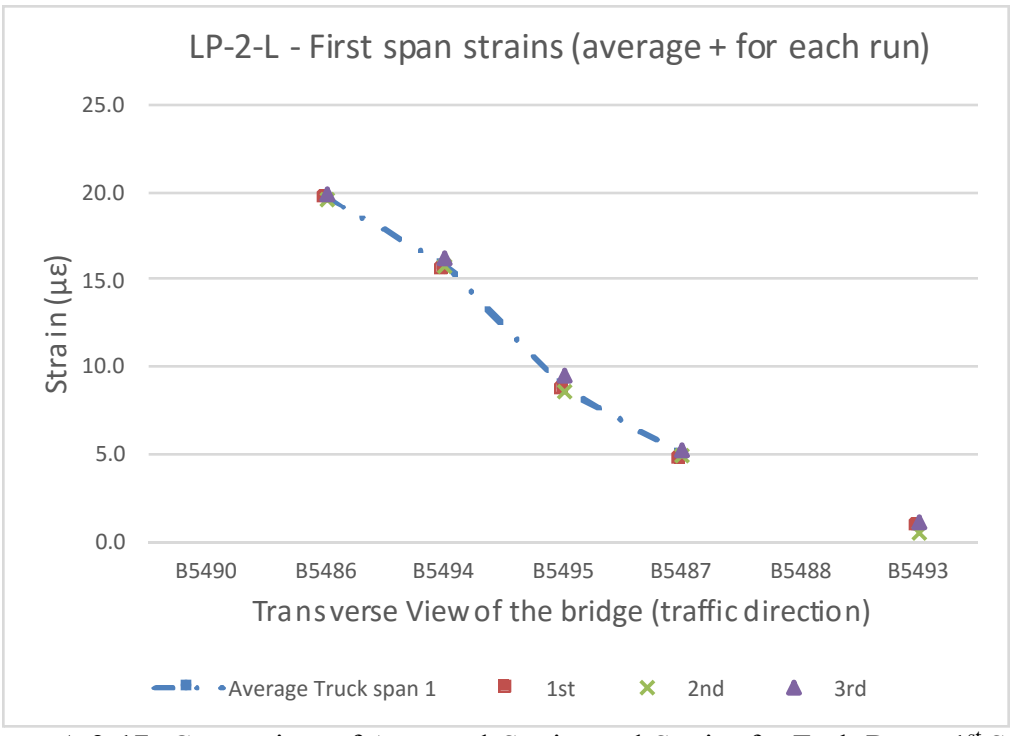

Figure A-2-17: Comparison of Averaged Strains and Strains for Each Run – 1st Span

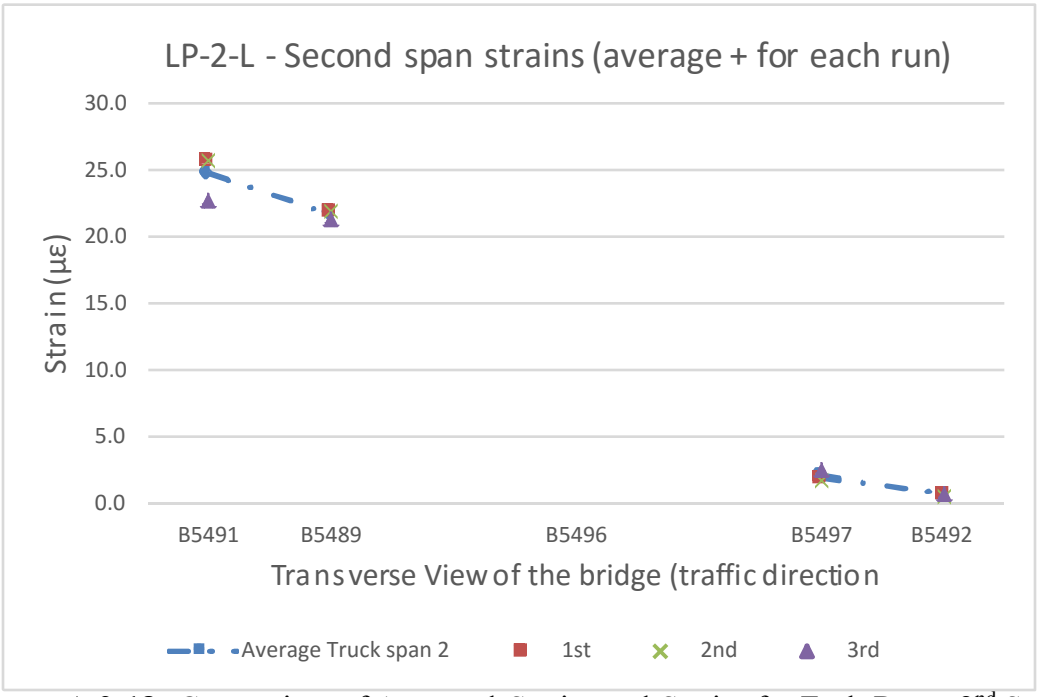

Figure A-2-18: Comparison of Averaged Strains and Strains for Each Run – 2nd Span

Load Pattern LP-2-R:

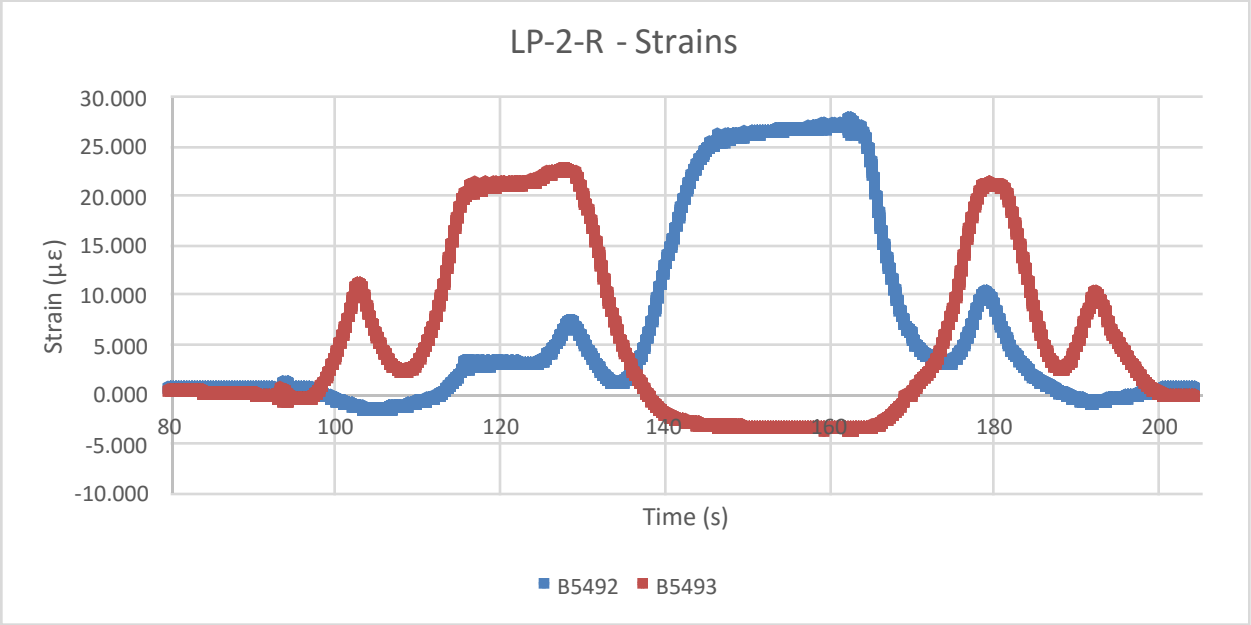

Figure A-2-19: Strains in Time for First Run

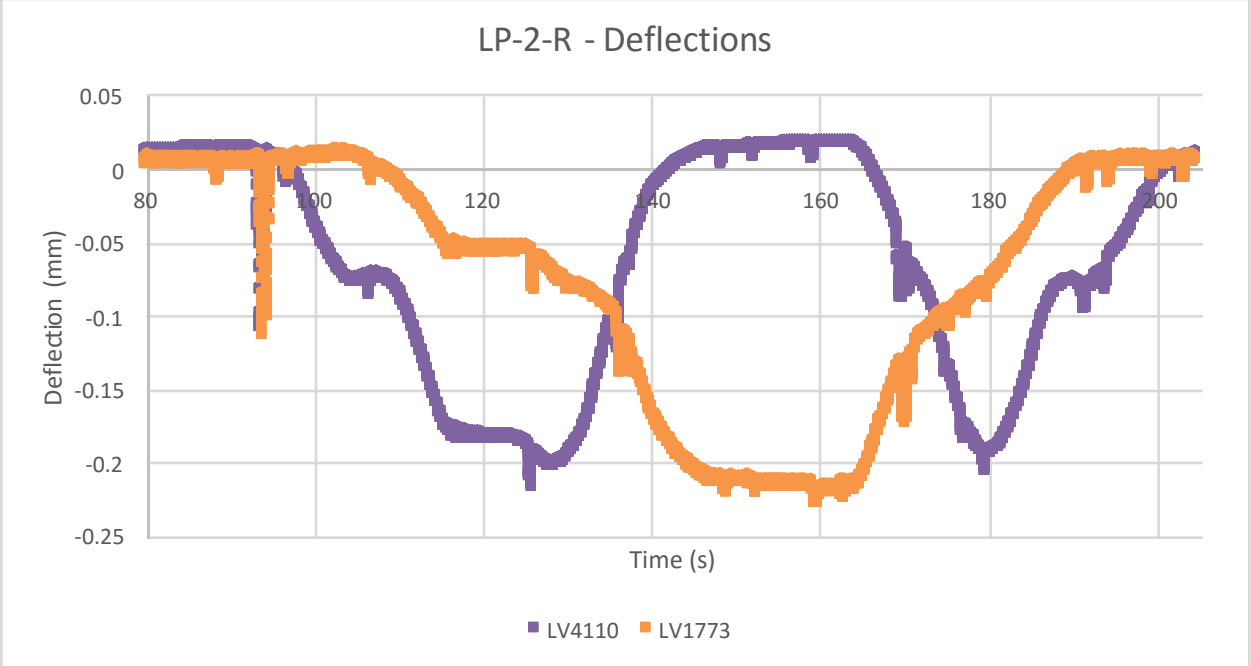

Figure A-2-20: Deflections in Time for First Run

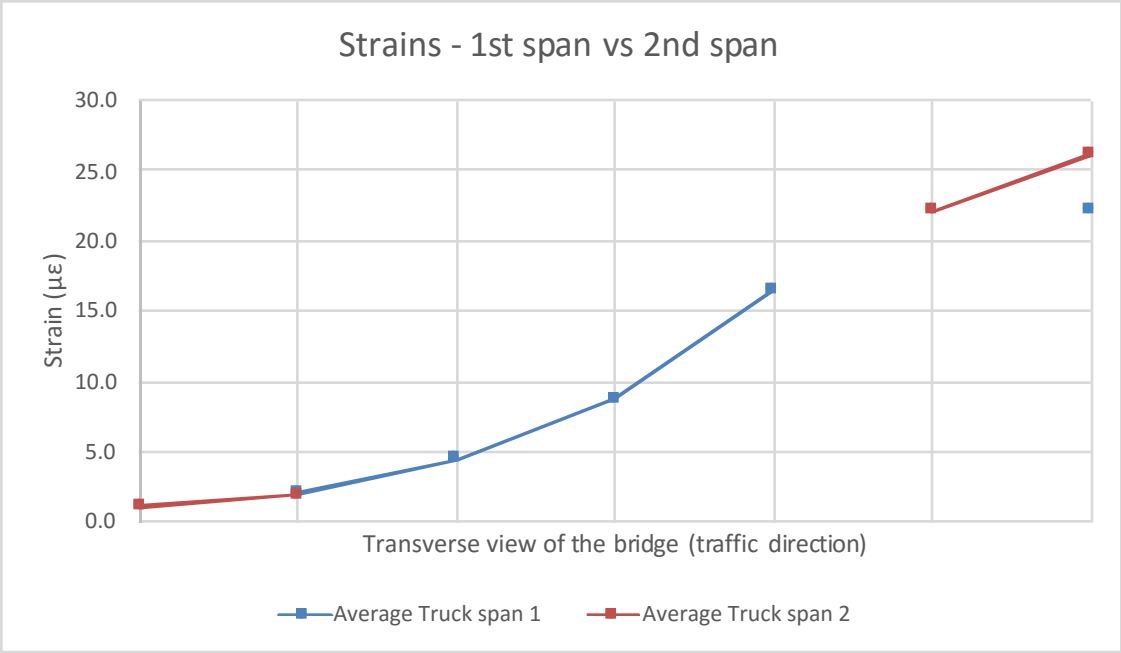

Figure A-2-21: Comparison of Averaged Strains for 1st and 2nd Span

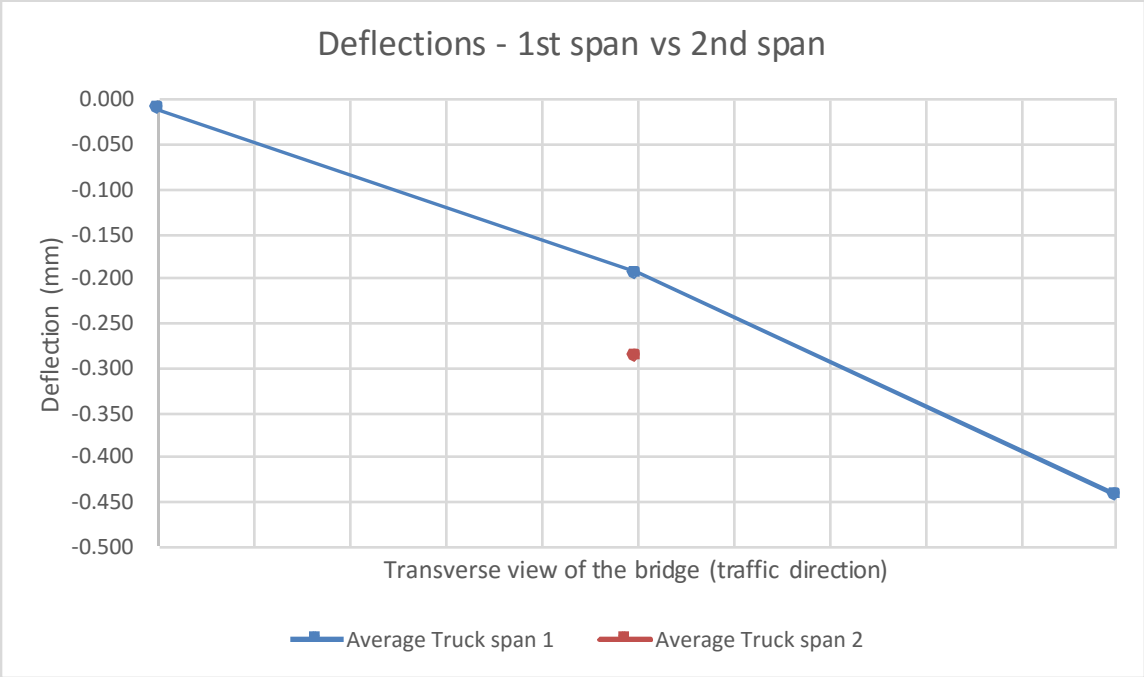

Figure A-2-22: Comparison of Averaged Deflections for 1st and 2nd Span

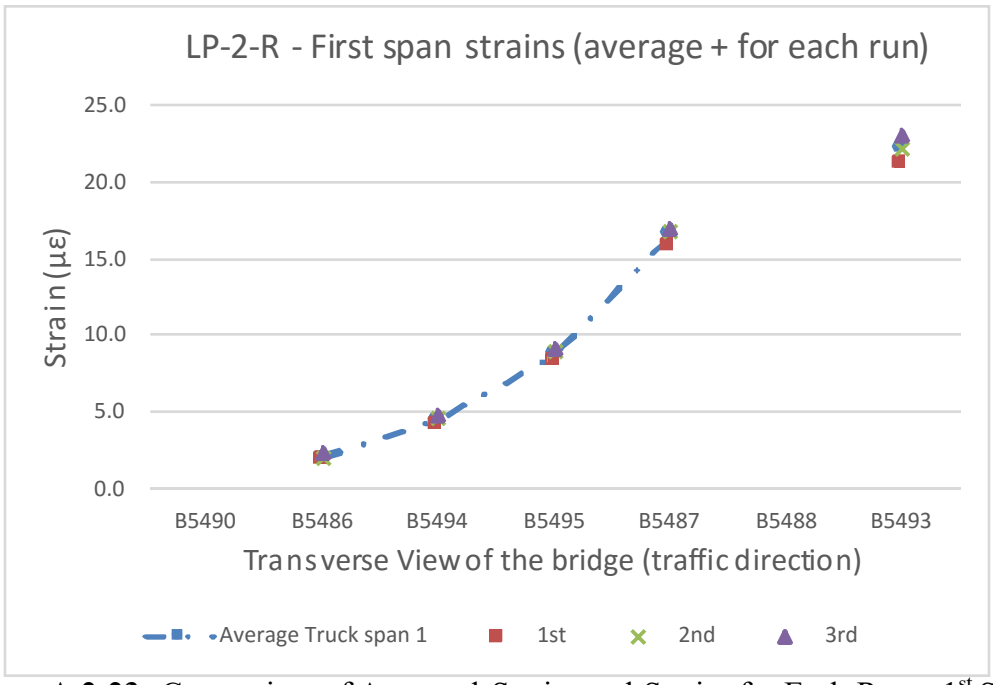

Figure A-2-23: Comparison of Averaged Strains and Strains for Each Run – 1st Span

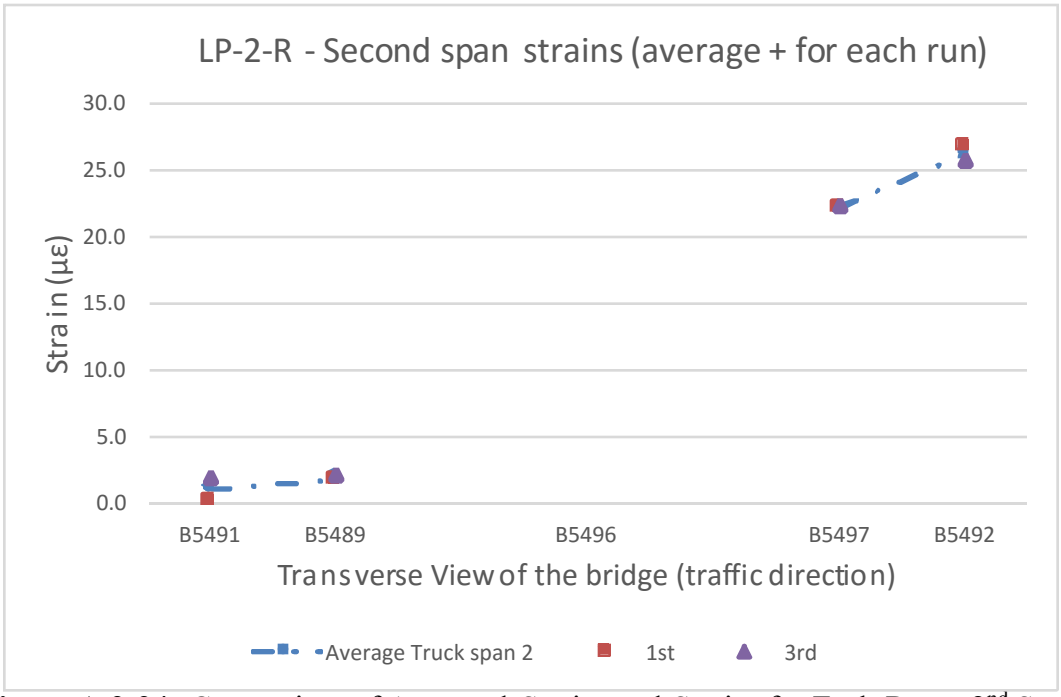

Figure A-2-24: Comparison of Averaged Strains and Strains for Each Run – 2nd Span

Load Pattern LP-4-L:

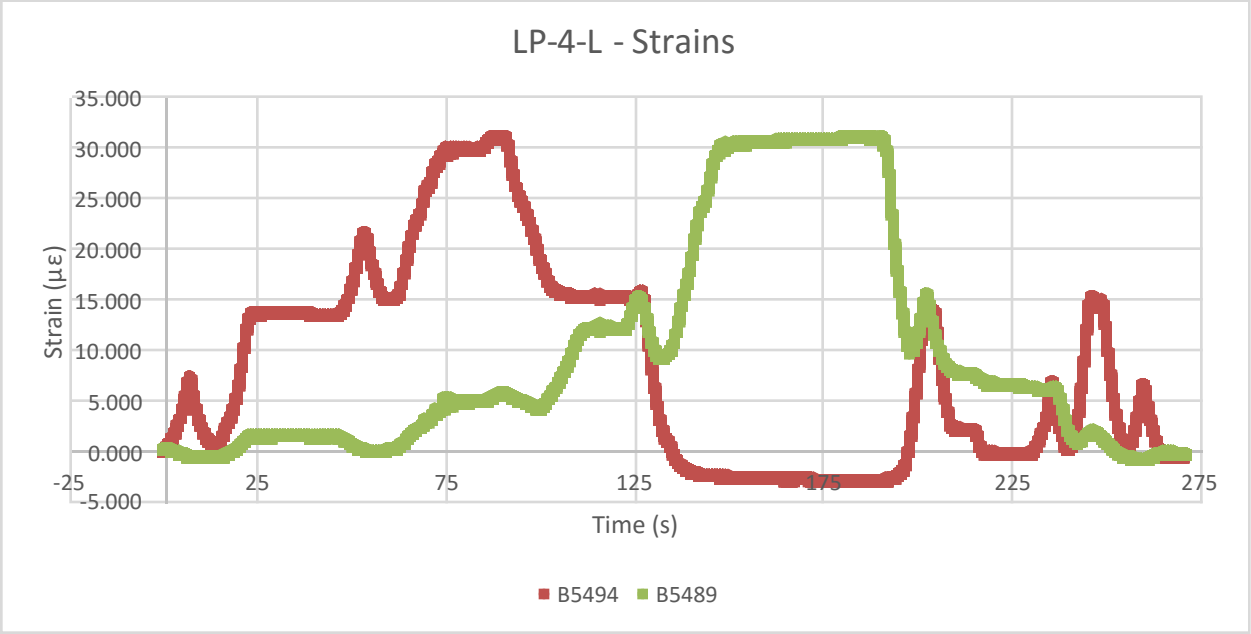

Figure A-2-25: Strains in Time for Second Run

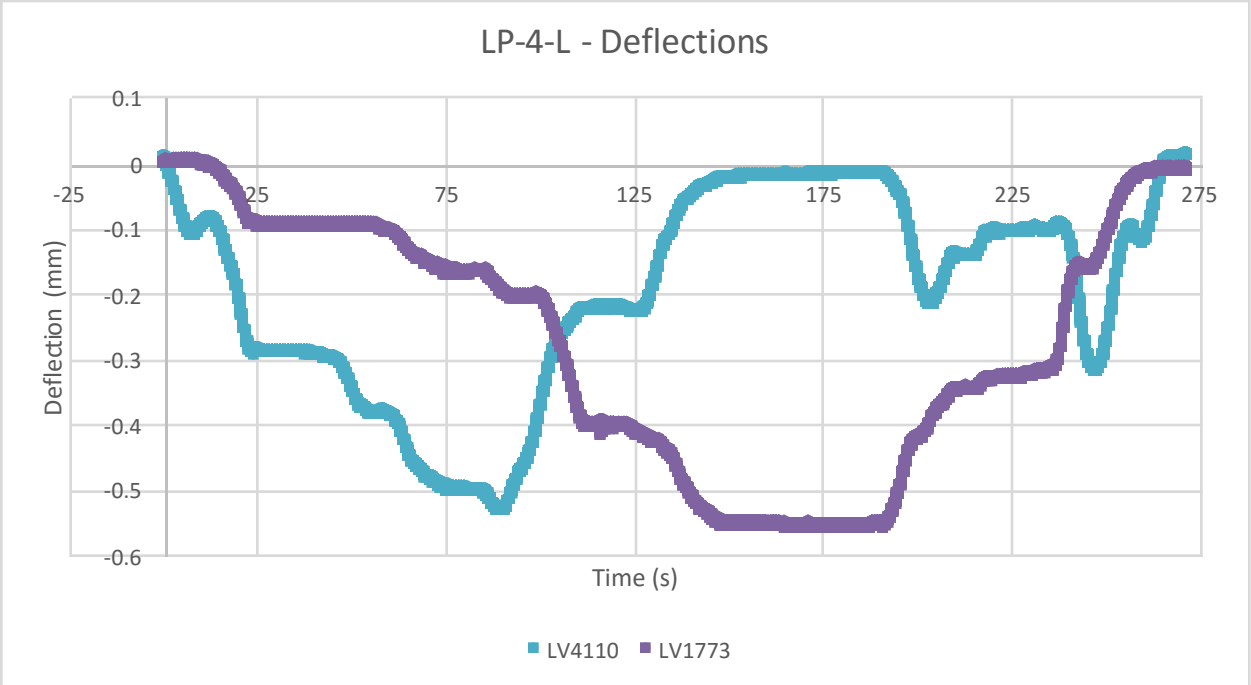

Figure A-2-26: Deflections in Time for Second Run

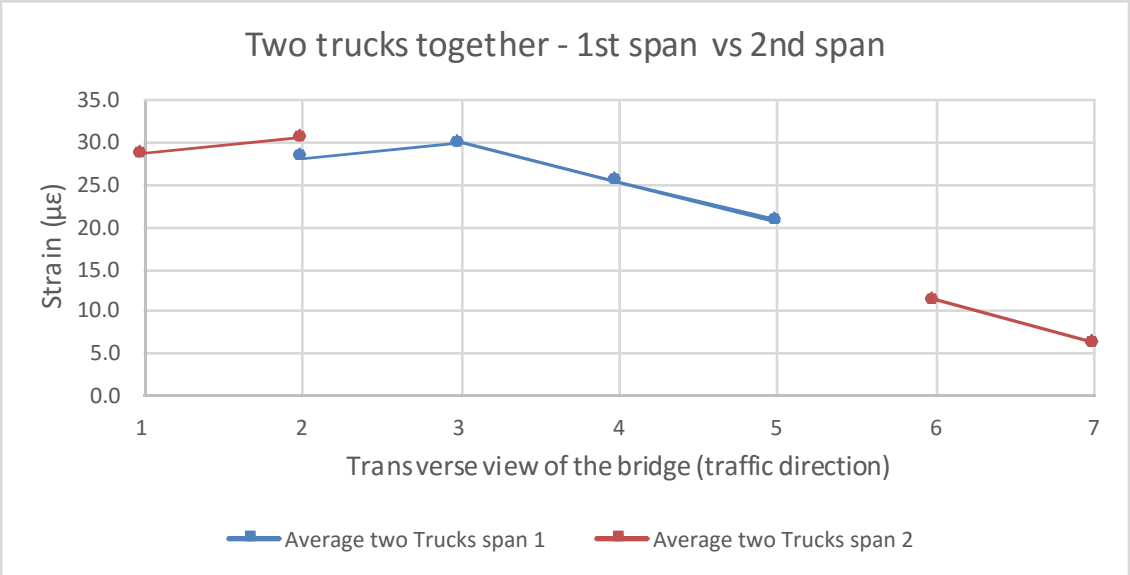

Figure A-2-27: Comparison of Averaged Strains for 1st and 2nd Span

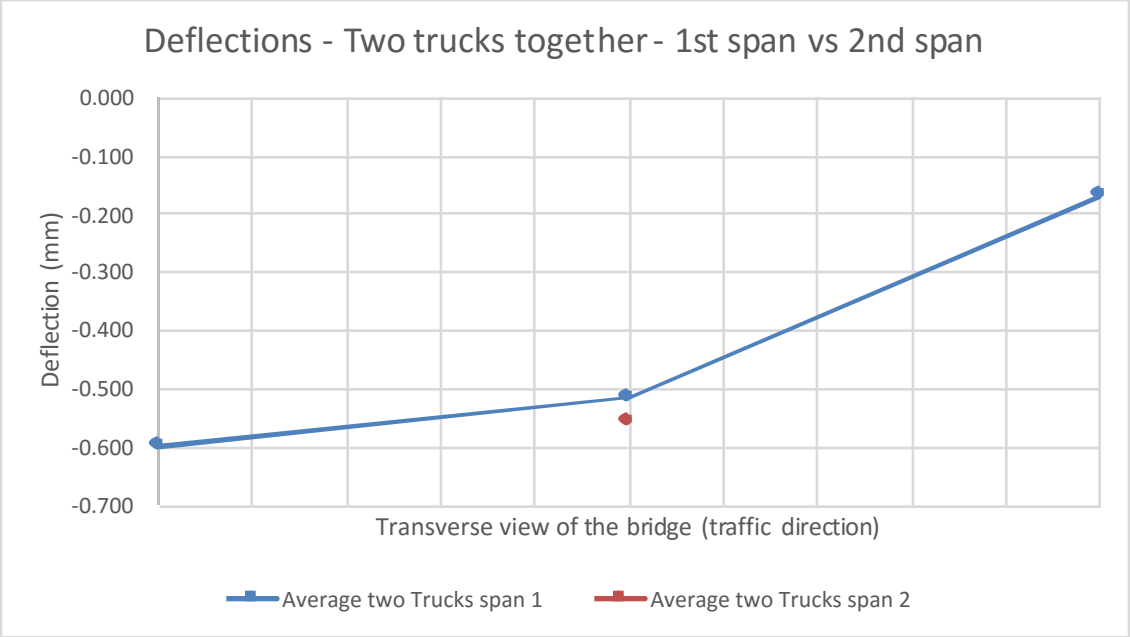

Figure A-2-28: Comparison of Averaged Deflections for 1st and 2nd Span

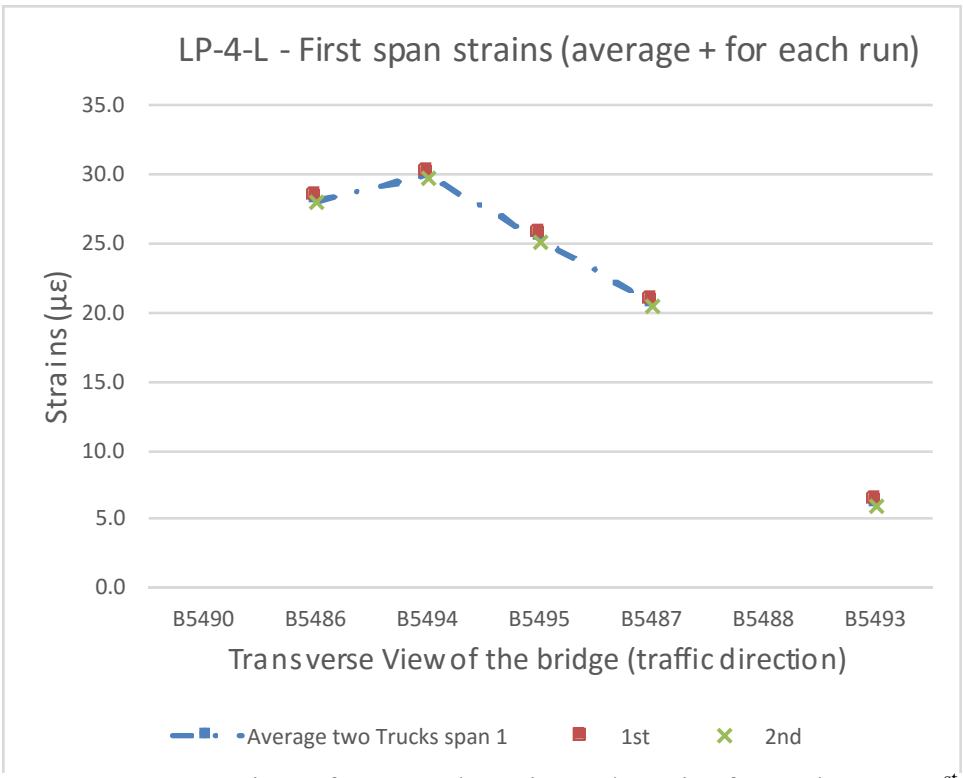

Figure A-2-29: Comparison of Averaged Strains and Strains for Each Run – 1st Span

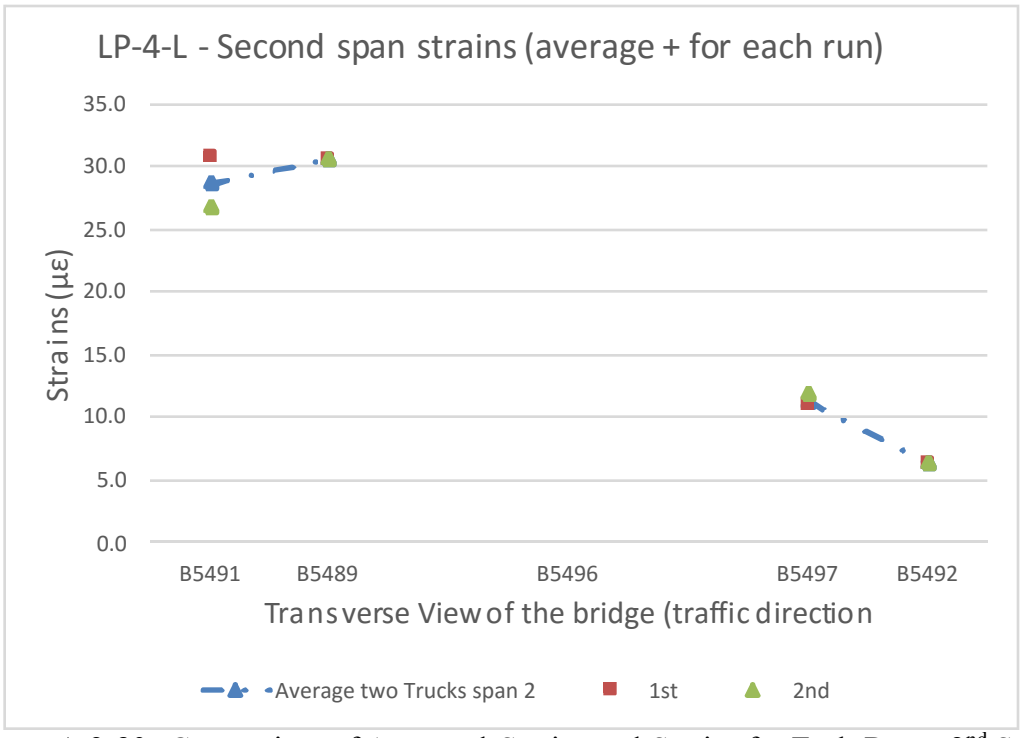

Figure A-2-30: Comparison of Averaged Strains and Strains for Each Run – 2nd Span

Load Pattern LP-4-R:

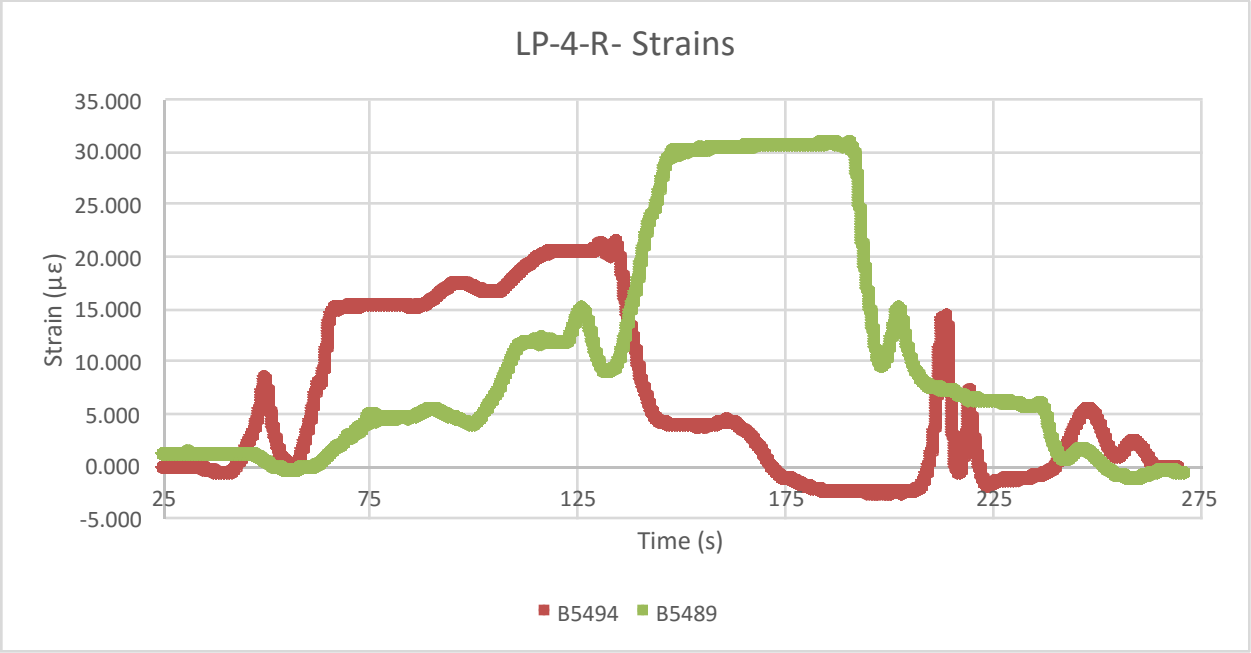

Figure A-2-31: Strains in Time for Second Run

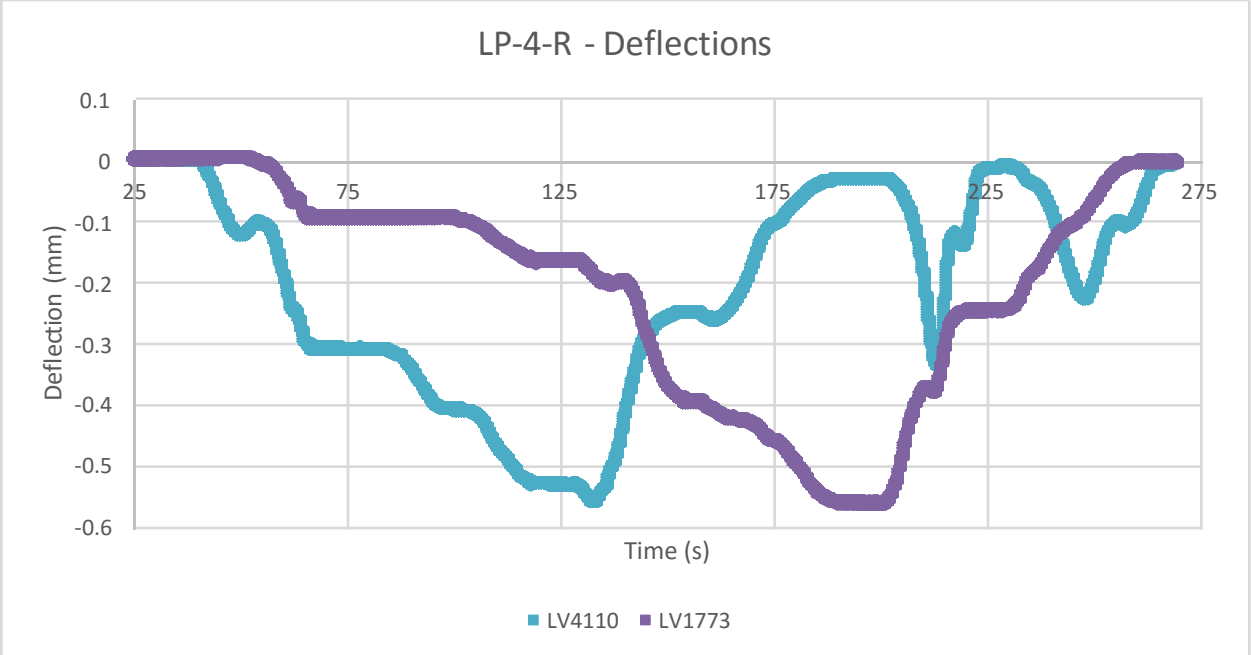

Figure A-2-32: Deflections in Time for Second Run

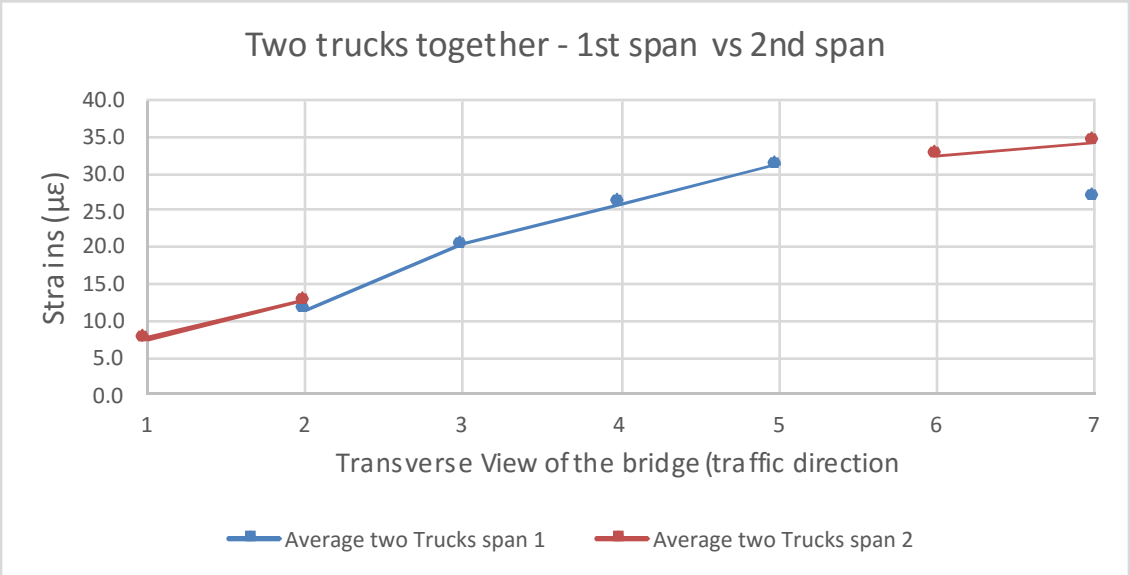

Figure A-2-33: Comparison of Averaged Strains for 1st and 2nd Span

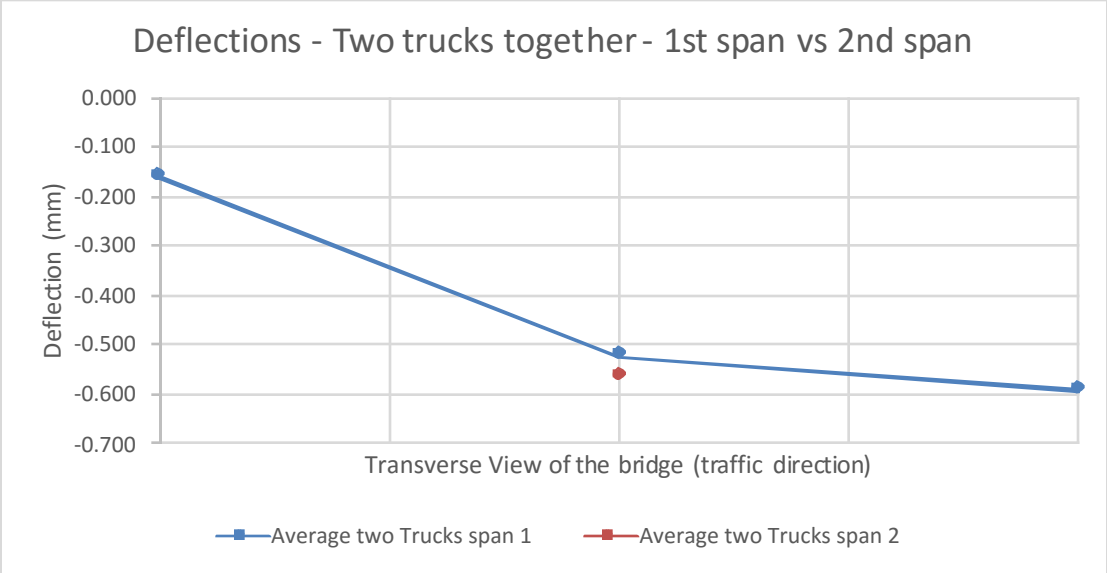

Figure A-2-34: Comparison of Averaged Deflections for 1st and 2nd Span

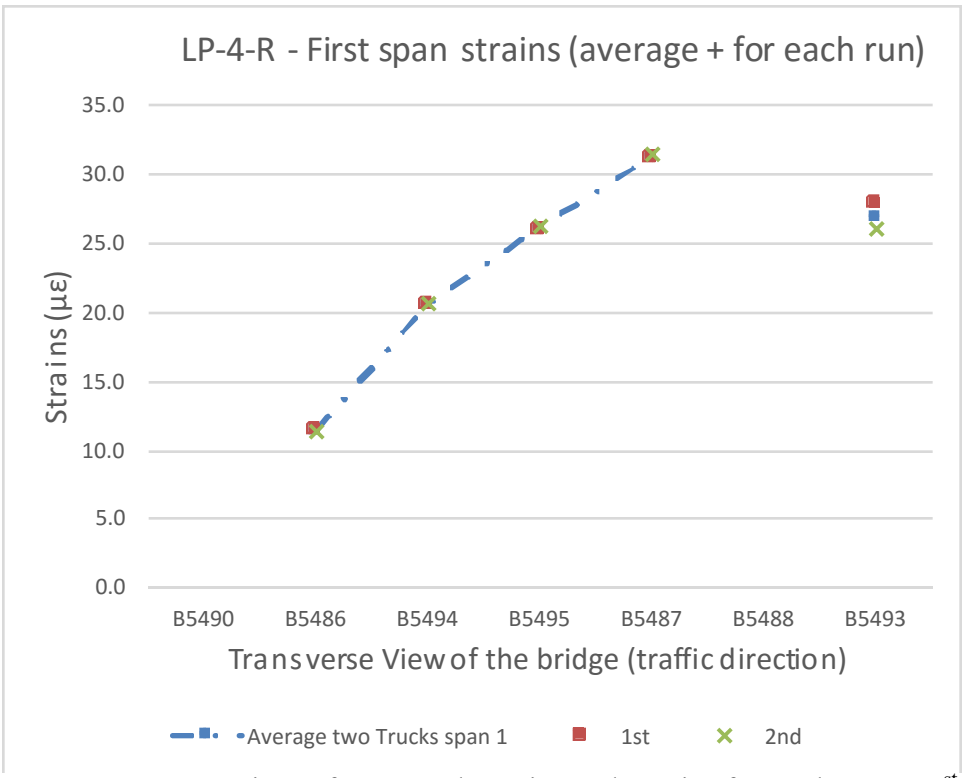

Figure A-2-35: Comparison of Averaged Strains and Strains for Each Run – 1st Span

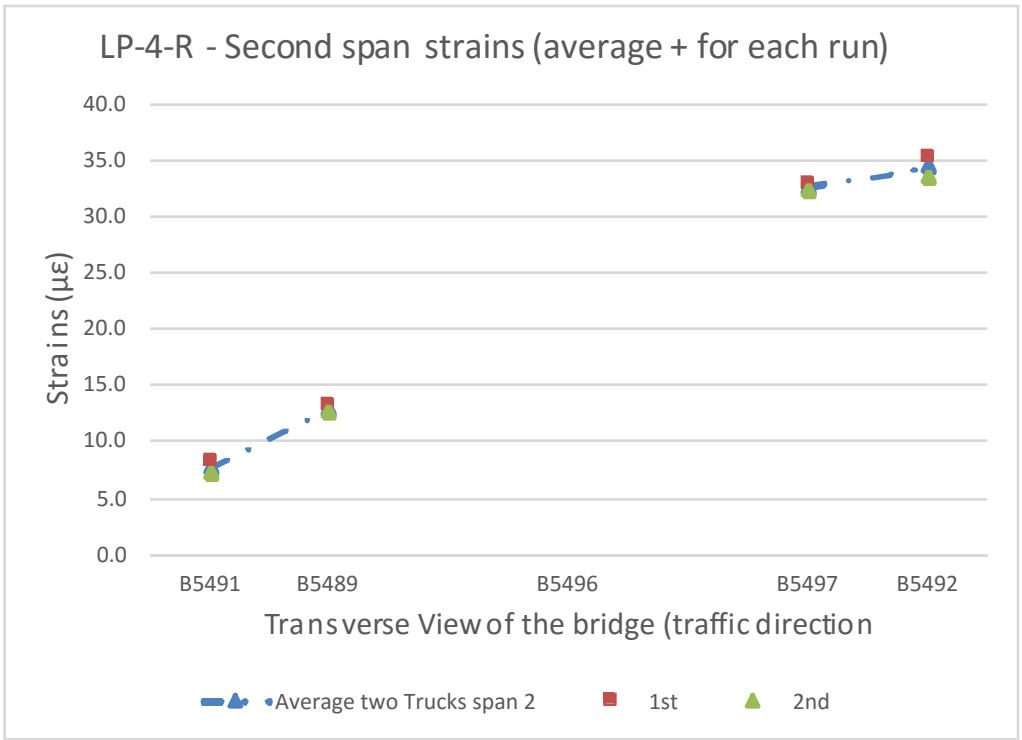

Figure A-2-36: Comparison of Averaged Strains and Strains for Each Run – 2nd Span

Load Pattern LP-3-L-CS:

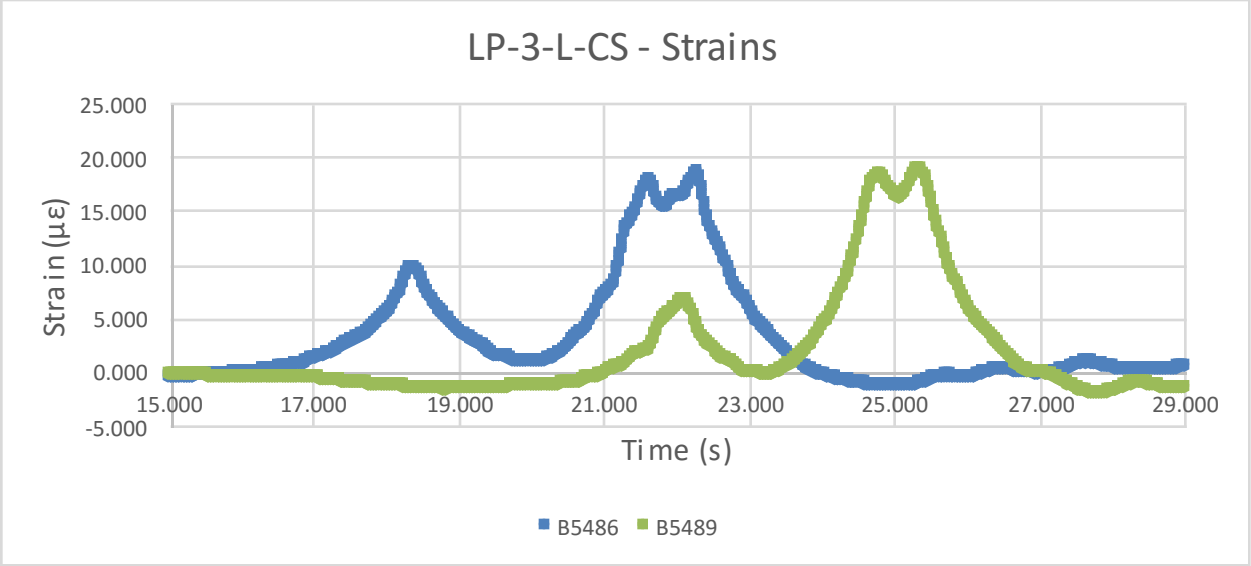

Figure A-2-37: Strains in Time for Third Run

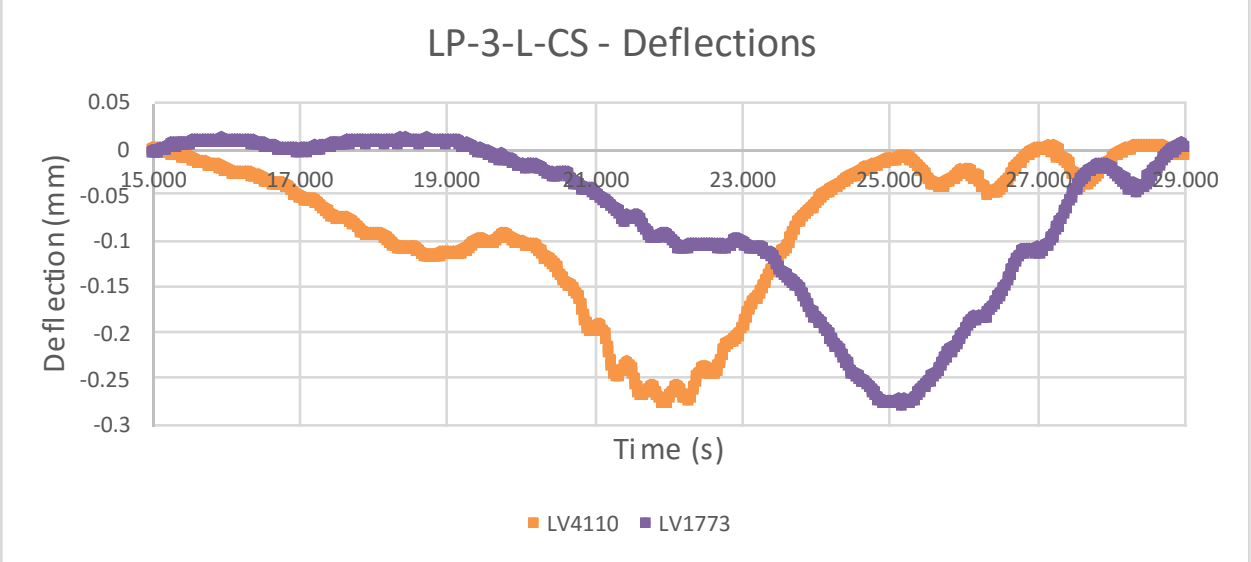

Figure A-2-38: Deflections in Time for Third Run

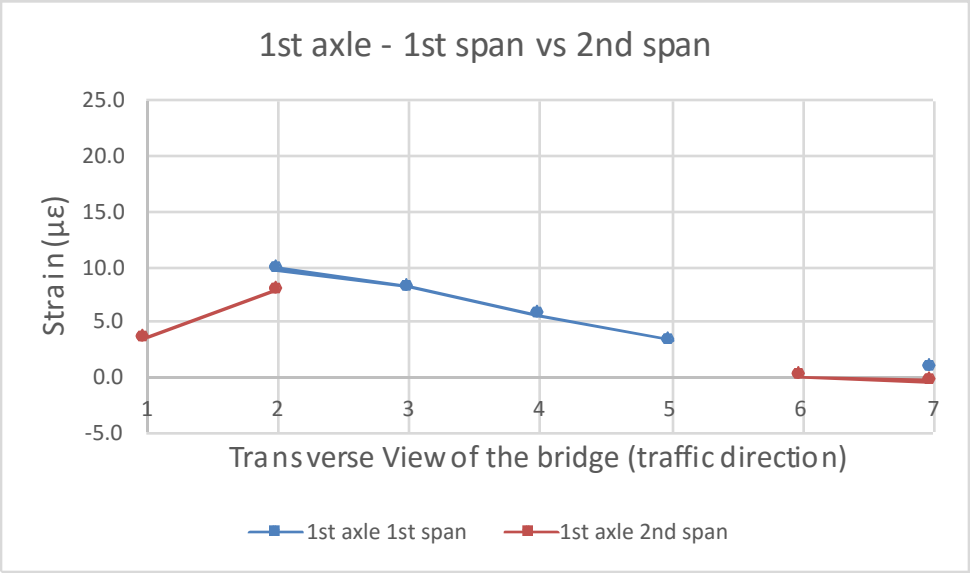

Figure A-2-39: Comparison of Averaged Strains for 1st and 2nd Span – First Axle

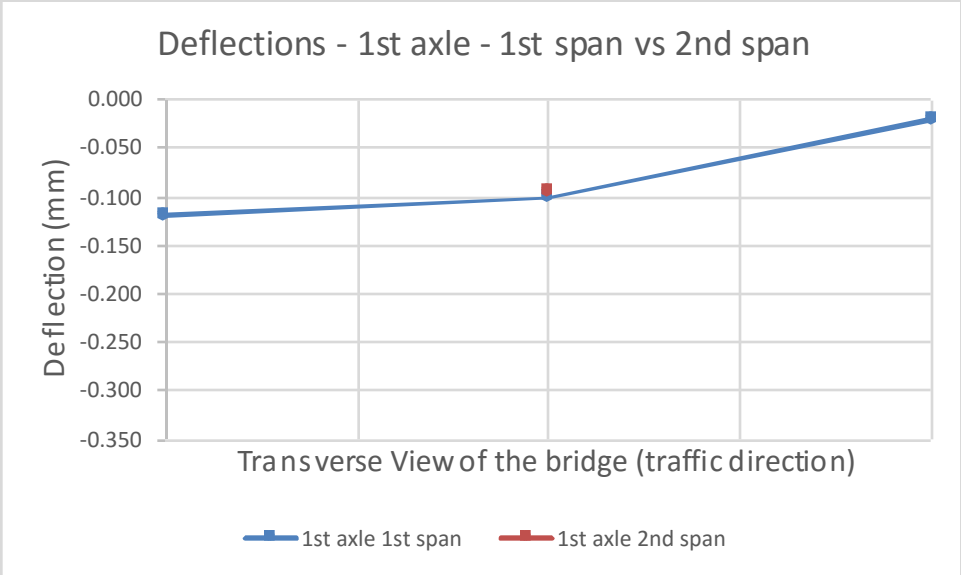

Figure A-2-40: Comparison of Averaged Deflections for 1st and 2nd Span – First Axle

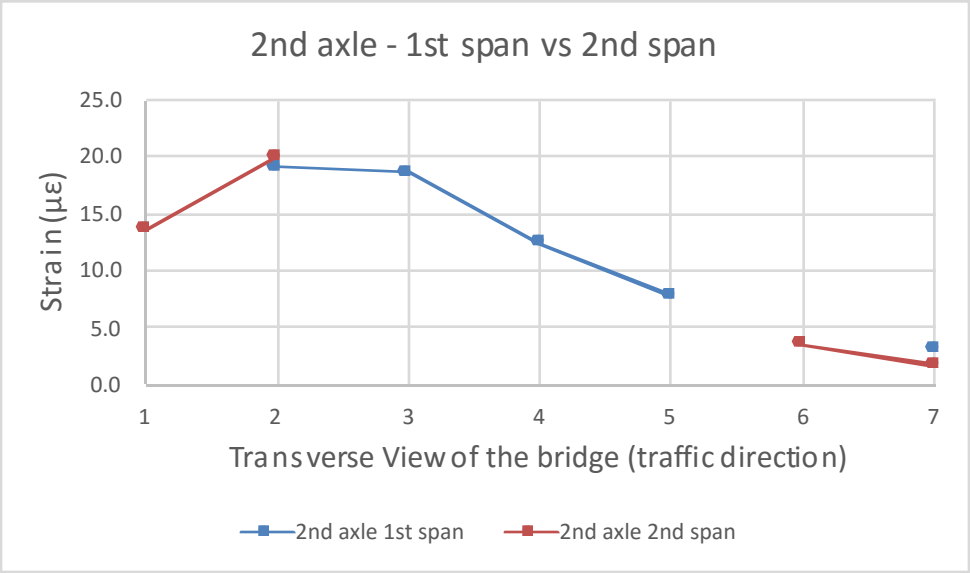

Figure A-2-41: Comparison of Averaged Strains for 1st and 2nd Span – Second Axle

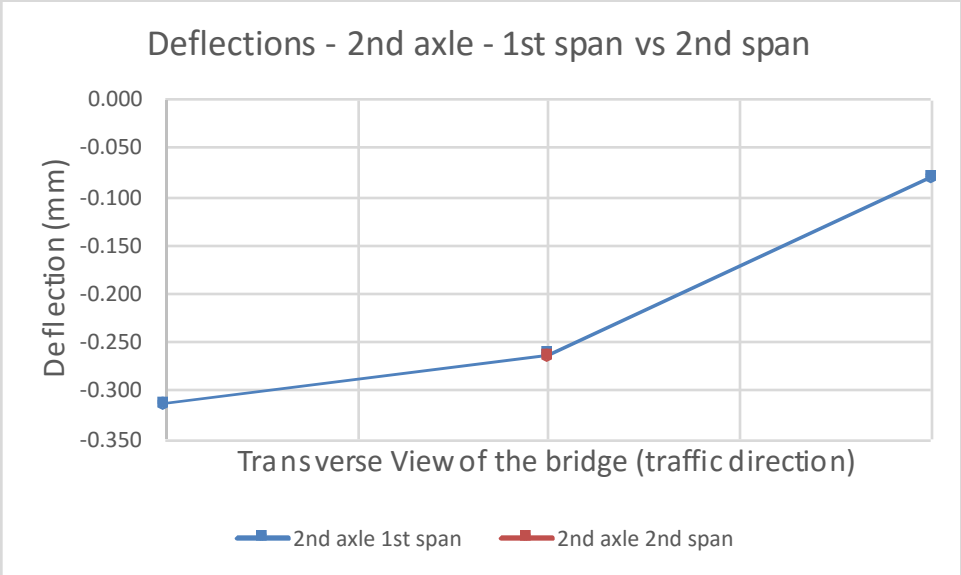

Figure A-2-42: Comparison of Averaged Deflections for 1st and 2nd Span – Second Axle

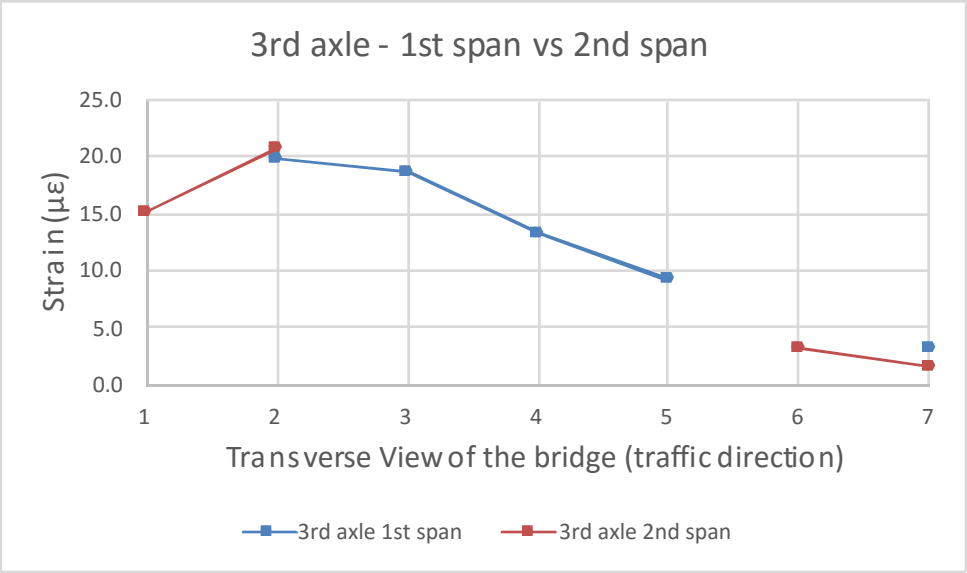

Figure A-2-43: Comparison of Averaged Strains for 1st and 2nd span – Third Axle

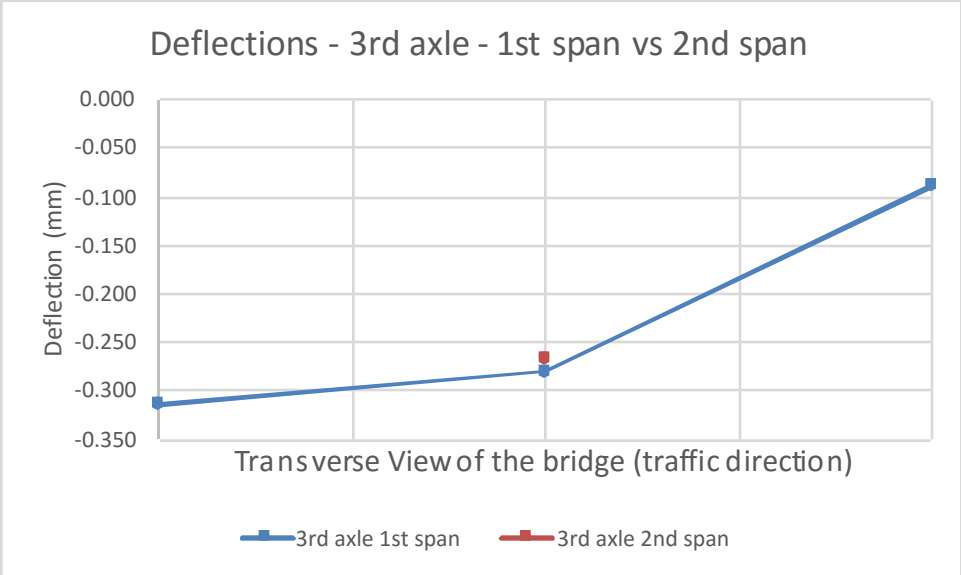

Figure A-2-44: Comparison of Averaged Deflections for 1st and 2nd Span – Third Axle

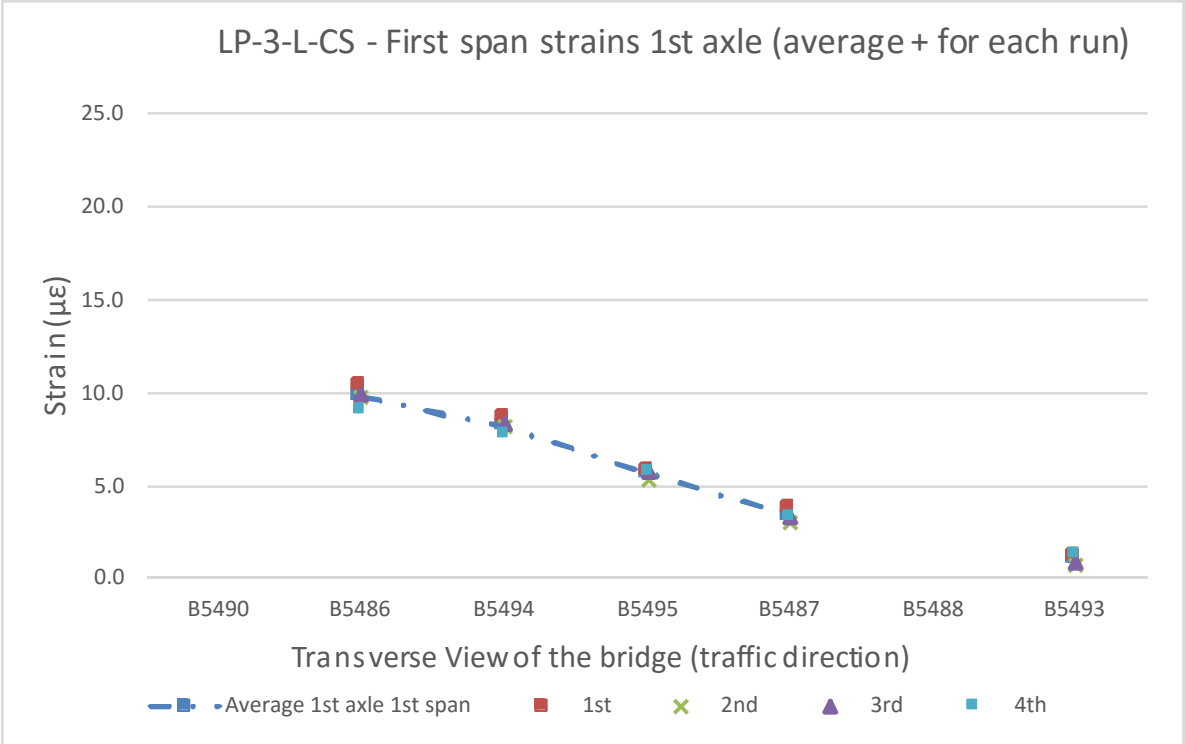

Figure A-2-45: Comparison of Averaged Strains and Strains for Each Run – 1st Span, 1st Axle

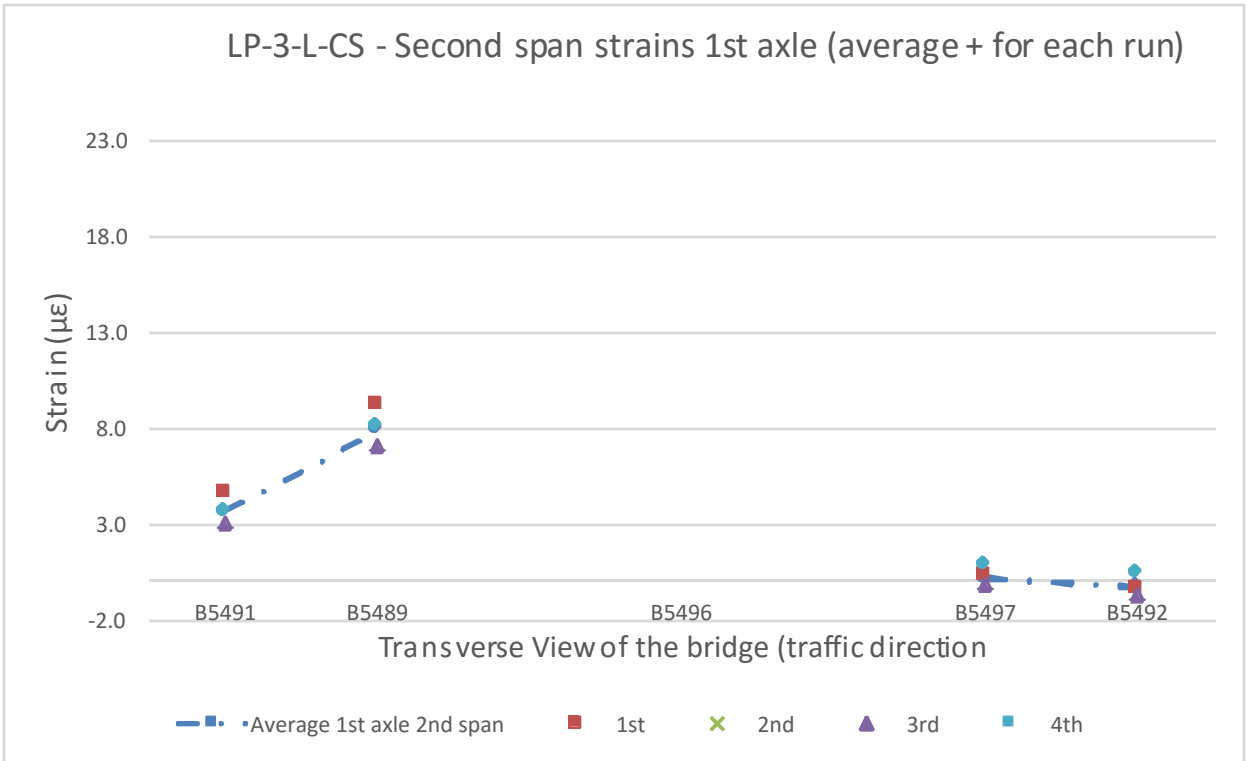

Figure A-2-46: Comparison of Averaged Strains and Strains for Each Run – 2nd Span, 1st Axle

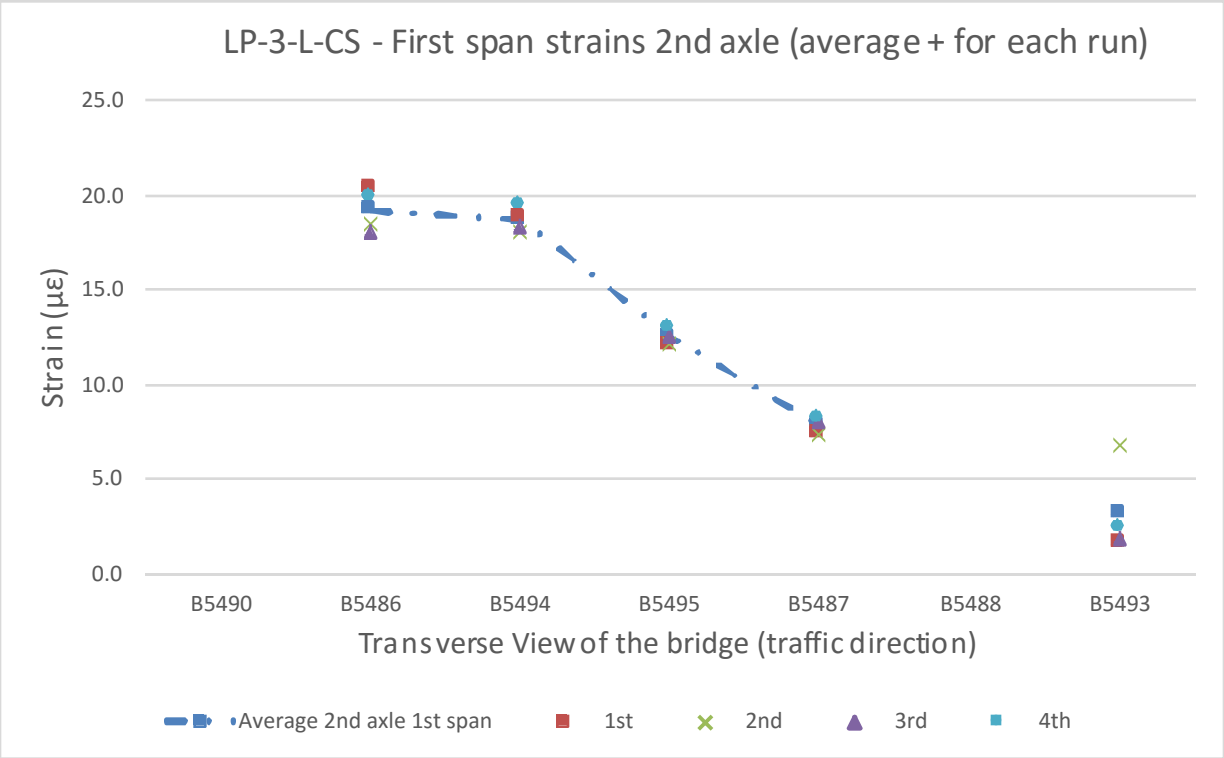

Figure A-2-47: Comparison of Averaged Strains and Strains for Each Run – 1st Span, 2nd Axle

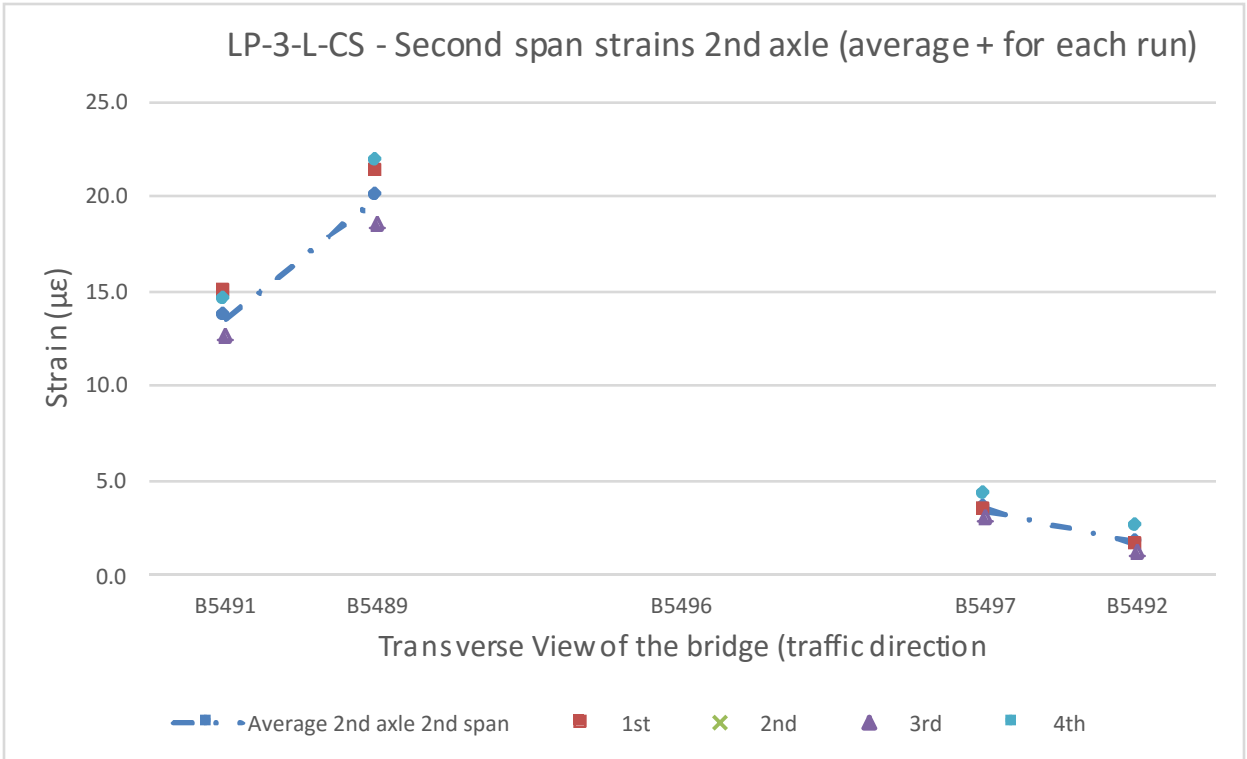

Figure A-2-48: Comparison of Averaged Strains and Strains for Each Run – 2nd Span, 2nd Axle

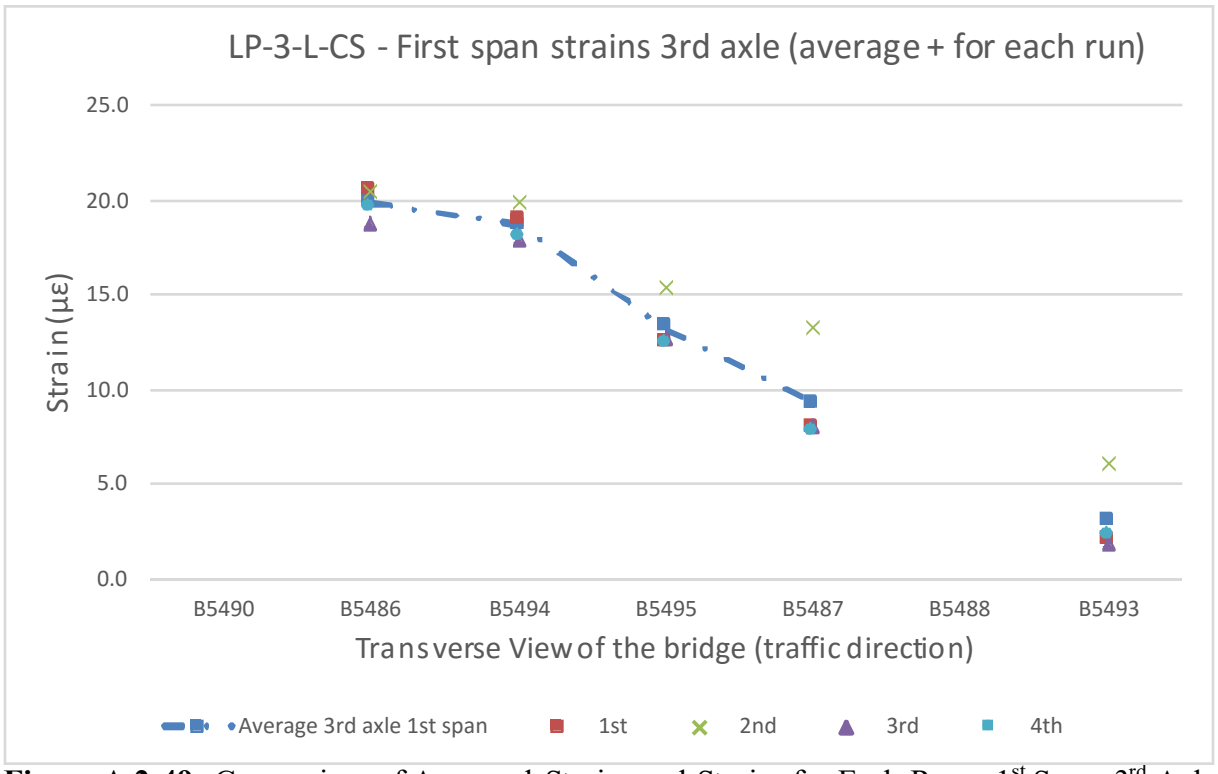

Figure A-2-49: Comparison of Averaged Strains and Strains for Each Run – 1st Span, 3rd Axle

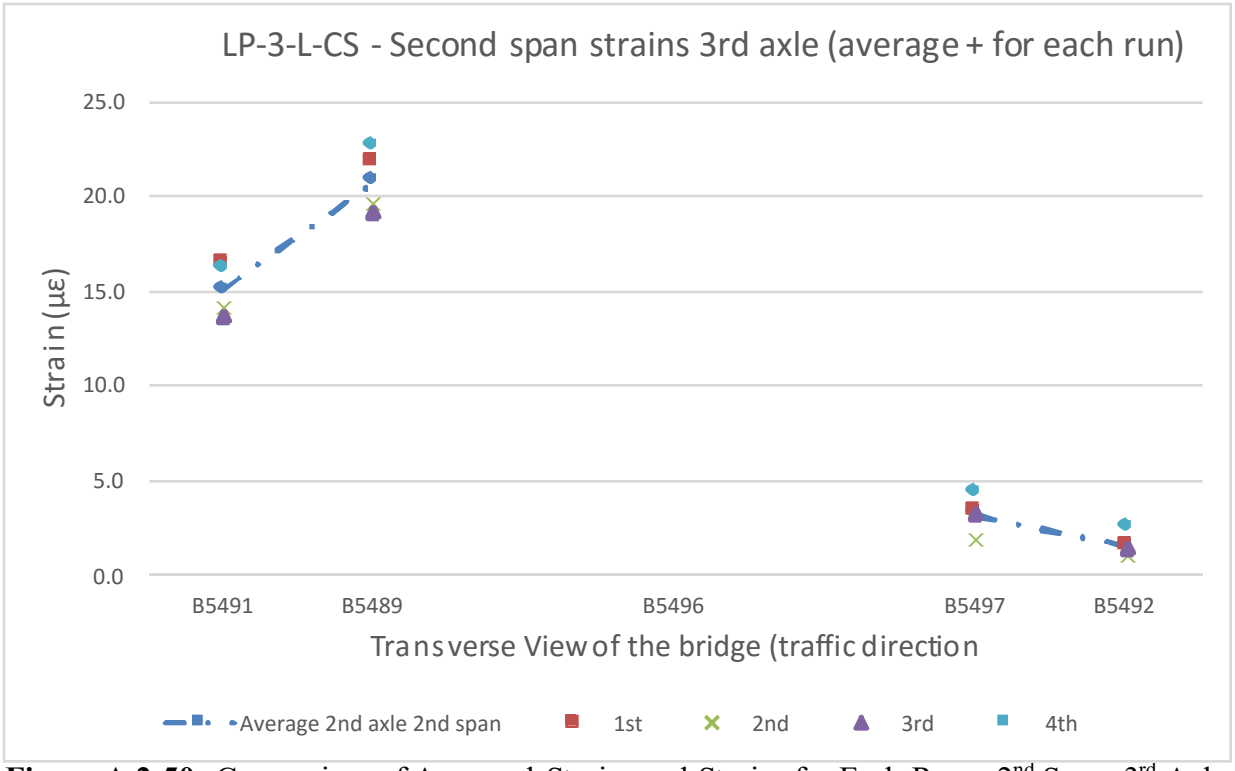

Figure A-2-50: Comparison of Averaged Strains and Strains for Each Run – 2nd Span, 3rd Axle

Load Pattern LP-3-R-CS:

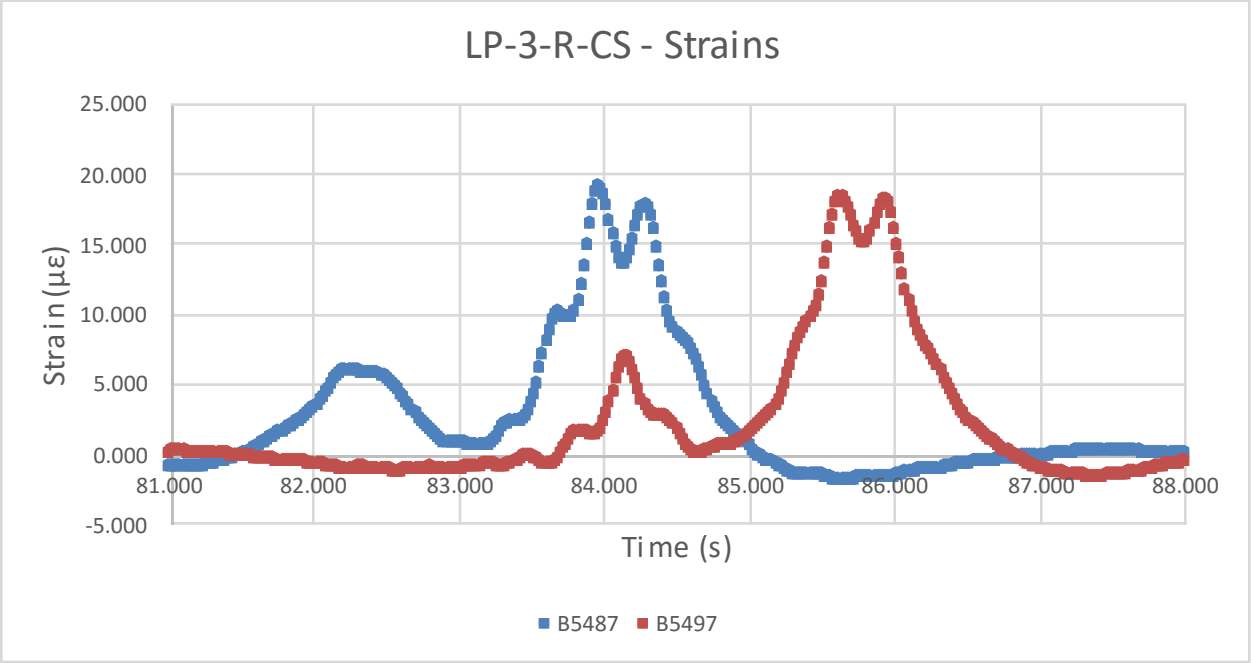

Figure A-2-51: Strains in Time for Third Run

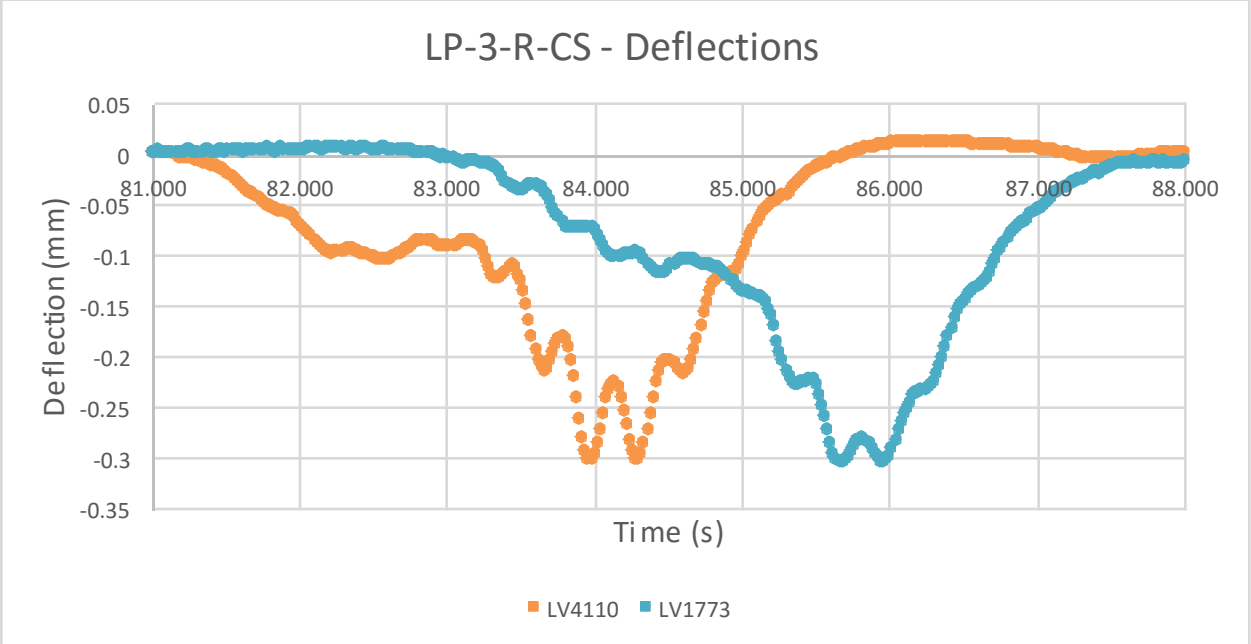

Figure A-2-52: Deflections in Time for Third Run

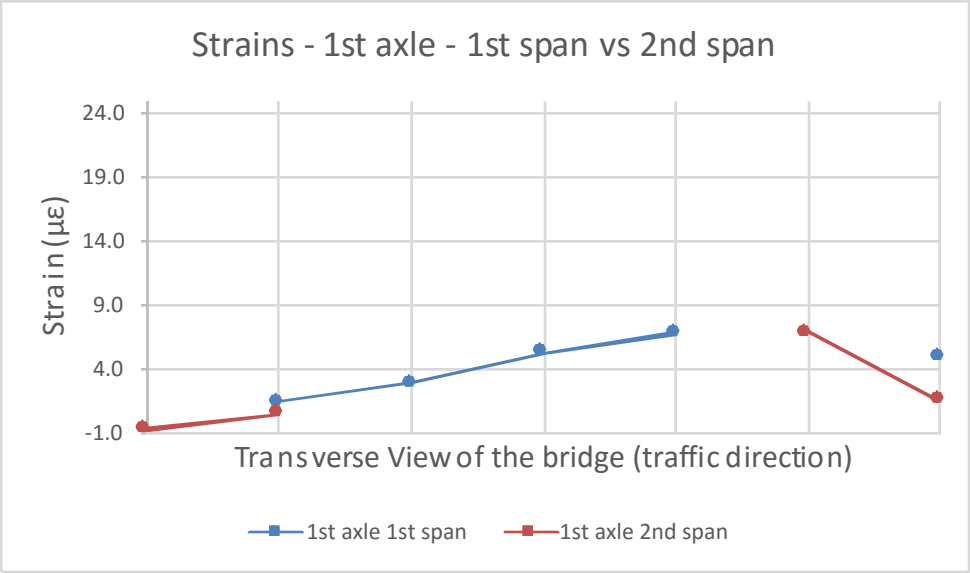

Figure A-2-53: Comparison of Averaged Strains for 1st and 2nd Span – First Axle

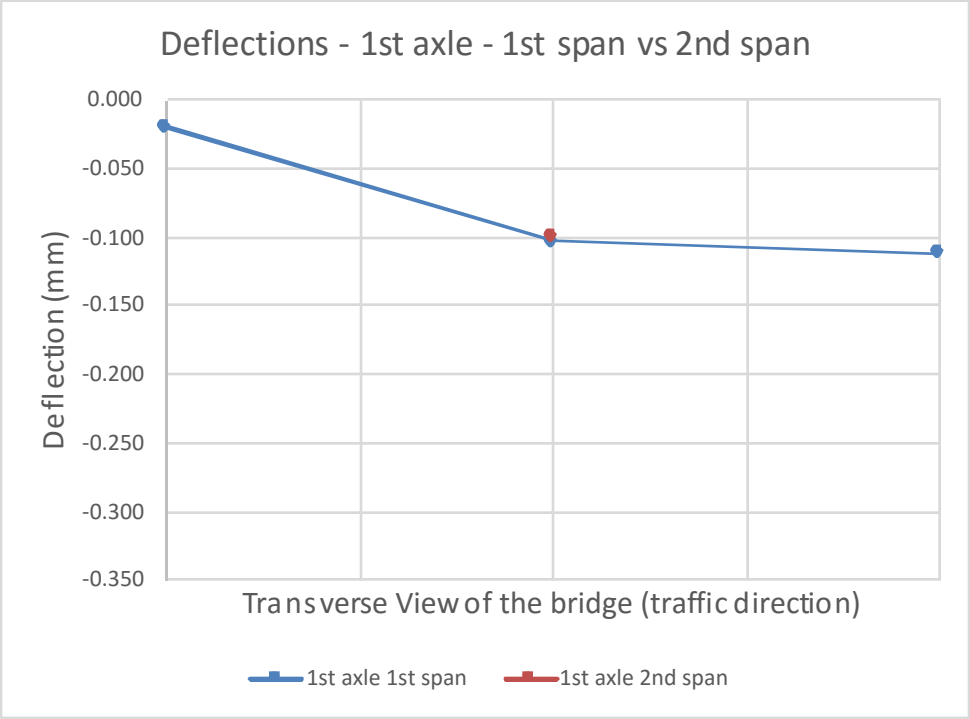

Figure A-2-54: Comparison of Averaged Deflections for 1st and 2nd Span – First Axle

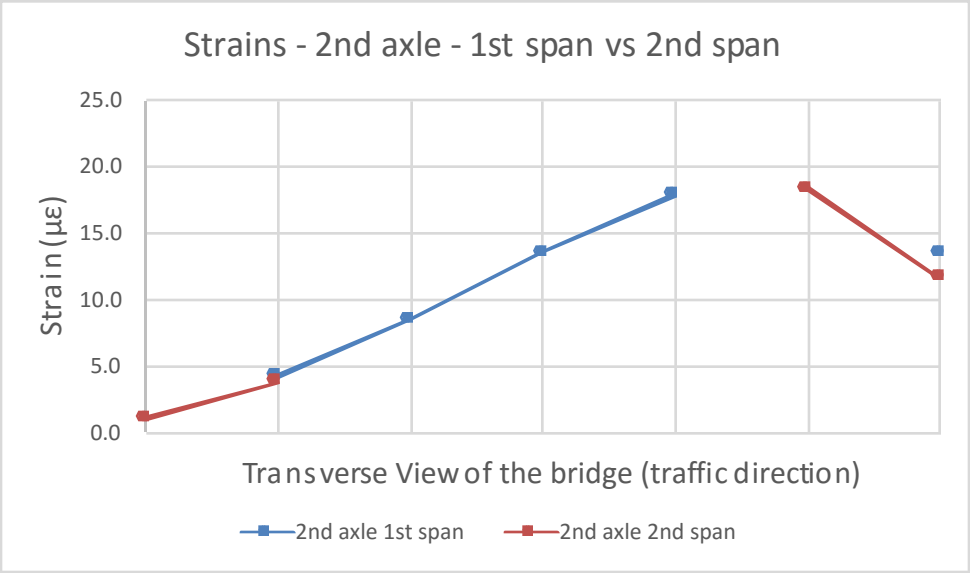

Figure A-2-55: Comparison of Averaged Strains for 1st and 2nd Span – Second Axle

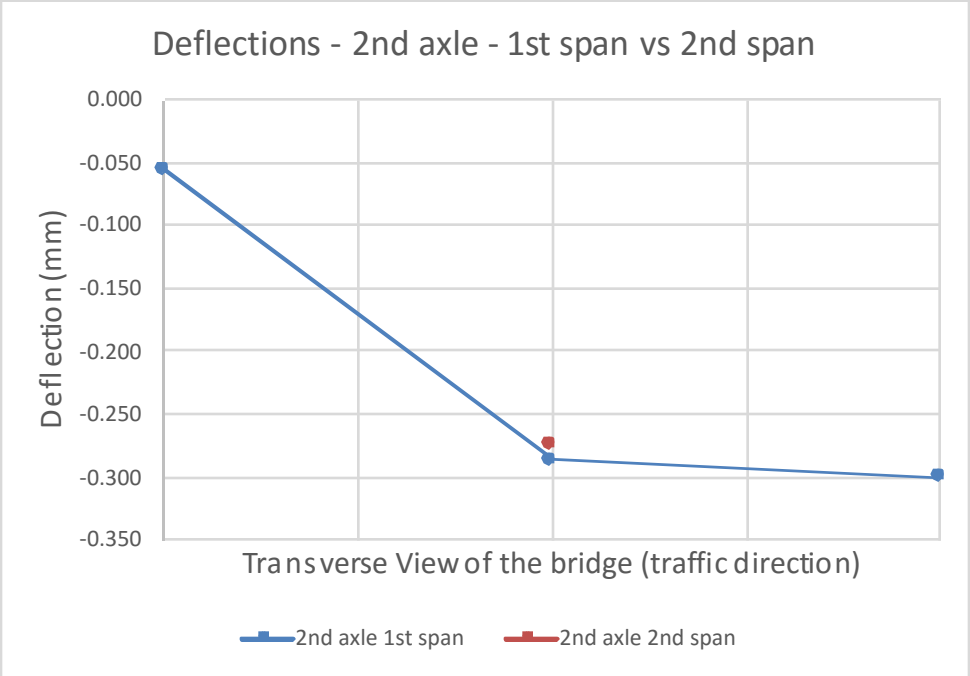

Figure A-2-56: Comparison of Averaged Deflections for 1st and 2nd Span – Second Axle

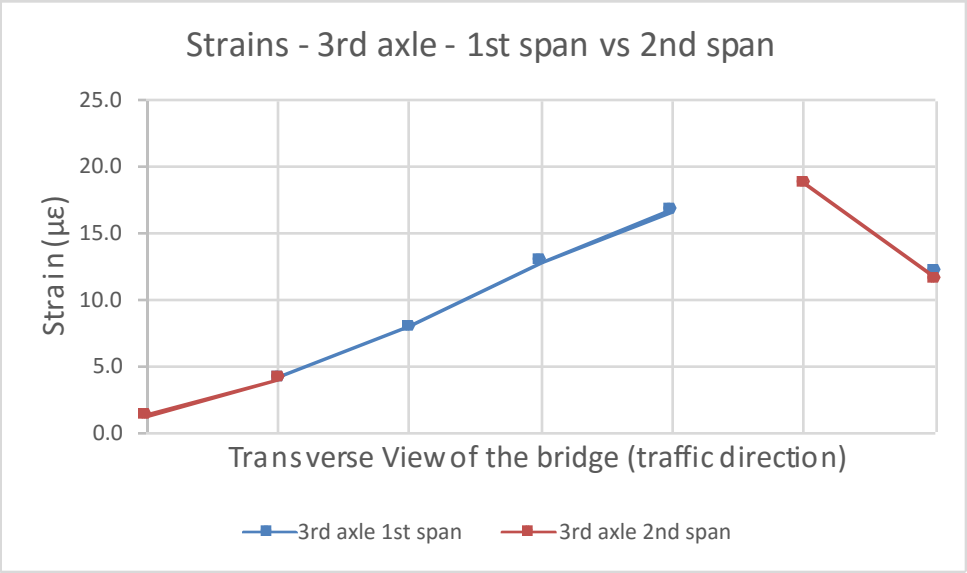

Figure A-2-57: Comparison of Averaged Strains for 1st and 2nd Span – Third Axle

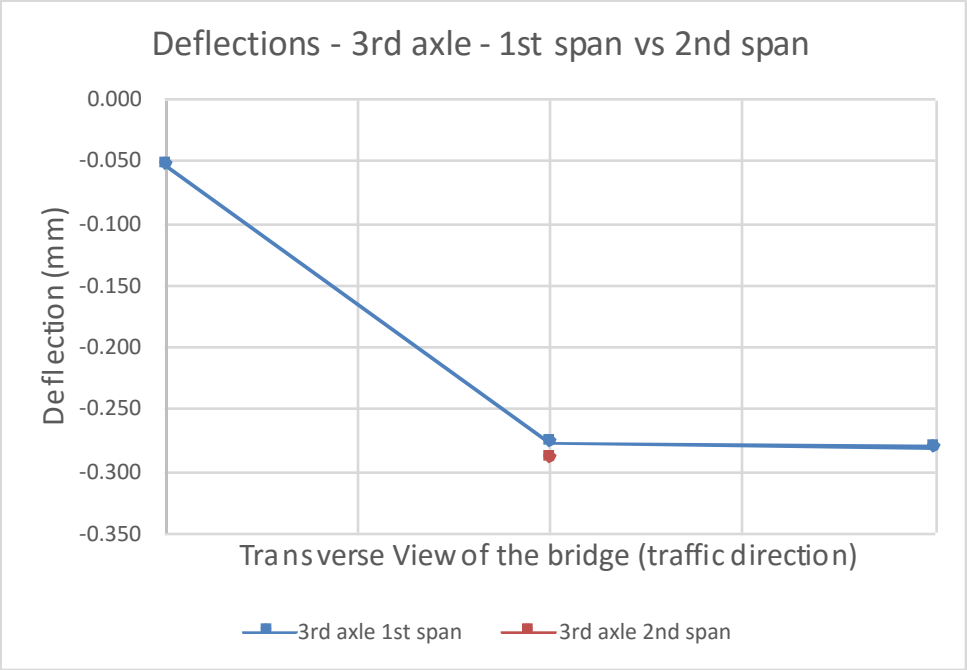

Figure A-2-58: Comparison of Averaged Deflections for 1st and 2nd Span – Third Axle

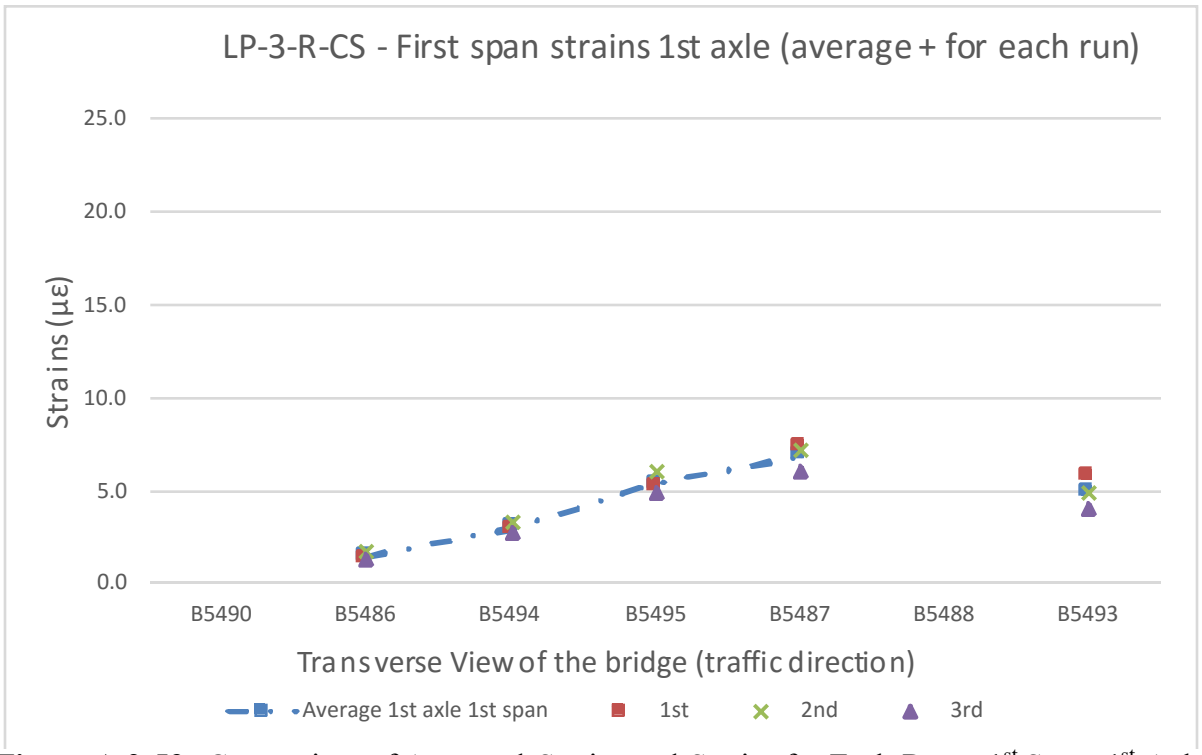

Figure A-2-59: Comparison of Averaged Strains and Strains for Each Run – 1st Span, 1st Axle

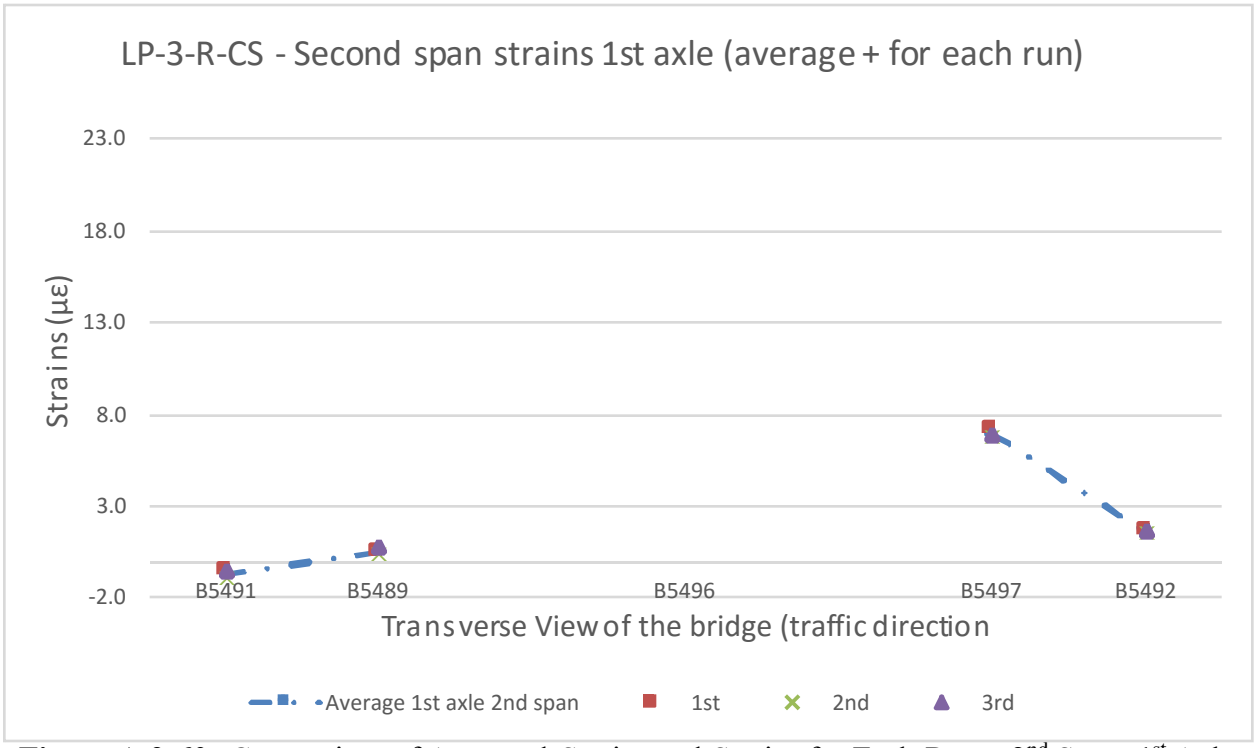

Figure A-2-60: Comparison of Averaged Strains and Strains for Each Run – 2nd Span, 1st Axle

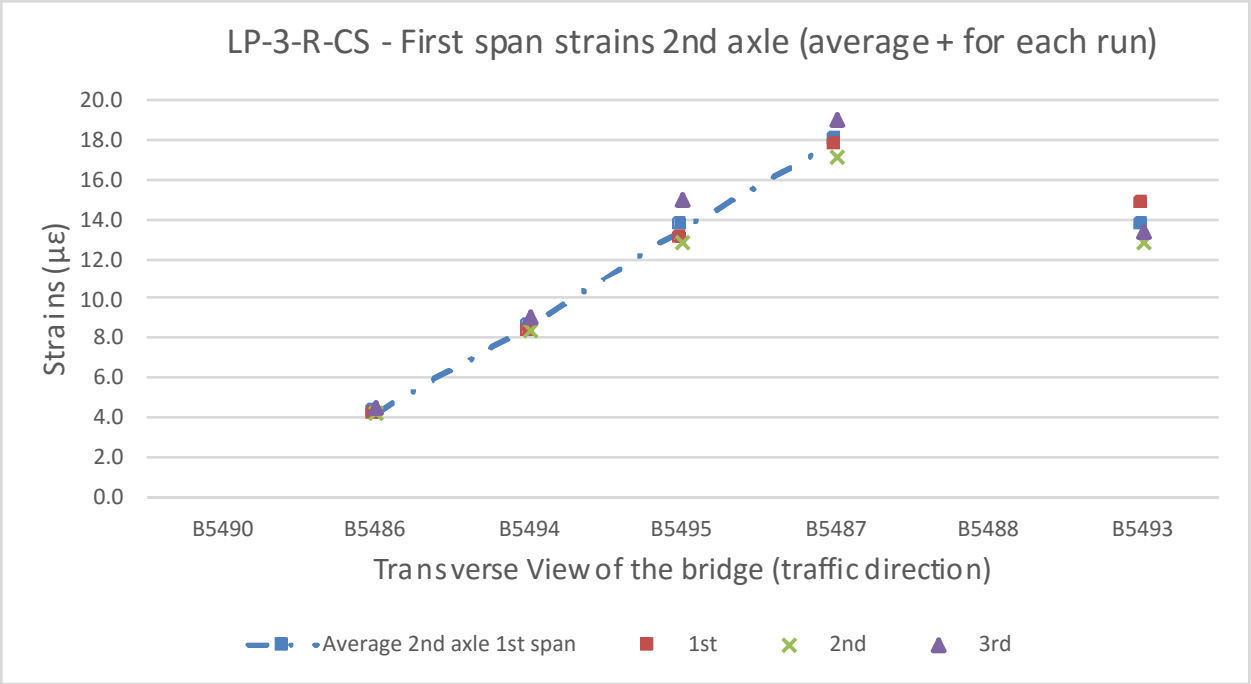

Figure A-2-61: Comparison of Averaged Strains and Strains for Each Run – 1st Span, 2nd Axle

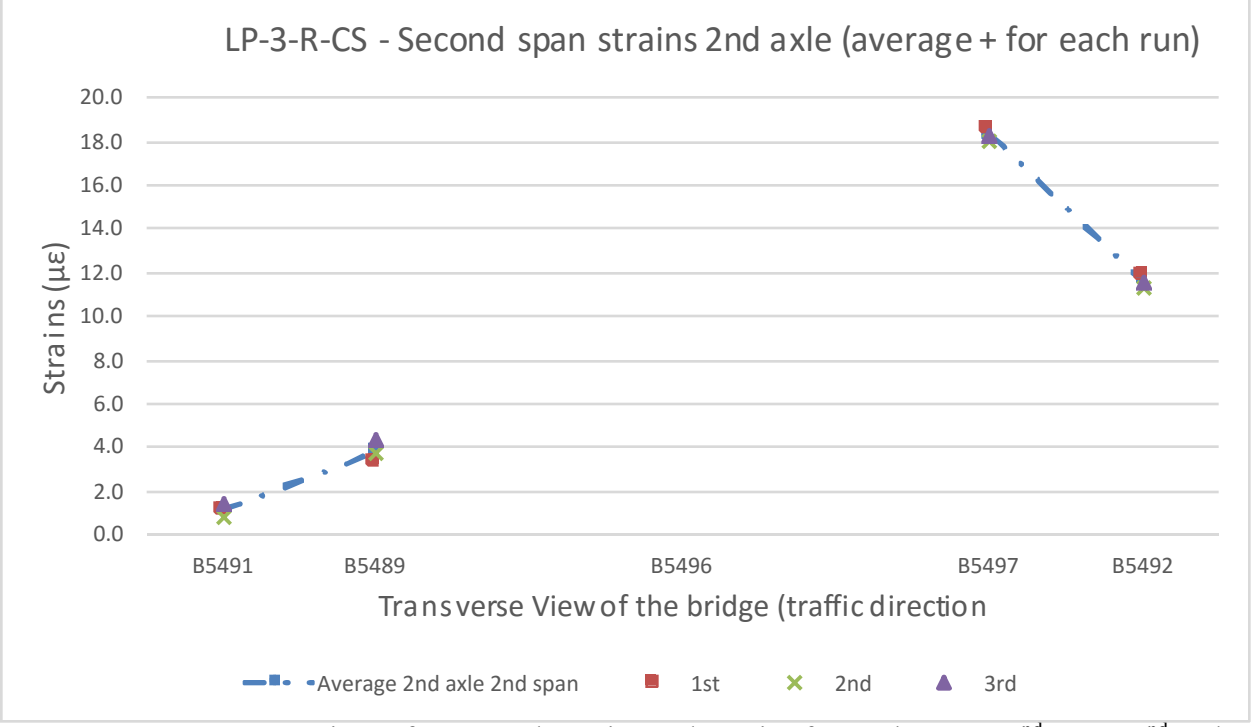

Figure A-2-62: Comparison of Averaged Strains and Strains for Each Run – 2nd Span, 2nd Axle

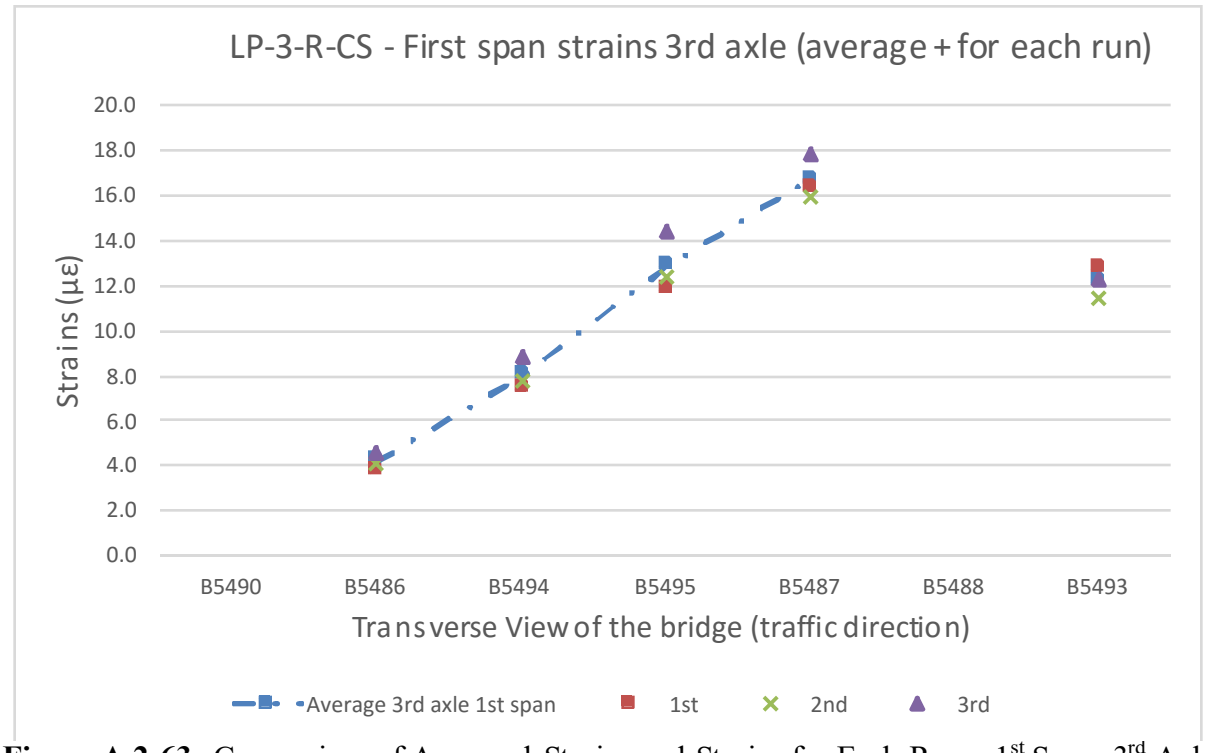

Figure A-2-63: Comparison of Averaged Strains and Strains for Each Run – 1st Span, 3rd Axle

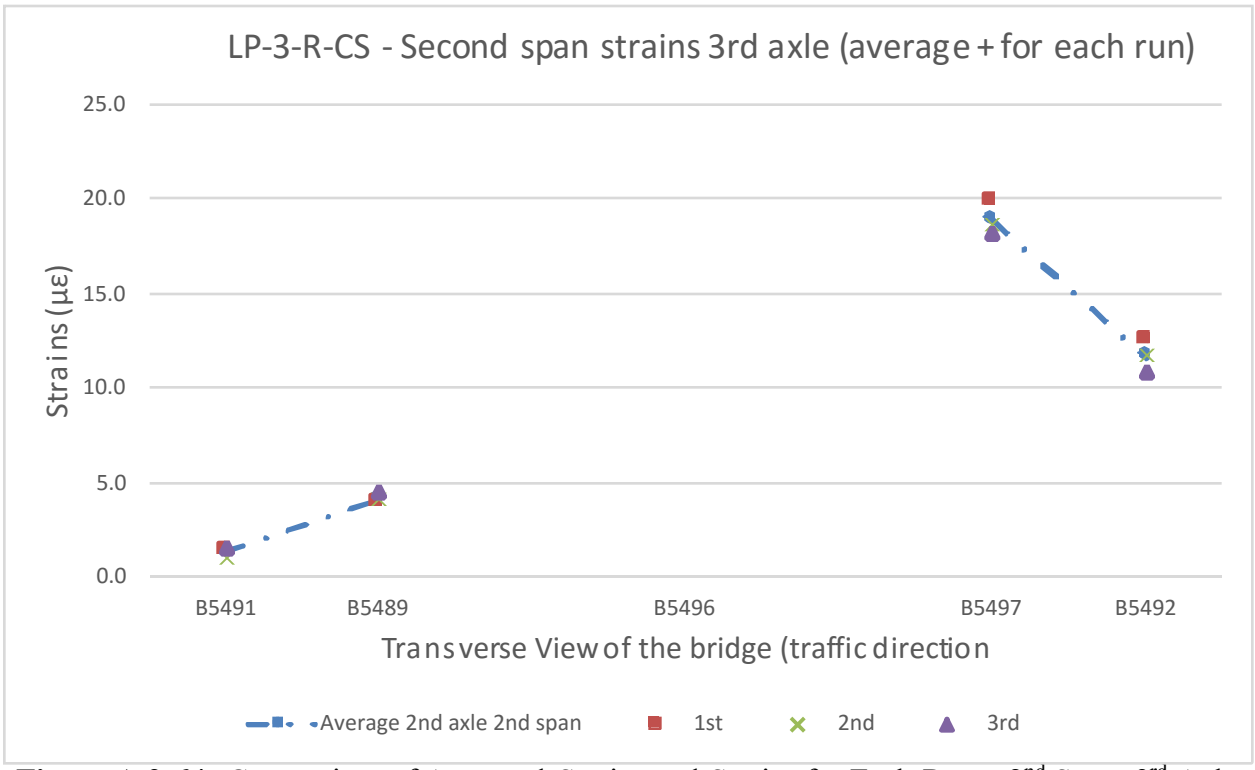

Figure A-2-64: Comparison of Averaged Strains and Strains for Each Run – 2nd Span, 3rd Axle

Load Pattern LP-5-R-Dyn:

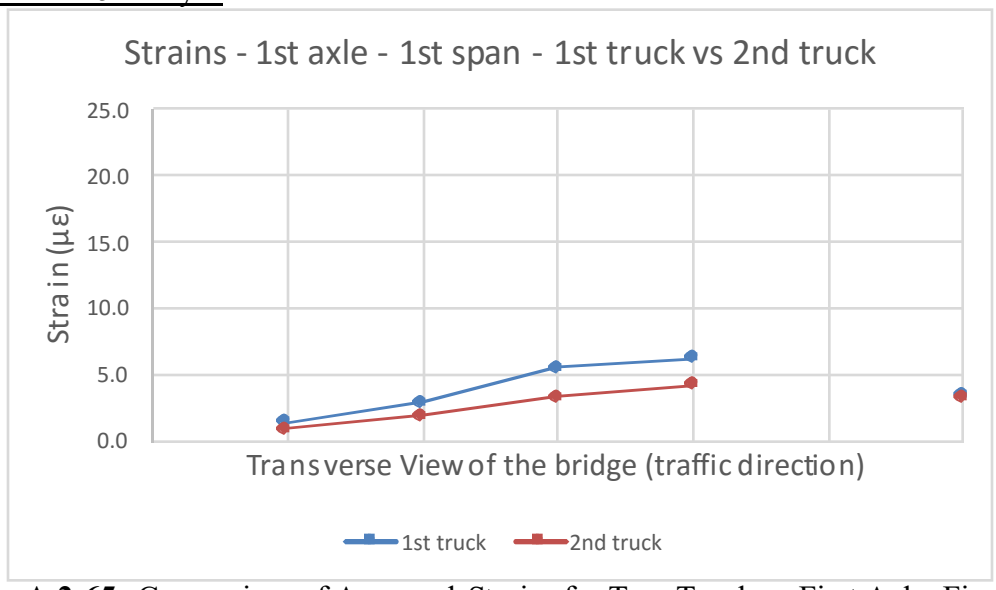

Figure A-2-65: Comparison of Averaged Strains for Two Trucks – First Axle, First Span

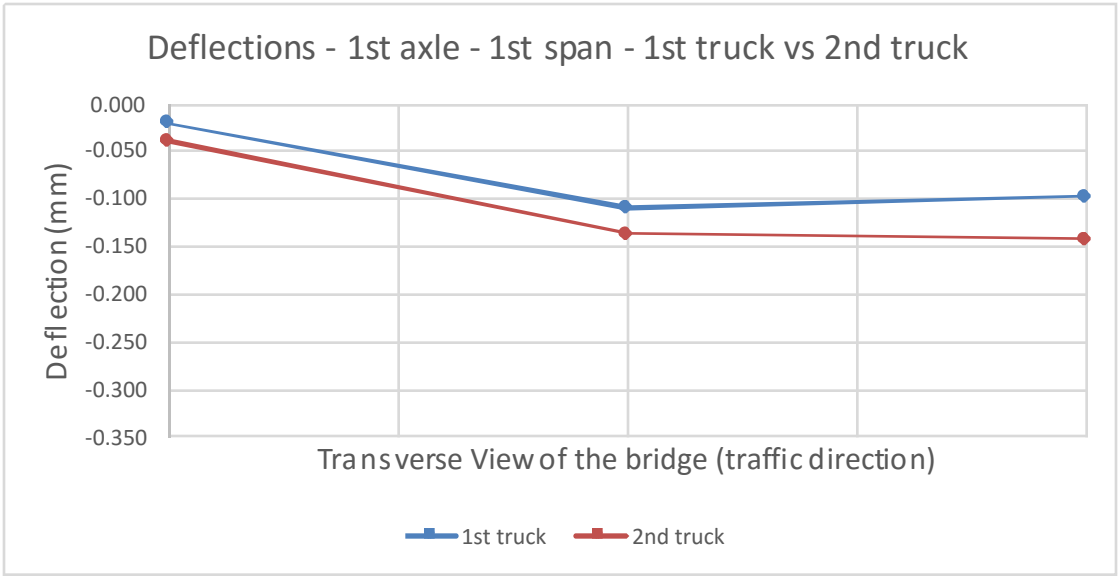

Figure A-2-66: Comparison of Averaged Deflections for Two Trucks – First Axle, First Span

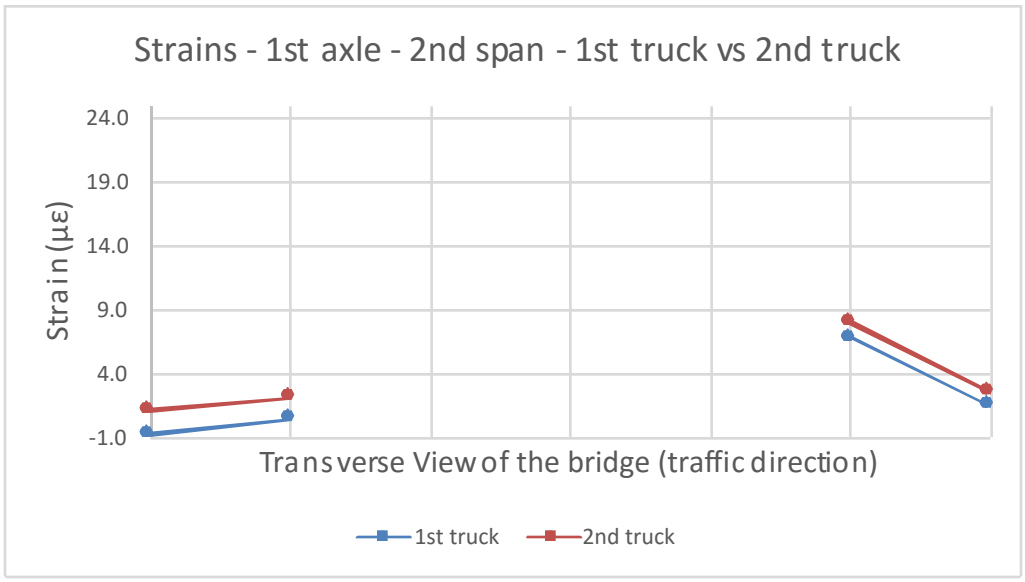

Figure A-2-67: Comparison of Averaged Strains for Two Trucks – First Axle, Second Span

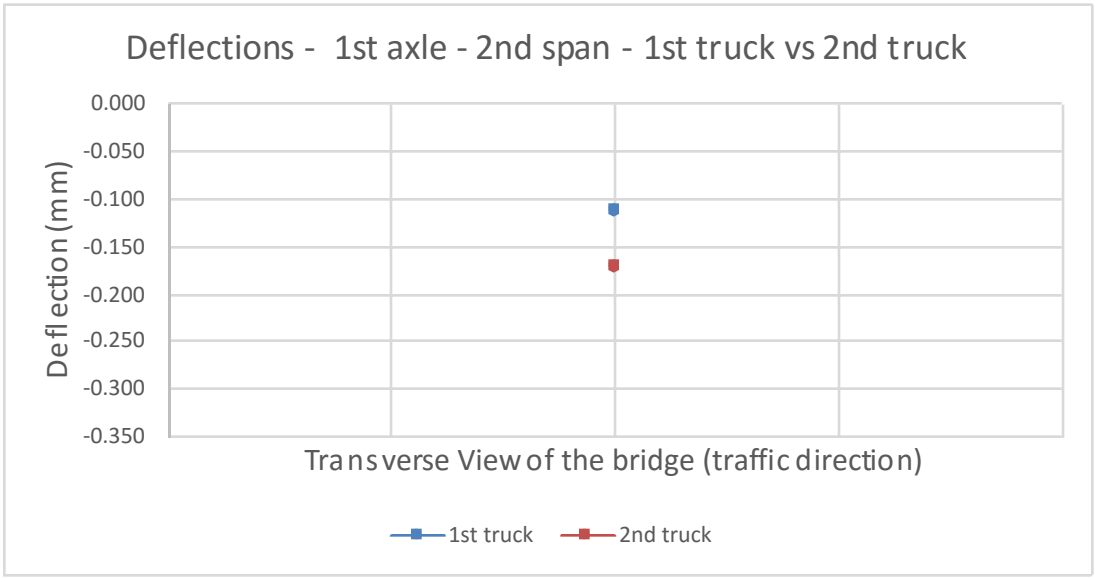

Figure A-2-68: Comparison of Averaged Deflections for Two Trucks – First Axle, Second Span

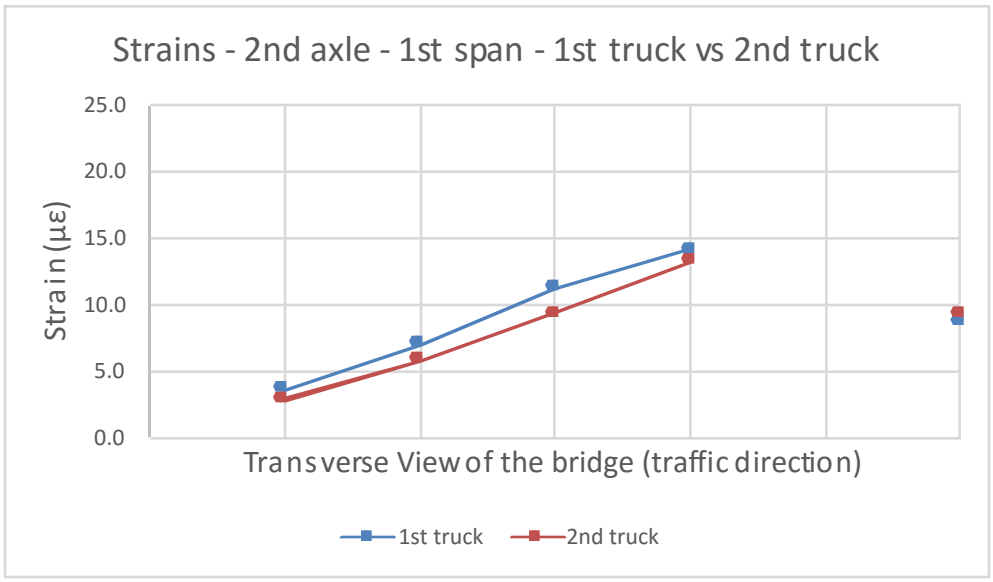

Figure A-2-69: Comparison of Averaged Strains for Two Trucks – Second Axle, First Span

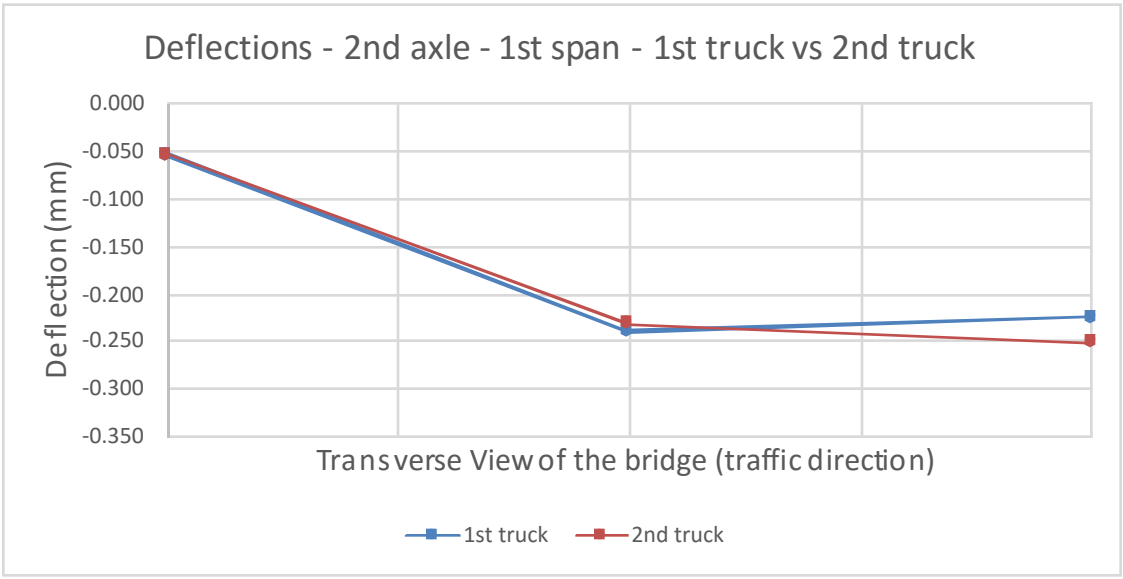

Figure A-2-70: Comparison of Averaged Deflections for Two Trucks – Second Axle, First Span

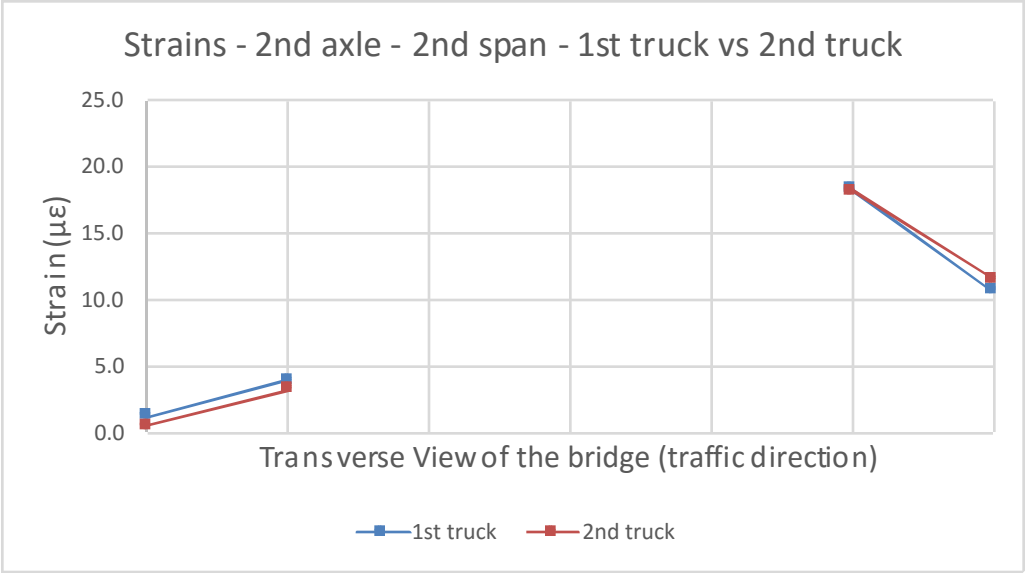

Figure A-2-71: Comparison of Averaged Strains for Two Trucks – Second Axle, Second Span

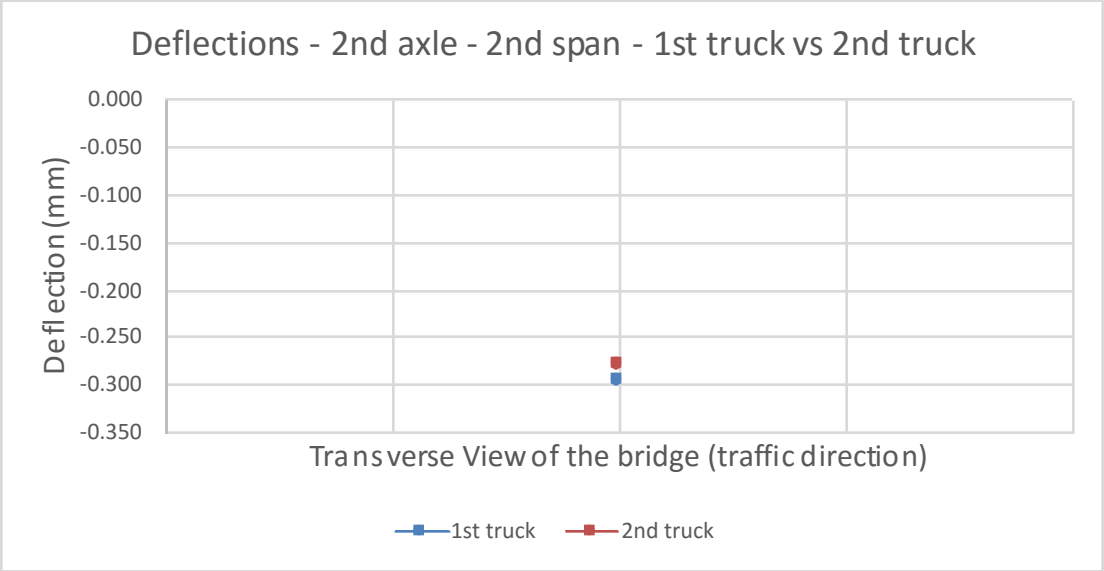

Figure A-2-72: Comparison of Averaged Deflections for Two Trucks – Second Axle, Second Span

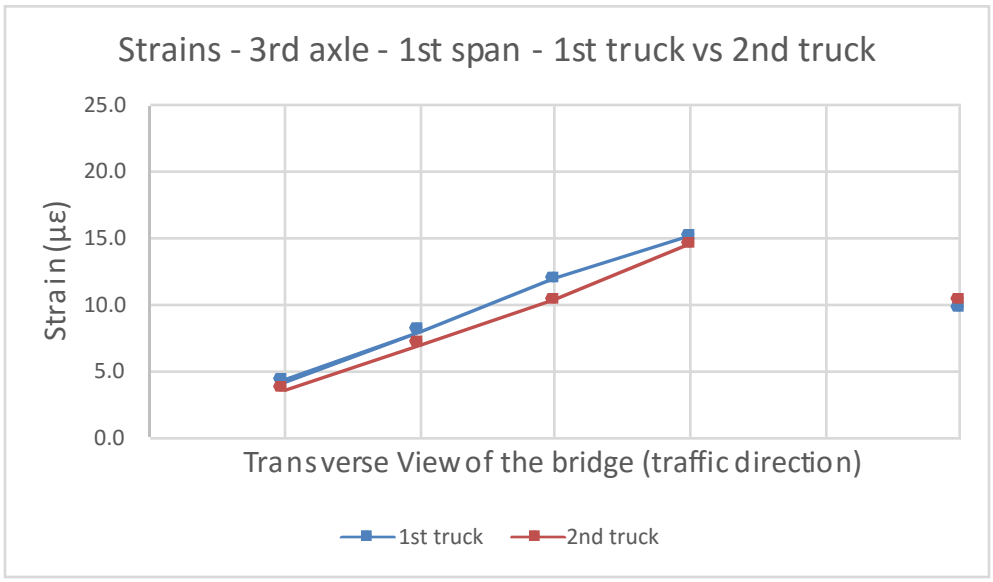

Figure A-2-73: Comparison of Averaged Strains for Two Trucks – Third Axle, First Span

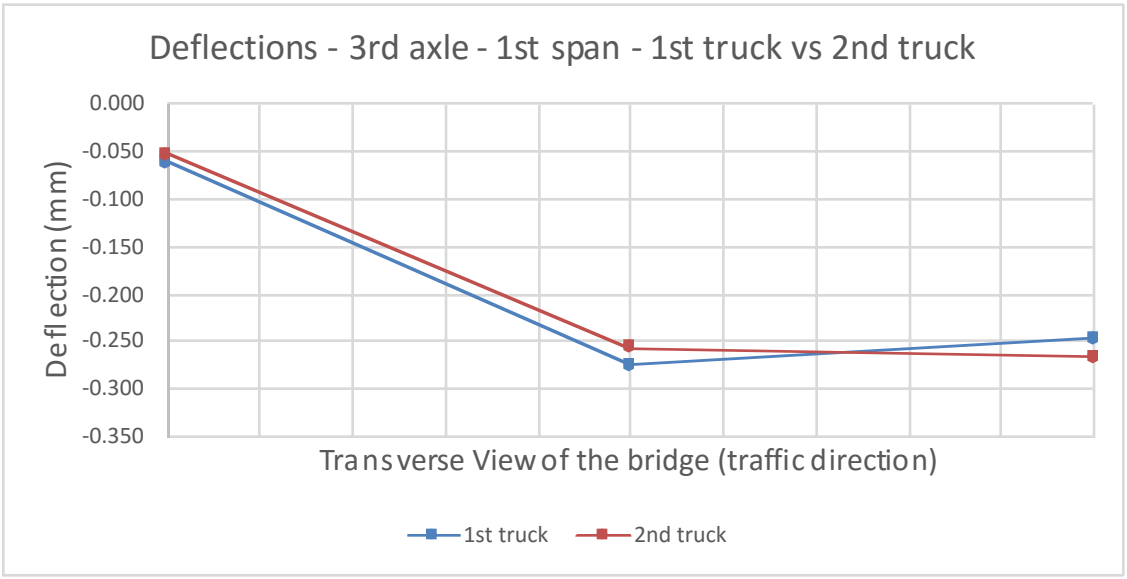

Figure A-2-74: Comparison of Averaged Deflections for Two Trucks – Third Axle, First Span

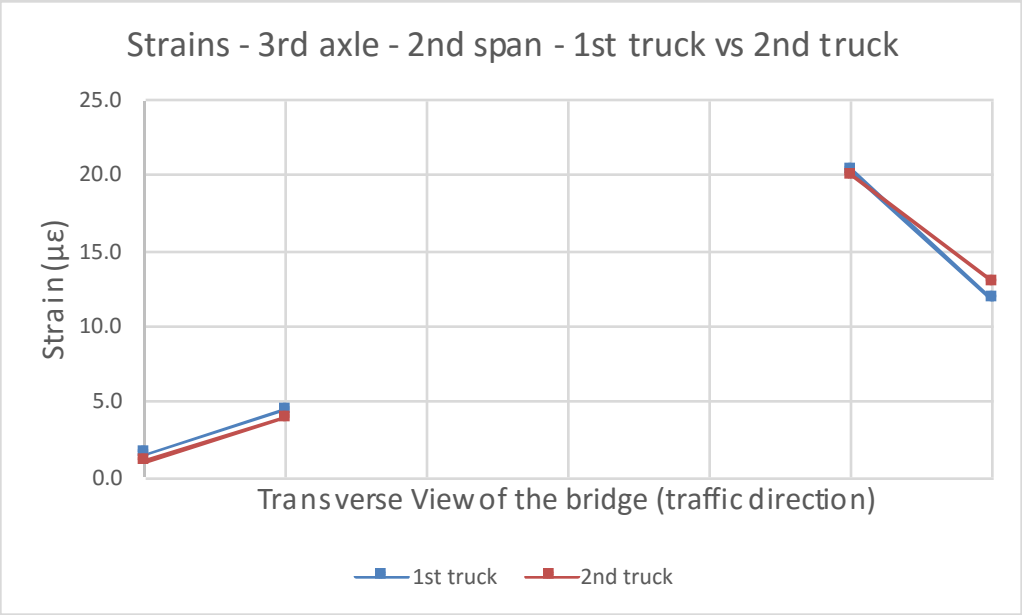

Figure A-2-75: Comparison of Averaged Strains for Two Trucks – Third Axle, Second Span

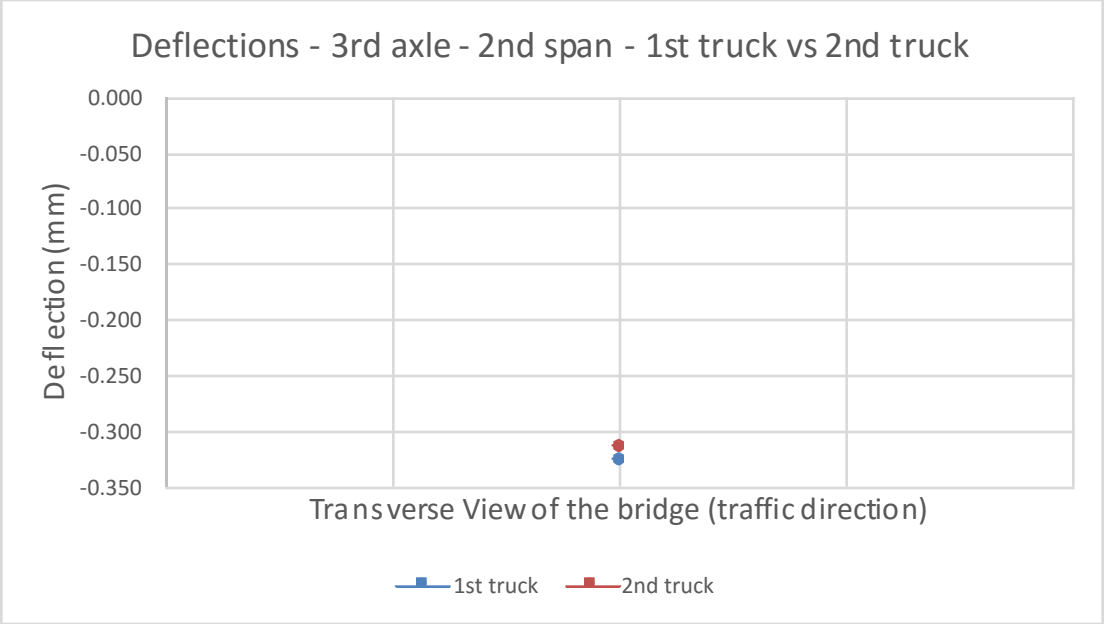

Figure A-2-76: Comparison of Averaged Deflections for Two Trucks – Third Axle, Second Span

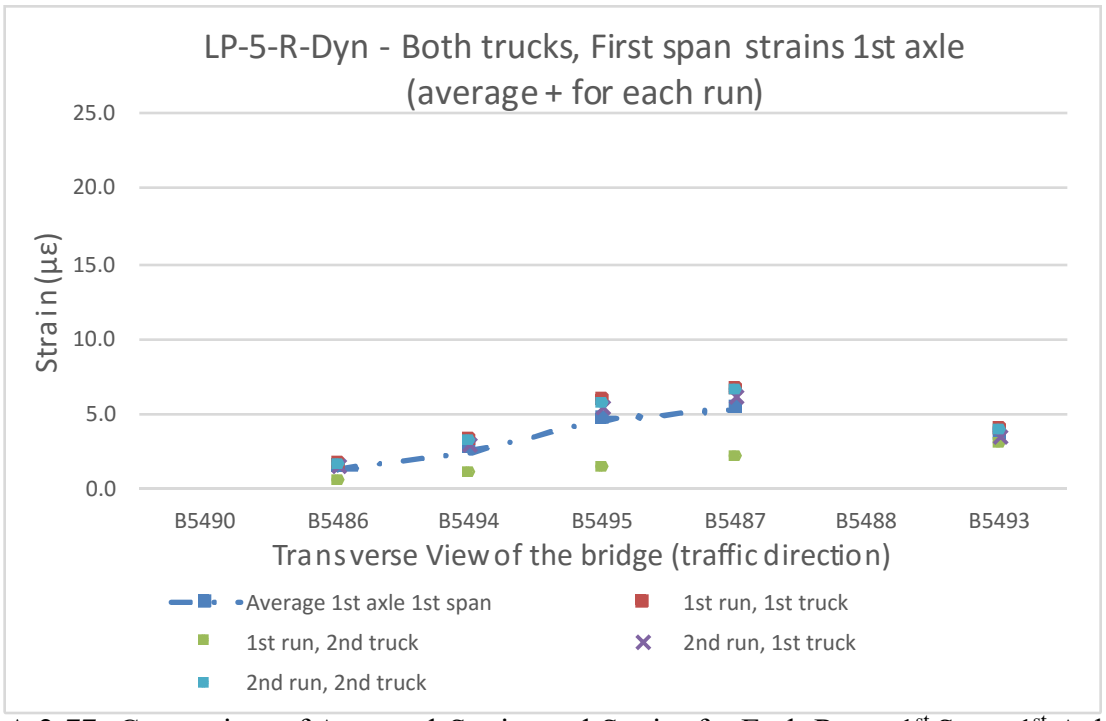

Figure A-2-77: Comparison of Averaged Strains and Strains for Each Run – 1st Span, 1st Axle, Both Trucks

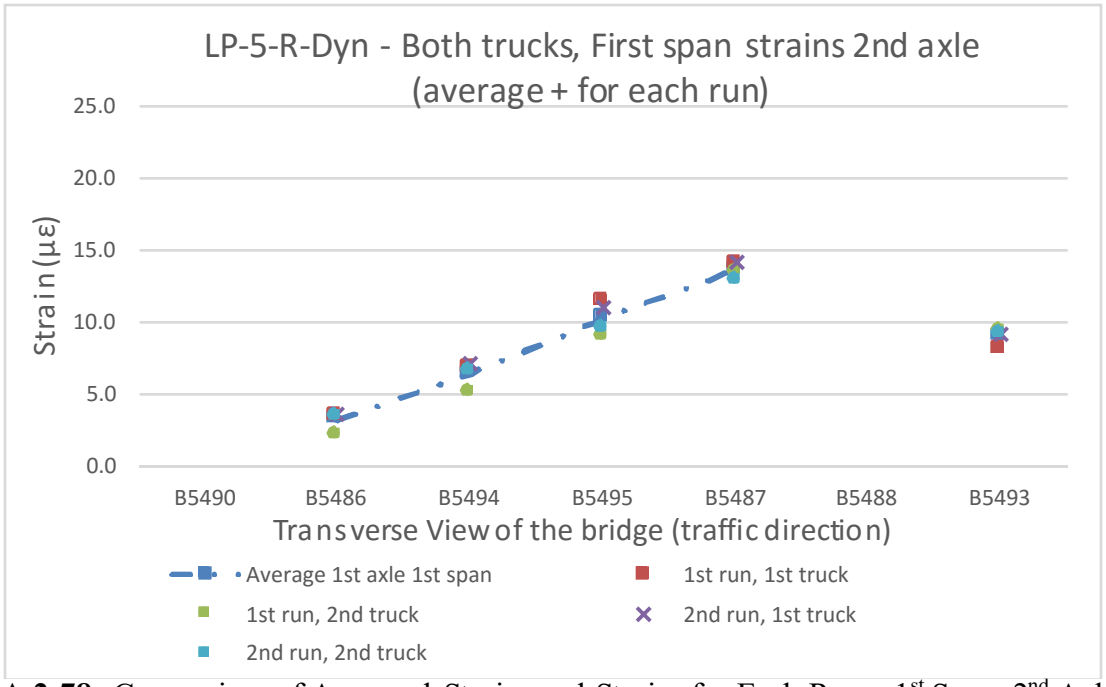

Figure A-2-78: Comparison of Averaged Strains and Strains for Each Run – 1st Span, 2nd Axle, Both Trucks

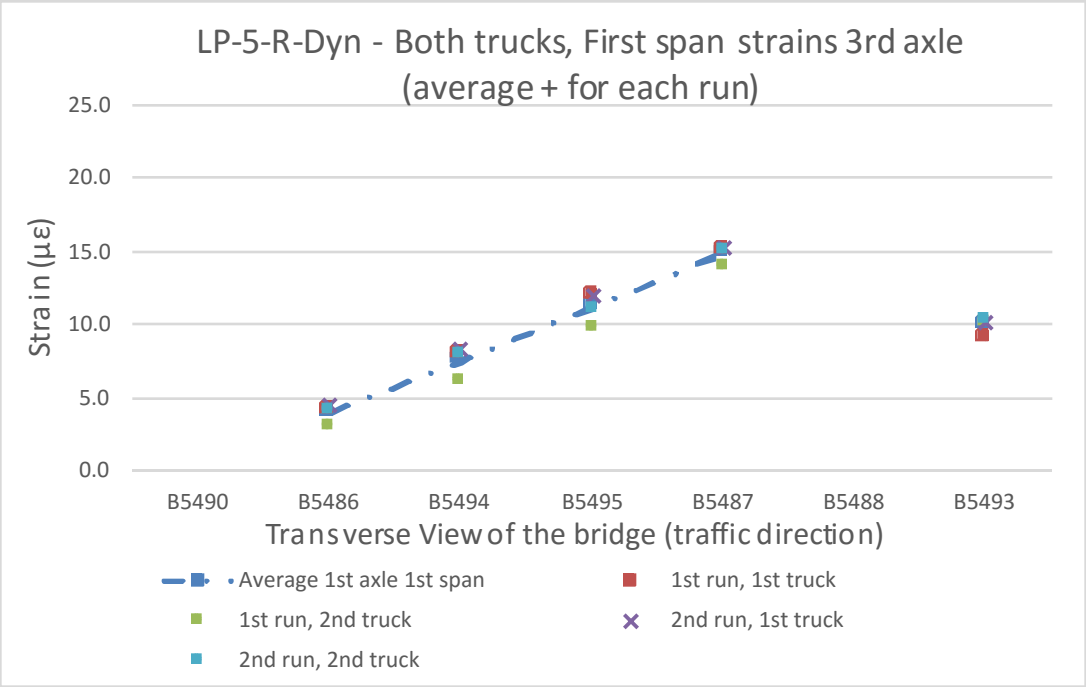

Figure A-2-79: Comparison of Averaged Strains and Strains for Each Run – 1st Span, 3rd Axle, Both Trucks

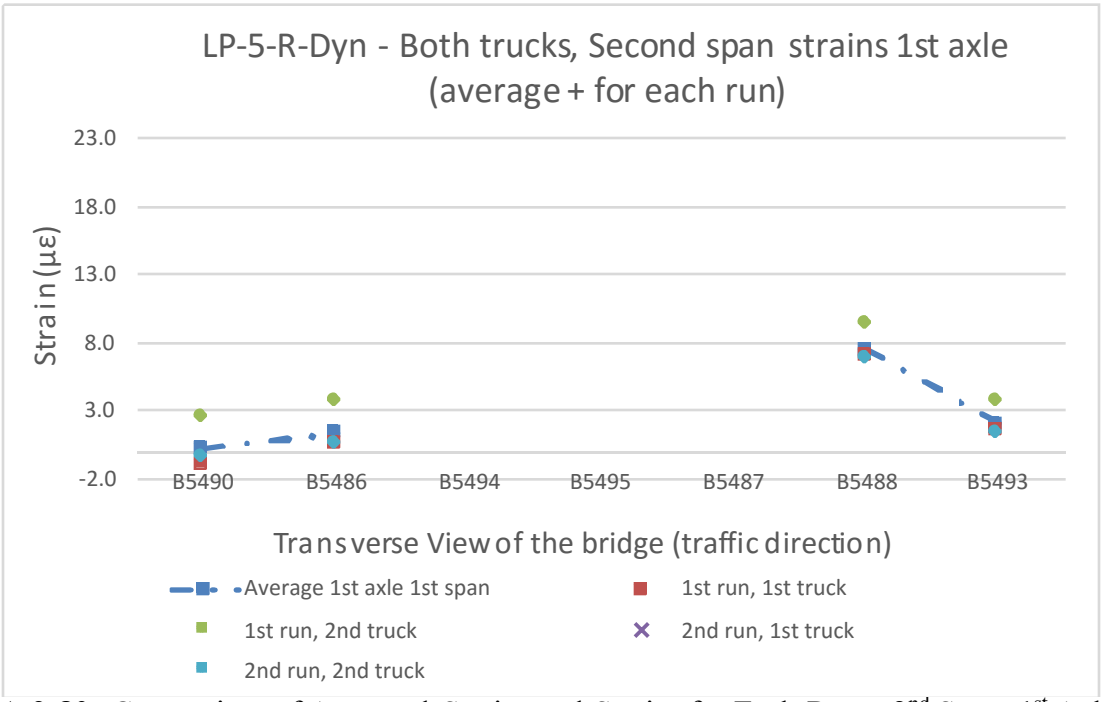

Figure A-2-80: Comparison of Averaged Strains and Strains for Each Run – 2nd Span, 1st Axle, Both Trucks

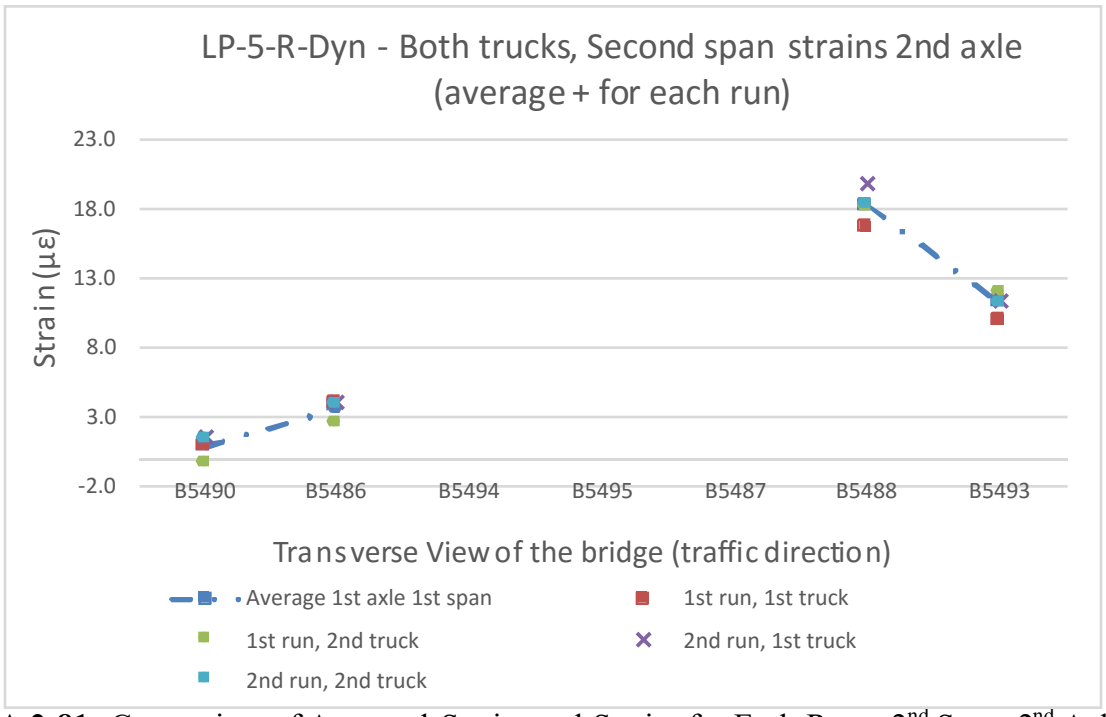

Figure A-2-81: Comparison of Averaged Strains and Strains for Each Run – 2nd Span, 2nd Axle, Both Trucks

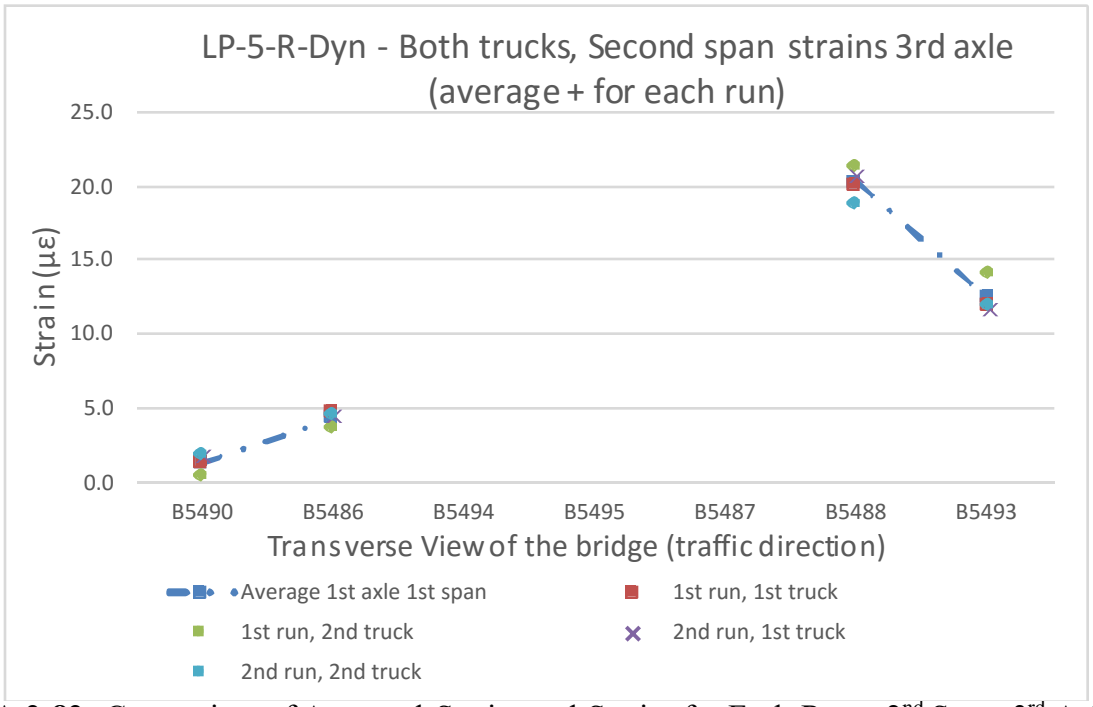

Figure A-2-82: Comparison of Averaged Strains and Strains for Each Run – 2nd Span, 3rd Axle, Both Trucks

Appendix B: Finite Element Analyses Results

This section provides results of FEA on calibrated model.

B-1: Comparison of FE results with on-site measured values

Appendix B-1 corresponds directly with Chapter 7.5.1 of the Report and shows comparison plots for static load cases LP-1 and LP-2. The values of deflections and longitudinal strains at sensor mounting locations along the width of the bridge are shown as points in the plots. FEM values present the actual distribution of longitudinal strains and deflections in the cross-section. Vertical dashed lines indicate different segments connection. Westbound of the bridge corresponds to the distance along the width of 0 inches, while Eastbound corresponds to the value of 376 inches.

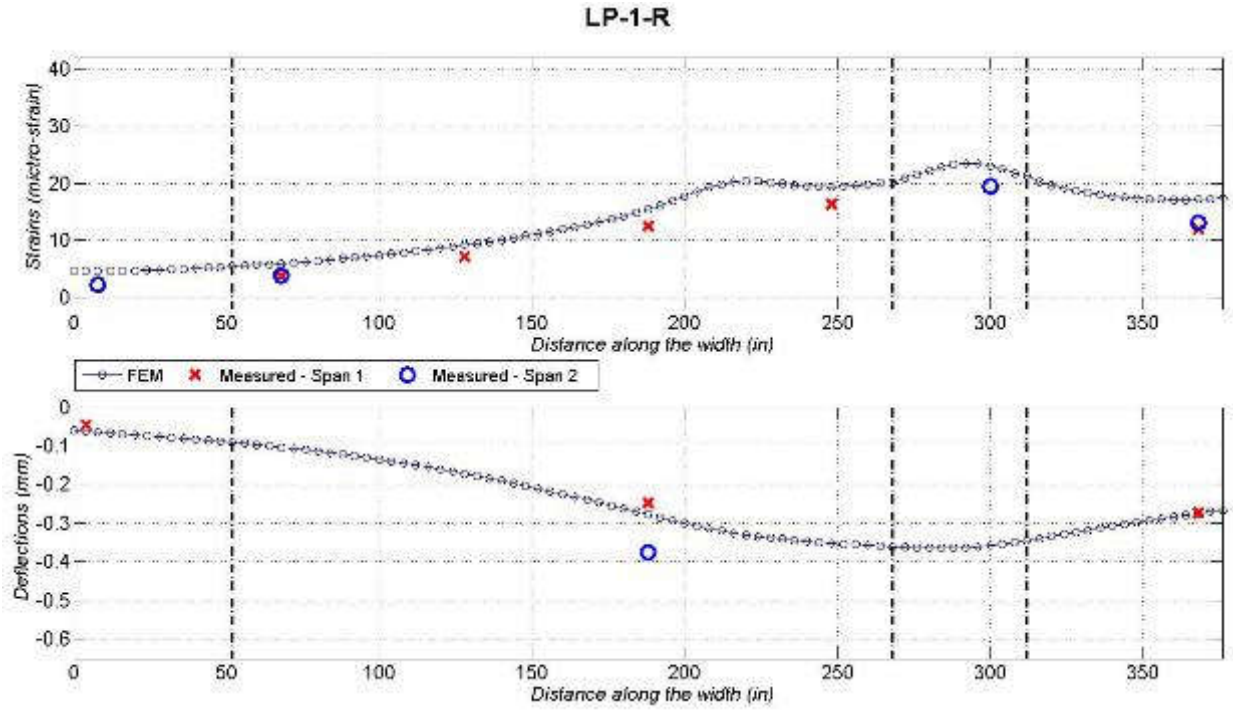

Figure B-1-1: Comparison Plot of Strains and Deflections for LP-1-R (1 mm = 0.02 in).

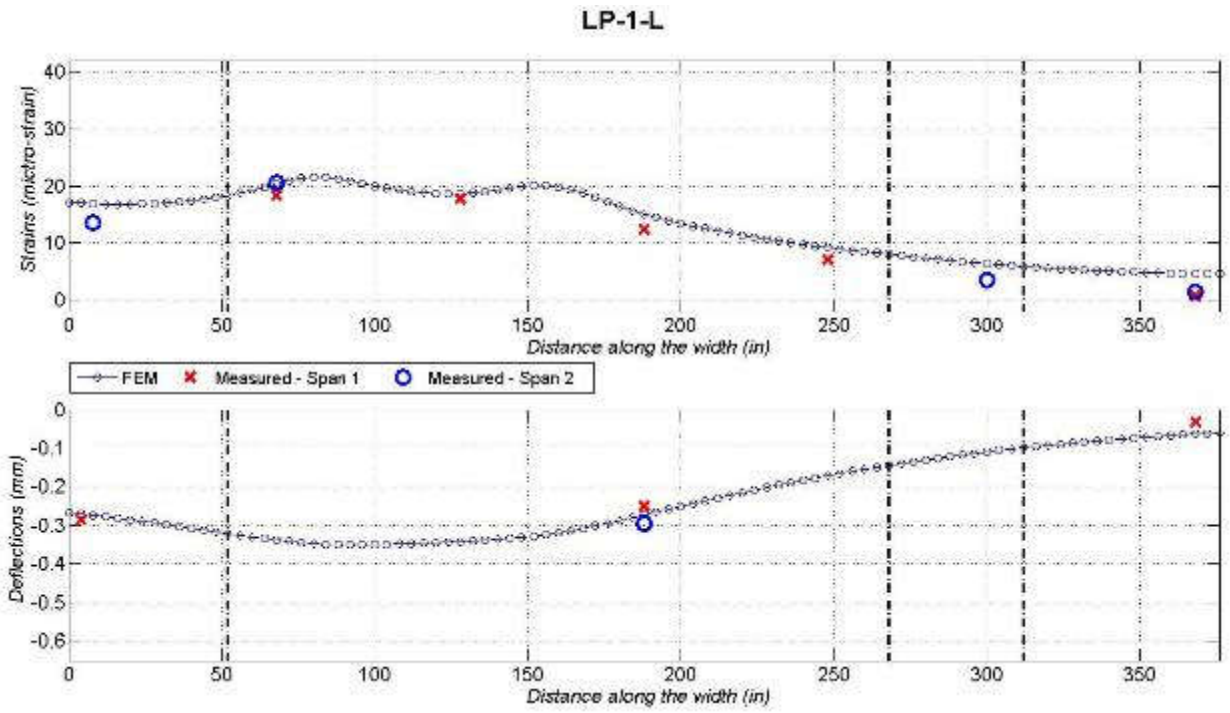

Figure B-1-2: Comparison Plot of Strains and Deflections for LP-1-L (1 mm = 0.02 in).

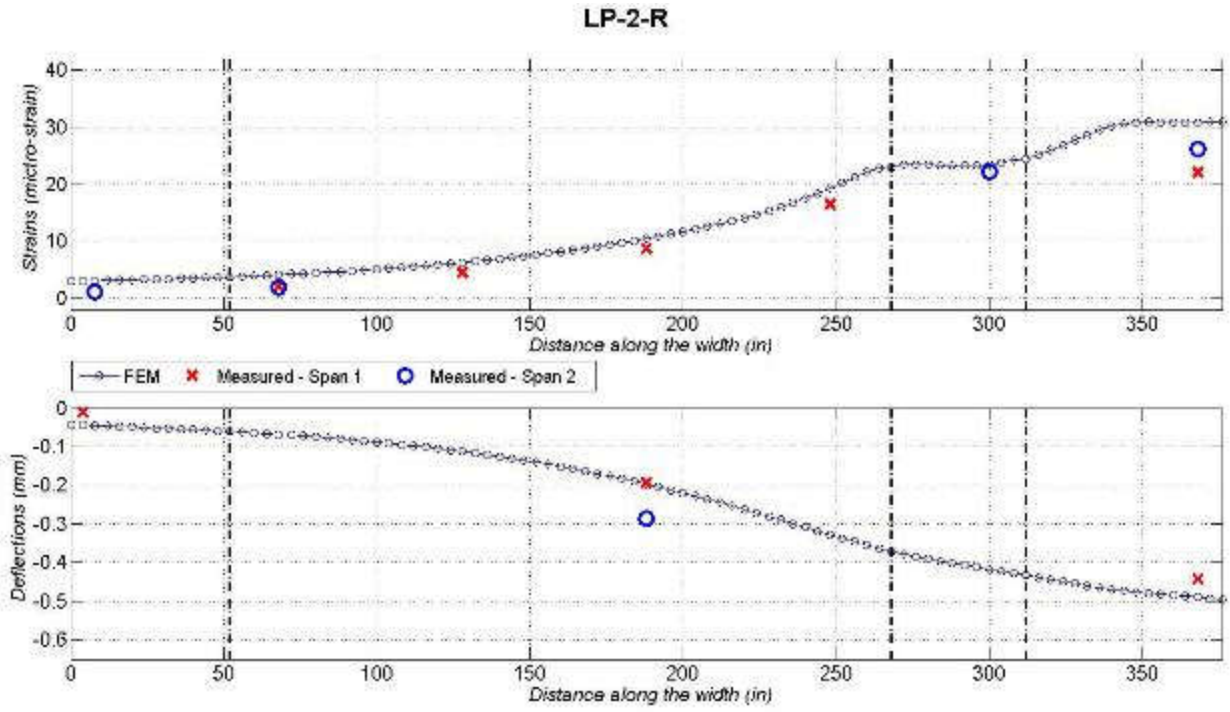

Figure B-1-3: Comparison Plot of Strains and Deflections for LP-2-R (1 mm = 0.02 in).

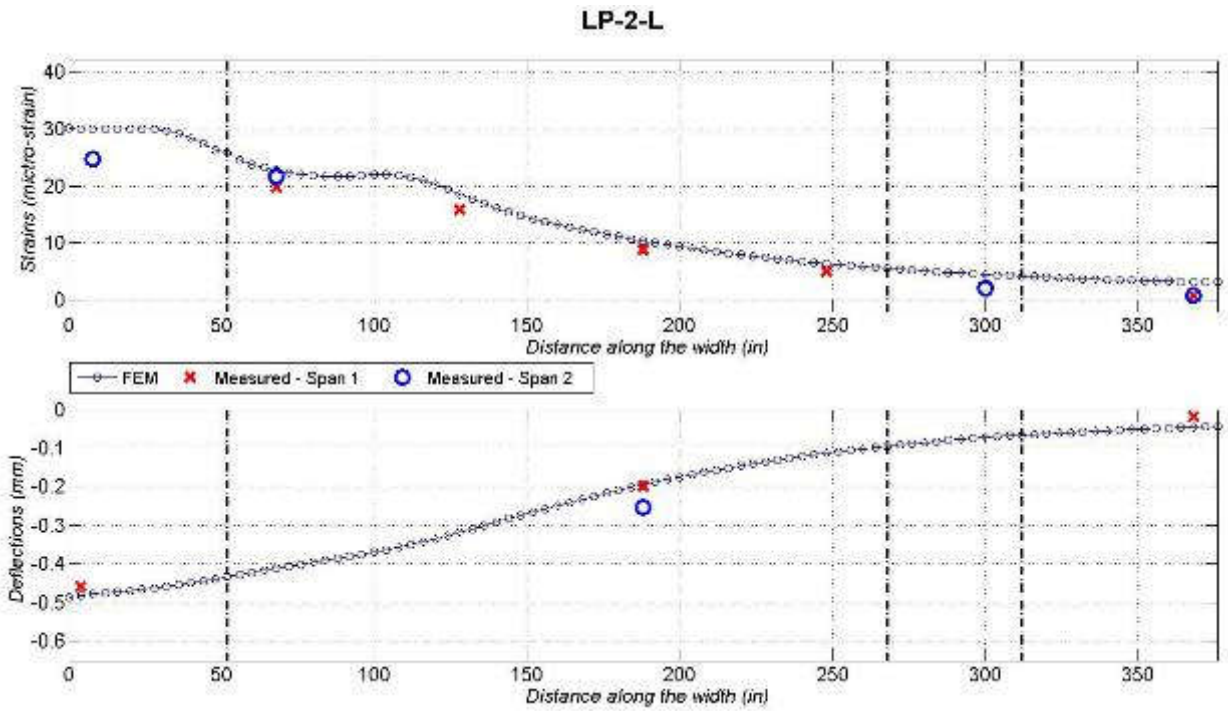

Figure B-1-4: Comparison Plot of Strains and Deflections for LP-2-L (1 mm = 0.02 in).

B-2: Stresses for static cases

Appendix B-2 corresponds directly with Chapters 7.5.2 and 7.6 of the Report. Selected maps of stresses, used in stress analysis and FE Model aided rating calculations are presented here.

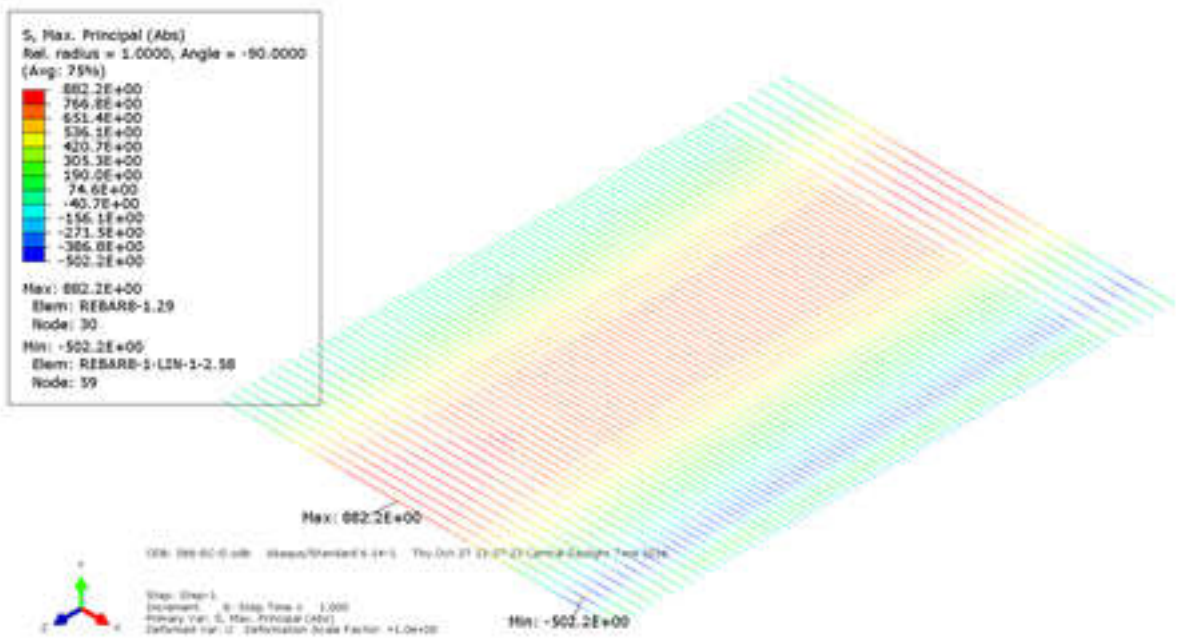

Figure B-2-1: Stresses in Reinforcing Bars for Dead Load (psi)

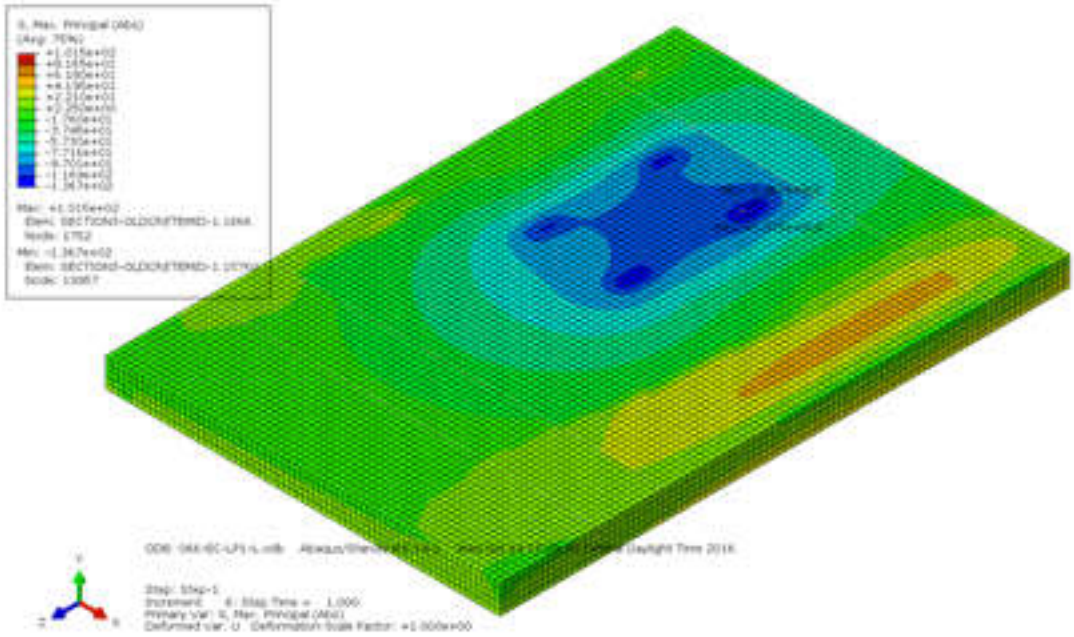

Figure B-2-2: Stresses in Concrete Slab for LP-1-L (psi)

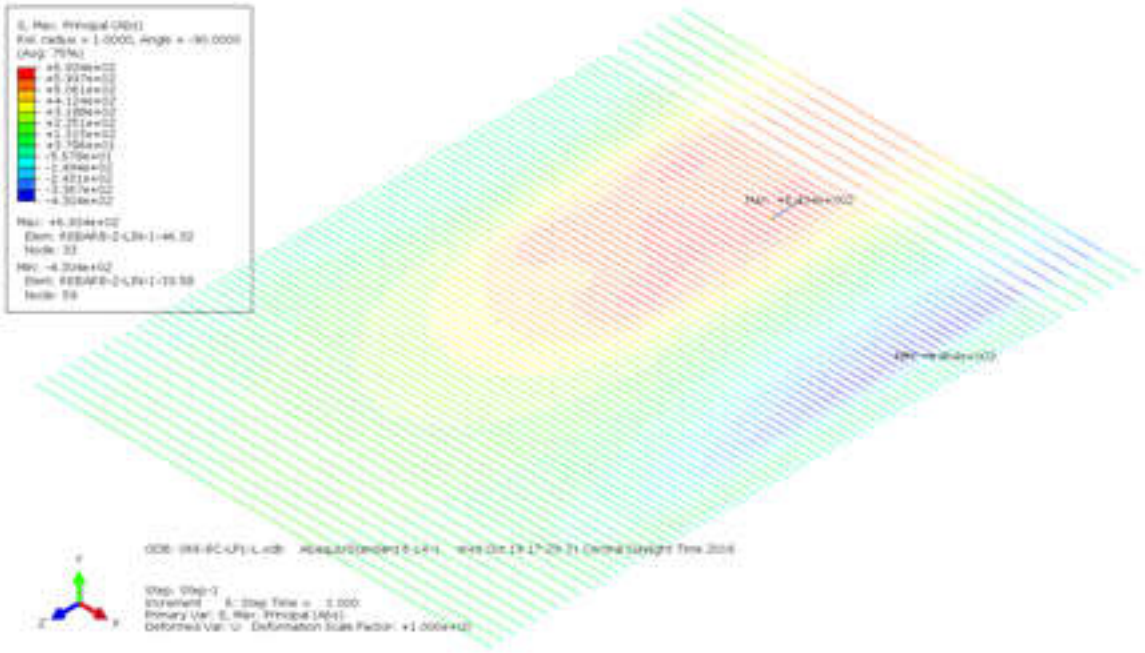

Figure B-2-3: Stresses in Reinforcing Bars for LP-1-L (psi)

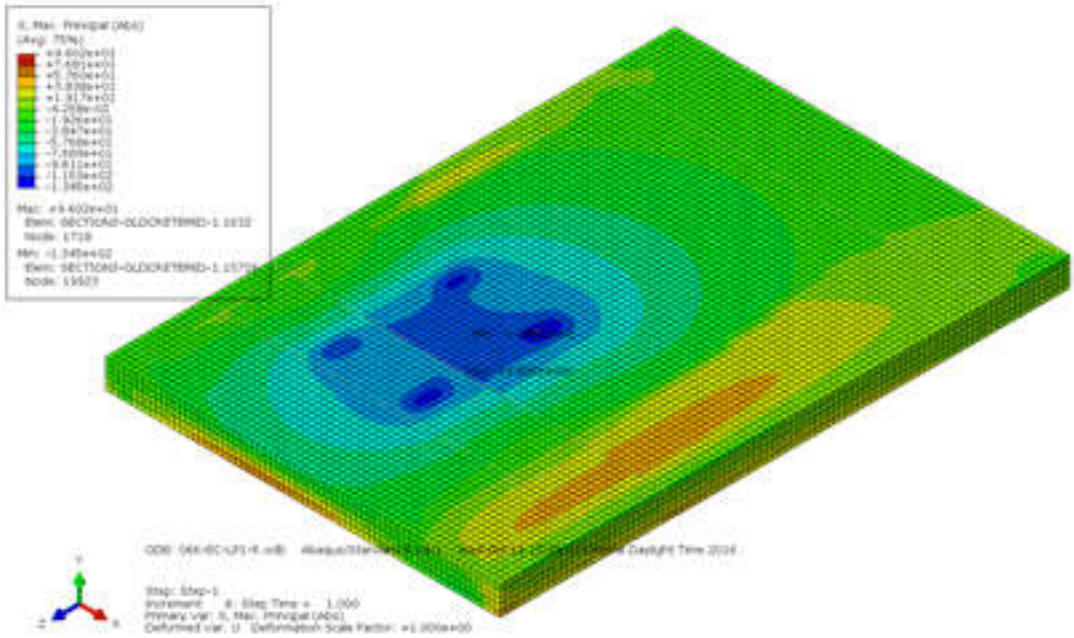

Figure B-2-4: Stresses in Concrete Slab for LP-1-R (psi)

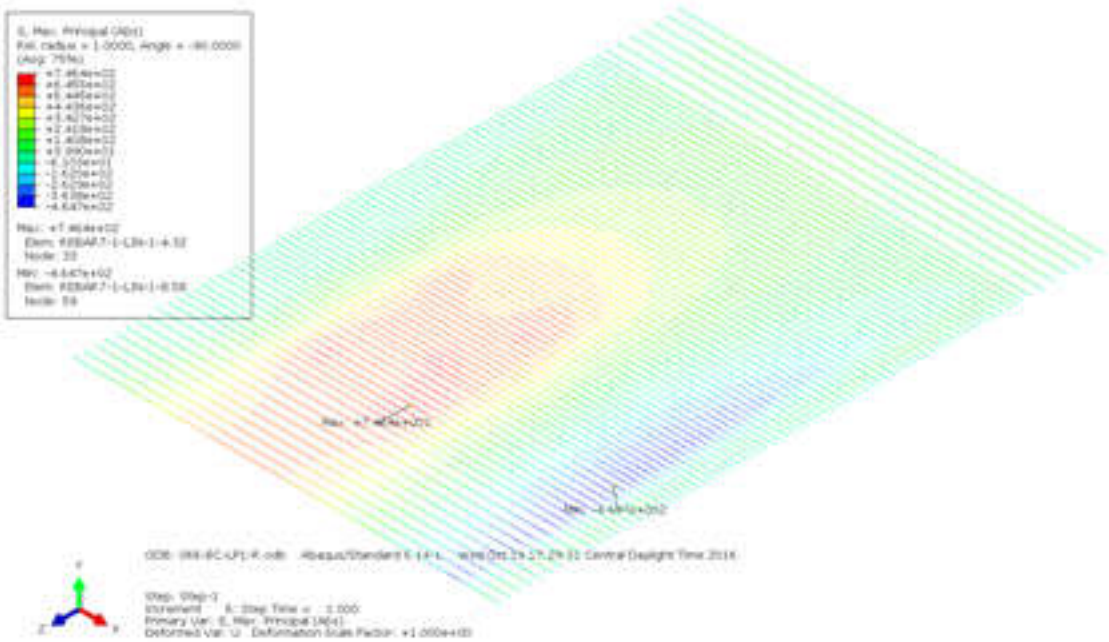

Figure B-2-5: Stresses in Reinforcing Bars for LP-1-R (psi)

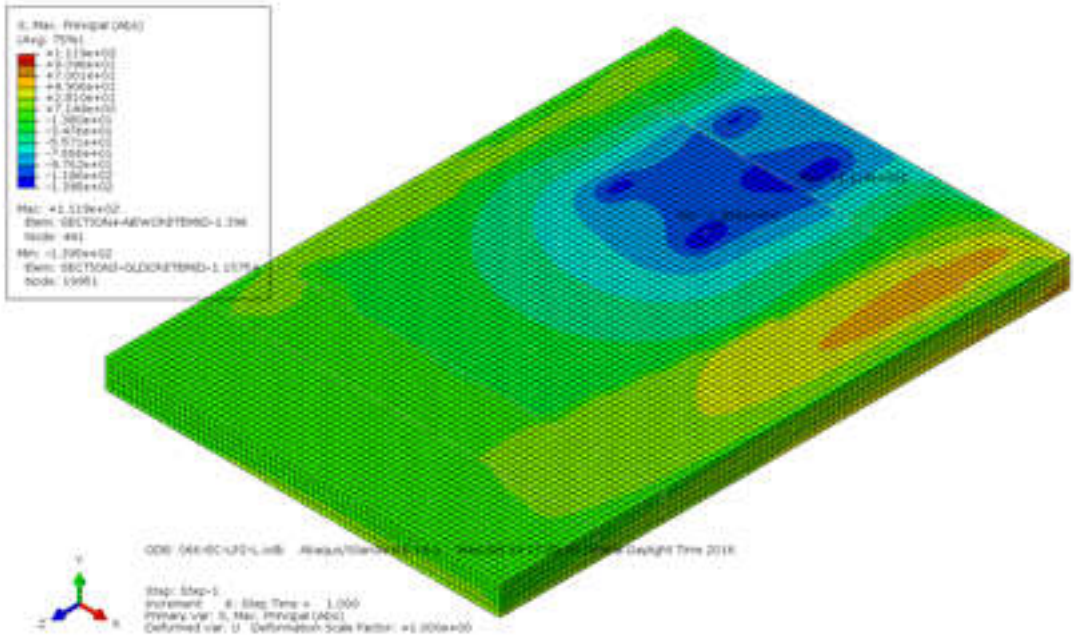

Figure B-2-6: Stresses in Concrete Slab for LP-2-L (psi)

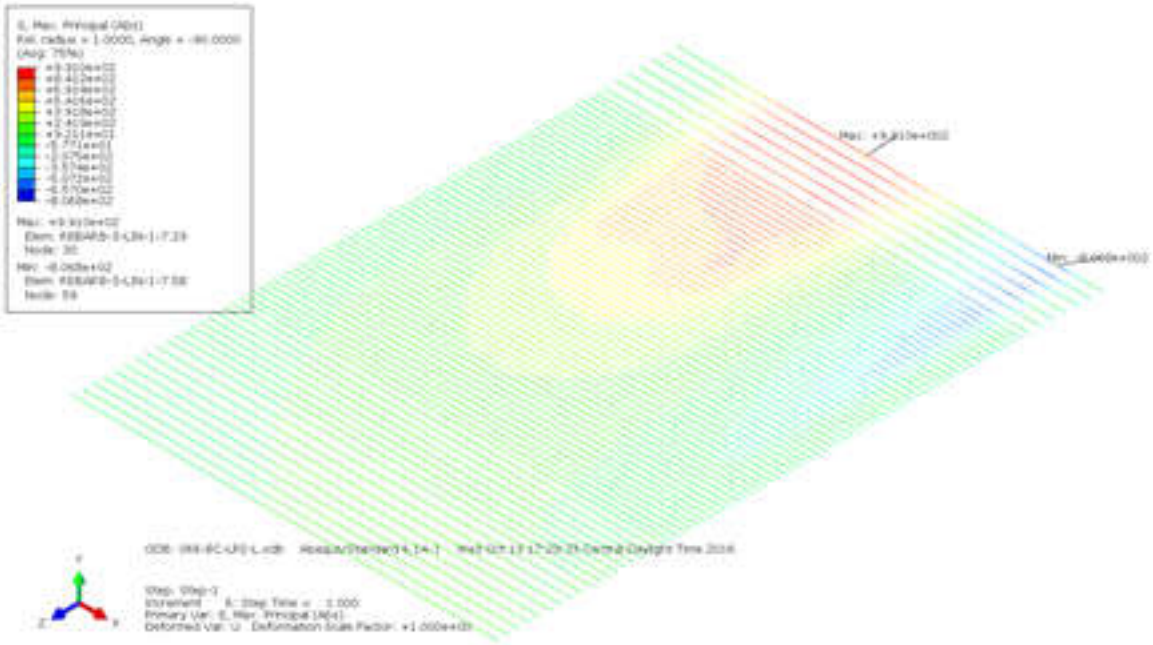

Figure B-2-7: Stresses in Reinforcing Bars for LP-2-L (psi)

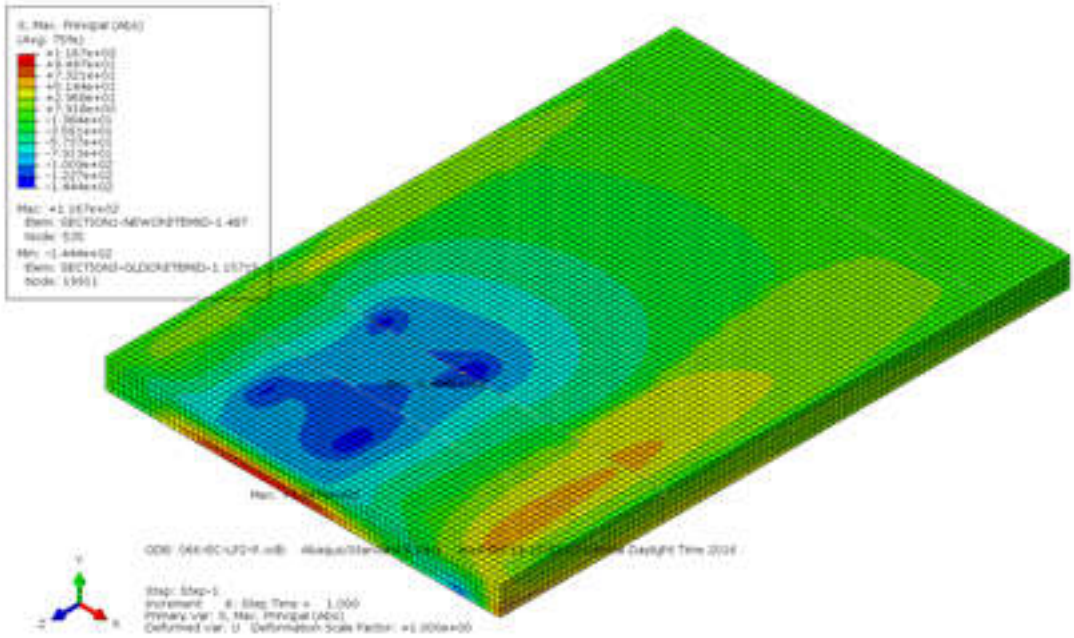

Figure B-2-8: Stresses in Concrete Slab for LP-2-R (psi)

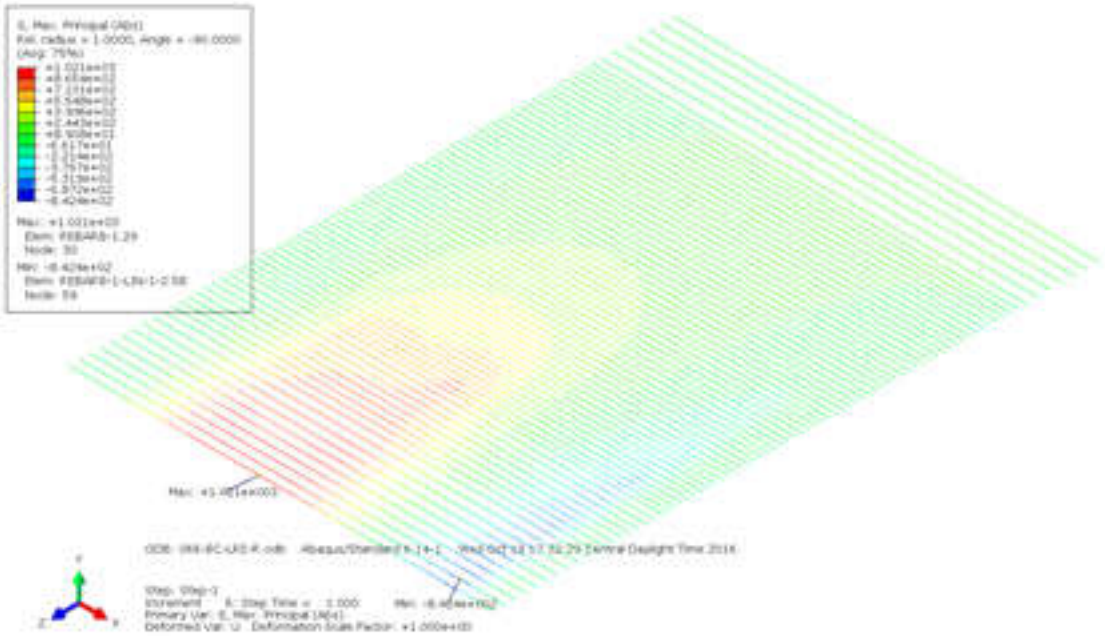

Figure B-2-9: Stresses in Reinforcing Bars for LP-2-R (psi)

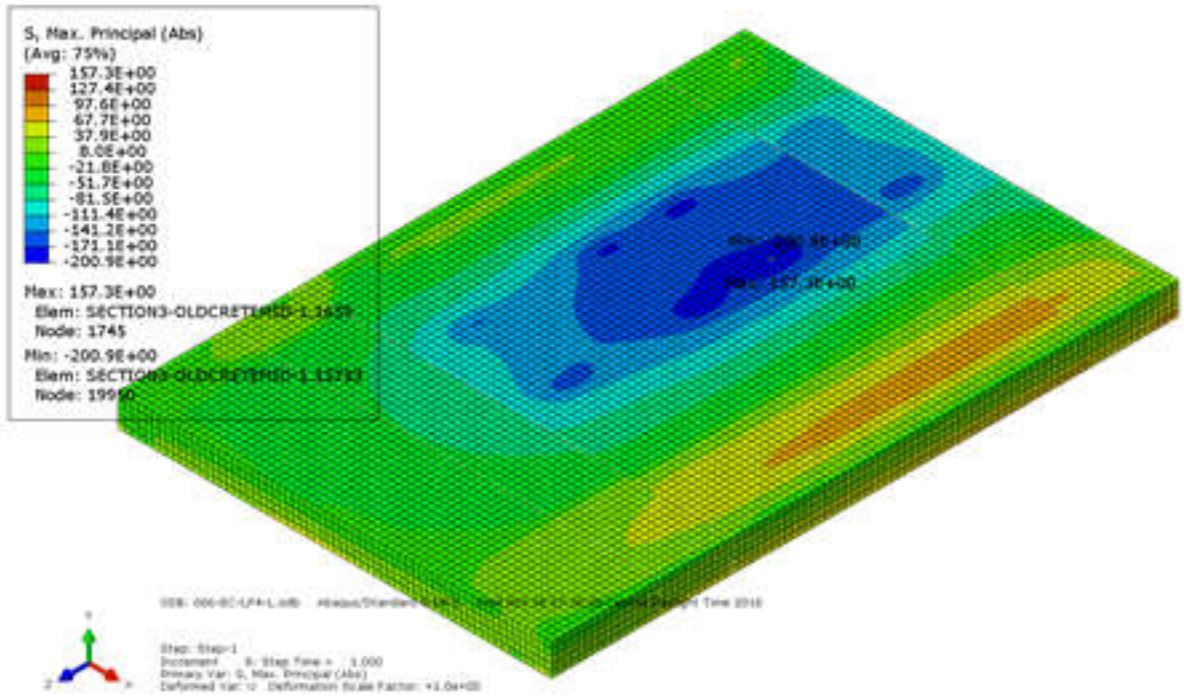

Figure B-2-10: Stresses in Concrete Slab for LP-4-L (psi)

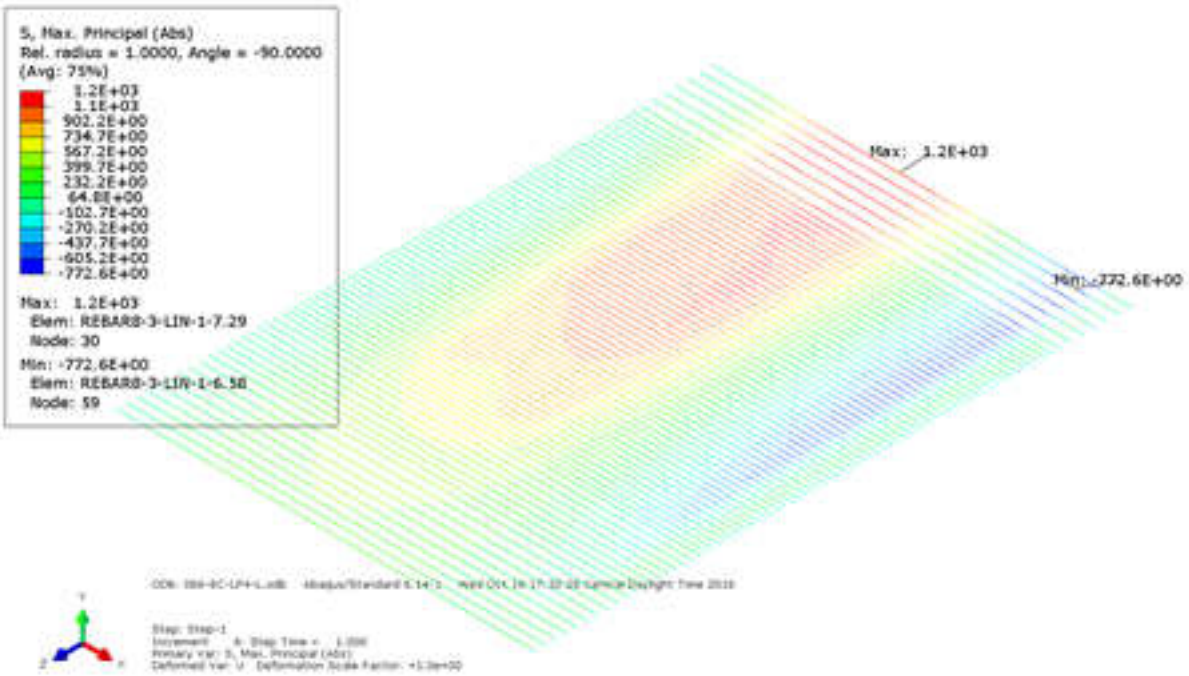

Figure B-2-11: Stresses in Reinforcing Bars for LP-4-L (psi)

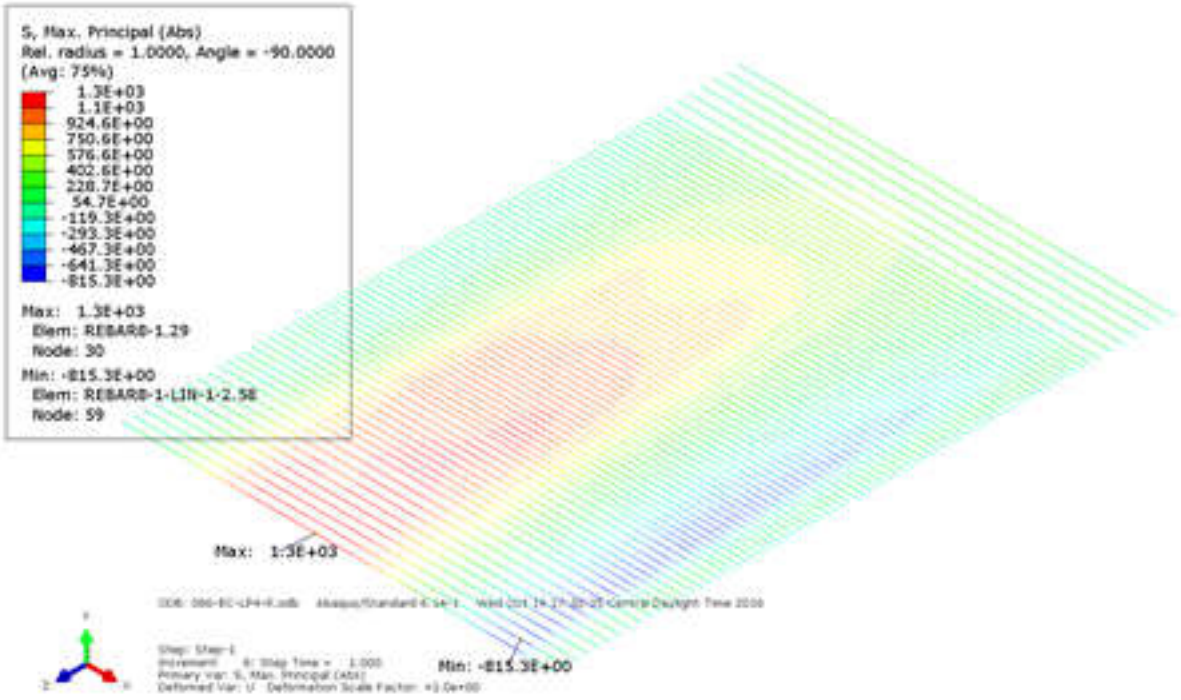

Figure B-2-12: Stresses in Reinforcing Bars for LP-4-R (psi)

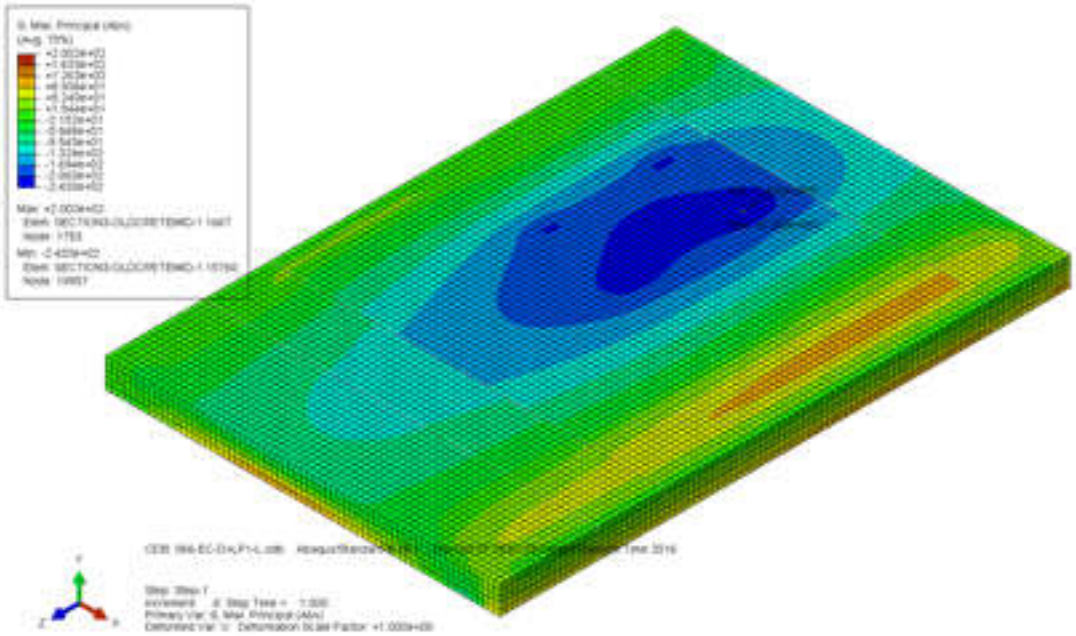

Figure B-2-13: Stresses in Concrete Slab for D+LP-1-L (psi)

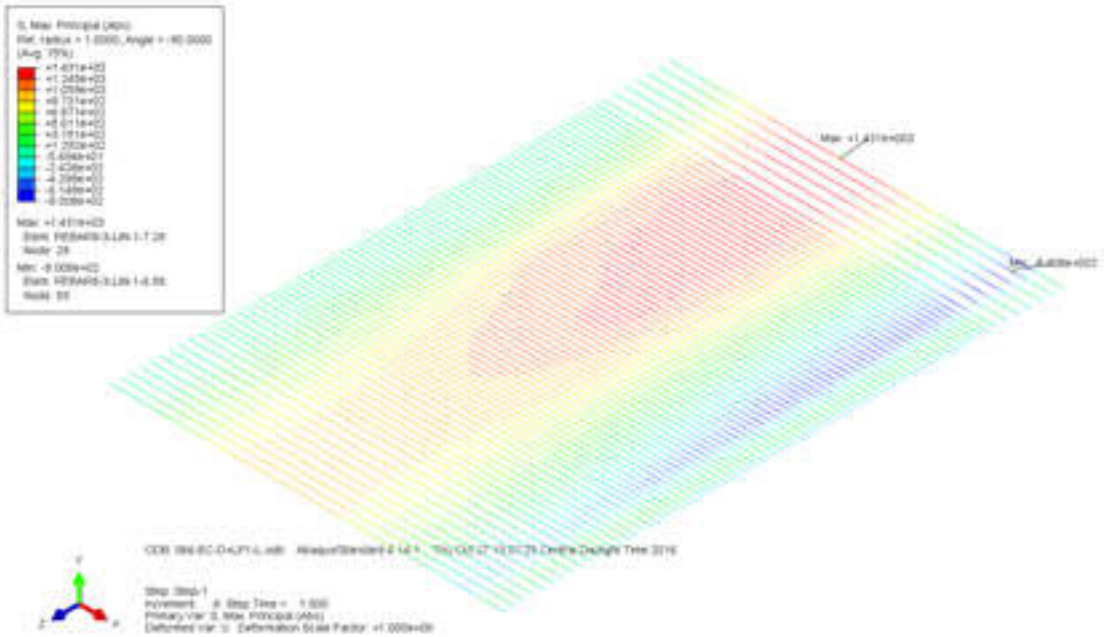

Figure B-2-14: Stresses in Reinforcing Bars for D+LP-1-L (psi)

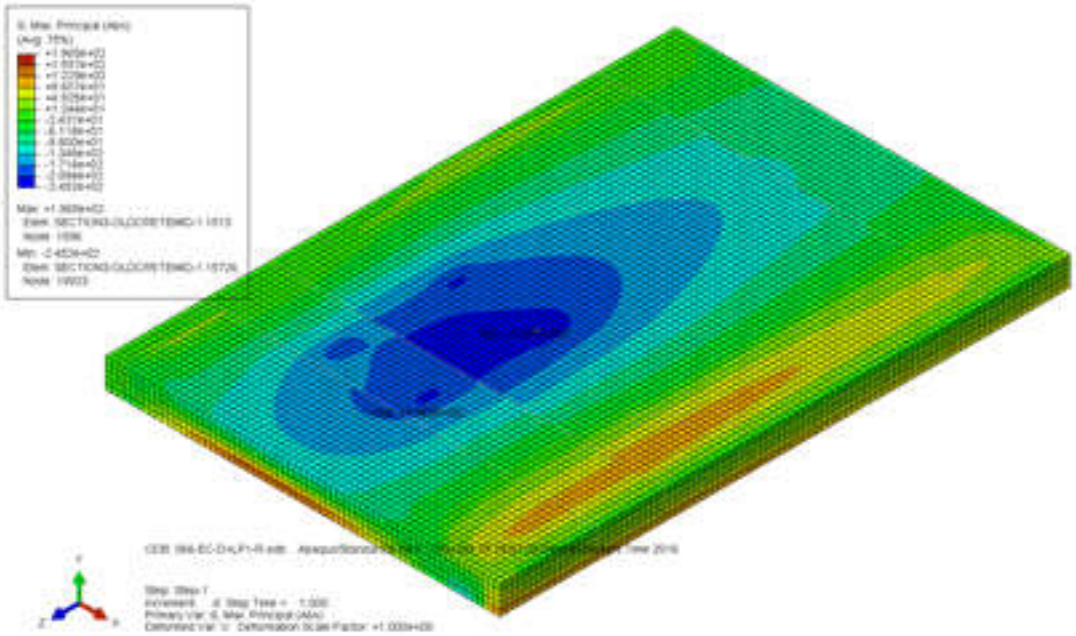

Figure B-2-15: Stresses in Concrete Slab for D+LP-1-R (psi)

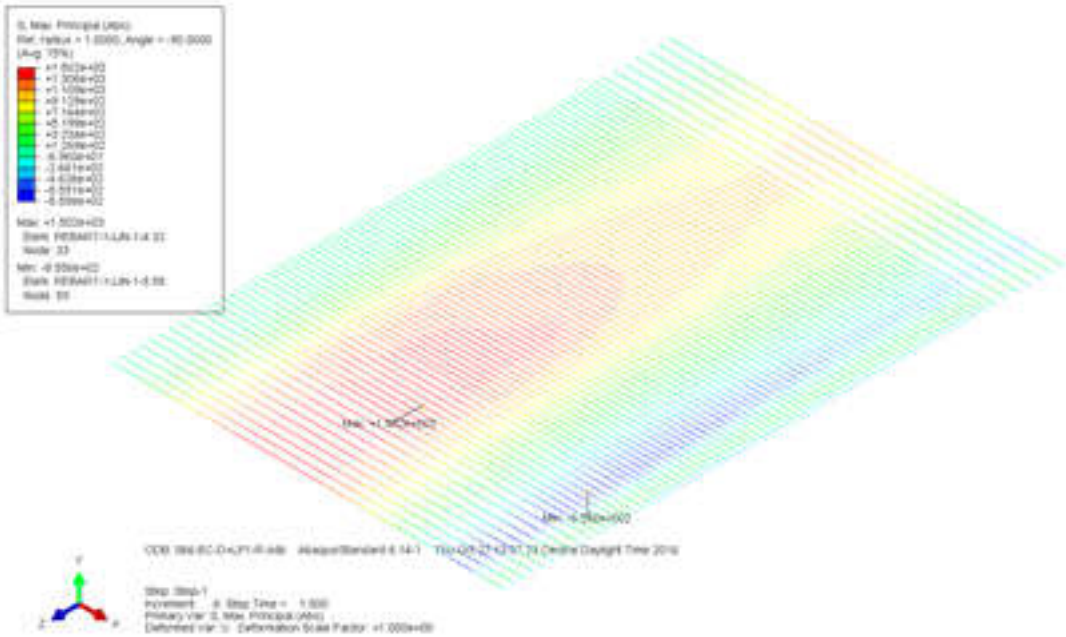

Figure B-2-16: Stresses in Reinforcing Bars for D+LP-1-R (psi)

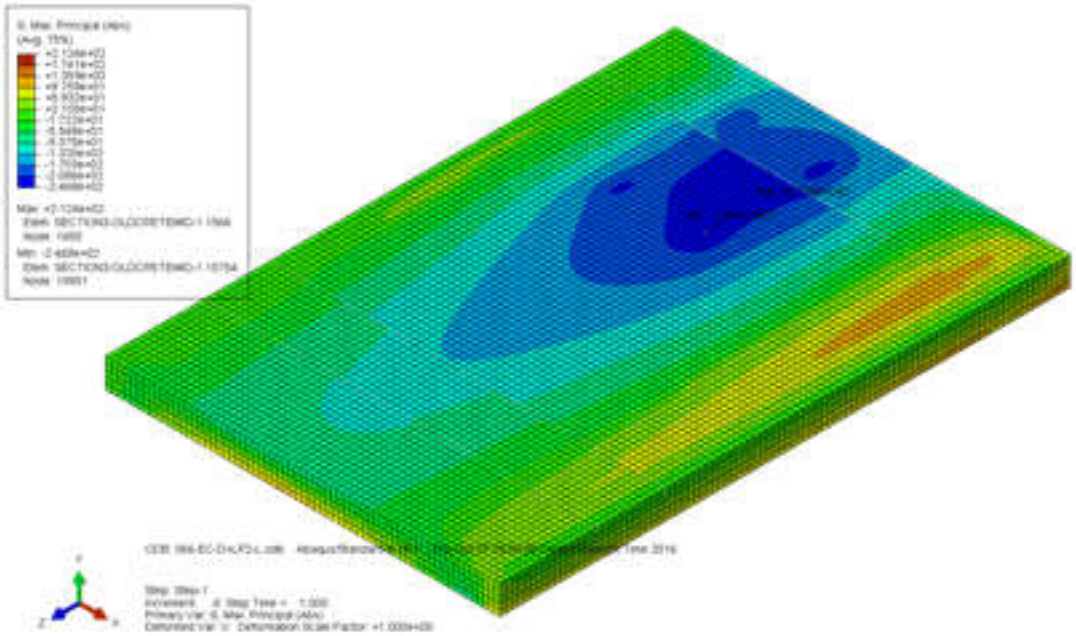

Figure B-2-17: Stresses in Concrete Slab for D+LP-2-L (psi)

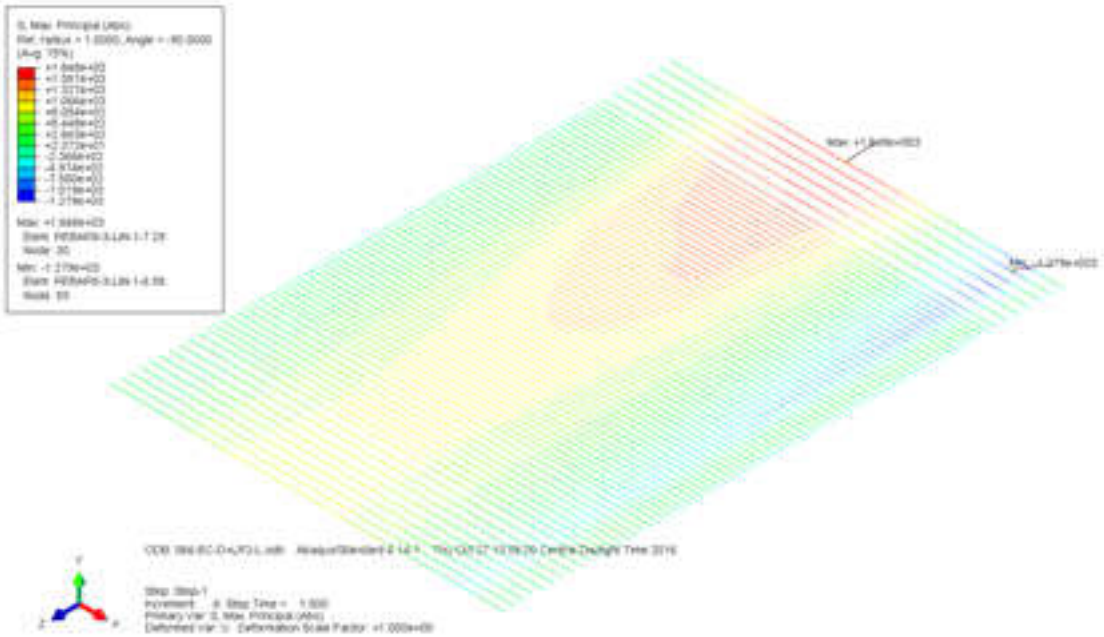

Figure B-2-18: Stresses in Reinforcing Bars for D+LP-2-L (psi)

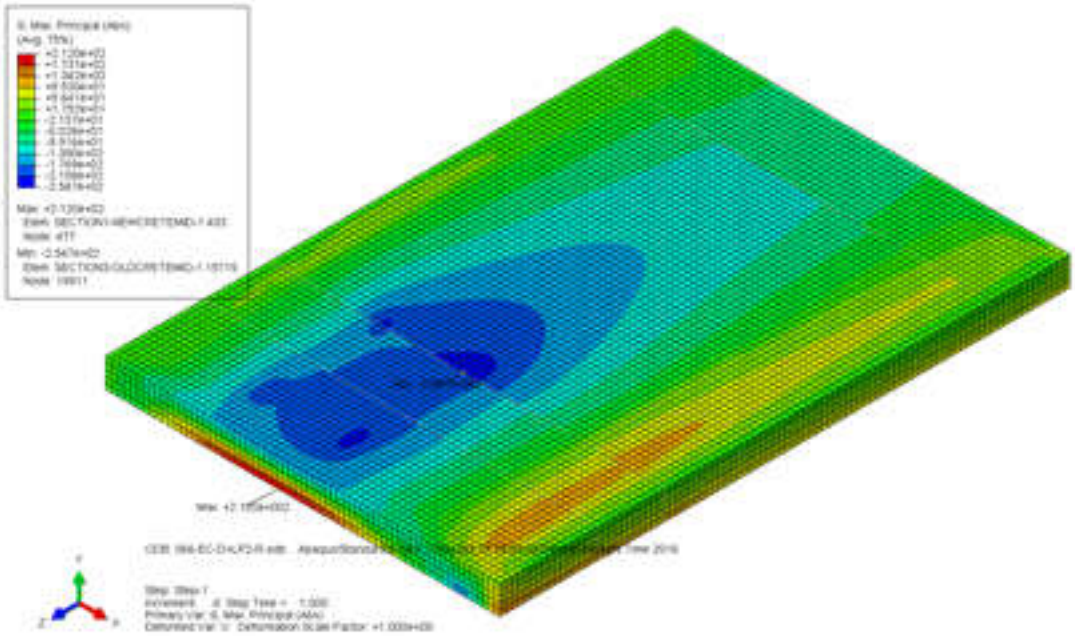

Figure B-2-19: Stresses in Concrete Slab for D+LP-2-R (psi)

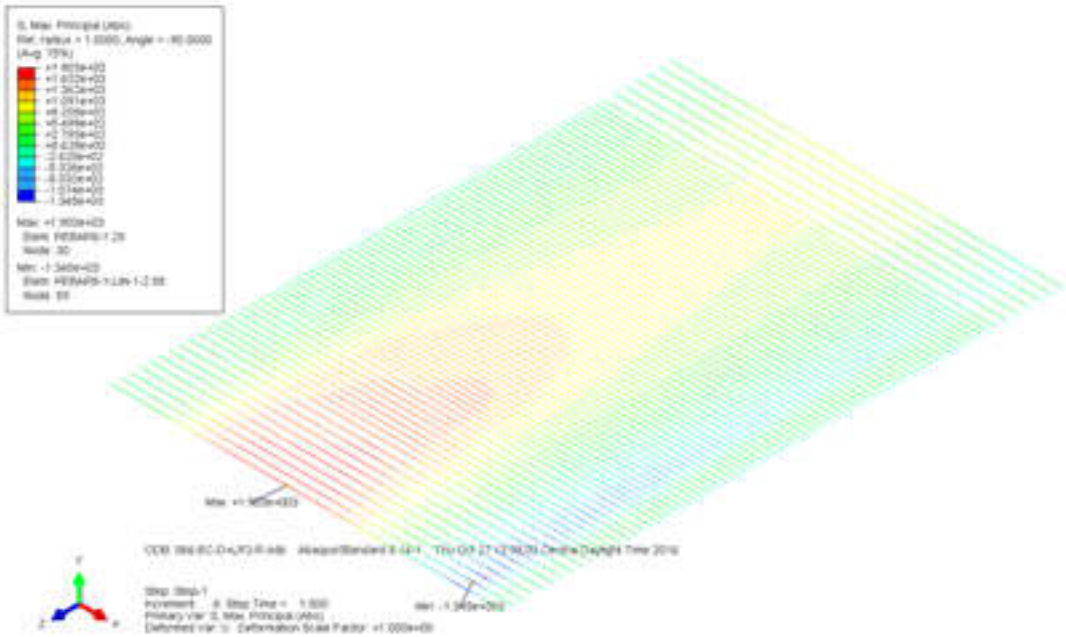

Figure B-2-20: Stresses in Reinforcing Bars for D+LP-2-R (psi)

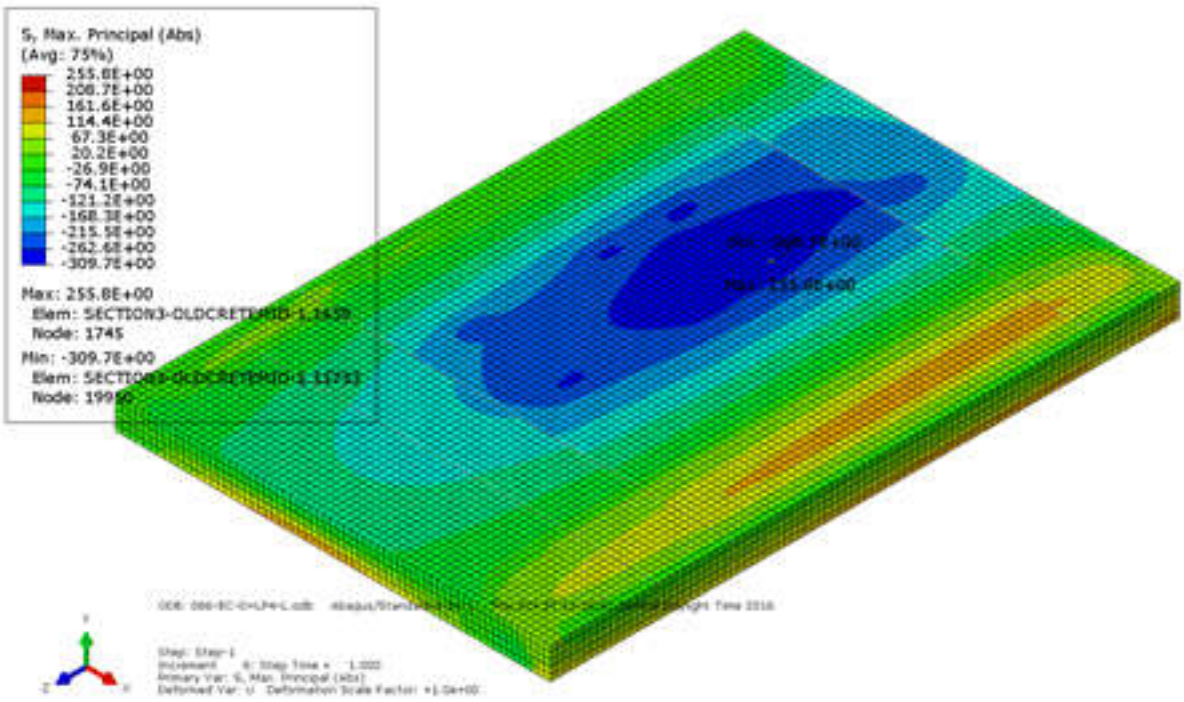

Figure B-2-21: Stresses in Concrete Slab for D+LP-4-L (psi)

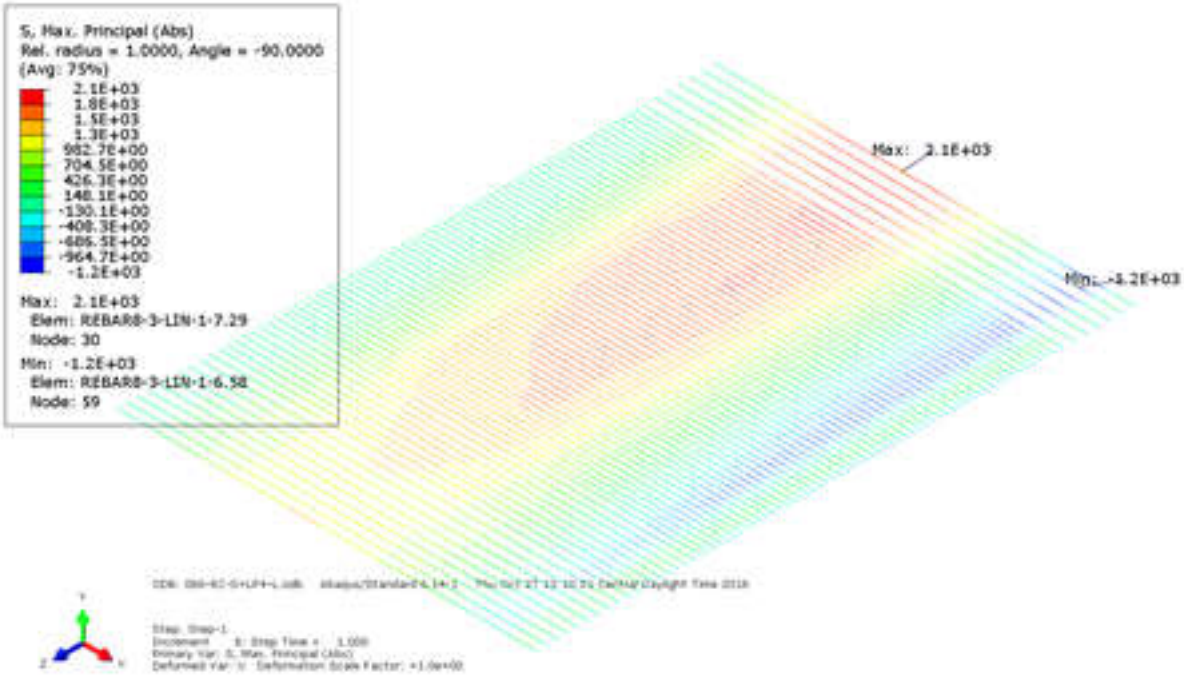

Figure B-2-22: Stresses in Reinforcing Bars for D+LP-4-L (psi)

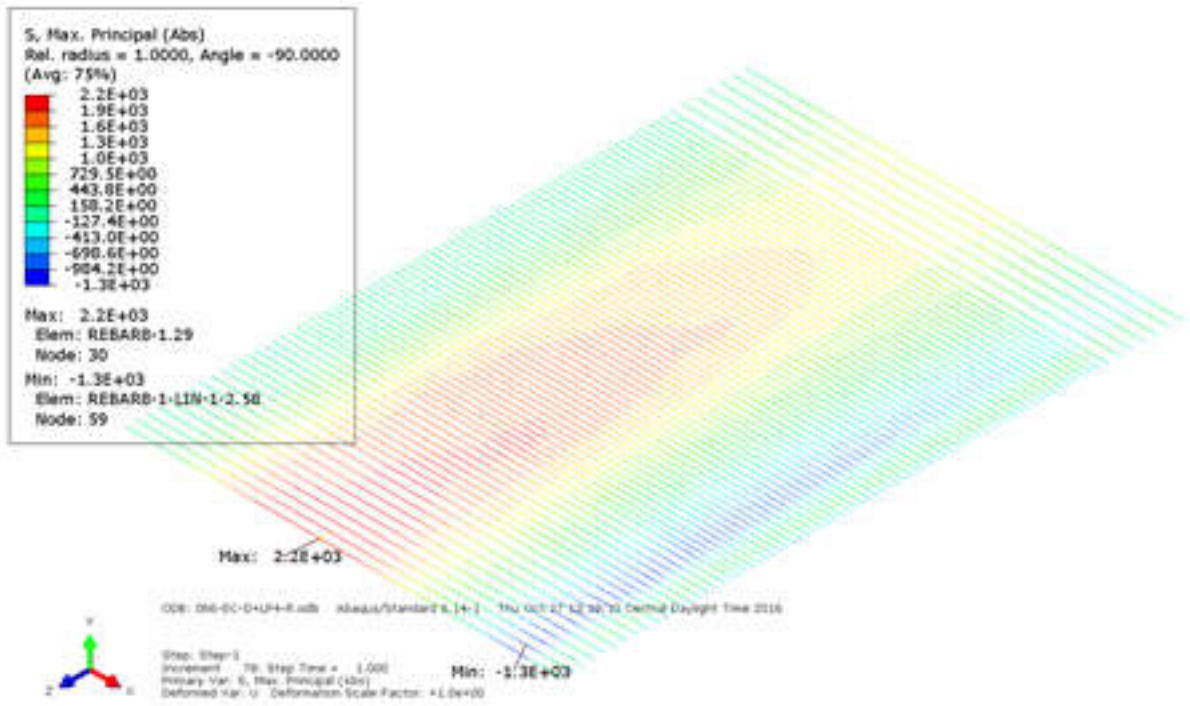

Figure B-2-23: Stresses in Reinforcing Bars for D+LP-4-R (psi)

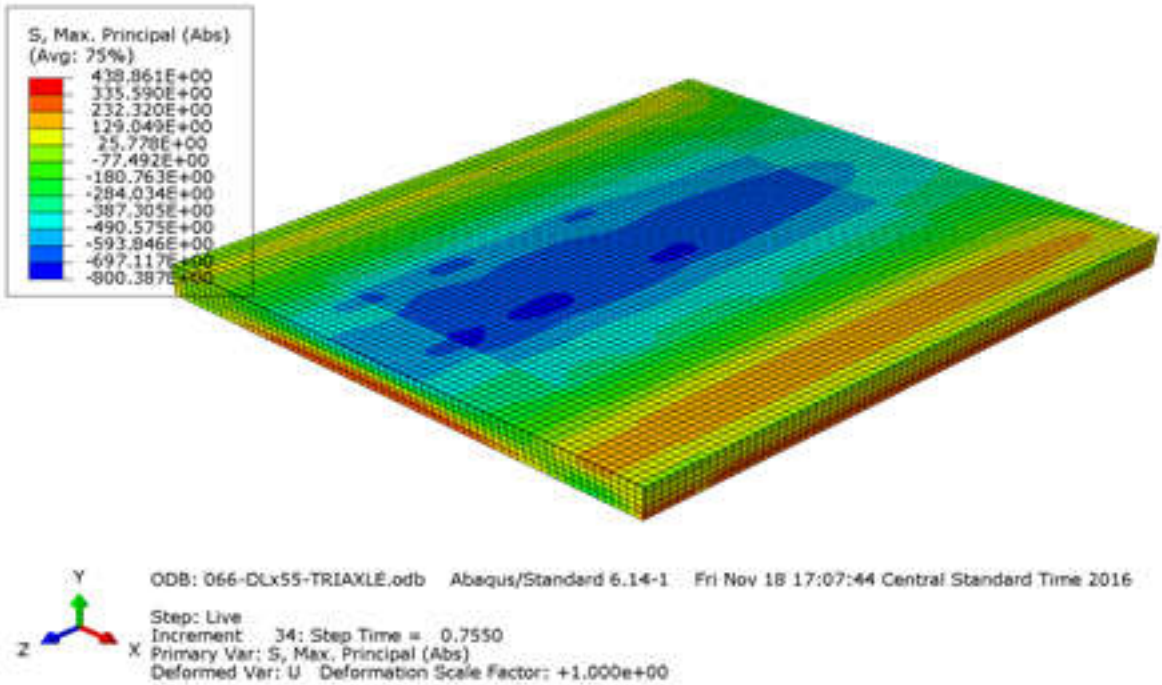

Figure B-2-24: Inventory Level Stresses in Concrete for Two TriAxle Trucks (psi)

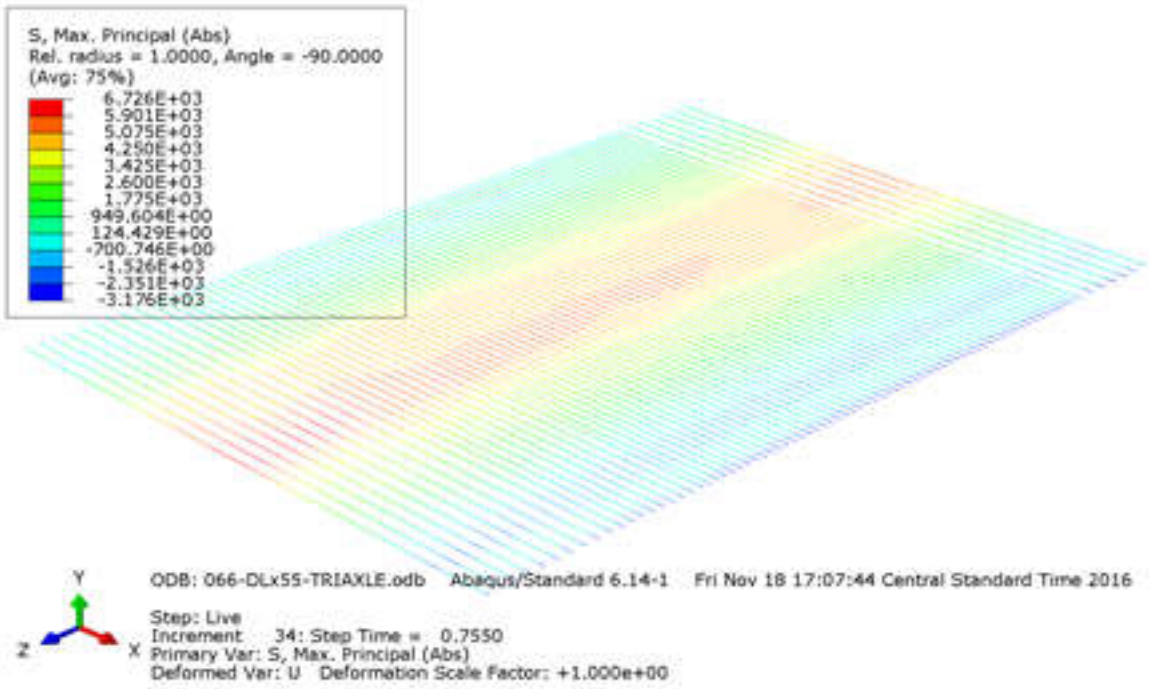

Figure B-2-25: Inventory Level Stresses in Reinforcing Bars for Two TriAxle Trucks (psi)

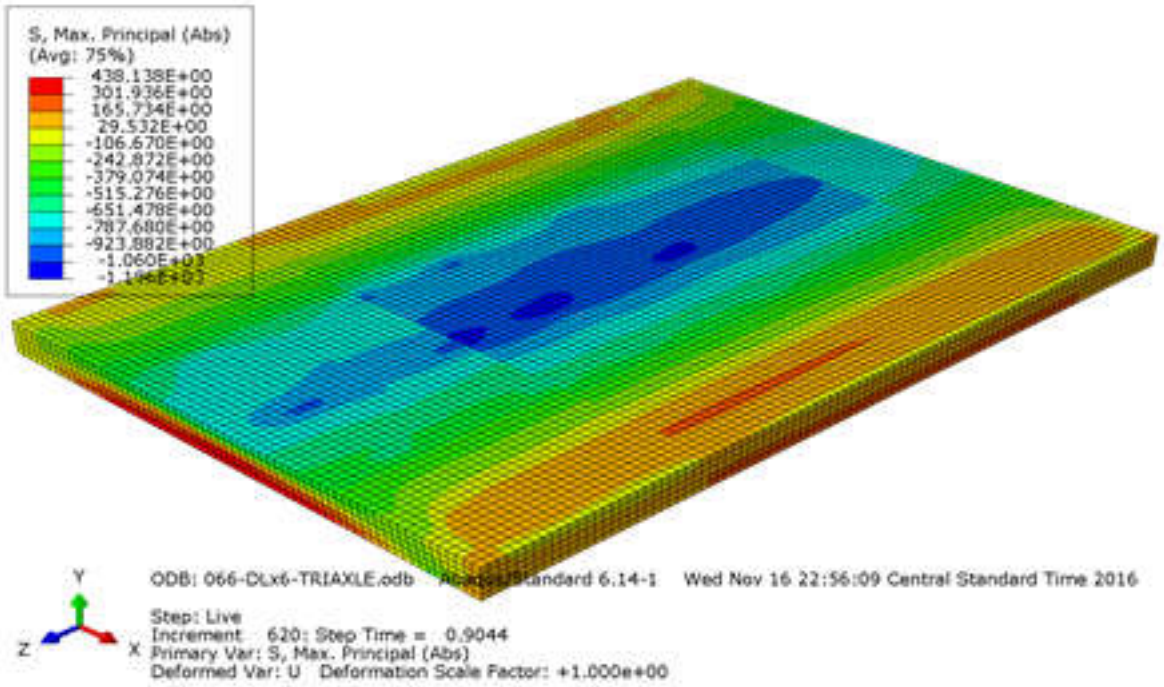

Figure B-2-26: Operating Level Stresses in Concrete for Two TriAxle Trucks (psi)

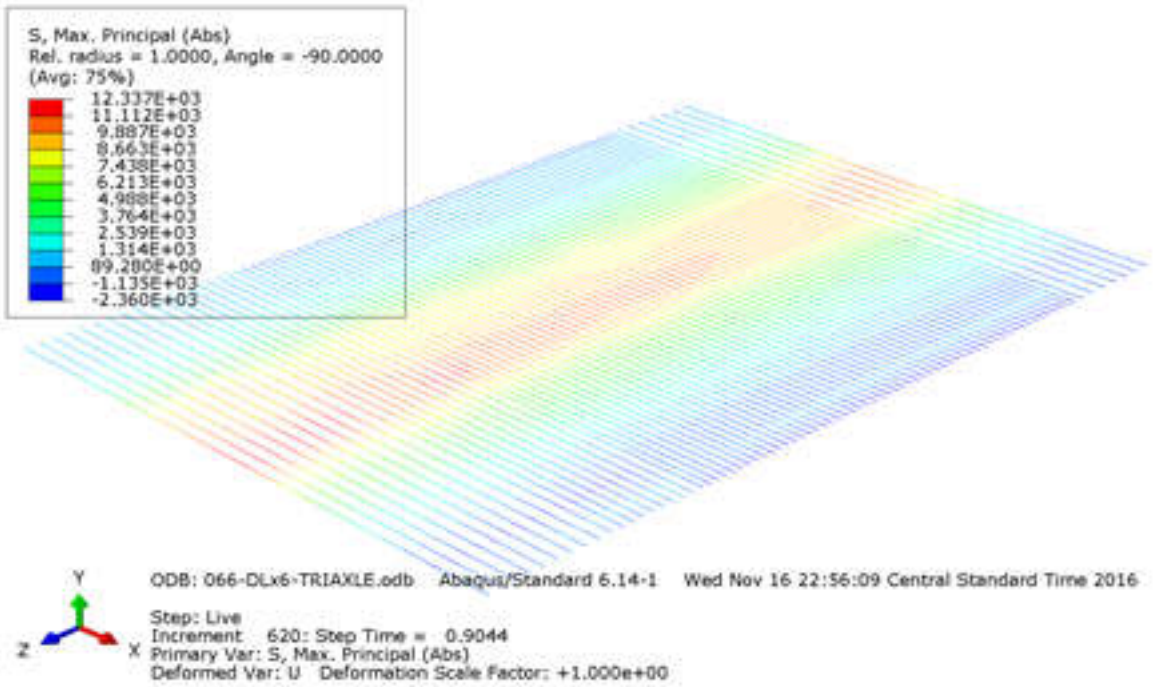

Figure B-2-27: Operating Level Stresses in Reinforcing Bars for Two TriAxle Trucks (psi)